



UNIVERSITY OF  

---

LIVERPOOL

## Reverse Engineering Glaucoma

---

Thesis submitted in accordance with the requirements of  
the University of Liverpool for the degree of Doctor of  
Philosophy by

**Karen Leah Lester**

**April 2018**

## Abstract

Primary open angle glaucoma (POAG) is a leading cause of irreversible blindness worldwide, and the only modifiable risk factor is intraocular pressure (IOP). Glaucoma is a complex disease with specific endophenotypes, and disease pathogenesis is likely to involve multiple pathways linking genetic and environmental interactions. Growth factors present in the aqueous humour in POAG increase outflow resistance and elevate IOP. TGF- $\beta$ 2 alters ECM production and turnover in the trabecular meshwork (TM) and has been shown in numerous studies to play a role in the pathogenesis of POAG. No current pharmacological interventions target the deleterious effects of TGF- $\beta$ 2 of the TM which produced elevated IOP. In addition to TGF- $\beta$  another well characterised glaucoma stimulus is corticosteroids. Corticosteroids are used in ophthalmology to decrease inflammation and preserve ocular function. However side effects including cataract, enhanced infection, and glaucoma are associated with their use. Small, naturally occurring regulatory genes, micro RNAs (miRNAs), target many genes downstream of TGF- $\beta$ 2 and are expressed in response to corticosteroids.

The current work set out to identify key differentially expressed genes by RNA-Seq in the human trabecular meshwork (TM) in response to two glaucoma stimuli; TGF- $\beta$ 2 and dexamethasone; and investigate the ability of miRNAs to manipulate gene expression within the TM to reduce pathological insults central to glaucoma.

Investigating the influence of TGF- $\beta$ 2 on gene expression in primary human TM cells demonstrated that the majority of the significantly differentially expressed genes were involved in extracellular matrix remodelling and actin cytoskeletal re-organisation likely via the RhoA signalling pathway. The influence of dexamethasone on gene expression in primary human TM cells identified genes involved in extracellular matrix remodelling and genes required for glucocorticoid receptor nuclear translocation. Differentially expressed miRNAs in healthy and glaucomatous human TM cells were identified by a miRNA microarray. Manipulation of validated mRNA targets by identified miRNAs indicated a complex regulatory network and *in vitro* functional analyses further identified regulation of actin cytoskeleton remodelling via miRNA inhibition.

The findings of this study indicate that TGF- $\beta$ 2 and dexamethasone have significant effects on extracellular matrix remodelling and actin cytoskeletal re-organisation in human TM cells. The RNA-Seq and miRNA array have identified potential novel therapeutic targets for glaucoma.

## Acknowledgments

First and foremost I would like to thank my supervisors Prof. Colin Willoughby (Bob), Dr. Carl Sheridan, and Mrs. Anshoo Choudhary. Thank you firstly for affording me the wonderful opportunity and for your continued help and support over the last three years. Carlos, thanks for keeping me going over the last few months! Bob, I understand now why you wanted to drag me from the lab and encourage my reading! I have learned so much under your guidance and everything you taught me will stick with me throughout my scientific career. You have encouraged me every step of the way and for this I will always be grateful.

Thank you to Dr. Kevin Hamill for being an honorary supervisor, an everyday llama expert and a teacher extraordinaire! Your enthusiasm for science is admirable.

Thank you to Dr. S. Senthilkumari (Aravind Medical Research Foundation, Madurai, India) for providing training on the H.O.C.A.S setup. Thank you to Dr. Abbot Clark (UNTHSC, Texas, USA) for providing glaucomatous TM samples for this research. Thank you to Dr. David Simpson and his team (Queens University Belfast, UK) for RNA-Sequencing services. Thank you to Dr. Natalie Pollock and Dr. Stephnie Kennedy for your help with primary cell culture. Thank you Neeru for your advice and collection of corneal rims.

Thank you NC3R, International Glaucoma Association/UK and Eire Glaucoma, International Glaucoma Association and Fight for Sight for funding this work.

In addition I would like to thank everyone in E.V.S who have made my time in U.of.L such an enjoyable experience, and have been so helpful throughout. Miss. Jessica Eyre, thank you for dragging me to yoga even when I protested and being there over the last year to provide the lols.

Thank you to my girls back home, your support has been phenomenal and I apologise for only knowing how to talk about one thing for the past three years.

To my best friend and partner in crime, Leeburt, thank you for being with me every step of the way since the very beginning. You have cheered me up no end every time I needed it and stood by me through it all. You've held my hand every step of the way and encouraged me always. Endless Netflix binges and Lindt chocolate was key. It has been the best experience ever doing this with you by my side every day.

I especially want to thank my Mum, Dad, and sister Amy. Mum and Dad, you've given me the best of everything, always, and I know without your support throughout my life I would not be where I am today. Amy, thanks for making me smile when all I wanted to do was cry, you've dealt with my ups and downs throughout this whole process expertly and I know I wouldn't have gotten through it without you all by my side.

~"Always look someone in the eye, even if they're blind, just say "I'm looking you in the eye."~

## Table of Figures

Figure 1.1: Optic Disc and Schematic Cross-section of the ONH to Show Central Cup.....	<b>3</b>
Figure 1.2: Characteristic Visual Field Defects in Glaucoma.....	<b>5</b>
Figure 1.3: Gonioscope Drainage Angle Images.....	<b>7</b>
Figure 1.4: Posterior View of the Iris and Ciliary Body Showing the Ciliary Processes.....	<b>16</b>
Figure 1.5: Active Secretion of Aqueous Humour.....	<b>17</b>
Figure 1.6: Cross Section of the Human Eye.....	<b>20</b>
Figure 1.7: Anatomical Structure of the Human Trabecular Meshwork.....	<b>21</b>
Figure 1.8: Structure and Transcriptional Isoforms of the Human GR Gene.....	<b>27</b>
Figure 1.9: Glucocorticoid Mechanisms of Action.....	<b>30</b>
Figure 1.10: TGF- $\beta$ Structure, Latency, Activation and Signalling.....	<b>36</b>
Figure 1.11: miRNA Biosynthesis- Canonical Pathway.....	<b>45</b>
Figure 1.12: miRNA Biosynthesis- Non-Canonical Pathway.....	<b>47</b>
Figure 2.1: Representative Images Depicting Human Anterior Segment Dissection Protocol.....	<b>55</b>
Figure 3.1: Representative Phase Contrast Microscope Images of Human Cultured TM Cells.....	<b>88</b>

Figure 3.2: Representative Fluorescent Confocal Microscope Images of Human TM Cells.....	<b>89</b>
Figure 3.3: Principal Component Analysis of RNA-Seq Data for Control Untreated TM Cells and TGF- $\beta$ 2 Treated TM Cells.....	<b>94</b>
Figure 3.4: Heat Map and Unsupervised Clustering of Human TM Cells Treated with TGF- $\beta$ 2.....	<b>96</b>
Figure 3.5: volcano Plot Showing the Relationship Between LogFC and the Average Log Counts-Per-Million (CPM) .....	<b>101</b>
Figure 3.6: Top Canonical Pathways of the Top 1% Differentially Expressed Genes in TGF- $\beta$ 2 Treated Human TM Cells Vs Control TM Cells.....	<b>107</b>
Figure 3.7: Canonical Pathway Map for RhoA Signalling Pathway.....	<b>108</b>
Figure 3.8 Expression Levels of Candidate Genes in Cultured Normal Human Tm Cells.....	<b>116</b>
Figure 3.9: Expression Levels of Candidate Genes in Cultured Normal Human TM Cells and Glaucomatous TM Cells.....	<b>120</b>
Figure 3.10: Schematic of Rho/ROCK Signalling Pathway.....	<b>124</b>
Figure 3.11: NOX4 Mediated TGF- $\beta$ -Induced Pro-Fibrotic Responses.....	<b>127</b>
Figure 3.12: Pathological Role of EDN1 in Glaucoma.....	<b>129</b>
Figure 3.13: Localisation of CDKN2B and CDKN2B-AS1 on Chr9p21.....	<b>131</b>
Figure 3.14: Effects of CDKN2B and CDKN2b-AS1 on Cell Cycle via CDK4 Inhibition.....	<b>131</b>

Figure 4.1: Principal Component Analysis of RNA-Seq Data for Control Untreated TM Cells and DEX Treated TM Cells.....	<b>151</b>
Figure 4.2: Heat Map and Unsupervised Clustering of RNA-Seq Data from Control Untreated TM Cells and DEX Treated TM Cells.....	<b>153</b>
Figure 4.3: Volcano Plot of the Relationship Between the LogFC and the Average Log Counts-Per-Million (CPM) in Control Untreated TM Cells Compared to DEX Treated TM Cells.....	<b>160</b>
Figure 4.4: Top Canonical Pathways of the Top 1% Differentially Expressed Genes in Human TM Cells +/- Dexamethasone.....	<b>164</b>
Figure 4.5: Heat Map of Highest Ranked Over-Lapping Canonical Pathways between TGF- $\beta$ 2 Treated Human TM Cells and DEX Treated Human TM Cells.....	<b>165</b>
Figure 4.6: Expression Levels of Glucocorticoid Receptor (GR $\alpha$ and $\beta$ ) in Paired Human TM Cells +/- DEX Treatments.....	<b>167</b>
Figure 4.7: Expression Levels of Candidate Genes in Cultures Human TM Cells.....	<b>170</b>
Figure 4.8: Alternate Splicing of Glucocorticoid Receptor Generates Two Functionally Distinct Splice Isoforms: GR $\alpha$ and GR $\beta$ .....	<b>175</b>
Figure 4.9: Putative Integrin Signalling Pathways Through PYK2 or FAK.....	<b>177</b>
Figure 4.10: FKBP51/FKBP5 Structure.....	<b>180</b>
Figure 4.11: The FKBP51 and FKBP52 Genes Regulate Glucocorticoid Receptor Nuclear Translocation.....	<b>181</b>
Figure 4.12: PAI-2 Inhibits tPA Activity.....	<b>184</b>
Figure 5.1: Interplay Between miR-200 Family, TGF- $\beta$ , and ZEB1/2 in EMT Regulation.....	<b>191</b>

Figure 5.2: Cross-talk Between TGF- $\beta$ and miRNAs.....	<b>193</b>
Figure 5.3: Present Calls and Threshold Filtering Plot.....	<b>206</b>
Figure 5.4: Volcano Plot Analysis of Untreated and TGF- $\beta$ 2 Treated Human TM Cells miRNA Expression.....	<b>210</b>
Figure 5.5: q-PCR Validation of Significantly Up-regulated miRNAs from Microarray Data of TGF- $\beta$ 2 Cultured Human TM Cells.....	<b>212</b>
Figure 5.6: Expression Levels of miR-143, miR-145, and miR-4328 in Cultured Human Glaucomatous TM Cells.....	<b>213</b>
Figure 5.7: Transfection Optimisation; Cell Viability Assessment.....	<b>215</b>
Figure 5.8: TGF- $\beta$ 2 Expression Profiles in TGF- $\beta$ 2 TM Cells Treated with a miR-145- 5p Mimic and Inhibitor.....	<b>217</b>
Figure 5.9: SMAD2 Expression Profiles in the Presence of Synthesised Mimics and Inhibitors for miR-145-5p.....	<b>218</b>
Figure 5.10: CTGF Expression Profiles in the Presence of Synthesised Mimics and Inhibitors for miR-145-5p.....	<b>219</b>
Figure 5.11: E-Cadherin Expression Profiles in the Presence of Synthesised Mimics and Inhibitors for miR-145-5p.....	<b>220</b>
Figure 5.12: N-Cadherin Expression Profiles in the Presence of Synthesised Mimics and Inhibitors for miR-145-5p.....	<b>221</b>
Figure 5.13: SLUG Expression Profiles in the Presence of Synthesised Mimics and Inhibitors for miR-145-5p.....	<b>222</b>
Figure 5.14: SNAIL Expression Profiles in the Presence of Synthesised Mimics and Inhibitors for miR-145-5p.....	<b>223</b>
Figure 5.15: Vimentin Expression Profiles in the Presence of Synthesised Mimics and Inhibitors for miR-145-5p.....	<b>224</b>

Figure 5.16: Principal Component Analysis Across All Sample Groups.....	<b>228</b>
Figure 5.17: Venn Diagram of Overlap of Differentially Expressed Genes Between Scrambled Negative Control, 143i, or 145i Transfected TM Cells Treated with TGF- $\beta$ 2.....	<b>238</b>
Figure 5.18: Comparison Analysis of Canonical TGF- $\beta$ Signalling Pathway between 143i, 145i and SNC Transfected TGF- $\beta$ 2 Treated Human TM Cells.....	<b>246</b>
Figure 5.19: Comparison Upstream Analysis of miR145 Between 143i, 145i, and SNC Transfected TGF- $\beta$ 2 Treated Human TM Cells.....	<b>247</b>
Figure 5.20: Comparison Upstream Analysis of ZEB1 Between 143i, 145i, and SNC Transfected TGF- $\beta$ 2 Treated Human TM Cells.....	<b>248</b>
Figure 5.21: q-PCR Analysis of ACTA2 Gene Expression in Transfected TGF- $\beta$ 2 Human TM Cells.....	<b>250</b>
Figure 5.22: ACTA2 Protein Expression Reduced in Presence of miRNA Inhibitors.....	<b>252</b>
Figure 5.23: The miR143/145 Cluster.....	<b>254</b>
Figure 5.24: Regulation of Vascular Smooth Muscle Cell Phenotype.....	<b>256</b>
Figure 5.25: Summary of miR143/145 Regulation.....	<b>261</b>
Figure 7.1: Anterior Segment Organ Culture Perfusion Setup.....	<b>290</b>

## Website Index

miRTarBase (v8): <http://mirtarbase.mbc.nctu.edu.tw/php/index.php>

Validated Target Module of miRWalk 2.0: <http://zmf.umm.uni-heidelberg.de/apps/zmf/mirwalk2>

PrimerBank: <https://pga.mgh.harvard.edu/primerbank/>

## List of Abbreviations

TM	Trabecular meshwork
AH	Aqueous humour
TGF- $\beta$	Transforming Growth Factor Beta
PBS	Phosphate buffered saline
DMEM	Dulbeccos modified eagles medium
POAG	Primary open angle glaucoma
q-PCR	Quantitative polymerase chain reaction
TC	Tissue culture
CLAN	Cross-linked actin network
miRNA	Micro-Ribonucleic Acid
RNA	Ribonucleic Acid
IOP	Intraocular pressure
OHT	Ocular hypertension
ONH	Optic nerve head
RGC	Retinal ganglion cells
DEX	Dexamethasone
GAGs	Glycosaminoglycans
WHO	World Health Organisation
PACG	Primary angle closure glaucoma
OCT	Optical coherence tomography
CCT	Central corneal thickness
DM	Diabetes mellitus
NPE	Non-pigmented epithelium
SC	Schlemms' canal

ECM	Extracellular matrix
JCT	Juxtacanalicular meshwork
BM	Basement Membrane
LC	Lamina Cribrosa
AGEs	Advanced glycation end products
MMPs	Matrix metalloproteinases
TNF- $\alpha$	Tumour necrosis factor alpha
GC	Glucocorticoids
GR	Glucocorticoid receptor
GREs	Glucocorticoid response elements
BMPs	Bone morphogenic proteins
LAP	Latency-associated protein
LTBP	Latent TGF- $\beta$ -binding proteins
r-SMADs	Receptor-mediated SMADs
co-SMADs	Common partner SMADs
CTGF	Connective tissue growth factor
ncRNA	Non-coding RNA
tRNA	Transfer RNA
rRNA	Ribosomal RNA
snoRNA	Small nucleolar RNA
bp	Base pairs
nt	Nucleotides
DGCR8	DiGeorge syndrome critical region 8
UTR	Untranslated region
RISC	RNA-induced silencing complex
SNP	Single nucleotide polymorphism
FPKM	Fragments per kilobase per million mapped fragments
FDR	False discovery rate
LogFC	Log fold change
CPM	Counts per million
GO	Gene ontology

IPA	Ingenuity Pathway Analysis
DEGs	Differentially expressed genes
GWAS	Genome-wide association studies
FECD	Fuchs endothelial corneal dystrophy
ROS	Reactive oxygen species
FN	Fibronectin



1.6.3	microRNA Mechanism of Action.....	48
1.6.3.1	microRNA-Mediated mRNA Decay.....	48
1.6.3.2	microRNA Translational Repression.....	49
1.6.4	miRNAs and Human Disease.....	49
<b>2.</b>	<b>Materials and Methods.....</b>	<b>51</b>
2.1	Tissue Culture.....	52
2.1.1	Tissue Samples.....	52
2.1.2	Dissection of Anterior Segment From Porcine and Human Eyes.....	53
2.1.3	Dissection of Trabecular Meshwork from Anterior Segment.....	53
2.1.4	Cell Culture Maintenance.....	56
2.1.5	Mycoplasma Testing and Treatment of Cells.....	56
2.1.6	Sub-Culturing Cells.....	56
2.1.7	Long-Term Storage of Cells.....	57
2.2	Cells for Experimentation.....	58
2.2.1	Characterisation of TM Cells.....	58
2.2.1.1	Morphological Assessment TM Cells.....	58
2.2.1.2	Fluorescent Staining of TM Cells <i>In Vitro</i> .....	58
2.2.2	Cell Stimulations with TGF- $\beta$ 2 and Dexamethasone.....	60
2.2.3	Transfection for miRNA Manipulation Experiments.....	61
2.3	Protein Based Methods.....	62
2.3.1	Whole Cell Lysis-Protein Extraction.....	62
2.3.2	SDS-Polyacrylamide Gel Electrophoresis (SDS-PAGE) .....	62
2.4	Nucleic Acid Based Methods.....	63
2.4.1	Ribonucleic Acid (RNA) Extraction.....	63
2.4.2	Nucleic Acid Concentration Measurements by NanoDrop 2000 Spectrophotometer.....	63
2.4.3	RNA Quality Assurance with Agilent Bioanalyser 2100.....	64
2.4.4	cDNA Synthesis.....	64
2.4.5	End-Point PCR.....	65
2.4.6	Agarose Gel Electrophoresis.....	66

2.4.7	Primer Design and Optimisation.....	66
2.4.8	Relative Quantification real-time PCR (q-PCR) .....	67
2.5	RNA-Seq and Microarray Analyses.....	73
2.5.1	Bioinformatic Methodology.....	73
2.5.1.1	Exiqon RNA-Seq Analysis.....	73
2.5.1.2	IPA RNA-Seq Analyses.....	73
2.5.1.3	R/Bioconductor RNA-Seq Analyses.....	74
2.5.2	Statistical Analysis.....	75
<b>3.</b>	<b>Transforming Growth Factor-<math>\beta</math>2 Modulates Gene Expression in the Human Trabecular Meshwork.....</b>	<b>76</b>
3.1	Introduction.....	77
3.2	Aim.....	80
3.3	Materials and Methods.....	81
3.3.1	Sample Collection, Preparation and Tissue Culture Establishment.....	81
3.3.2	Characterisation of Human Trabecular Meshwork Cells.....	83
3.3.3	TGF- $\beta$ 2 Stimulations.....	83
3.3.4	Total RNA Extraction and QC.....	83
3.3.5	RNA-Seq of Cultured Normal Human Trabecular Meshwork Cells.....	84
3.3.5.1	Template Preparation, rRNA Depletion, and cDNA Library Construction, Purification and QC.....	84
3.3.6	RNA-Seq Data Analysis.....	84
3.3.7	mRNA-Seq Data Validation.....	85
3.4	Results.....	88
3.4.1	Characterisation of Human Trabecular Meshwork Cells.....	88
3.4.2	RNA-Seq Analysis of Human Trabecular Meshwork Cells in the Absence of Presence of TGF- $\beta$ 2.....	90
3.4.2.1	RNA-Seq Summary.....	90
3.4.2.2	Principal Component Analyses.....	93

3.4.2.3	Heat Map and Unsupervised Clustering.....	95
3.4.3	Functional Analysis of Gene Pathways Involved in TGF- $\beta$ 2 Stimulation of Human Trabecular Meshwork Cells.....	97
3.4.3.1	Differentially Expressed Genes in Human Trabecular Meshwork Cells in the Presence of Absence of TGF- $\beta$ 2 Obtained from RNA-Seq Analysis .....	97
3.4.3.2	Visual Identification of RNA Transcripts Obtained by RNA-Seq Analysis.....	100
3.4.3.3	TGF- $\beta$ 2 Activated Processes in Cultured Human Trabecular Meshwork Cells.....	102
3.4.4	q-PCR Assay Validation of Top Differentially Expressed Genes in Cultured Human TM in the Presence or Absence of TGF- $\beta$ 2.....	111
3.5	Discussion.....	121
3.5.1	Genome-Wide Transcriptome Profiling in TGF- $\beta$ 2 Treated Human TM Cells.....	121
3.6	Summary.....	137
<b>4.</b>	<b>A Comparison of Global Gene Expression Profiles in Human Trabecular Meshwork Cells Treated with Dexamethasone using RNA-Sequencing.....</b>	<b>139</b>
4.1	Introduction.....	140
4.2	Aim.....	143
4.3	Materials and Methods	
4.3.1	Sample Collection, Preparation and Tissue Culture Establishment.....	144
4.3.2	Dexamethasone Stimulations.....	144
4.3.3	Total RNA Extraction and QC.....	145
4.3.4	RNA-Seq of Cultured Normal Human Trabecular Meshwork Cells.....	145
4.3.5	RNA-Seq Data Analysis.....	145
4.3.6	RNA-Seq Data Validation.....	145
4.4	Results.....	147

4.4.1	RNA-Seq Analysis of Human Trabecular Meshwork Cells in the Absence or Presence of Dexamethasone.....	147
4.4.1.1	RNA-Seq Summary.....	147
4.4.1.2	Principal Component Analysis.....	150
4.4.1.3	Heat Map and Unsupervised Clustering.....	152
4.4.2	Functional Analysis of Gene Pathways Involved in Dexamethasone Stimulation of Human Trabecular Meshwork Cells.....	154
4.4.2.1	Differentially Expressed Genes in Human Trabecular Meshwork Cells in the Presence or Absence of Dexamethasone Obtained from RNA-Seq Analysis.....	154
4.4.2.2	Visual Identification of RNA Transcripts Obtained by RNA-Seq Analysis.....	159
4.4.2.3	Dexamethasone Activated Processes in Cultured Human Trabecular Meshwork Cells.....	159
4.4.3	q-PCR Assay Assessment of Glucocorticoid Receptor Isoforms Expressed in Cultured Human TM Cells +/- Dexamethasone.....	166
4.4.3.1	q-PCR Assay Validation of Top Differentially Expressed Genes in Cultured Human TM in the Presence or Absence of Dexamethasone.....	168
4.5	Discussion.....	173
4.6	Summary.....	187
<b>5.</b>	<b>Identification of TGF-<math>\beta</math>2 Inducible miRNAs in Human Trabecular Meshwork Cells.....</b>	<b>188</b>
5.1	Introduction.....	189
5.1.1	miRNAs in Glaucoma.....	189
5.2	Aim.....	193
5.3	Materials and Methods.....	194

5.3.1	Tissue Culture and TGF- $\beta$ 2 Stimulations.....	194
5.3.2	miRNA Isolation and QC.....	196
5.3.3	Microarray Analysis of Human TM Cells.....	196
5.3.4	MicroRNA Array Data Validation.....	197
5.3.5	Human Trabecular Meshwork Transfection Optimisation.....	198
5.3.5.1	q-PCR Assessment of miRNA Mimics and Inhibitors of miR-145-5p on Target Genes and EMT-related Genes.....	199
5.3.6	RNA-Seq Analysis of Genome-wide Transcriptional Effects of miRNA Inhibitors of miR-145-5p and miR-143-3p to Identify Target Genes.....	202
5.3.7	RNA-Seq of TGF- $\beta$ 2 Positive Cells Co-Transfected with miRNA Inhibitors (miR-143i and miR- 145i).....	202
5.3.7.1	cDNA Library Construction, Purification and QC.....	203
5.3.7.2	RNA-Seq Data Analysis of TGF- $\beta$ 2 Positive Cells Co- Transfected with miRNA Inhibitors (miR-143i and miR-145i).....	203
5.3.8	RNA-Seq Validation.....	204
5.3.8.1	ACTA2 Differential Gene Expression Validation by q- PCR.....	204
5.3.8.2	ACTA2 Differential Protein Expression Validation by Western Blot Analysis.....	204
5.4	Results.....	206
5.4.1	miRNA Array Data Analyses.....	206
5.4.1.1	Calls and Threshold Filtering.....	206
5.4.1.2	miRNA Expression Analysis of TGF- $\beta$ 2 Treated TM Cells.....	207
5.4.1.2.1	volcano Plot Analysis of Untreated and TGF- $\beta$ 2 Treated Human TM Cells.....	209

5.4.2	q-PCR Assay Validation of Top Differentially Expressed miRNA in Cultured Human TM +/- TGF- $\beta$ 2.....	211
5.4.3	Human Trabecular Meshwork Transfection Optimisation.....	214
5.4.3.1	Human TM Cell Viability with Varying Volumes of HiPerfect Reagent.....	214
5.4.3.2	Effects if miRNA Inhibitors (miR-143i and miR-145i) on Target Gene and EMT-related Gene Expression.....	216
5.4.4	RNA-Seq Analysis of hsa-miR-145-5p and hsa-miR-143-3p Inhibitor Target Expression Profiles.....	225
5.4.4.1	mRNA-Seq Summary.....	225
5.4.4.2	Principal Component Analysis.....	227
5.4.5	Functional Analysis of Genes Associated with miR-143 and miR-145 Inhibition Following TGF- $\beta$ 2 Treatment.....	229
5.4.5.1	Differentially Expressed Genes in Human Trabecular Meshwork Cells Post miR-143/miR-145 Inhibition Following TGF- $\beta$ 2 Treatment.....	229
5.4.5.2	Comparison Analysis of 143i and 145i in Human TM Cells +/- TGF- $\beta$ 2.....	245
5.4.5.3	Validation of hsa-miR-145-5p and hsa-miR-143-3p Inhibitor Effects of ACTA2 at mRNA Level.....	249
5.4.5.4	Validation of hsa-miR-145-5p and hsa-miR-143-3p Inhibitor Effects of ACTA2 at Protein Level.....	251
5.5	Discussion.....	253
5.6	Summary.....	262
<b>6.</b>	<b>Emerging and Novel Glaucoma Therapeutics.....</b>	<b>264</b>
<b>7.</b>	<b>Summary and Future Work.....</b>	<b>280</b>

**Chapter 1**  
**Introduction**

# 1. Introduction

## 1.1 Glaucoma

In 2002 the World Health Organisation (WHO) estimated that 161 million individuals worldwide had visual impairment and 37 million were blind<sup>1</sup>. Glaucoma accounted for 12.3% of global blindness<sup>2</sup>. Glaucoma is second only to cataracts as a leading cause of blindness worldwide; glaucoma is the leading cause of irreversible visual loss<sup>1</sup>. Visual impairment due to glaucoma is a huge socio-economic burden, and affects adults more than children and females more than males<sup>1</sup>.

Glaucoma is a heterogeneous group of disorders primarily divided into open angle and close angle glaucoma<sup>3</sup>. By the year 2020 it is estimated that there will be 79.6 million individuals in the world with either primary open angle glaucoma (POAG) or primary angle-closure glaucoma (PACG); the majority of which will have POAG<sup>2</sup>. It is inevitable with increasing population sizes that the health and social burden of vision loss will also increase. Visual loss and related health conditions, including glaucoma in the ageing population impacts families, caregivers and society as a whole. Mobility and daily activities are among lifestyle factors that are affected that can often lead to injury, long-term care, and depression. It is therefore paramount that progress be made with regards to innovative solutions for prevention and treatment of this disease<sup>4,5</sup>.

### Clinical Diagnosis of Glaucoma

An international consensus panel published definitions of POAG and PACG in 2002<sup>6</sup>. Glaucoma is a progressive optic neuropathy, characterised by specific structural changes to the optic nerve head and associated visual field changes. Often referred to as “The Silent Thief” of sight, glaucoma patients (POAG) do not exhibit any symptoms or discomfort until very late in the progression of the disease. A familial history of the disease increases risk of glaucoma and mandates careful eye examinations. Myopia patients are at higher risk for POAG<sup>7</sup> and hypermetropia patients are at higher risk for PACG<sup>8</sup>.

The diagnosis of glaucoma in its earliest stages requires the accurate measurement of functional disturbances of the eye and is a challenge for clinical

ophthalmology. POAG is a progressive disease distinguished only from other optic neuropathies by its slow progression over months or years<sup>9</sup>, and characteristic appearance of the optic nerve head<sup>10</sup>. The progressive optic neuropathy in glaucoma results from apoptosis of the retinal ganglion cells (RGC) whose axons make up the optic nerve head (ONH)<sup>11</sup>. Pathogenesis of RGC apoptosis is poorly understood however it is thought to be a cascade initiated by mechanical factors, such as elevated intraocular pressure (IOP), or vascular factors, or a combination of both<sup>12</sup>. Diagnosis of glaucoma is made when both the structural and functional changes, that are the consequence of apoptosis, can be identified by clinical examination, visual field analysis and imaging.

The ONH has a central depression where retinal vessels enter the eye, this is known as the 'cup'<sup>13</sup>. Peripheral nerve fibres are lost in glaucoma resulting in compensation of function by remaining fibres, and a larger 'cup' (Figure 1.1)<sup>14</sup>.

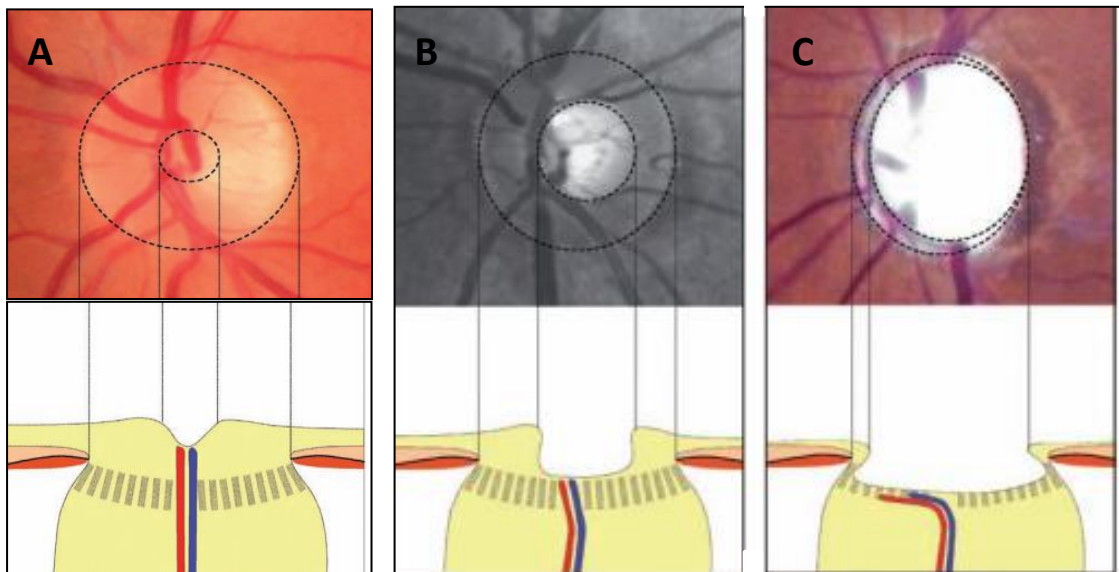


**Figure 1.1: Optic Disc and Schematic Cross-section of the ONH to Show Central Cup.** Modified from Williams *et al.* 2001<sup>14</sup>. (A) Normal optic disc, (B) Moderate optic disc cupping, and (C) Cavernous optic atrophy- fully cupped disc.

Funduscopy images allow for the visualisation of optic disc cupping as an area of central pallor. Although during early stages of glaucoma, disc-cupping may occur faster than area of pallor<sup>15</sup>. Therefore, interpreting optic nerve head cupping can be

challenging and must involve identification of the area of pallor and the identification of kinking of vessels found within the periphery of optic disc cupping. Some degree of cupping is normal, and individuals may have physiologically large cups, so quantitative measures are required. The degree of cupping is measured as a ratio of the cup size to disc size and must be greater than 0.5mm, vertical cup/disc ratio must be greater than horizontal cup/disc ratio, and asymmetry between cup/disc ratios of the two eyes should be more than 0.2mm<sup>14</sup>. The degree of cupping is evaluated by objective assessment using slit-lamp biomicroscopy, stereophotography and optical coherence tomography (OCT) imaging.

The diagnosis of glaucoma cannot be made purely on structural changes but by a combination of structural and functional defects. The RGC axonal loss which produces optic disc-cupping, begins in the periphery of the nerve<sup>16</sup>. The origin of these axons are in the RGCs of the mid-peripheral retina and so, glaucoma results in characteristic visual field loss in these regions. This early visual field loss is often unnoticed by patients. Visual field testing identifies these defects using targets of differing intensity at different points within the patient's visual field. Visual field threshold at these different points are analysed to identify the size of the 'blind spot' which corresponds to the ONH<sup>17</sup> and any disease associated visual loss. In glaucoma there is an initial enlargement of the 'blind spot' followed by mid-peripheral curved scotomas<sup>18</sup>. End stage glaucoma patients present with tunnel vision when all but central area of fixation is involved<sup>19</sup>. Visual field loss is significant if it occurs in the context of cupping and if the degree of visual field loss corresponds with the degree of cupping<sup>20</sup>. Primary open angle glaucoma is bilateral, but asymmetric<sup>21</sup>. If left untreated, or, inadequately treated, POAG leads to irreversible blindness or severe visual impairment respectively.

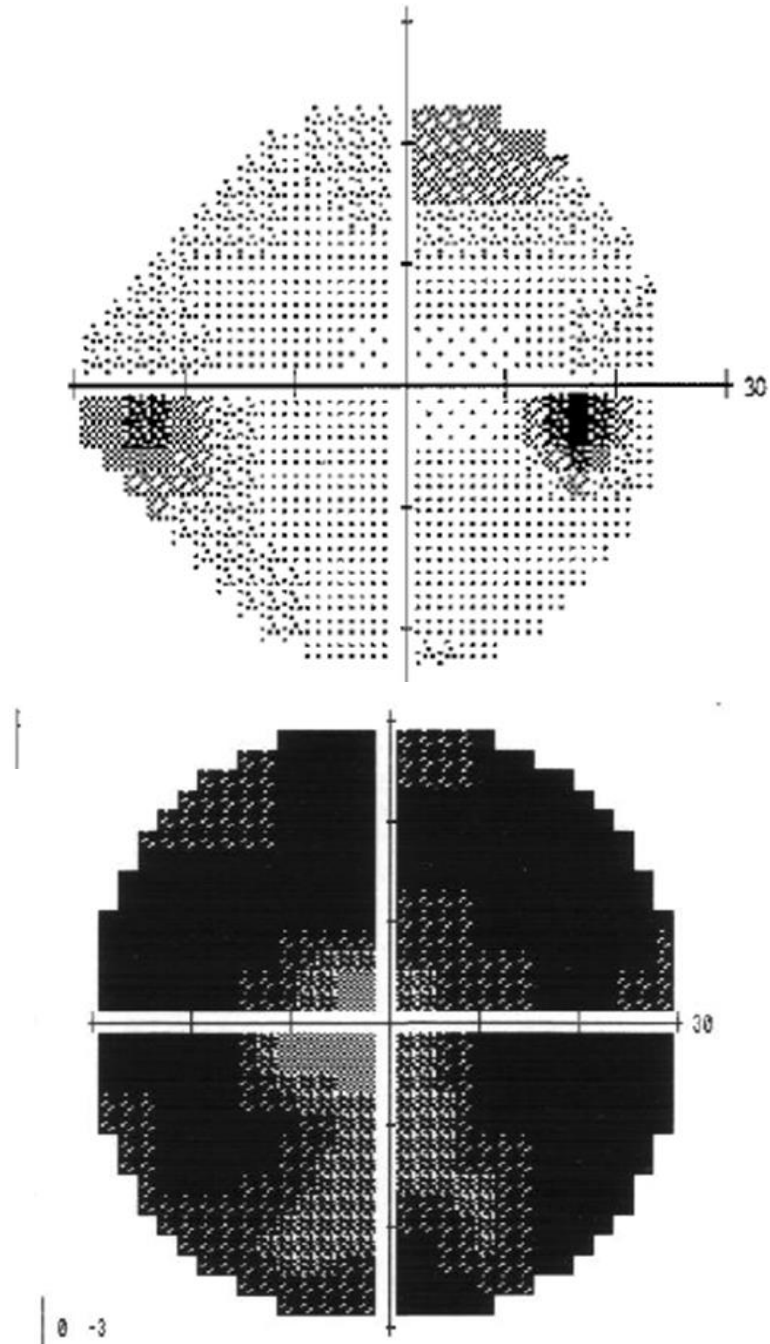


**Figure 1.2: Characteristic Visual Field Defects in Glaucoma.** (Top) A normal visual field. Black spot on the right side is the normal 'blind spot'. (Bottom) Progressive glaucoma visual field, tunnel vision.

Glaucoma can be broadly classified into open-angle glaucomas (POAG) and closed-angle (PACG) after an evaluation of the anterior chamber drainage angle. The drainage angle in the anterior segment cannot be directly visualised because of the principle known as the critical angle; the critical angle is related to the properties of light passing through media with different indices of refraction<sup>22</sup>. Light from the anterior chamber angle exceeds this critical angle and is therefore reflected back into the anterior chamber, thus preventing direct visualisation of the drainage angle. This can be overcome using gonioscopy to eliminate the cornea-air interface and involves the use of a mirrored contact lens to eliminate the optical effect of the front of the corneal surface. Gonioscopy identifies the angle structures: from posterior to anterior these include the ciliary body, scleral spur, trabecular meshwork, and Schwalbe line<sup>23</sup>. Grading of angle width is essential to assess glaucoma patients and glaucoma suspects<sup>24</sup>. Gonioscopy aims to identify the functional status of the angle, degree of closure, and risk of future closure. Angles are graded based on the shape and contour of the iris, the deepest structure visible, the amount of trabecular pigmentation and the presence of peripheral anterior synechia<sup>25</sup>.

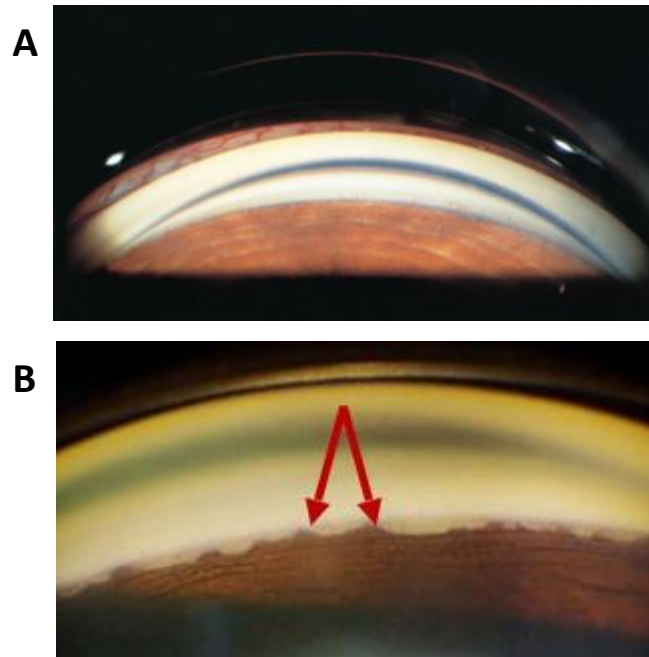


**Figure 1.3: Gonioscopic Drainage Angle Images.** (A) Gonioscopic image of an open angle as seen in POAG (American Academy of Ophthalmology, online resource<sup>26</sup>). (B) Gonioscopic image of peripheral anterior synechiae as seen in PACG. Red arrows identify iris-cornea adherence points (Glaucoma Associates of Texas, online resource<sup>27</sup>).

In the general population the mean intraocular pressure (IOP) is 16mmHg and two standard deviations either side of the mean gives a “normal” IOP range of 11 to 21mmHg<sup>28</sup>. In the ageing population the mean IOP is higher, with women typically showing propensity for elevated IOP over men. The “normal” IOP range in elderly women is increased to 24mmHg<sup>29</sup>. Elevated IOP is an important functional risk factor in glaucoma because risk of optic disc damage and RGC loss increases as IOP rises. Patients may have glaucoma in the absence of elevated IOP (normal tension glaucoma) and may have raised IOP (ocular hypertension: OHT) without glaucoma. However, IOP is currently the only modifiable risk factor of glaucoma and therefore assessment and management of IOP is still of great clinical importance.

IOP is determined by the dynamics of aqueous humour and outflow as will be discussed in section 1.2. The Goldmann tonometer is the gold standard for IOP measurement<sup>30</sup> and is based on the principle that IOP equals the force divided by the area of application of that force, with one major assumption that the eye is perfectly spherical. Importantly, diurnal fluctuations in IOP of up to 5mmHg occurs in approximately 30% of normal individuals and this fluctuation is increased to 90% in POAG patients<sup>31</sup>. To detect fluctuations IOP should be measured at different intervals throughout the day. It is also important to note that asymmetry in IOP measurements from two eyes is also possible and can be a feature of glaucoma<sup>32</sup>. At present decreasing IOP is the only currently available therapeutic intervention to treat glaucoma and this is accomplished with pharmacological and surgical intervention.

### Primary and Secondary Glaucoma

Glaucoma is an umbrella term<sup>33</sup> used to describe a group of neuropathies and is not a single disease entity. Glaucoma is subdivided into open-angle and closed-angle and also whether or not the disease is caused by primary or secondary factors. The term primary glaucoma (POAG and PACG), is used when there is no underlying disease whereas secondary glaucoma arises as a result of an initiating disease or intervention: such as trauma, inflammation, tumours, surgery or medical therapies such as corticosteroids<sup>34</sup>. Secondary glaucoma often results from

decreased aqueous humour outflow<sup>35</sup> due to inflammatory debris<sup>36</sup>, red blood cells from intraocular haemorrhage<sup>37</sup> and growth of new blood vessels in the drainage angle<sup>38</sup>. Neo-vascularisation in the drainage angle is most common in patients with diabetes and individuals with occlusions of major retinal blood vessels<sup>38</sup>.

## 1.2 Primary Open Angle Glaucoma

Primary open angle glaucoma (POAG) is an insidious sight threatening optic neuropathy which affects a growing proportion of the ageing population worldwide. According to WHO, approximately 70% of POAG cases are found in the developing world. The prevalence of POAG is high in Africa and in established market economies where the proportion of the population over 40 years old is above average<sup>39</sup>. The incidence of POAG increases with age and there is a female preponderance<sup>40</sup>. In the United Kingdom, POAG is the second most common cause of blind registration after macular degeneration and is estimated to cost over 300 million per annum<sup>41</sup>.

Numerous epidemiological studies, conducted across continents, have investigated the prevalence of POAG. Case definition has been problematic in epidemiological studies and standardised definitions of POAG have been established<sup>42</sup>. More than 50 populations studies have been conducted worldwide<sup>43-51</sup> and these studies have highlighted that prevalence of POAG varies worldwide and that differential risk factors may be involved.

### 1.2.1 Risk Factors for Primary Open Angle Glaucoma

POAG is a heterogeneous and multifaceted disease and an extensive list of risk factors possibly or probably associated with the development of the disease have been identified from a variety of studies including observational and experimental work<sup>52</sup>. For the purpose of this thesis these risk factors have been separated to include demographic, ocular, systemic, environmental, and genetic risk factors. The overall risk of developing POAG increases with both number and severity of risk factors<sup>53</sup>.

#### 1.2.1.1 Demographic Risk Factors

##### Age

The main demographic factor associated with increased POAG risk is age. Increasing age has been associated consistently with increasing risk across numerous studies, not only observational studies but in large multi-centre

randomised controlled trials including the Ocular Hypertension Treatment Study<sup>54</sup> and the European Glaucoma Prevention Study<sup>55</sup>. The magnitude of risk also consistently multiplies with increasing age, increasing several fold from 40-50 years of age to over 80 years of age<sup>56-58</sup>. No other demographic factor, other than ancestry, has been consistently associated with increased risk.

## Gender

The relationship between gender and primary open angle glaucoma has been debated for many years with inconsistent findings across many studies<sup>45,48,59,60</sup>. Prevalence studies have identified increased frequency in men, increased frequency in women, and others have demonstrated little difference between the two genders. For example, the Baltimore Eye Survey<sup>59</sup> and the Beaver Dam Eye Study<sup>48</sup> showed no significant difference between gender and POAG prevalence. However, the Rotterdam Study<sup>45</sup> and the Framingham Eye Study<sup>61</sup> both showed an increase in prevalence among the male cohort, whereas the Blue Mountains Eye Study<sup>46</sup> showed an increase among the female cohort.

The reason for these inconsistencies are not clear, they may relate to case definition with the used of different study criterion across different populations. A Bayesian meta-analysis, identified variation in POAG prevalence with age, gender, race, year of publication, and survey methods<sup>57</sup>. Biologically, there is evidence to suggest that female sex hormones may be protective against raised IOP<sup>62</sup>. Oestrogen receptors have been found in the ciliary body and outflow tract<sup>63</sup> and it is therefore possible that it could influence glaucoma via the AH formation and outflow facility. Evidence from population based studies suggests that females who undergo early menopause are at an increased risk of developing POAG as oestrogen protective qualities decrease<sup>40,64</sup>.

## Race and Ethnicity

Ethnicity is a category of people who identify with each other based on similarities such as common ancestry, language, culture or society. Race is associated with biology in which populations are distinguished from one another based on physical traits<sup>65</sup>. Several studies have been performed that examine race and ethnicity and their potential involvement in POAG development and progression. Using a meta-analysis of published epidemiological studies, race and ethnicity influenced POAG prevalence<sup>57</sup>. The highest prevalence was among the African-Caribbean populations at all ages compared to Caucasian and Asian populations<sup>57</sup>. POAG prevalence was estimated as 16% in those over 70 years of age in the African-Caribbean population compared to 6% and 3% in the Caucasian and Asian populations respectively<sup>57</sup>. Individuals of African descent who develop POAG tend to exhibit a more aggressive form of the disease and blindness is more likely to follow in these cases<sup>66</sup>. Inter-population differences in ONH structure, central corneal thickness (CCT), and IOP levels have been cited as potential explanations for differential incidences<sup>67</sup>.

Classification of population diversity remains a challenging, complex and sensitive issue; statistics of POAG prevalence should be interpreted with caution. It is worth noting that individuals of African descent belong to one of the most genetically diversified populations in the world. Therefore, if the prevalence of POAG in populations deemed to be “of the same race” there can be significant variations in POAG prevalence between populations<sup>68</sup>. For example, POAG prevalence amongst individuals of African descent is significantly lower ( $p < 0.001$ ) in South Africa, Nigeria, Tanzania, and Baltimore compared to Ghana, St. Lucia or Barbados. Amongst Caucasian populations prevalence is significantly higher in white Australians than in the Dutch ( $p < 0.001$ )<sup>69</sup>.

### 1.2.1.2 Systemic Risk Factors

#### Hypertension and Primary Open Angle Glaucoma

There are a number of systemic diseases associated with the development and progression of POAG<sup>52</sup>. Hypertension is proposed to increase the risk of developing POAG. Hypertension, or elevated blood pressure, is defined by either; blood pressure measurements at a screening exam, or, the reported taking of medication for hypertension, or both<sup>70</sup>. Several mechanisms have been suggested to explain the association between hypertension and POAG development. Firstly, hypertension may lead to microvascular impairment in the retina and optic nerve head region, which may, in turn, result in reduced blood flow to the anterior ONH<sup>71</sup>. Secondly, hypertension may impair auto-regulation of posterior ciliary circulation which is the main source of blood supply for the ONH<sup>72</sup>. Thirdly, previous studies have suggested that anti-hypertensives may induce excessive nocturnal dipping in blood pressure which may inadvertently lead to lower ocular perfusion to the ONH<sup>73</sup>. Finally, hypertension can also lead to retinal vasculature narrowing, which may also affect the blood supply to the ONH<sup>74</sup>. Despite these findings, previous epidemiological studies have so far led to inconclusive findings across large varying populations over longitudinal studies<sup>59,75</sup>.

The Blue Mountains Eye Study reported that individuals with systemic hypertension were 1.5 times as likely to have POAG<sup>75</sup>. In contrast, the Baltimore Eye Study reported that hypertension did not increase the risk of POAG in a population<sup>59</sup>. Instead, it was observed that younger hypertensives were less likely to develop POAG in comparison to an ageing cohort, suggesting that age was a surrogate for duration of hypertension, and some aspects of hypertensive effects on vessels or their function over years of exposure could lead to a predisposed risk for developing POAG<sup>75,76</sup>. Inconsistencies like these suggest that the effects of these factors are potentially modified by the presence of other confounding risk factors (e.g. age in this instance).

## Diabetes and Primary Open Angle Glaucoma

The potential association between diabetes mellitus (DM) and POAG has been studied by many groups, with most studies reporting a weak association between the two diseases<sup>77-79</sup>. An early meta-analysis indicated that DM is associated with an increased risk for developing POAG<sup>80</sup>. However, the meta-analysis did not include any cohort studies, but instead was performed on seven cross-sectional and five case-controlled studies of DM and the risk of POAG. This meant that a temporal relationship between exposure and outcome could not be established. Since this, numerous epidemiological studies, including cohort studies, of an association between DM and POAG have been reported<sup>77-79</sup>, however, the relationship has been deemed somewhat contradictory and inconclusive.

### 1.2.1.3 Ocular Risk Factors

#### Intraocular Pressure

The relationship between glaucoma and intraocular pressure dates back as far as 986 AD when Arabic ophthalmologist Abdul Tabari first describes “migraine in the eye” which involved a pressure sensation<sup>81</sup>. Since then, IOP has become an established risk factor for POAG with the risk of POAG increasing with increasing levels of IOP<sup>82</sup>. The relationship between elevated IOP and POAG risk however is best examined from population-based data on incidence over prevalence.

Several different population-based studies have investigated the distribution of IOP in both normal and glaucomatous eyes and findings have suggested that mean IOP can vary between populations. For example, the mean IOP in white Caucasian adult populations has consistently been estimated to being between approximately 15-16mmHg, with standard deviations reaching as high as 3.2mmHg<sup>45,46</sup>. However, higher mean IOP between 16.5 and 18.7 mmHg were reported in populations of Afro-Caribbean origin<sup>49,59</sup>. Persons having elevated IOP and no optic nerve damage are termed “ocular hypertensives” with population frequencies varying widely from study to study. The prevalence of “ocular hypertension” is typically between 5-10% in persons of European descent and lower in Japanese or Mexican-American populations<sup>54</sup>.

Population cross-sectional studies conducted across all continents have provided strong evidence to suggest IOP is intimately related to glaucoma. Studies from the USA<sup>60</sup>, Australia<sup>46</sup>, to India<sup>50</sup> have yielded findings that show an increased IOP is associated with an increased prevalence of glaucoma. Furthermore, in individuals with bilateral POAG, the eye with higher IOP tends to lose visual field more rapidly than if both IOPs were in the “normal” range. Randomised clinical trials have shown that lowering of IOP by means of medication, surgery, or laser all slow the onset/progression of optic neuropathy and visual field defects<sup>83,84</sup>. In the Early Manifest Glaucoma trial<sup>84</sup>, patients with early POAG were randomised into observational or treatment cohort; treatment consisted of reduction of IOP by selective laser trabeculoplasty or medication ( $\beta$ -blocker: betaxolol). Reduction in IOP clearly reduced the progression of glaucoma by 17% in the treatment group. Overall, it is believed that elevated IOP induces a series of events which will eventually lead RGC death by apoptosis and irreparable visual loss.

## 1.3 Aqueous Humour Dynamics

### 1.3.1 Aqueous Humour Formation

Aqueous humour (AH) formation is related to circadian rhythms<sup>85</sup>. The main structures associated with AH are the ciliary body, the trabecular meshwork, and the uveoscleral pathway. The ciliary body is the site of AH production<sup>86</sup> where AH is formed by the ciliary processes, which are finger-like projections consisting of a double layered epithelium associated with a core of stroma supplied by a rich plexus of fenestrated capillaries<sup>87</sup>. Each of the ciliary processes contain many capillaries that are sourced from the major arterial circle of the iris. The ciliary body has both an inner non-pigmented layer and outer pigmented layer; the epithelium of both layers face each other and are joined by tight junctions. These tight junctions are essential to maintain the blood-aqueous barrier. The inner non-pigmented epithelia contain a number of mitochondria and microvilli and is the main site of AH production<sup>88</sup>.

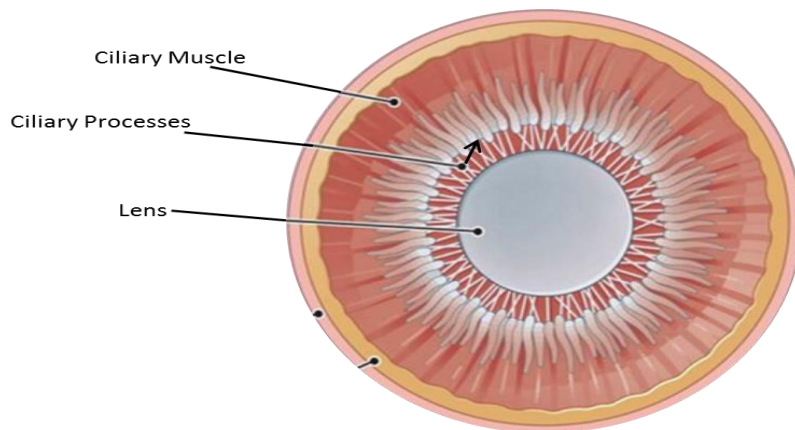


**Figure 1.4: Posterior View of the Iris and Ciliary Body Showing the Ciliary Processes.** Image modified from online resource<sup>860</sup>.

AH formation and secretion to the posterior chamber is a combination of three processes; active secretion, ultrafiltration, and diffusion<sup>89</sup>. AH is derived from plasma ultra-filtrate. Diffusion and ultrafiltration are responsible for the accrual of plasma ultrafiltrate in the stroma, behind the tight junctions of non-pigmented ciliary epithelium cells<sup>90</sup>. Diffusion involves the transport of lipid soluble solutes through lipid portions of the membrane, whereas ultrafiltration is the flow of water-soluble substances across the fenestrated capillaries of the ciliary body, in to the ciliary stroma. These occur in response to an osmotic gradient or hydrostatic pressure.

Active secretion is the major part of AH formation, responsible for up to 90% of total AH formation<sup>91</sup>. The main site of active transport is the non-pigmented epithelia of the ciliary processes (Figure 1.5). Active transport involves the selective transport of anions, cations, among other molecules across a concentration gradient in the blood-aqueous barrier. Protein transporters located in the epithelial cell membranes mediate this process. Aquaporins, facilitate the transport of fluids when there is insufficient osmotic pressure<sup>92</sup>; aquaporin 1, and 4 contribute to AH secretion<sup>93</sup>. Carbonic anhydrase II, and enzymes found in the non-pigmented and pigmented ciliary epithelia are also involved in the active transport of AH<sup>94</sup>. Carbonic anhydrase II initiates bicarbonate formation to influence fluid transport and the energy required for active transport is catalysed by  $\text{Na}^+\text{-K}^+\text{-ATPase}$ ; an

enzyme found within the pigmented and non-pigmented epithelial cells of the ciliary body<sup>95</sup>.  $\text{Na}^+\text{-K}^+\text{-ATPase}$  can be regulated by a number of molecules<sup>85,96</sup> and is a target for pharmacological agents (such as dorzolamide and brinzolamide) to alter AH dynamics and lower IOP to treat glaucoma<sup>52</sup>.

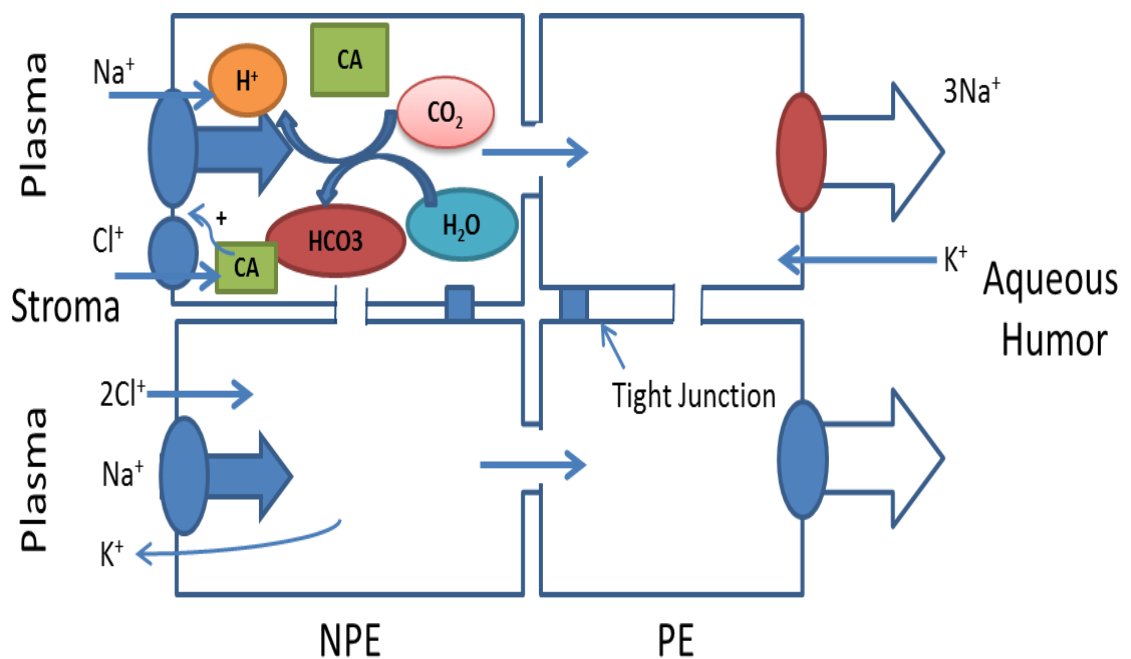


**Figure 1.5: Active Secretion of Aqueous Humour.** The NPE (non-pigmented epithelium) of the ciliary processes are responsible for the bulk of active secretion of AH. AH secretion is catalysed by carbonic anhydrase II and  $\text{Na}^+\text{-K}^+\text{-ATPase}$ . Image adapted from Marcel *et al* 2002<sup>97</sup>.

AH is secreted into the posterior chamber of the eye and is transported to the anterior chamber to provide nourishment for avascular structures including the lens, the posterior surface of the cornea and the trabecular meshwork. As well as nourishment of avascular structures, AH dynamics also help in the maintenance of intraocular pressure<sup>98</sup>.

Compared to blood plasma, the composition of AH has an excess of hydrogen and chloride ions and ascorbate but is deficient of bicarbonate. Protein levels are relatively low in AH (approximately 0.2mg/mL) to maintain visual clarity and include: albumin which accounts for nearly half of the total protein content, SERPIN family members, and prostaglandin D2 synthase (PTGDS)<sup>98,99</sup> as examples.

Additional components of the AH include growth factors: TGF- $\beta$ , transferrin<sup>100</sup>, endothelin-1<sup>101</sup> and indoleamine 2,3-dioxygenase<sup>102</sup>, enzymes: carbonic anhydrase<sup>87</sup>, lysozyme<sup>87</sup>, diamine oxidase<sup>103</sup>, plasminogen activator<sup>104</sup>, and prostaglandins; cAMPs<sup>105</sup>, steroid hormones<sup>106</sup> and hyaluronic acid<sup>107</sup>.

AH turnover rate differs throughout the day and the mechanism of this biological rhythm is still unknown. However, it is hypothesised that circulating epinephrine may have an influence on circadian rhythm<sup>108</sup>. The rate of AH turnover is estimated to be between 1-1.5% of the anterior chamber volume per minute, which is  $2.4 \pm 0.6\mu\text{L}/\text{min}$  in adults on average<sup>109</sup>.

## 1.4 The Trabecular Meshwork

### 1.4.1 Trabecular Meshwork and Aqueous Humour Outflow

The trabecular meshwork (TM) and Schlemm's canal (SC) comprise the drainage tissues of the anterior chamber of the human eye<sup>85</sup>. Aqueous humour exits the eye via two outflow pathways, the conventional pathway and non-conventional pathway. The physiology of these two outflow pathways differ in several important aspects.

Unlike the conventional outflow pathway, the non-conventional pathway, or, the uveoscleral pathway, is relatively independent of intraocular pressure (IOP)<sup>110</sup>. AH secreted by the ciliary processes enters the ciliary muscle and exits the eye via the supraciliary space and across the anterior and posterior sclera via canals around the vortex veins or into choroidal vessels<sup>111</sup>. In the ageing population, uveoscleral outflow decreases<sup>112</sup> leading to compensation by the conventional outflow pathway in order to maintain IOP.

The conventional outflow pathway consists of the TM and Schlemm's canal. The TM is a filter made up of extracellular matrix (ECM) derived beams ensconced by TM cells, (see 1.4.2 below). Fluid movement takes place down a pressure gradient from the TM to Schlemm's canal which has a passive-pressure dependent mechanism such as giant vacuoles and pores. The organisation of trabecular beams and presence of SC pores all influence AH outflow. Pore sizes range from 0.1-3 $\mu$ m in diameter and their presence can be influenced by changes in the IOP.

After exiting Schlemm's canal, AH enters aqueous veins and subsequently mixes with circulating blood in the episcleral veins. The pressure within the episcleral veins, combined with resistance of the conventional AH drainage pathway, results in an average IOP in humans of  $15.5 \pm 2.6$ mmHg for the general population<sup>85</sup>.

## 1.4.2 Anatomical Structure and Function

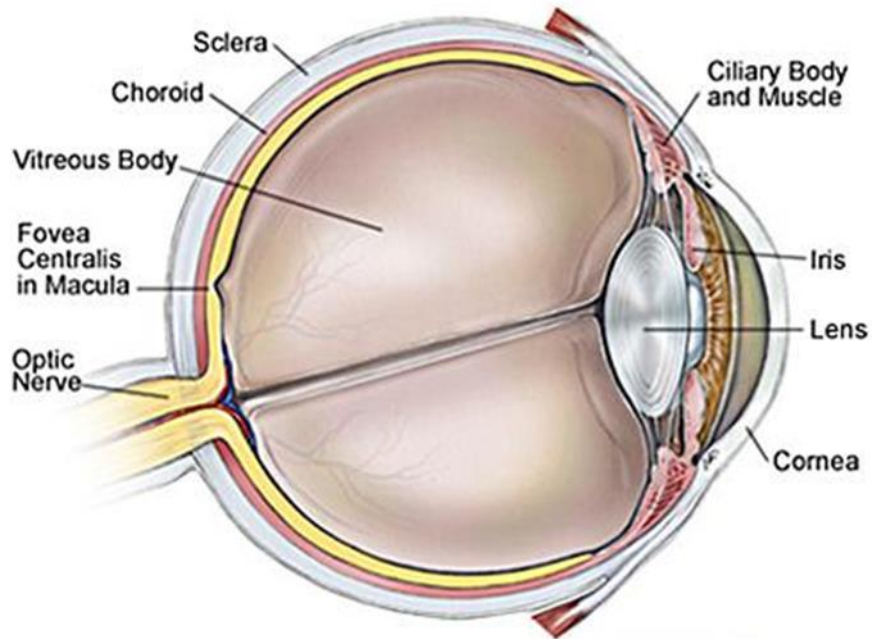


**Figure 1.6: Cross Section of the Human Eye.** AH is produced by the ciliary body, namely the non-pigmented ciliary epithelium. The ciliary body is indicated in the top right of the cross sectional image. Modified from online resource<sup>113</sup>.

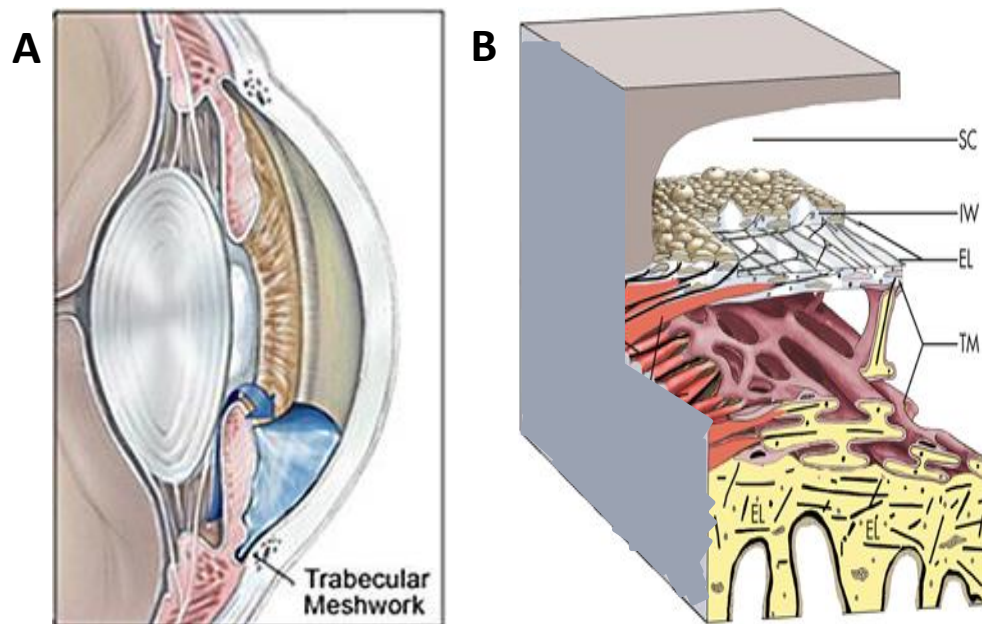


**Figure 1.7: Anatomical Structure of the Human Trabecular Meshwork.** (A) A build-up of AH produced by the ciliary body is transported across the TM following the route (arrow) indicated. (B) Structurally the TM is comprised of a number of layers surrounded by elastic fibres (EL) necessary for contractility. The AH first flows through the TM before reaching the inner wall (IW) of Schlemm's canal (SC) and exiting via the surrounding circulatory system. Modified from Overby *et al*<sup>114</sup>.

The TM is located within the iridocorneal angle, where the iris and cornea meet, and the sclera transitions in to the cornea. The TM is anatomically a miniscule triangular tissue of approximately 350 X 50-150µm in cross section<sup>115</sup>. Structurally the TM comprises of layers made up of connecting fenestrated beams and sheets of ECM overlaid by trabecular cells<sup>116</sup>. TM beams, or lamellae, contain a central core composed of collagens and elastic fibres embedded in hyaluronan and proteoglycans<sup>117</sup>. Elastic fibres contained within the lamellae core differ in both structure and composition to other fibres found throughout the body, and, have therefore, previously been termed “elastic-like” fibres<sup>118</sup>. TM cells located on these beams have a robust basement membrane, and long cellular projections quite often traverse adjacent beams<sup>119</sup>. Although relatively basic in structure, variation in the orientation of the lamellae has led to the description of distinct regions of the TM. The three distinct differentiated layers of the TM include; the uveal meshwork, the corneoscleral meshwork and the juxtacanalicular meshwork (JCT; also known as the cribriform meshwork)<sup>120</sup>. Previous studies, using electron microscopy, have revealed that the arrangement of the trabecular lamellae and intra-trabecular spaces noticeably change from the inner to the outer-most sections of the TM<sup>121</sup>.

The inner-most layer, the uveal meshwork, is fixed to connective tissue located in front of the ciliary body and to the iris root and is continuous posteriorly to the uvea. The uveal meshwork is the furthest from the JCT region and thus is the first layer to come in to contact with AH. The uveal portion is approximately three layers of interconnecting lamellae covered by flat confluent TM cells which form large irregular intra-trabecular fenestrations<sup>115</sup>. TM beam cells are aggressively phagocytic and are thought to act as a pre-filter to remove debris from the AH<sup>119,122</sup>. The elastic fibre net of the uveal meshwork is continuous posteriorly with some fibres embedded in the connective tissue between the ciliary muscle tips in front of the circular muscle portion<sup>123</sup>. The irregular arrangement of intra-trabecular spaces allows for the relatively unrestricted movement of AH to the deeper layers of the TM.

The corneoscleral meshwork is contiguous with the uveal meshwork and completes the lamellated portion of the TM. The corneoscleral meshwork is the

most extensive part of the TM consisting of approximately 8-15 lamellae layers<sup>124</sup>. The corneoscleral meshwork is characterised by the presence of lamellae, previously seen in the uveal portion, ensconced by TM cells attached to a basement membrane (BM). Unlike the uveal portion however the lamellae and intra-trabecular spaces are much more highly organised. Intra-trabecular spaces also narrow the closer they get to the JCT region resulting in an increased resistance to AH outflow not previously observed.

The third and smallest region of the TM, the JCT, is the deepest area anatomically located adjacent to the inner wall endothelium of SC extending from the last trabecular beam<sup>120</sup>. Typically 2-15µm thick, the JCT has many large, empty spaces and is considered to be more porous than most other connective tissues<sup>125</sup>. Unlike the uveal and corneoscleral meshwork, the JCT is not arranged into lamellae structures. Conversely the JCT is comprised of loosely arranged ECM to which TM cells are sparsely embedded<sup>125</sup>. The ECM in which the JCT cells are embedded is highly hydrated and provides a channel for AH to traverse the JCT to exit the eye via Schlemm's canal<sup>126</sup>. The ECM components include collagen types, I, III, IV, V, and VI but not type II, elastin, laminin-γ1, fibronectin and glycosaminoglycans<sup>126-128</sup>. It is generally agreed that the inner wall region formed by the JCT and endothelium of SC is the site of trabecular outflow resistance however exact location is still debated<sup>129</sup>. The SC inner endothelium has one of the highest conductivities in the body, comparable only with that of the fenestrated endothelia<sup>130</sup>.

### 1.4.3 The Trabecular Meshwork and Intraocular Pressure

Intraocular pressure is generated within the TM outflow pathways by providing resistance to aqueous humour outflow. IOP builds in response to reduced outflow facilities until it is high enough to drive AH across the TM into Schlemm's canal. In a healthy eye, IOP is a strict balance between aqueous formation by the ciliary body and outflow resistance<sup>131</sup>. In ageing, and various forms of POAG, the resistance to outflow increases leading to elevated IOP.

IOP homeostasis has been defined as *“corrective adjustments of the AH outflow resistance, which occur in direct response to sustained pressure*

*changes*<sup>122</sup>. This definition is primarily based on evidence from perfused human anterior segment organ culture or perfused *ex-vivo* eyes. In disease states, such as POAG, mechanisms through which IOP homeostasis is interrupted have not been fully elucidated. However, it has been hypothesised, that elevated IOP forces produce mechanical stretching on the JCT and SC inner wall in the TM resulting in distortion of the extracellular matrix (ECM) since much of the resistance is putatively provided by the ECM itself<sup>122,119</sup>. Distortion and changes to the ECM can be sensed by TM cells which could possibly lead to activation of specific signalling pathways triggering key gene expression changes, including, but not limited to, specific ECM turnover components<sup>129</sup>.

Increasing age is associated with several naturally occurring physiological changes to the eye and its associated blood supply- changes like these may promote the pathogenesis of POAG. The trabecular meshwork is the key route of aqueous humour outflow in the eye. AH outflow pathways show a natural decrease in outflow with age and it has been postulated that this is due to both the loss of TM cells and the accumulation of extracellular plaque-like deposits within the meshwork<sup>132</sup>. Furthermore, there is an increased amount of fibronectin<sup>133</sup>, progressive formation of collagen aggregates<sup>134</sup>, decreased levels of hyaluronic acid<sup>135</sup>, and accumulation of chondroitin sulphates<sup>134,135</sup>. In the endothelial cells of Schlemm's canal there is also a reduction of intracellular pores and giant vacuoles<sup>136</sup>. These age-related changes in the TM and SC can cause a decrease in AH outflow which may be attributed to observed age related elevated intraocular pressure noted in numerous population-based studies<sup>82,137-140</sup>.

The cell bodies of the retinal ganglion cells make up the inner most layer of the retina. They receive input from the photoreceptors via bipolar and amacrine cells. Unmyelinated axons of the RGCs exit the eye via the optic nerve head which is supported by the lamina cribrosa (LC). Glial cells provide structural support for retinal ganglion cells as well as functional support including metabolism, regulation of extracellular environment and the phagocytosis of neuronal debris<sup>141</sup>. Microglia function to protect neurons from destructive inflammatory cytokines<sup>142</sup>. Viability and regenerative capacity of the microglial cells of the central nervous system are

negatively affected by ageing<sup>143</sup>. Similar age dependent attrition may be seen in the glial cells of the retina and optic nerve and it is possible that these changes may adversely affect their neuro-supportive and neuro-protective functions. With ageing there is a decrease in the amount of RGCs<sup>144</sup> and optic nerve fibres as well as decreasing thickness of the retinal nerve fibre layer<sup>145</sup>.

The lamina cribrosa (LC) is a fibrous network encapsulated by astrocytes which supports the ONH. Astrocytes are the main cell types of the ONH and are essential for RGCs health<sup>146</sup>. The main function of astrocytes is ECM remodelling and removal of waste products<sup>147</sup>. Upon ageing, the LC has been observed to increase in thickness<sup>148</sup> and becomes increasingly collagenous<sup>149</sup>. These structural changes result in increased stiffness and decreased resilience making older populations more susceptible to axonal damage<sup>150</sup>. The retina and optic nerve of donor eyes have been demonstrated to show an increased accumulation of advanced glycation end (AGE) products<sup>151</sup>. Accrual of AGEs may contribute to biomechanical changes of the LC and may also promote intracellular changes in the RGCs and glial cells that encourage impaired function and apoptosis<sup>152</sup>.

#### 1.4.4 Extracellular Matrix in the Trabecular Meshwork

A wide range of ECM components have been identified within the TM which have different functional roles depending on their location in the TM<sup>153</sup>. Collagens, elastic fibre components, proteoglycans, glycosaminoglycans (GAGs), fibronectin and matricellular proteins have all been found at different levels throughout all layers of the TM<sup>154-156</sup>. Although majority of these are similar to components identified in other tissues, apparent unique isoforms have also been identified<sup>157</sup>. Matrix and contractile genes have been shown to be highly expressed in the JCT cells in comparison to inner wall cells of Schlemm's canal<sup>158</sup>.

Extracellular matrix turnover is a highly co-ordinated process consisting of ECM production, remodelling and degradation. Numerous stimuli that affect outflow facility change the activity of matrix metalloproteinases (MMPs), which are known to be responsible for the majority of ECM turnover. These MMP-inducing

stimuli include tumour necrosis factor alpha (TNF- $\alpha$ ), dexamethasone (DEX), elevated IOP and mechanical stress<sup>159</sup>. MMP activity triggers changes in ECM protein expression levels and the replacement ECM is slightly different in composition and/or amount each time in order to maintain outflow facilities<sup>116,122</sup>.

The extracellular matrix of the TM is a source of latent growth factors and small regulatory molecules; the activity of which needs to be tightly regulated<sup>159,160</sup>. Maintenance remodelling by MMPs may aid in removal of bound molecules to prevent saturation of the ECM. When the ECM becomes saturated, for example in response to elevated IOP, these regulatory molecules gain access to outflow channels and modify resistance accordingly. The ECM of the TM provides a microenvironment with distinctive properties necessary for normal biological function. In comparison to other adult tissues throughout the body, TM cells express high levels of MMP-2, tenascin C, and  $\alpha$ -smooth muscle actin, typically associated with tissues undergoing remodelling during development or disease<sup>116</sup>. Elevated expression of these molecules in the TM suggests that TM cells may have evolved transient remodelling processes as a normal function in order to maintain outflow facilities<sup>120</sup>.

## 1.5 Role of Known Glaucoma Stimuli Resulting in Raised IOP

Glaucoma is a complex disease with specific endophenotypes, and disease pathogenesis is likely to involve multiple pathways linking interactions between genetics and environmental interactions<sup>161,162</sup>. In addition, there are several known glaucoma stimuli that exert their effects by a combination of over-lapping and distinct pathophysiological processes. The most well characterised stimuli resulting in raised IOP and glaucoma are corticosteroids and transforming growth factor beta (TGF- $\beta$ )<sup>162-164</sup>.

### 1.5.1 Corticosteroids

Corticosteroids are subdivided into glucocorticoids and mineralocorticoids<sup>165</sup>. Glucocorticoids (GC) are synthesised by the adrenal cortex in humans and secreted into blood plasma where levels fluctuate according to circadian rhythm<sup>166</sup>. The naturally occurring glucocorticoid in humans is

hydrocortisone synthesised in the adrenal cortex from its precursor cortisone. Beneficial effects of glucocorticoids in inflammatory disorders have been described since the early 1950s, and since then a number of synthetic glucocorticoids have been developed<sup>167,168</sup>.

### 1.5.1.1 Glucocorticoid Mechanism of Action

Despite the identification of GCs some years ago, the exact mechanism of action is still not fully understood. GCs exert both genomic and non-genomic functions<sup>169</sup>. At the cellular level every individual GC functions through the same receptor mechanism<sup>170</sup>. GC receptors are present on all cell types except anuclear cells<sup>171</sup>. Activation of the GC receptor is brought about by binding of naturally occurring or synthetic GCs, known as ligands, and results in a change in the regulation of gene expression. The GC receptor gene is composed of nine exons and alternative splicing results in four isoforms, glucocorticoid receptor (GR)- $\alpha$ , GR- $\beta$ , GR- $\delta$ , and GR- $\gamma$ <sup>172</sup>.

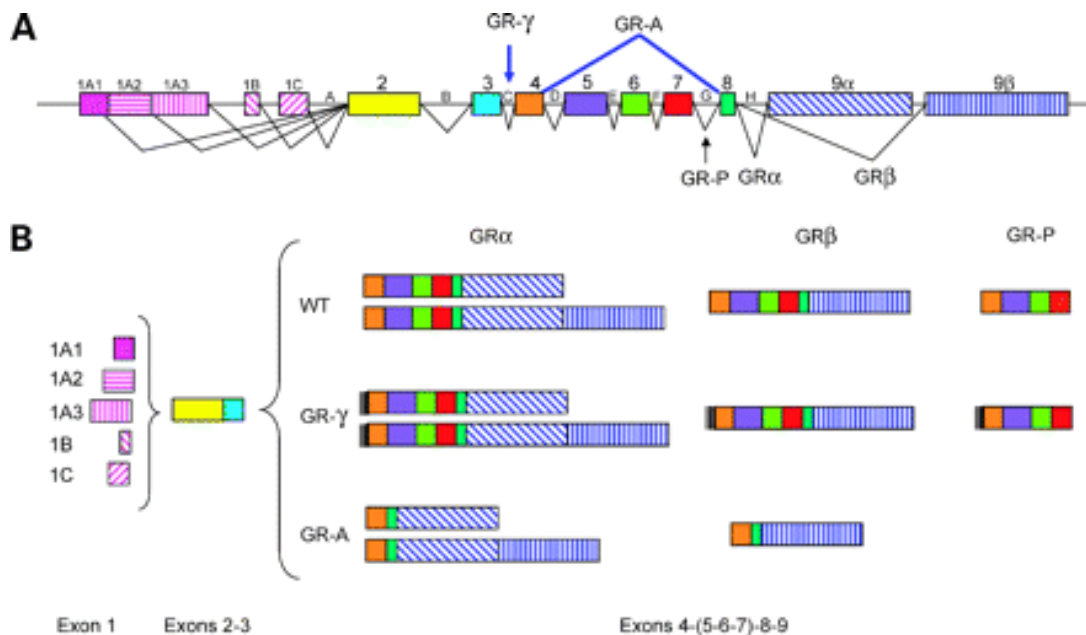


**Figure 1.8: Structure and Transcriptional Isoforms of the Human GR Gene.** Modified from Vega *et al* 2006<sup>173</sup>. (A) 9 different exons comprise the human GR gene. (B) Different isoforms are generated by alternative splicing; GR- $\alpha$  and GR- $\beta$  represent the major isoforms.

GR- $\alpha$  is the only fully active isoform, while GR- $\beta$ , GR- $\delta$ , and GR- $\gamma$  retain structural similarities for the active receptor (Figure 1.9)<sup>173</sup>. GR- $\beta$  is shorter than the active  $\alpha$  isoform by 35 amino acids and lacks a ligand binding domain, but retains its DNA binding domain; allowing it to competitively bind DNA and negatively regulate the actions of GR- $\alpha$ <sup>174</sup>. Furthermore, Gr- $\beta$  can bind to GR- $\alpha$  and form a non-active heterodimer, additionally inhibiting GR- $\alpha$  activity. Gr- $\beta$  also has a half-life two times longer than that of GR- $\alpha$ , and given its antagonist role, GR- $\beta$  can inhibit signalling of GR- $\alpha$  and cause secondary resistance to glucocorticoids<sup>175</sup>.

The wide range of actions of glucocorticoids has been attributed to the cellular distribution of their receptors; glucocorticoid receptors (GRs) are found in the cytoplasm, nucleus, and cell membranes (Figure 1.9). GRs can be cytoplasmic, or membrane bound on the cell surface, or present as homo/hetero-dimers in the nucleus<sup>176,177</sup>. Cytoplasmic GR are monomers until a GC ligand is bound wherein ligand-binding induces the formation of GR homodimer<sup>178</sup>, and translocation to the nucleus via microtubules<sup>179</sup>. GRs remain within the nucleus as dimers and exert positive or negative effects on gene expression. This is the proposed mechanism of action for genomic roles of GCs<sup>180</sup>. Membrane bound GRs initiate rapid changes in various signalling pathways when ligands bind and perform a non-genomic role<sup>177</sup>.

As a homodimer, GRs can bind to DNA-regulatory glucocorticoid response elements (GREs) in the nucleus. GREs are found within the promoter region of glucocorticoid regulated genes<sup>170</sup>. Positive GREs lead to gene expression activation, whereas negative GREs result in suppression of gene expression<sup>181</sup>. GR binding to DNA initiates the recruitment of co-activator CRB proteins (CREB binding proteins), and steroid receptor co-activator 1 (SRC-1)<sup>182</sup>. Co-activators use inner histone deacetylases to weaken DNA strands and facilitate RNA Polymerase II and TATA box-binding protein actions to begin transcription<sup>183</sup>.

In addition, GC-GR monomers within the cytoplasm can inhibit gene expression without the need to bind DNA, this is termed 'indirect trans-repression'<sup>184</sup>. GC-GR monomers interact with numerous proteins in the cytoplasm, including signalling pathway kinases and transcription factors<sup>185</sup>. GCs can inhibit transcription factors such as nuclear factor kappa B (NF $\kappa$ B)<sup>186</sup>. NF $\kappa$ B activates the

expression of genes involved in inflammation, and cellular processes such as proliferation. NFkB protein-protein interaction with GC-GR complex inhibits regulatory gene expression functions<sup>186</sup>.

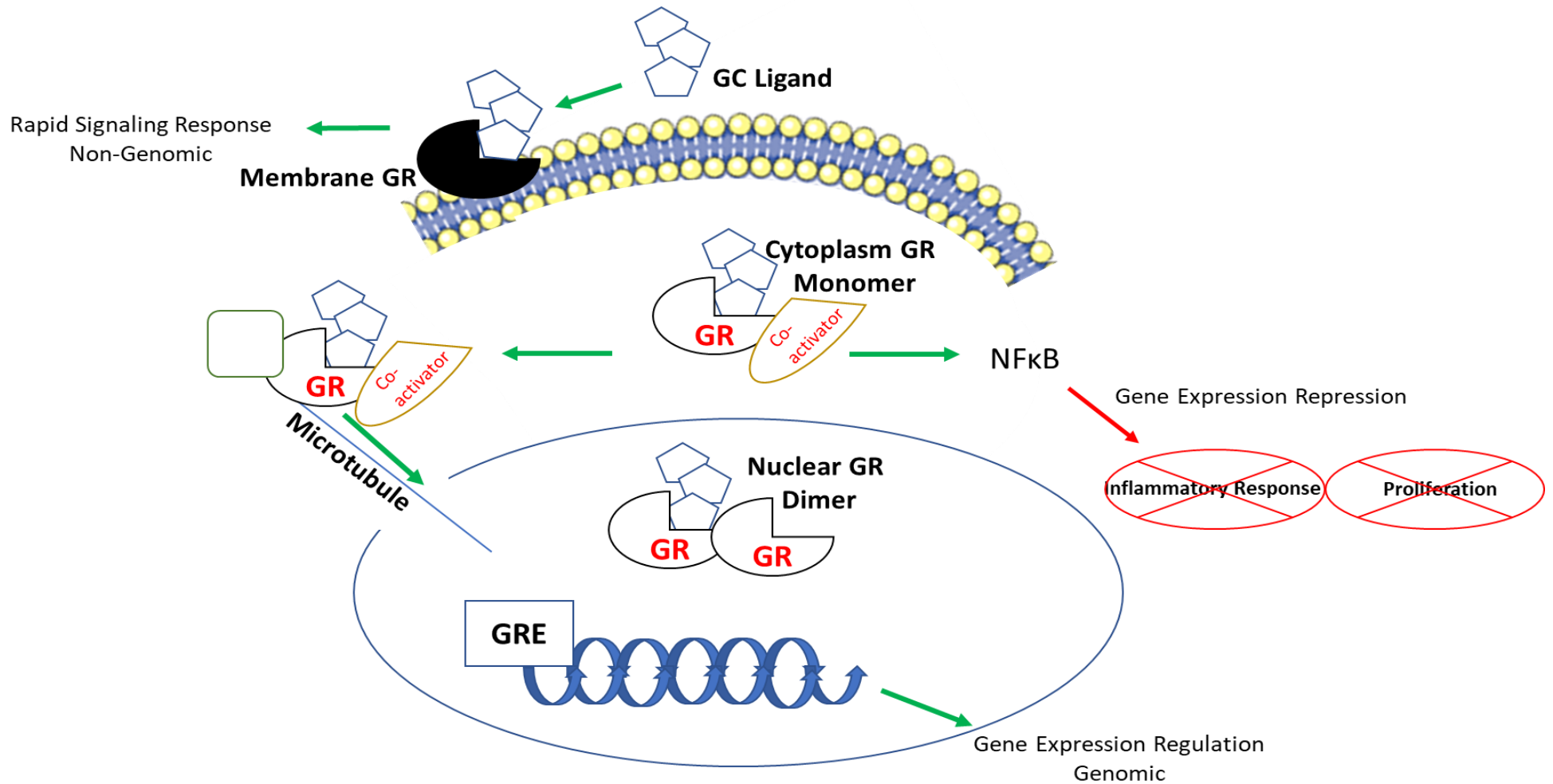


**Figure 1.9: Glucocorticoid Mechanisms of Action.** GCs exert their effects via membrane bound, cytoplasmic, and nuclear GC receptors. Effects may be non-genomic or genomic depending on the activation of specific receptors. GREs within the promoter region of steroid-regulated genes allow binding of GC-GR dimer complexes to initiate gene expression regulation. Cytoplasmic monomers inhibit gene expression via protein-protein interactions. Modified from online resource Tulane University<sup>861</sup>.

### 1.5.1.2 Corticosteroids Effect in the Eye

Synthetic glucocorticoids are of great interest in ophthalmology due to their ability to decrease inflammation and preserve ocular function<sup>187</sup>. The actions of corticosteroids on ocular tissues has been widely studied<sup>188</sup>. Cortisone was seen to inhibit the formation of fibrotic material, reduce cellular infiltration, fibroblastic repair and endothelial regeneration in corneal wounds<sup>189</sup>. In addition, high doses of cortisone were able to prevent wound healing entirely<sup>190</sup>. Apart from their effects in reducing wound scarring, the major use for corticosteroids is for their anti-inflammatory traits. Early studies identified that cortisone reduced permeability of ocular capillaries during inflammation, and withdrawal of treatment saw capillary recovery<sup>191</sup>.

Despite their benefits in wound healing and inflammation, corticosteroids mode of action, and in turn, complications, are largely dependent on dose and duration<sup>192</sup>. Relatively high doses of corticosteroids can result in adverse systemic side effects<sup>193</sup>. Several ocular diseases require steroids daily in order to maintain the condition. Interestingly, ocular side effects are seen irrespective of whether the steroid is taken for systemic or ocular disease<sup>194</sup>. Corticosteroid ocular side effects include cataract, enhanced infection and glaucoma<sup>192</sup>.

### 1.5.1.3 Corticosteroid-Induced Glaucoma

Elevated IOP is one of the major risk factors for developing glaucoma, and ocular hypertension (OHT) due to secondary factors, can convert to glaucoma. IOP elevation can occur as an adverse side effect of corticosteroid therapy. GC therapies reduce phagocytic capabilities of the TM<sup>195</sup>, resulting in a build-up of ECM debris which can block and reduce outflow facilities in the drainage angle<sup>196</sup>. Reduced outflow facility results in elevated IOP. If the effect of OHT is of sufficient magnitude, for a significant amount of time, damage to the ONH may arise resulting in steroid-induced glaucoma. Clinical use of corticosteroids was first described in the 1950's and shortly thereafter the phenomenon of corticosteroid induced elevated IOP was first described in literature<sup>197,198</sup>. Adrenocorticotrophic hormone

(ACTH) and cortisone when administered systemically and locally induced elevated IOP<sup>199</sup>.

The corticosteroid-IOP response is not limited to a specific method of steroid administration but has been shown to be most commonly associated with topical administration of drugs such as dexamethasone and prednisolone. The ocular hypertensive response observed in patients is however relative to the intraocular potency of the steroid administered<sup>200</sup>. Differences have been reported in the level of steroid response, in known high steroid responders, to different steroid preparations. The mode of therapy is important when one considers corticosteroid use in individuals with pre-existing risk factors (discussed below), to developing secondary glaucoma. Previous studies have identified that patients treated topically with corticosteroids exhibited an IOP response within several weeks in comparison to several months when treated systemically<sup>201,202</sup>.

Risk factors for developing secondary glaucoma include; markedly elevated IOP in response to corticosteroids and familial history of glaucoma and systemic diseases such as arthritis. 30% of the general population are steroid responders, and this increases to 46-92% in a cohort with primary open angle glaucoma (POAG)<sup>203</sup>. Familial history of diseases such as POAG, diabetes mellitus, high myopia, and connective tissue diseases such as rheumatoid arthritis have also been identified as a risk factor for IOP alterations in response to corticosteroids than in other populations<sup>199</sup>.

#### 1.5.1.4 Corticosteroid-Induced Glaucoma Pathophysiology

The main pathophysiological response to corticosteroid-induced IOP is increased resistance to AH outflow. The trabecular meshwork undergoes structural changes in response to corticosteroids supporting the theory that corticosteroids increase outflow resistance. TM cells express GRs, and in response to receptor activation, the TM cellular morphology changes with an increased nuclear size and DNA content. The microstructure of the TM is also altered in response to steroids. Extracellular matrix deposition and turnover is dysregulated in glaucoma. Steroid-responsive patients have shown an excessive ECM deposition within the TM and

GAGs, fibronectin, and elastin were all found to be deposited at higher rates in response to dexamethasone treatment<sup>204</sup>. Excessive ECM obstructs intercellular space within the TM causing decreased outflow facility. Furthermore, prolonged steroid exposure elicited a further increase in GAG deposition and it has been proposed that corticosteroids stabilise lysosomal membranes, exacerbating GAG deposition by decreasing the availability of catabolic enzymes. Additionally, indigestible GAGs, when hydrated, can cause oedema and subsequently a narrowing of trabecular spaces. The effects of corticosteroids on the aqueous outflow pathway have been investigated using cellular, animal and perfusion models<sup>205,206</sup>. Human anterior segments perfused with DEX ( $10^{-7}$  mol/L) in organ culture for 12 days not only showed an increase in IOP but also an increase in amorphogranular and fibrillar material in the ECM spaces within the JCT<sup>207</sup>. Cultured human TM cells also showed decreased phagocytic activity<sup>208,209</sup> and increased ECM protein expression in response to DEX (100nM) after 24 hours or long-term respectively<sup>210</sup>.

### 1.5.2 Transforming Growth Factor Beta (TGF- $\beta$ )

The transforming growth factor beta (TGF- $\beta$ ) superfamily belongs to the cytokine family that have crucial roles in tissue development and differentiation in vertebrates, as well as control of immunological responses and tissue healing<sup>211</sup>. The TGF- $\beta$  superfamily is a large group of regulatory polypeptides including the potent TGF- $\beta$  family and other families such as bone morphogenic proteins (BMPs), growth and differentiation factors (GDFs), activins (ACTs), inhibins (INHs), and glial-derived neurotrophic factors (GDNFs), as well as nodal growth differentiation factor (Nodal), and left-right determination factor (LEFTY)<sup>211</sup>. The TGF- $\beta$  superfamily is characterised by its pleiotropic and redundant effects<sup>212</sup>. TGF- $\beta$  members act in an autocrine, paracrine, and endocrine manner<sup>212</sup>.

TGF- $\beta$ s are synthesized as precursor proteins, which are biologically inactive. They consist of pre-pro-peptides, which require a 2-step process to give rise to active TGF- $\beta$ s (for review see Matthews *et al* 1991)<sup>213</sup>. A first proteolytic cleavage leads to the elimination of a hydrophobic signal peptide, in the N-terminal region of the precursor protein, yielding pro-TGF- $\beta$ <sup>214</sup>. A second cleavage leads to the separation of the pro-region of the protein from the TGF- $\beta$  mature peptide (Figure 1.10)<sup>215</sup>. The bioactive forms of TGF- $\beta$ s are composed of 2 mature peptide chains linked by di-sulfide bonds. TGF- $\beta$ s are usually produced as homodimers, but natural heterodimeric molecules have also been identified<sup>216</sup>.

Once synthesized and processed, TGF- $\beta$ s are released by cells as latent complexes, which are biologically inactive<sup>217</sup>. Two forms of latent complexes have been described: the “small” and “large” latent complexes (Figure 1.10)<sup>215</sup>. In the small latent complex, one molecule of mature, active TGF- $\beta$  is non-covalently associated with latency-associated protein (LAP)<sup>218</sup>. In the large latent complex, LAP is linked by di-sulfide bonds to one member of the latent TGF- $\beta$ -binding proteins (LTBPs)<sup>219</sup>. LTBPs induce association of the complex with the extracellular matrix, permitting the storage of TGF- $\beta$  (for review see Taipale and Keski-Oja, 1998<sup>220</sup>). A number of LTBPs isoforms exist, therefore, the bioavailability of TGF- $\beta$  and its specific targeting to different organs can be regulated, in part, by the formation of large latent complexes with different LTBP isoforms<sup>221</sup>. The release of latent TGF- $\beta$

from the extracellular matrix is triggered by proteolytic enzymes such as plasmin, which are able to cleave LTBPs<sup>222</sup>. Plasmin cleaves the non-covalent bonds within the N-terminal of LAP resulting in the release of active TGF- $\beta$ <sup>223</sup>. Thrombospondin (TSP), an extracellular matrix protein, also promotes the activation of TGF- $\beta$ <sup>224</sup>. In contrast to what has been described for plasmin, TSP-mediated activation of latent TGF- $\beta$  occurs through a cell- and protease-independent mechanism<sup>225</sup>. TSP induces a conformational change of LAP, which then results in the release of active TGF- $\beta$ <sup>226</sup>.

Multiple receptors interact with TGF- $\beta$ s<sup>227,228</sup>. TGF- $\beta$  receptor 1 (TGF- $\beta$ R1) and TGF- $\beta$ R2 are directly involved in signal transduction<sup>211</sup>. TGF- $\beta$ R1 and TGF- $\beta$ R2 are serine/threonine kinases that interact to form heterotetrameric complexes<sup>211</sup>. TGF- $\beta$  ligands first bind TGF- $\beta$ R2. TGF- $\beta$ R1 is then recruited to the complex and phosphorylated by TGF- $\beta$ R2 which propagates the TGF- $\beta$  intracellular signalling cascade<sup>229</sup>.

SMAD proteins are intracellular substrates of TGF- $\beta$  signalling<sup>230</sup>. Three groups of SMADs exist: receptor-mediated SMADs (rSMADs) which are directly phosphorylated by TGF- $\beta$ R1; common partner SMADs (co-SMADs), which interact directly with phosphorylated rSMADs to form heterodimeric complexes<sup>231</sup>. These are then translocated to the nucleus where they interact with DNA binding elements that can regulate gene expression<sup>232</sup>. Finally, inhibitory SMADs prevent interaction between rSMADs and co-SMADs thereby acting as a negative feedback to repress TGF- $\beta$  signalling<sup>233</sup>.

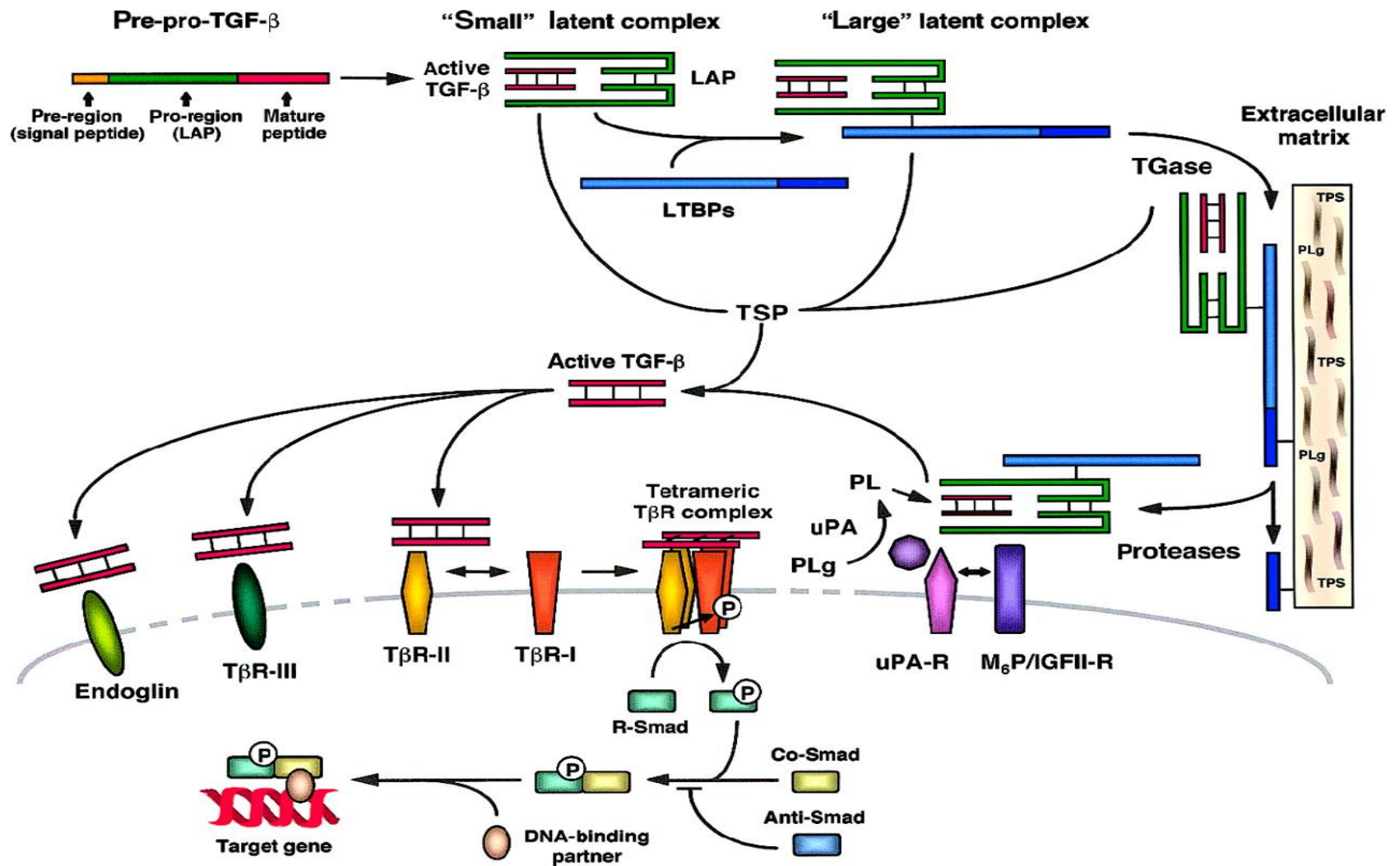


Figure 1.10: TGF- $\beta$  Structure, Latency, Activation, and Signalling. Modified from Fortunel *et al* 2000<sup>215</sup>.

### 1.5.2.1 TGF- $\beta$ -Induced Glaucoma Pathophysiology

Primary open angle glaucoma is the most common form of glaucoma<sup>21</sup>. Several prospective studies have identified IOP as the most critical risk factor for developing POAG<sup>45,46</sup>. TGF- $\beta$ 2 is the predominant isoform in the eye and is found in elevated concentrations in the AH of POAG patients<sup>234</sup>. Expression of TGF- $\beta$ 2 in the trabecular meshwork and optic nerve head of normal eyes<sup>235</sup>, and its increased expression in POAG eyes has been reported<sup>236</sup>. Increased expression of TGF- $\beta$ 2 appears to be a characteristic phenomenon in eyes with POAG<sup>237</sup>. Cultured trabecular meshwork cells secrete both TGF- $\beta$ 1 and TGF- $\beta$ 2, and express TGF- $\beta$  receptors<sup>238,239</sup>, indicating its function in the AH outflow pathway. Furthermore, it is reasonable to assume that the TM is under the influence of TGF- $\beta$ 2 present in the AH that bathes the anterior segment.

#### 1.5.2.1.1 TGF- $\beta$ and Extracellular Matrix

Disruption of ECM secretion and turnover is central to the pathophysiology of glaucoma<sup>240</sup>. TGF- $\beta$  signalling has been implicated in multiple disorders throughout the body as a mediator of the pathological increase in ECM secretion and deposition and negatively involved in fibrosis<sup>241</sup>. Numerous *in-vitro* studies indicate that elevated TGF- $\beta$  levels in POAG are involved in ECM deposition within the TM<sup>237,242–244</sup>. *In-vitro* studies of TM cells stimulated with TGF- $\beta$ 2 have increased expression of ECM-related proteins including: collagens (Type I, III, IV, and VI), laminin, elastin, cochlin, fibronectin, and thrombospondin-1<sup>237,242–244</sup>. Connective tissue growth factor (CTGF), a downstream mediator of TGF- $\beta$ 2 activities, is also elevated in response to TGF- $\beta$ 2, and is believed to mediate fibronectin synthesis<sup>237,242–244</sup>. TGF- $\beta$ 2 not only exerts its effects on ECM synthesis but also decreases the expression of key matrix metalloproteinases required for ECM degradation<sup>243</sup>. Decreased ECM degradation within the TM leads to a pathological accumulation resulting in elevated IOP and eventually glaucoma. TGF- $\beta$ 2 induces the expression of plasminogen activator inhibitor-1 (PAI-1), a potent inhibitor of matrix metalloproteinases (MMPs)<sup>243</sup>. Additionally, PAI-1 levels are also elevated in the AH of POAG patients<sup>243</sup>.

#### 1.5.2.1.2 TGF- $\beta$ and the Trabecular Meshwork Cytoskeleton

Increased stiffness of the trabecular meshwork has been observed in POAG patients<sup>245</sup>. Increased stiffness reduces intercellular spaces thus reducing the outflow capacity of the TM<sup>246</sup>. TGF- $\beta$ 2 enhances TM stiffness via the activation of tissue transglutaminase<sup>247</sup>. Tissue transglutaminase is found in normal eyes and expression is increased in POAG eyes<sup>248</sup>. TGF- $\beta$ 2 enhances cross-linking of fibronectin via tissue transglutaminase in the TM, increasing overall TM stiffness<sup>247</sup>. Lysyl oxidase (LOX) family members have also been localised to the TM and are influenced by TGF- $\beta$ 1-3<sup>249</sup>. LOX family members crosslink ECM components such as elastin and collagens which are present in the TM<sup>249</sup>.

The normal TM is more labile than the TM of POAG patients, thus outflow facilities function well. Increased contractility of TM cells prevents substantial AH outflow<sup>250</sup>. In general, TGF- $\beta$  is a potent enhancer of myofibroblast contractile phenotypes via increased expression of alpha smooth muscle actin ( $\alpha$ -SMA) in actin stress fibres<sup>251</sup>. Trabecular meshwork cells in culture treated with TGF- $\beta$ 2 have increased expression of  $\alpha$ -SMA<sup>252</sup>. However, it is yet to be shown that increasing TGF- $\beta$ 2 levels in POAG is directly correlated to increased expression of  $\alpha$ -SMA.

The cellular architecture of TM cells is altered in POAG patients and in response to TGF- $\beta$ 2<sup>253,254</sup>. TM cells of POAG patients have cross-linked actin networks (CLANs)<sup>253</sup>. CLANs are more commonly associated with glucocorticoid-treated and glaucomatous cultured TM cells<sup>255-257</sup>. Recently, however, studies have shown CLANs can also be induced by TGF- $\beta$ <sup>254</sup>.

## 1.6 The microRNA

Non-coding RNAs (ncRNA) is a term that encompasses RNAs that do not code for protein such as transfer RNA (tRNA), ribosomal RNA (rRNA), small nucleolar RNA (snoRNA), long non-coding RNA (lncRNA), and micro RNA (miRNA). Individual RNAs have specific functions<sup>258</sup>. tRNA is responsible for the transfer of amino acids to the ribosome during translation where it then interacts with rRNA which catalyses peptide bond formation for each amino acid required for the polypeptide being synthesised<sup>259</sup>. In order to become functional, both tRNAs and rRNAs need to undergo modifications such as methylation or pseudouridylation which is facilitated by snoRNAs<sup>259</sup>. Small RNAs were first discovered in 1993 with identification of *lin-4* during genetic screening of nematodes<sup>260</sup>. Further research in the same year lead to the discovery that *lin-14* could be regulated by *lin-4* demonstrating the regulatory abilities of small RNAs for the first time<sup>261</sup>. Presently, the shorter *lin-4* RNA is now recognised as the origin of a class of small regulatory RNAs also known as micro RNAs (miRNAs)<sup>262</sup>. With the advent of high-throughput sequencing techniques and enhanced bioinformatics hundreds of different miRNAs have been identified and their regulatory targets and potential function continually elucidated<sup>263,264</sup>. A number of miRNAs have been identified as central to diverse processes such as cell death, cell proliferation, metabolism, neuronal patterning and hematopoietic differentiation<sup>265-271</sup>. Developments in the miRNA field are ongoing and increasing at a steady rate; this is evident by the increasing number of studies implicating miRNAs in disease states such as Alzheimer's disease, diabetes and cancer<sup>272-281</sup>. Technological advancements in RNA-based therapies aid the progression in miRNA research and have shown a movement towards investigating the potential of miRNAs as a therapy<sup>262</sup>.

### 1.6.1 microRNA Biosynthesis- The Canonical Story

The biogenesis of miRNAs is under strict temporal and spatial control and their dysregulation is associated with many human diseases<sup>282</sup>. miRNAs regulate the expression of genes encoded for by mRNAs<sup>283</sup>. Targeting most protein-coding

transcripts, miRNAs are involved in nearly all developmental and pathological processes in animals<sup>283</sup>.

It has been predicted that miRNAs make up 1-5% of the human genome and regulate approximately 30% of protein coding genes<sup>284,285</sup>. miRNAs make up a large family of small, evolutionary conserved, non-coding RNAs between 21-25 nucleotides in length<sup>286</sup>. miRNAs are single stranded RNAs, which are derived from double-stranded RNA hairpin precursors<sup>287,288</sup>. miRNA precursors are commonly found in clusters throughout different regions of the genome, with a preference for intergenic regions and introns of protein-coding genes<sup>289</sup>. miRNAs are less commonly found in exons of transcripts and in antisense transcripts<sup>282</sup>. Frequently, several miRNA loci are located within close-proximity to each other which results in a polycistronic transcription unit<sup>290</sup>. miRNAs found within the same cluster are normally co-transcribed however individual miRNAs can undergo modifications at a post-transcriptional level<sup>291,292</sup>.

RNA polymerase III (POL-III) was initially thought to mediate miRNA transcription due to its role in tRNA and U6 snRNA transcription<sup>293</sup>. Research efforts have identified a caveat in this theory; primary miRNAs (pri-miRNAs) can sometimes be over several kilobases in length and contain stretches of more than four U bases; these stretches would result in the termination of POL III activity<sup>293</sup>. This evidence suggests an alternative method of miRNA transcription which is now known to be driven by RNA polymerase II (POL-II)<sup>294</sup>. The precise location of miRNA promoters have not yet been elucidated, however, from RNA sequencing data, CHIP-seq (chromatin immunoprecipitation followed by sequencing), and CpG island analyses it can be inferred that some miRNAs share the promoter of the host genes from which miRNAs reside within the introns<sup>295</sup>. It has also been noted that miRNAs can have multiple start sites of transcription and that their promoters may be distinct from host gene promoters<sup>296</sup>.

#### 1.6.1.1 Nuclear Events in microRNA Biosynthesis

Mammalian miRNAs can be classified into two broad categories, canonical and non-canonical, based on how the pri-miRNA is processed to form the mature

miRNA. Canonical mature miRNAs are generated by a two-step cleavage process of primary miRNA (pri-miRNA)<sup>293,297</sup> (Figure 1.11<sup>298</sup>). pri-miRNA processing is a critical event in miRNA biogenesis<sup>299</sup>. pri-miRNAs are larger than mature miRNA (~1kb) and may contain 5' and 3' modifications identical to those present in mRNAs or pre-mRNAs<sup>300</sup>. pri-miRNAs contain a stem-loop structure from which the mature miRNA sequence is derived<sup>301</sup>.

Only pri-miRNAs which contain the appropriate stem length, a large flexible terminal loop of approximately 10 base pairs (bp) and the capability to produce 5' and 3' single-stranded RNA overhangs will be efficiently processed and mature to functional miRNA<sup>302</sup>. The nuclear processing step of pri-miRNAs to stem-loop precursors of ~70 nucleotides (nt) in length is initiated by a core nuclease, RNase III, human Drosha<sup>299</sup>. Drosha forms part of a protein complex termed the microprocessor complex which also contains an essential RNA binding protein DiGeorge syndrome critical region 8 (DGCR8)<sup>299</sup>. DGCR8 identifies pri-miRNA sequences and induces cleaving via Drosha to form a pre-miRNA<sup>303</sup>. The exact mechanism through which DCGR8 recognises pri-miRNA sequences is unknown. It is clear however from bio-informatic analyses that no sequence is universally conserved among human pri-miRNAs<sup>304</sup>, it is therefore assumed that processing proteins, such as DCGR8, have to recognise the structural features of pri-miRNAs<sup>305</sup>. Unique cross-regulation between Drosha and DGCR8, which is essential for the control of miRNA biogenesis, has been previously described<sup>306</sup>. DGCR8 stabilises Drosha via protein-protein interactions and assists in controlling Drosha protein levels<sup>306</sup>. Meanwhile, Drosha negatively regulates DGCR8 mRNA post-transcriptionally by cleavage of a hairpin like structure in the 5' untranslated region (UTR) leading to destabilisation of the transcript<sup>307</sup>. Germline deficiency of Drosha causes lethality in embryogenesis, highlighting the importance of miRNAs in development<sup>308</sup>.

Precise identification of the pri-miRNA is essential for Drosha-mediated cleavage of miRNA termini<sup>301</sup>. During the pri-miRNA processing event the 'basal' junction acts as the major reference point in determining the cleavage site, the 'apical' junction itself is essential for efficient processing<sup>309</sup>. Alternative factors,

independent of Drosha and DGCR8, are involved in the processing of pri-miRNAs<sup>310</sup>. These elements reside within the 'basal' region (UG motif and the CNNC motif) and terminal 'apical' loop (UGUG motif) of human pri-miRNAs<sup>311</sup>. SRp20, a splicing factor, binds the CNNC motif and increases processing of human pri-miRNAs<sup>310</sup>.

Intronic miRNA processing by Drosha does not affect the processing of host genes pre-mRNA as cleavage of pri-miRNA is thought to occur co-transcriptionally prior to splicing catalysis<sup>312</sup>. miRNAs encoded by exonic regions destabilise the host mRNA<sup>313</sup>. Drosha antagonises follistatin-like 1 (FSTL1) expression through cleavage of miR-198 hairpin structure located within the 3'UTR of the FSTL1 mRNA. KSRP (KH-type splicing regulatory protein) binds to the terminal loop of miR-198 and facilitates cleavage<sup>307,314</sup>. Upon injury, TGF- $\beta$  signalling represses KSRP resulting in the upregulation of FSTL1<sup>307,314</sup>.

### Nuclear Events- Regulation of the Microprocessor Complex

Drosha mediated processing is essential in establishing miRNAs<sup>315</sup>. Many mechanisms exist that control expression level, activity and specificity of Drosha (1.6.1.1). This cross regulation enables homeostasis of the microprocessor activity and is highly conserved in animals<sup>309</sup>. Post-translational modifications of Drosha can also affect the processing activity of the microprocessor<sup>316,317</sup>. Acetylation of Drosha by unknown enzymes can inhibit its degradation and increase stability<sup>317</sup>. Phosphorylation of DGCR8 by ERK can increase stability of the protein<sup>318</sup>. As well as this, deacetylation of DGCR8 by histone deacetylase 1 (HDAC1) can increase DGCR8 affinity for pri-miRNAs<sup>316,317</sup>.

Specific control of Drosha mediated processing is mediated by RNA-binding proteins that can selectively interact with Drosha and/or certain pri-miRNAs<sup>300</sup>. R-SMAD proteins, SMAD1-3 and SMAD5 promote microprocessor activity via interactions with p68<sup>319</sup>. For example, when R-SMAD proteins are activated by TGF- $\beta$ , they interact with p68 and the stem of pri-miRNAs to stimulate Drosha-mediated processing of miR21 and miR-199a<sup>320,321</sup>.

### 1.6.1.2 Nuclear Export

Following Drosha processing, pre-miRNAs are transported to the cytoplasm of the cell for further processing to produce mature miRNAs<sup>262</sup>. Exportin 5 (EXP5) exports pre-miRNAs<sup>322</sup>. EXP5 forms a complex with guanosine triphosphate (GTP)-binding nuclear protein RAN, GTP/RAN, and the pre-miRNA<sup>323</sup>. The GTP/RAN, pre-miRNA complex is translocated through a nuclear pore to the cytoplasm where GTP undergoes hydrolysis and is replaced by guanosine diphosphate (GDP)<sup>323</sup>. Hydrolysis of GTP results in the disassembly of the transport complex and the release of the pre-miRNA into the cytosol<sup>324</sup>. EXP5/GDP/RAN complex provides support and protection for the pre-miRNA in the cytosol via interactions between the double stranded RNA (ds-RNA) stem-loop overhang at the 3' of the pre-miRNA and a tunnel like structure on the export complex<sup>324</sup>.

### 1.6.1.3 Cytoplasmic Processing of pre-miRNA

#### Dicer-mediated Processing

The nuclear cleavage process by Drosha (1.6.1.1), defines one end of the mature miRNA. The pre-miRNA released into the cytosol is cleaved by a Pol III, Dicer, near the terminal loop to liberate a small RNA duplex<sup>325</sup>. Dicer is an RNase III endonuclease of ~200kDa. The C-terminal RNase III domains of Dicer form intramolecular dimers to create catalytic centres similar to those found in Drosha<sup>299</sup>. Dicer contains a PAZ domain which binds to pre-miRNA termini<sup>326</sup>. Dicer binds to pre-miRNA with a preference for the 3' overhang generated by Drosha processing<sup>326</sup>.

#### Dicer Regulation

Dicer proteins interact with double stranded RNA binding domain proteins (ds-RBD). Dicer interacts with TAR-RNA binding protein (TRBP); TRBP modulates efficiency of Dicer-mediated processing of certain pre-miRNAs and fine tunes the length of mature miRNA<sup>327</sup>. Conversely, human Dicer interactions with ds-RBDs do not seem to be essential for Dicer-mediated pre-miRNA processing but instead can act as positive or negative regulators of the process<sup>327</sup>. Following the generation of the RNA duplex by Dicer, the duplex is subsequently loaded on to an Ago family

protein to form an effector complex termed RNA-induced Silencing Complex (RISC)<sup>328</sup>. RISC assembly involves two steps; the loading of the miRNA duplex and its subsequent unwinding<sup>309</sup>. Ago proteins are ubiquitously expressed and are associated with miRNAs and siRNAs<sup>329</sup>.

miRNA duplexes are made up of a passenger strand and a guide strand, and incorporation of a miRNA duplex to an AGO protein forms a pre-RISC complex<sup>309</sup>. The passenger strand of the duplex (termed miRNA\* (miRNA star)) is discarded and the guide strand is incorporated to form a mature RISC<sup>330</sup>. The strand retained in the Ago:RNA complex is determined by the relative thermodynamic stability of the two ends of the duplex intermediate<sup>331</sup>. Mismatches in the guide strand promote unwinding of the miRNA duplexes<sup>332</sup>. The miRNA guides the RISC to its target mRNA resulting in silencing via degradation or repression<sup>333</sup>.

### Intrinsic Regulation of miRNA

Alterations in sequence and/or structure of miRNAs can alter their maturation and turn-over rates<sup>309</sup>. Single nucleotide polymorphisms (SNPs) have been identified in miRNAs and can have direct effects on their biosynthesis or alter their target specificity<sup>309</sup>. A 'C' to 'T' SNP in the first C of CNNC motif in pri-miR-15a~16-1 reduces Drosha-mediated processing resulting in lower miRNA production<sup>310</sup>. Mature miRNA and pre-miRNA are also susceptible to intrinsic regulation<sup>309</sup>. RNA tailing, a process whereby untemplated nucleotidyl addition to the 3' end of RNA occurs, can alter the synthesis and function of both pre-miRNA and mature miRNA<sup>334</sup>. Uridylation and adenylation are forms of tailing seen most commonly identified on miRNAs<sup>309</sup>. miRNAs can be regulated at the RNA stability level<sup>335</sup>. The turnover of mature miRNA has been studied extensively and several nucleases have been proposed to be involved in the cleavage and decay of miRNAs<sup>309</sup>. It is unknown how these nucleases achieve target specificity and whether this is conserved machinery for miRNA decay<sup>309</sup>.

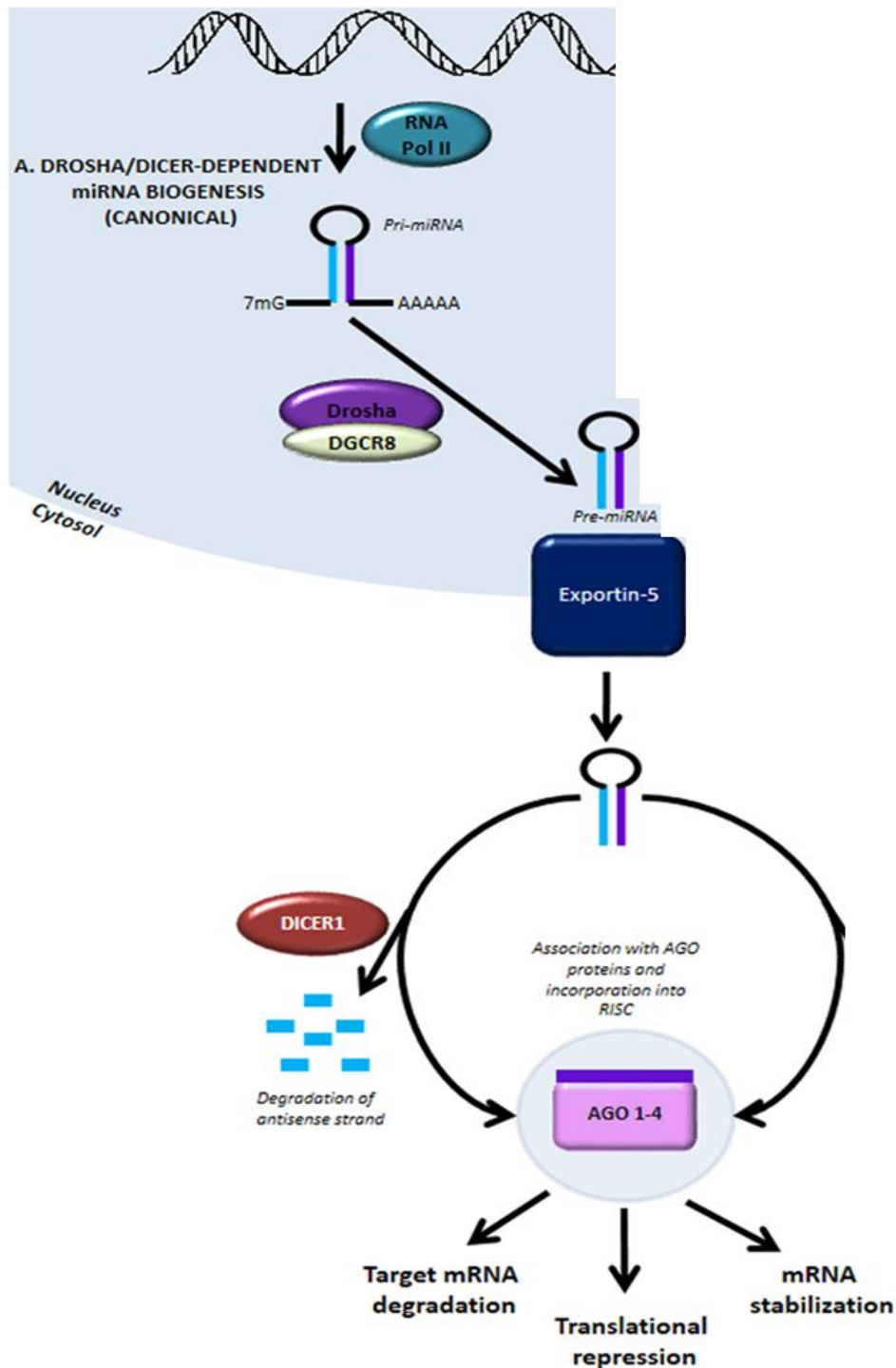


**Figure 1.11: miRNA Biosynthesis- Canonical Pathway.** Modified from Heman-Ackah *et al* 2013<sup>298</sup>. The canonical miRNA biogenesis pathway is Drosha/Dicer mediated. RNA POL II mediates transcription of genomic loci containing miRNA genes. Primary transcript is referred to as pri-miRNA. pri-miRNA is processed in the nucleus by Drosha and DGCR8 to produce pre-miRNA. Exportin 5 transports pre-miRNA to the cytoplasm where it is further processed by RNA POLIII Dicer. The mature miRNA strand complexes with AGO proteins to form a functional RISC complex.

## 1.6.2 Non-Canonical Biosynthesis

Biosynthesis of miRNAs can be achieved using various alternative methods which do not follow canonical biosynthesis<sup>336</sup>; these alternative mechanisms make up the non-canonical pathway of miRNA biosynthesis<sup>298</sup> (Figure 1.12). Typically, non-canonical miRNAs are distinguished from canonical miRNAs by changes in their expression when a certain miRNA processing factor, such as Drosha, Dicer, or DGCR8, is removed<sup>337,338</sup>. Almost all miRNA species in mammals follow the canonical pathway for biosynthesis<sup>300</sup>. Non-canonical miRNAs account for only 1% of conserved miRNAs and are typically in low abundance<sup>300</sup>. The non-canonical pathway was first described during mirtron production<sup>339</sup>, in which, the Drosha-mediated processing step was bypassed and instead the production of a small RNA was facilitated by an mRNA splicing event<sup>339</sup>. Biogenesis of miR-451 does not require Dicer<sup>340</sup>. Pre-miR-451 is cleaved by AGO2, bypassing Dicer<sup>341</sup>. Drosha-mediated processing cleaves a short hairpin structure that is too small to be processed by Dicer hence direct loading by AGO2 to form mature miRNA<sup>342,343</sup>.

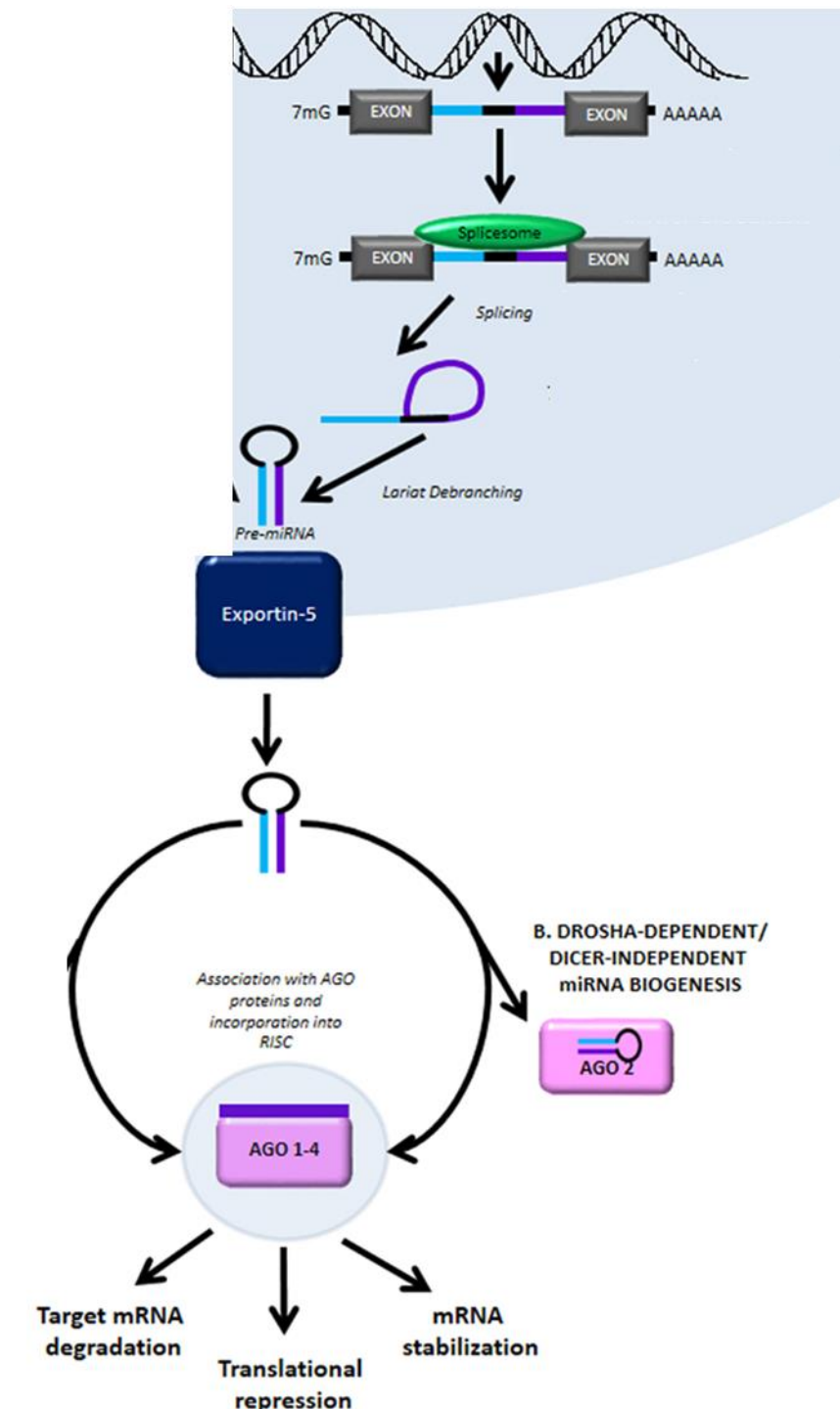


**Figure 1.12: miRNA Biosynthesis- Non Canonical Pathway.** Modified from Heman-Ackah *et al* 2013<sup>298</sup>. The non-canonical miRNA biogenesis pathway is Drosha/Dicer independent. Cytoplasmic pri-miRNA undergoes processing by AGO2.

### 1.6.3 microRNA Mechanism of Action

Individual miRNAs control the expression of one or more target mRNAs and each mRNA may be regulated by one or more miRNA<sup>344</sup>. Experimental evidence has suggested that the 5' end of the miRNA is responsible for the specificity and activity in binding a target mRNA<sup>345</sup>. This 5' region is termed the "seed" region. In animals the "seed" region is approximately 6-8nt in length and is highly conserved across species<sup>346</sup>, even slight alterations in the sequence may alter the miRNAs target spectre<sup>347</sup>.

miRNAs incorporated within the RISC complex guide RISC to specifically recognise target mRNAs and down regulate gene expression by one of two post-transcriptional mechanisms: (i) translational repression or (ii) mRNA cleavage<sup>262</sup>. miRNAs interact with their target mRNAs by base pairing to specific sequences, found in the 3' untranslated region (UTR) of mRNAs<sup>348</sup> by perfect or near perfect complementarities<sup>349</sup>. Genes with longer 3'UTRs usually have higher density of miRNA-binding sites and are mainly involved in developmental processes whereas genes with shorter 3'UTRs usually have lower density of miRNA-binding sites and are involved in basic cellular mechanisms<sup>350</sup>.

The degree of miRNA-mRNA complementarity is a major determinant of the regulatory mechanism process be it repression or degradation<sup>351</sup>. High degree of complementarity enables Ago-catalysed degradation of the mRNA target sequences through the mRNA cleavage mechanism process<sup>351</sup>. In contrast, a central mismatch omits degradation of the target mRNA as an option and instead facilitates the translational repression mechanism<sup>351,352</sup>.

#### 1.6.3.1 microRNA-Mediated mRNA Decay

In animals, most miRNAs are only partially complimentary to their targets<sup>353</sup>. In this case, AGO proteins are not sufficient to mediate silencing and therefore they must interact with GW182 family proteins<sup>354</sup>. AGO-GW182 complexes silence mRNA targets by repressing translation enhancing degradation<sup>354</sup>. The mechanism through which this is achieved is not very well understood, although new insights in to the role of GW182 in these processes have emerged<sup>354,355</sup>. Initially it was believed that

miRNAs only repress translation of target mRNAs with little or no effect on mRNA abundance<sup>356</sup>; however it is now known that miRNAs can also promote destabilisation of target mRNAs by recruiting deadenylases onto target mRNAs via GW182 proteins<sup>357</sup>.

#### 1.6.3.2 microRNA Translational Repression

Numerous studies have examined the mechanisms through which miRNAs mediate translational repression. miRNAs inhibit the initiation step of translation and three major mechanisms have been proposed<sup>358</sup>: (i) GW182-mediated PABP displacement<sup>359</sup>, (ii) recruitment of translational repressors via GW182<sup>360</sup> and (iii) dissociation of eIF4A from the cap binding complex eIF4F<sup>361</sup>. None of these mechanisms are mutually exclusive and, they may overlap, occur concurrently, or occur with different kinetics to augment the overall silencing effect<sup>358</sup>.

#### 1.6.4 miRNAs and Human Disease

miRNAs play important roles in several physiological and pathological processes<sup>362</sup>. miRNAs are involved in developmental processes including metabolism, cell proliferation, apoptosis, and neuronal cell fate<sup>363</sup>. miRNAs have also been implicated in regulation of inflammatory microenvironments<sup>364</sup> and fibrosis<sup>365</sup>. The identification of miRNAs involvement in human disease and metabolic disorders has led to research focused on the role of miRNAs as important regulatory molecules. Altered miRNA expression has been linked to numerous diseases including; myocardial infarction<sup>366</sup>, neurological disorders such as Parkinson's disease<sup>298</sup> and Alzheimer's disease<sup>278</sup>, diabetes<sup>277</sup>, and numerous forms of cancer<sup>367</sup>. Increased expression of miRNAs can function as both oncogenes (by down-regulation of tumour suppressor genes) or as regulators of cellular differentiation<sup>368</sup>. Unique miRNA profiles have been identified for a number of reproductive cancers; breast and ovary as well as endometroid adenocarcinoma, haematological cancers, and thyroid cancer<sup>369</sup>.

Over the preceding decade, the miRNA transcriptome of the retina and other ocular tissues (lens and cornea) have been established<sup>370</sup>. miRNAs often show unique tissue-specific expression patterns suggesting potential unique roles for

miRNAs in ocular tissues<sup>370,371</sup>. miRNAs have already been implicated in several ocular diseases such as cataract<sup>372</sup>, myopia<sup>373</sup>, age related macular degeneration<sup>374</sup>, and retinoblastoma<sup>375</sup>. Differentially expressed miRNAs have been identified in cataract and non-cataract lens epithelium capsules<sup>376,377</sup>. In the lens, miRNAs mainly target redox homeostasis transcription factor genes<sup>378</sup>, dysregulation of which leads to cataract and cellular abnormalities. The miRNA transcriptome of the aqueous humour has identified several differential miRNAs in healthy and disease states<sup>377,379</sup>. miRNA expression in the AH has been shown to be altered in cataract patients<sup>378</sup> and more recently glaucoma patients<sup>379</sup>. It is therefore no surprise that miRNA dysregulation in the AH may have pathological effects on ocular tissues involved in glaucoma due to permanent AH interactions. Recently miRNAs have been localised to the trabecular meshwork and it is thought that they function to maintain homeostasis within the TM<sup>380,381</sup>. Dysregulation of miRNAs in the TM will be discussed in Chapter 5 (5.1.1.1).

## **Chapter 2**

### **Materials and Methods**

## 2.1 Tissue Culture

### 2.1.1 Tissue Samples

Cadaveric eyes were provided by the Liverpool Research Eye Bank and approved by the local ethics review board (RETH000833) handled in accordance to the tenets of the Declaration of Helsinki. Written consent was obtained from the next of kin of the deceased donor. Eyes were obtained from the Royal Liverpool University Hospital Mortuary by an in-house team of qualified eye-retrievers. Donor eyes were excluded if the maximum post-mortem time exceeded 48 hours. Clinical and demographic data (age, sex, and ethnicity) was available and tissue was obtained from both non-glaucomatous (normal TM) and glaucomatous patients (GTM). GTM730-03 and GTM307-04 were a kind gift from Dr. Abbot Clark, University of North Texas.

<b>Donor ID</b>	<b>Age</b>	<b>Sex</b>	<b>Medical History</b>
NTM LGP-1	57	Male	No Glaucoma
NTM LGP-2	65	Male	No Glaucoma
NTM 009	57	Male	No Glaucoma
NTM 119	94	Male	No Glaucoma, Cataract Surgery
NTM 002	57	Male	No Glaucoma
NTM 720	64	Male	No Glaucoma
NTM 020	88	Female	No Glaucoma
NTM 012	71	Unavailable	No Glaucoma
NTM 013	85	Unavailable	No Glaucoma
NTM 029	65	Unavailable	No Glaucoma
GTM 304-04	74	Female	POAG
GTM 730-03	88	Male	POAG
GTM 034	86	Male	POAG

**Table 2.1 Human TM Cell Donor Information**

### 2.1.2 Dissection of Anterior Segment From Porcine and Human Eyes

Dissection of the anterior segment was performed under sterile conditions (Figure 2.1). Extra-ocular tissue was removed and only intact eyes were used. The eyes were immersed in 10% iodine solution for 5 minutes and washed twice in sterile 1X Dulbecco's Phosphate Buffered Saline (DPBS) (DB8537, Sigma, UK) before dissection. Holding the globe firmly, but without undue pressure the scleral tissue was circumferentially scored approximately 3-5mm posterior to the limbus using a #15 scalpel. The anterior segment was dissected by making a circumferential cut along the initial score. The vitreous, lens, iris, and choroidal layer were carefully removed. The remaining anterior segment was rinsed three times with sterile PBS to remove remaining pigment and placed in incubating media (see 2.1.4).

### 2.1.3 Trabecular Meshwork Dissection and Explant Culture

Dissection of the TM from the anterior segment was carried out upon receiving anterior segments from the internal Research Eye Bank (REB) and following whole globe anterior segment dissection. Growth medium as per specifications highlighted below (2.1.4) was incubated at 37°C in preparation for the tissue. Anterior segments were washed with sterile PBS and it was ensured that the iris, lens, and choroid layer were removed. The ciliary body was then carefully dissected using a blunt curved forceps. The TM could be visualised as a light grey layer close to where the ciliary body was located under a dissection microscope. TM was removed carefully using a blunt forceps in a stripping technique and the tissue obtained was placed directly in to incubating growth medium. The strip of TM obtained was cut into sections of approximately 2-4mm in length and was explanted to generate primary human TM cells. Using a sterile forceps an "X" was indented to the base of individual wells of a 6 well dish. The TM tissue was carefully placed in this region to aid attachment. To further prevent disruption to the TM tissue a sterile coverslip was use to keep the tissue in place. Incubating media was carefully pipetted dropwise until the tissue was covered. Tissue was allowed to attach for up to 4 hours and incubating media was topped up. Media was changed carefully daily ensuring no disruption to the tissue occurred. Primary TM cells were prone to fungal infections therefore for the initial growth period 2.5µg/mL

amphotericin B (A2942, Sigma, UK) supplemented media was used. Older donor eyes had a slower growth rate in comparison to younger donor eyes, this was counteracted by the addition of basic fibroblast growth factor (1µg/mL) (humanBFGF, F0291, Sigma, UK). Failure to produce primary outgrowths from the anterior segments or donor corneal rims was observed in eyes that remained in culture medium over 3 days prior to dissection, and was frequently caused by fungal infections. The latent period prior to cell growth was between several days to 4 weeks, which was donor dependent as conditions remained the same throughout.

Primary TM cells that grew to form a monolayer were gently dissociated from the donor tissue using 0.25% Trypsin/EDTA solution (T4049, Sigma, UK). Cells were not centrifuged as cell count was low and risk of cell damage or loss was high. Dissociated cells were placed directly into a T25 tissue culture flask (Greiner, Bio-One, UK) with surplus culture medium containing 10% FCS (BioSera, Labtech, UK) to counteract the Trypsin/EDTA solution. Primary TM cells were allowed to attach for up to 6 hours, following this media containing Trypsin/EDTA was removed and cultures were maintained as follows (2.14).

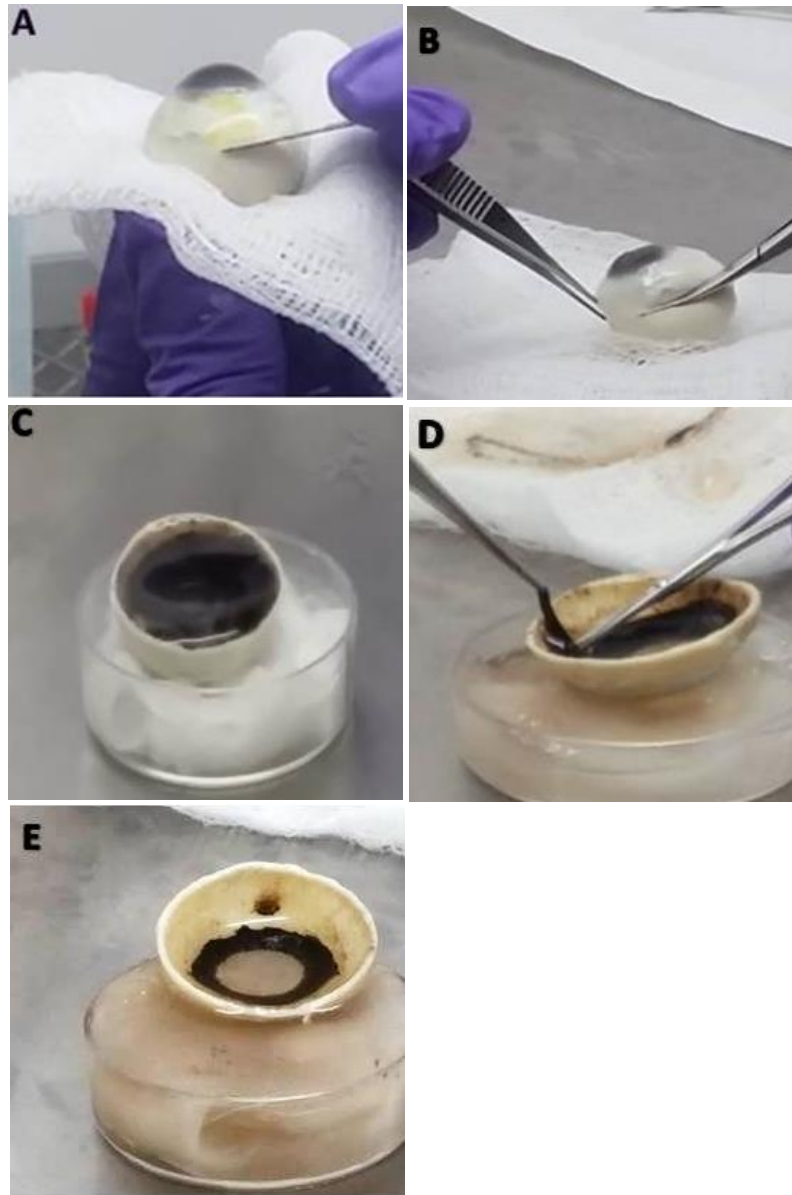


**Figure 2.1: Representative Images Depicting Human Anterior Segment Dissection Protocol.** Photographs depicting the dissection of the anterior segment of a human globe. A; Whole human globe in preparation for central scoring with #15 blade. B; Circumferential cutting of the whole globe to obtain anterior segment. C; Detached anterior segment containing some vitreous, the iris, the lens, and the choroid layer. D; Careful removal of the choroid layer via “stripping”. E; Final anterior segment section containing only the ciliary body and trabecular meshwork.

#### 2.1.4 Cell Culture Maintenance

Human trabecular meshwork cells were cultured in Dulbecco's Modified Eagle's Medium- low glucose (Sigma, UK) supplemented with 10% fetal calf serum (FCS)(Biosera, LabTech UK), 2mM L-glutamine, 100 units'/mL penicillin/100µg/mL streptomycin (Pen/Strep), and 2.5µg/mL amphotericin B (Fungizone) (all from Sigma, UK). Media was changed every 2-3 days. Cell growth was arrested 24 hours prior to experimentation in serum free DMEM supplemented with 2mM L-glutamine, Pen/Strep, and Fungizone as concentrations above.

#### 2.1.5 Mycoplasma Testing and Treatment of Cells

Mycoplasma testing was routinely carried out on all primary human trabecular meshwork cells prior to experimentation with the Sigma LookOut® Mycoplasma PCR detection kit (Sigma, UK) according to manufacturers' specifications. Briefly, 100µL of conditioned media was obtained from confluent cell cultures. Conditioned media was boiled for 5 minutes at 95°C and placed directly on ice for use in End Point PCR described in 2.4.6.

#### 2.1.6 Sub-Culturing Cells

Human trabecular meshwork cells were maintained in a 37°C humidified incubator (MCO-18AC Panasonic Biomedical, UK) with 5% CO<sub>2</sub>. Continuous cultures were maintained within standard sterile T75 tissue culture (TC) flasks (Greiner Bio-One, UK). When cells reached confluency they were sub-cultured. Briefly, cells were washed with sterile PBS before addition of 0.25% Trypsin/EDTA solution (Sigma, UK) for up to 10 minutes or until all cells had detached from the flask. The trypsin was neutralised with twice the volume of culture medium. The cell suspension was then removed and centrifuged at 1000 revolutions per minute (RPM) for 15 minutes, and split as appropriate into new TC flasks, or culture plates. Cell culture media was replenished every 2-3 days. Primary cells have increased susceptibility to infection, both bacterial and fungal, therefore cultures were observed daily to ensure no infection was present. Frequently cultures were lost to this. To counteract this, a new incubator specifically for primary cultures was made available which greatly decreased infection rates.

### 2.1.7 Long Term Storage of Cells

For long term storage trabecular meshwork cells were stock frozen at varying passages for use at a later date. Trypsinised cell suspensions were re-suspended in freezing medium consisting of 80% culture medium, 10% FCS and 10% dimethylsulphoxide (DMSO) (Sigma, UK. The suspension was transferred cryoprotective vials were placed in a 'Mr Frosty' freezing container containing isopropanol (Fischer Scientific) at room temperature. The container was then placed in a freezer at  $-80^{\circ}\text{C}$  for up to 24 hours after which the vials were removed and placed in liquid nitrogen. Frozen cells were thawed at  $37^{\circ}\text{C}$  and placed in tissue culture flasks containing pre-heated culture media. Liquid nitrogen maintenance is essential for long term cell storage. A number of primary cells were lost when liquid nitrogen levels were not efficiently maintained, upon thawing cells were unable to recover presenting difficulties proceeding with experimentation.

## 2.2 Cells for Experimentation

Human trabecular meshwork cells were used for experimentation between passage 3 and passage 6. Cell health and growth were continually observed based on morphological changes (2.2.1.1) and growth rate, between passaging<sup>382</sup>. Trabecular meshwork cells were not used after passage 10 in experiments as they began to show a decrease in growth rate and gross morphological changes. Cells were seeded at a density of 20,000 cells per cm<sup>2</sup> for immunocytochemistry (ICC) and transfection experiments. Cells were seeded at 100,000 cells per cm<sup>2</sup> for protein and nucleic acid experiments.

### 2.2.1 Characterisation of TM Cells

#### 2.2.1.1 Morphological Assessment of Trabecular Meshwork Cells

Preceding experimentation the trabecular meshwork cells were observed throughout their life-span under outlined cell culture conditions. These cells were viewed under a Brightfield microscope and images were taken using a Nikon TiE microscope (Nikon, Surrey, UK). Images were taken serially throughout cell culture to monitor growth of the cells ensuring appropriate morphology was maintained (Figure 3.1).

#### 2.2.1.2 Fluorescent Staining of Trabecular Meshwork Cells *In Vitro*

Trabecular meshwork cells were characterised by immunocytochemistry (ICC) to stain for the positive presence of TM associated proteins; caveolin-1, caveolin-2, aquaporin-4, myocilin, and vimentin. Primary human tenon fibroblasts were used as a positive control (Chapter 3, Figure 3.2).

Sterile coverslips were placed in 6 well TC plates. Trypsinised cells were counted using cell counter slides (Bio-Rad, UK) and 20'000 cells per cm<sup>2</sup> were plated per well and culture plates were maintained as described above (2.1.4). Wells intended for myocilin antibody staining were serum starved for 24 hours at 70% confluency. Cells were treated with 100nM dexamethasone (DEX) for 16hours prior to myocilin staining. All remaining wells were maintained as usual.

After treatment media was removed and cells were washed with PBS. All cells were fixed with 4% paraformaldehyde for 15 minutes. Fixed cells were washed with PBS and permeabilised with 0.05% Triton-X 100 in PBS for 10 minutes. Coverslips were washed with 3 changes of PBS for 15 minutes. To reduce non-specific binding, coverslips were blocked in 5% goat serum (Sigma, UK) in PBS for 90 minutes. Coverslips were washed with 3 changes of PBS for 15 minutes and incubated in primary antibodies diluted in 5% goat serum in PBS overnight at 4°C. Primary antibody concentrations can be found in Table 2.2 below. Following overnight incubation the coverslips were washed with PBS as above, and incubated with appropriate Fluorescein isothiocyanate (FITC) conjugated secondary antibody (Abcam, 6785, UK) at assay dependent concentrations for 90 minutes at room temperature. Coverslips were washed as above, and were prepared for mounting. Coverslips were carefully removed from corresponding wells and excess liquid was removed. Coverslips were mounted onto slides using Fluoroshield Mounting Medium with DAPI (Abcam, UK), and allowed to set overnight at 4°C. Slides were visualized using a confocal microscope (Zeiss LSM800, Zeiss, UK). Slides were kept for long term storage at -20°C and protected from light.

<b>Antibody</b>	<b>Supplier</b>	<b>Raised In</b>	<b>Concentration</b>
Anti-Caveolin-1 (ab32577)	Abcam	Rabbit	0.22 µg/mL
Anti-Caveolin-2 (ab79397)	Abcam	Rabbit	0.22 µg/mL
Anti-Myocilin (55477)	Abcam	Mouse	3.1 µg/mL
Anti-Vimentin (MA5-11883)	Invitrogen	Mouse	1 µg/mL
Anti-Aquaporin-4 (46182)	Abcam	Rabbit	10 µg/mL

**Table 2.2: Details for Primary Antibodies Used for ICC**

### 2.2.2 Cell Stimulations with TGF- $\beta$ 2 and Dexamethasone

TM cells were grown to 70-80% confluency and prior to stimulation cell growth was arrested for 24 hours in starvation media containing only L-glutamine, and Pen/Strep. Human TM Cells were stimulated with either recombinant human TGF- $\beta$ 2 (302-B2-010, R&D Systems, UK) at a concentration of 5ng/mL for 4hours or 24hours (Chapter 3 and 5) or 100mM dexamethasone (D4902, Sigma, UK) for 16hours (Chapter 4). The concentration and time chosen for TGF- $\beta$ 2 treatment was based on previously carried out optimization that looked at effects of 1ng/mL, 5ng/mL and 10ng/mL TGF- $\beta$ 2 on normal TM cells over a time period ranging from 0hours to 72hours (Figure 8.1, Appendix). Vehicle control cells were treated with equal volumes of 4mM Hydrogen Chloride (HCl) and 0.1% bovine serum albumin (BSA) solution (Sigma, UK), and negative control cells were maintained in starvation media only over the specified time period.

### 2.2.3 Transfection for miRNA Manipulation Experiments

TM cells were seeded at a density of 20,000 cells per cm<sup>2</sup> 48hours prior to transfection experiments. At 50% confluence cell growth was arrested using starvation medium as above (2.14) for 24hours. TM cells were treated with 5ng/mL TGFβ-2 and transfected with synthetic human microRNA mimic for miR-145-5p and miR-143-3p, miRNA inhibitor for miR-145-5p and miR-143-3p or a scrambled negative control (Qiagen, UK). Details of synthetic mimics and inhibitors are outlined in Table 2.3. The transfection mix was prepared according to the manufacturers' protocol using a ratio of 15μL HiPerfect Transfection reagent (301704, Qiagen, UK) for every 50nMol of miRNA transfected. Ambion® a fluorescently labelled negative control siRNA (AM4620, ThermoFisher Scientific, UK) was used to monitor transfection efficiency over 24 hours. Media was removed after 24 hours and wells were washed with PBS. siRNA negative control cells were imaged using Nikon TiE microscope (Nikon, Surrey, UK ) to assess uptake of miRNA mimics and inhibitors. TM cells were then prepped for total RNA isolation.

Candidate miRNA	Sequence	Qiagen ID
<b>hsa-miR-145-5p Mimic</b>	5'GUCCAGUUUCCCAGGAAUCCCU	MSY0000437
<b>hsa-miR-145-5p Inhibitor</b>	5'GUCCAGUUUCCCAGGAAUCCCU	MIN0000437
<b>hsa-miR-143-3p Mimic</b>	5'UGAGAUGAAGCACUGUAGCUC	MSY0000435
<b>hsa-miR-143-3p Inhibitor</b>	5'UGAGAUGAAGCACUGUAGCUC	MIN0000435
<b>Scrambled Negative Control</b>	Random	ID: 1027271

**Table 2.3: miScript miRNA Mimic and Inhibitors.**

## 2.3 Protein Based Methods

### 2.3.1 Whole Cell Lysis- Protein Extraction

Adherent cell lysates were prepared for immunoblotting against proteins of interest. Confluent cells, grown on a 10cm tissue culture treated dish, were washed with PBS following TGF- $\beta$ 2 treatments. Cells were then lysed using SDS/Urea lysis buffer (10mM Tris-HCL [pH=6.8], 6.7M Urea, 35nM SDS, 10% Glycerol and 7.4 $\mu$ M bromophenol blue) containing 50 $\mu$ M phenylmethanesulfonyl fluoride (PMSF) and 50 $\mu$ M N-methylmaleimide) to inhibit endogenous proteases. Prior to use 5%  $\beta$ -Mercaptoethanol (final volume) was added to each lysate to reduce for SDS-PAGE. Protein lysates were stored at -20°C.

### 2.3.2 SDS-Polyacrylamide Gel Electrophoresis (SDS-PAGE)

Prepared protein lysates and 6 $\mu$ L protein ladder (Precision Plus Protein™ Dual Color Standards, Bio-Rad, UK) were loaded into a 10% Precast Ready Gel (Bio-Rad, UK) in running buffer (10X Running buffer; 25mM Tris base (Sigma, UK), 190 mM glycine, (Sigma, UK) 0.1% sodium dodecyl sulfate (SDS) (Sigma, UK)), and separated at 120V. The gel, filter paper and nitrocellulose membrane were soaked in transfer buffer (10X Transfer buffer; 25mM Tris base (LiCor, UK), 190 mM glycine, (LiCor, UK) 20% Methanol (SDS) (Sigma, UK)), for approximately 10 minutes. Separated protein samples were then transferred onto a nitrocellulose membrane using semi-dry Bio-Rad TurboBlot transfer system at 25V (1.3A) for 7 minutes. Membranes were blocked for 1 hour at room temperature (RT) in Odyssey® TBS-Blocking Buffer (Li-Cor Biosciences, Nebraska, USA) prior to primary antibody incubation. Primary antibody information is outlined in Table 2.4. Primary antibodies were diluted in blocking buffer at assay dependent concentrations, and membranes were probed overnight at 4°C. Membranes were washed in 3 changes of TBS/0.1% Tween (TBS-T) for 15 minutes and probed for 90 minutes at 37°C with IRDye® 800CW or IRDye®680RD conjugated secondary antibodies (Li-Cor) diluted in blocking buffer at a concentration of 60ng/mL. Membranes washed as above in TBS-T and imaged using an Odyssey® CLx 9120 Infrared Imaging System.

<b>Antibody</b>	<b>Supplier</b>	<b>Raised In</b>	<b>Concentration</b>
Anti-SMAD2/3 (8828S)	Cell Signalling	Rabbit	0.22 µg/mL
Anti-pSMAD2/3 (8685S)	Cell Signalling	Rabbit	3.1 µg/mL
Anti-α-SMA (5694)	Abcam	Rabbit	0.1 µg/mL
Anti-GAPDH (8245)(181602)	Abcam	Mouse/Rabbit	0.01 µg/mL

**Table 2.4 Primary Antibody Details for Protein Analyses.**

## 2.4 Nucleic Acid Based Methods

### 2.4.1 Ribonucleic Acid (RNA) Extraction

Total RNA from primary normal TM and GTM cells was extracted using AllPrep® DNA/RNA/miRNA Universal Kit (Qiagen, UK) as per manufacturers' specifications. Briefly, cells grown in a monolayer were trypsinized and lysed. The lysate was passed through a QIAshredder column (Qiagen, UK, catalogue number 79654). DNase 1 "on column digestion" was carried out prior to subsequent steps as per manual. The RNA was washed several times before elution of total RNA, including miRNAs, with 40µL of RNase free water centrifuged for 1 minute at ≤8000xg. A second elution with 30µL RNase free water was carried out in the same manner to ensure a higher RNA yield. RNA quality and concentration was analysed prior to long term storage at -80°C until experimental use.

### 2.4.2 Nucleic Acid Concentration Measurements on NanoDrop 2000 Spectrophotometer

Total RNA concentration of a sample can be determined spectrophotometrically by measuring absorbance at 260nm. Absorbance can also be measured at 280nm to determine presence of protein contamination. Thus, a 260/280 ratio is used to identify pure RNA. A ratio of approximately 2.0 is defined as pure RNA. 1µL of "blank" sample (RNase free water) was used to calibrate the instrument. 1µL of RNA samples was pipetted directly on to the instruments pedestal then used to measure absorbance at 260nm and 280nm as well as RNA

sample concentrations (ng/ $\mu$ L) and purity by the NanoDrop 2000 (ThermoFisher Scientific, UK).

### 2.4.3 RNA Quality Assurance with Agilent Bioanalyser 2100

Bioanalyser 2100 (Agilent Technologies, UK) is the first commercially available assay that utilises Chip based technologies for nucleic acid separations. The LabChip Technology separates nucleic acids using a microfluidic platform. The Chip contains micro-channels of glass which are filled with polymer and a fluorescent dye. Fluorescent dye molecules are inserted into the RNA to enable them to be detected by the systems lasers. Once the RNA is loaded they are separated according to size migrating towards the positively charged ions. Size and concentration of the RNA is correlated with fluorescence. Bioanalyser software utilises an algorithm to present the data as electropherograms and “slab gel like images”. RNA loaded is compared to a ladder consisting of randomised RNA sizes in order to determine unknown concentrations. 18S and 28S ribosomal RNA peaks are used to determine the integrity of RNA samples loaded. RNA integrity is presented as an RNA Integrity Number (RIN) between 1 and 10. RNA samples with a RIN of 10 are considered high quality RNA samples.

The RNA 6000 Nano Kit was used to perform quality assurance on both normal TM and GTM RNA samples. Procedure was followed based on Agilent RNA 6000 Nano Kit<sup>®</sup> as per manufacturers’ specifications. Briefly, 550 $\mu$ L of RNA 6000 Nano gel matrix was passed through a spin filter and centrifuged at 1,500xg for 10 minutes. Aliquots of 65 $\mu$ l were transferred into RNase-free microfuge tubes and 1 $\mu$ l of RNA 6000 Nano dye concentrate was added before the gel/dye mix was centrifuged at 13,000xg for 10 minutes. Gel-dye mix (9  $\mu$ l), Agilent RNA 6000 Nano Marker (5 $\mu$ l) and ladder (1 $\mu$ l) or RNA samples (1  $\mu$ l) were pipetted into marked wells on the chip. The fully prepared chip was vortexed at 2400 rpm at 1 minute. The chip was run on the Bioanalyser 2100 system. Results can be seen in Figures 8.2 and 8.3 (Appendix).

### 2.4.5 cDNA Synthesis

0.5-1.0µg RNA was reverse transcribed with miScript II RT kit (Qiagen, UK) as per manufacturers' specifications. Briefly, template RNA and H<sub>2</sub>O mixture was added to the reverse transcription master mix containing 5x HiFlex Buffer, 10x Nucleics Mix and miScript Reverse Transcriptase (volumes highlighted in Table 2.5). The mixture was incubated for 60 minutes at 37°C then for 5 minutes at 90°C to inactivate the miScript reverse transcriptase, using a Veriti 96 well Thermal Cycler (Applied Biosystems™, ThermoFischer Scientific, UK). cDNA quality was assessed via End Point Polymerase Chain Reaction (PCR).

<b>Component</b>	<b>Volume</b>
5x miScript HiFlex Buffer	4µL
10x Nucleics Mix	2µL
miScript Reverse Transcriptase	2µL
H <sub>2</sub> O	Variable (Up to 12µL)
RNA Template (0.5-1.0µg)	Variable (Up to 12µL)
<b>Total volume</b>	<b>20µL</b>

**Table 2.5: Reverse Transcription Reagent Volumes for cDNA Synthesis.**

### 2.4.6 End-Point PCR

End-point PCR thermocycling reagent volumes are outlined in Table 2.6. Diluted cDNA template was added to the end-point master mix and products were amplified using the Veriti Thermal Cycler.

<b>Component</b>	<b>Volume</b>
cDNA template	1µL
Red Taq Enzyme (Sigma)	12.5µL
Primer Pair	2.5µL
H <sub>2</sub> O	9 µL
<b>Total Volume</b>	<b>25 µL</b>

**Table 2.6: End-Point PCR Reagent Volumes for Primer Efficiency and cDNA Integrity Analysis.**

#### 2.4.6 Agarose Gel Electrophoresis

End-Point PCR products were separated on 1.5%-2% agarose gels. Agarose gels were prepared by boiling 1.5-2g agarose (Sigma, UK) in 1X Tris-acetate-EDTA (TAE) buffer (Sigma, UK). Once cooled 3.5 $\mu$ L/100mL ethidium bromide (EtBr) was added to allow DNA visualisation under UV light. Gel was poured in to gel cast and allowed to set in a fume hood at RT. The gel was placed in an electrophoresis tank filled with 1X TAE. Up to 4 $\mu$ L 1kB DNA ladder (NEB, UK) was added to the first well and 10 $\mu$ L of PCR product was added to each well thereafter. Product separation was carried out at 120V for up to 45 minutes and bands were visualised using ChemiDoc Gel Imaging System (Bio-Rad, USA).

#### 2.4.7 Primer Design and Optimization

All primers used in this thesis were designed by Primerdesign Ltd (Primerdesign Ltd, UK) or sequences were obtained from Primer Bank website (<http://pga.mgh.harvard.edu/primerbank/>). Hybridization of the primers to the desired section of DNA was verified using NCBI nucleotide BLAST ([https://blast.ncbi.nlm.nih.gov/Blast.cgi?PAGE\\_TYPE=BlastSearch](https://blast.ncbi.nlm.nih.gov/Blast.cgi?PAGE_TYPE=BlastSearch)).

For each primer set, pairs were diluted to 10 $\mu$ M final concentration (10 $\mu$ L sense primer, 10 $\mu$ L antisense primer and 80 $\mu$ L H<sub>2</sub>O). End Point PCR was used as described above (2.4.6) to assess a range of different annealing temperatures for each primer pair to identify optimal working conditions. For each primer pair, a standard curve was prepared using 3-fold serial dilutions of a mixture of cDNA from RNA extracted from human TM cells. Dilutions were made for at least 5 concentrations ranging from 300ng-4ng to ensure complete coverage of the range of expected gene expression. Each concentration was performed in duplicate. Slope of the standard curve and q-PCR efficiency for each primer pair was determined. Primer pairs with an efficiency of 1.8-2 were accepted. Melt curve analyses were also used to determine efficiency and specificity of primer pairs. Glyceraldehyde-3-phosphate dehydrogenase (GAPDH) is a commonly used housekeeping gene for mRNA expression analyses<sup>383</sup> and is stably expressed in TM cells. GAPDH expression

is not affected by TGF- $\beta$ 2 or corticosteroid treatments and was therefore chosen as a reference gene for mRNA expression analyses and protein analysis experiments.

miRNA primer assays were obtained from Qiagen (miScript Primer Assays, Qiagen, UK) for the detection of miRNA targets: hsa-miR-143-3p (MS00003514, miScript Primer Assay, Qiagen, UK), hsa-miR-145-5p (MS00003514, miScript Primer Assay, Qiagen, UK) and hsa-miR-4328 (MS00021665, miScript Primer Assay, Qiagen, UK). Small nucleolar RNA 61 (MS00033705, miScript Primer Assay, Qiagen, UK) (SNORD61) was used as a reference gene for miRNA q-PCR experiments as other small RNAs have relevant expression levels to miRNAs and are likely to have similar behaviour during extraction and reverse transcription compared to longer transcripts<sup>384</sup>.

#### 2.4.8 Relative quantification real-time PCR (q-PCR)

Relative quantification ( $\Delta\Delta C_t$  method) real-time PCR was performed to investigate the expression of specific mRNA targets in normal TM and GTM samples. q-PCR was performed on LightCycler480 or LightCycler96 instruments (Roche, UK) according to manufacturers' specifications. Unlabelled gene-specific primers listed in Table 2.9 and PrecisionPLUS SYBR q-PCR Master Mix (Primerdesign Ltd, UK) or microRNA probes listed in Table 2.10 (Qiagen, UK) and miScript SYBR<sup>®</sup> Green PCR mix with miScript universal primer (miScript primer assays, Qiagen, UK) were used in q-PCR reactions as below (Table 2.7 and Table 2.8).

<b>PrecisionPLUS SYBR q-PCR</b>	
<b>Components</b>	<b>Volume</b>
PrecisionPLUS SYBR Master Mix	5µL
H <sub>2</sub> O	3µL
cDNA Template (1µg)	1µL
Primer Pair (1:10)(1µM final concentration)	1µL
<b>Total Volume</b>	<b>10µL</b>

**Table 2.7: mRNA q-PCR Reagent Volumes.**

<b>miScript SYBR®Green PCR Mix</b>	
<b>Components</b>	<b>Volume</b>
2x Quantitect SYBR®Green Master Mix	12.5µL
10x miScript Universal Primer	2.5µL
10x miScript Primer Assay	2.5µL
H <sub>2</sub> O (RNase free)	Up to 7.5µL
cDNA Template (0.5-1.0ug)	Up to 7.5µL
<b>Total Volume</b>	<b>25µL</b>

**Table 2.8: miRNA q-PCR Reagent Volumes.**

Primer I.D	Primer Sequence
EDN1	F;5'CCAGGAGCTCCAGAAACAG3' R;5'GAGCAGGAGCAGCGCTT3'
NOX4	F;5'CACAGACTTGGCTTTGGATTTC3' R;5'GGATGACTTATGACCGAAATGATG3'
FSTL3	F;5'GACTTCATCAGGAACAAGTGGTC3' R;5'AGGTCCGTAGCCATGAGGAT3'
FNDC1	F;5'GACTTCATCAGGAACAAGTGGTC3' R;5'AGGTCCGTAGCCATGAGGAT3'
KANK4	F;5'CATCTTCAGCCTTGAATTCCTCAT3' R;5'TTCTAATGTGCTAATGTGCTCCTG3'
LDLRAD4	F;5'AAGAGTTGGAGCACAGGCTT3' R;5'TTACAGACCAGCGAACCAAGA3'
RASL11B	F;5'CCTCACCAAACGATTCATCGG3' R;5'ACCTGGAGTGTCTTGAACCTG3'
WNT2B	F;5'TTGGAGTGGTAGCCATAAGCAT3' R;5'TTGAACGCTGACTGTGTAGGT3'
ATP10A	F;5'TCGGCATTGTCATCTACGCA3' R;5'AGGAGCAGGACACACCAGA3'
PMEPA1	F;5'TTAGACTCCGCTCTTGTTCTCC3' R;5'ATGCTCTCCTCTGGTCACCT3'
CDKN2B	F;5'GCAAGCCTGTCTGAGACTCA3' R;5'ACACACTCCTAAATATCCCTGGAA3'
CDKN2B-AS1	F;5'CCACATCAATGATGAAGCCAGAA3' R;5'TTGATCTCTGCTGTTGAATCAGAAT3'
OSR2	F;5'TCTCCACACAAATGTCCCACA3' R;5'TTTCGCCTGAACACTTTGCC3'

DACT1	F:5'CTTCATGCTGTGGCTGTGC3' R:5'GGACGGTAAGGAACTGTCTGT3'
LEFTY2	F:5'GGTGGTCTTAATGTAGGTCTTAACTT3' R:5'AGACAGGAAATGGAAGGACACA3'
FST	F:5'AGGCAAGATGTAAAGAGCAGC3' R:5'CAGTAGGCATTATTGGTCTGGTC3'
PDPN	F:5'AACCAGCGAAGACCGCTATAA3' R:5'CGAATGCCTGTTACTGTTGA3'
SERPINB2	F:5'TCCTGGGTCAAGACTCAAACC3' R:5'CATCCTGGTATCCCCATCTACAG3'
FKBP5	F:5'CTCCCTAAAATTCCCTCGAATGC3' R:5'CCCTCTCCTTTCCGTTTGGTT3'
MMP-1	F:5'ACGGATACCCCAAGGACATCT3' R:5'TCAGAAAGAGCATCGATATG3'
PTK2B	F:5'CCCCTGAGTCGAGTAAAGTTGG3' R:5'GATACGCACGTCCTCCTTTTC3'
RGCC	F:5'CGCCACTTCCACTACGAGG3' R:5'CAGCAATGAAGGCTTCTAGCTC3'
ZBTB16	F:5'CCTCAGACGACAATGACACGG3' R:5'CTCGCTGGAATGCTTCGAGAT3'
VEGFC	F:5'GAGGAGCAGTTACGGTCTGTG3' R:5'TCCTTTCCTTAGCTGACACTTGT3'
GR $\alpha$	F:5'GAAGGAAACTCCAGCCAGAA3' R:5'TAAGGGGCTCTACAATCGAC3'
GR $\beta$	F:5'TGACTCTACCCTGCATGTACGACCA3' R:5'CTATTTTTGAGCGCCAAGATTGTT3'
$\alpha$ -SMA	F:5'CCGACCGAATGCAGAAGGA3' R:5'ACAGAGTATTTGCGCTCCGAA3'
GAPDH	F:5'CGAGCCACATCGCTCAGACACC3' R:5'GGTCAATGAAGGGGTCATTGATGGCAAC3'

**Table 2.9: Unlabelled Gene Specific Human Primers.**

<b>miRNA</b>	<b>Probe Sequence</b>
hsa-miR-143-3p (MIMAT0000435)	5'UGAGAUGAAGCACUGUAGCUC
hsa-miR-145-5p (MIMAT0000437)	5'GUCCAGUUUCCAGGAAUCCCU
hsa-miR-4328 (MIMAT0016926)	5'CCAGUUUCCAGGAUU
SNORD 61	Unavailable; Transcript: NR_002735 (73bp)

**Table 2.10: miScript Universal Primer Sequences.**

cDNA template was added separately to corresponding wells of a 96 well semi-skirted PCR plate (Starlab, UK) followed by a master-mix as above. The run methods for mRNA and miRNA detection are outlined in Table 2.11 and Table 2.12, respectively.

Programme Name	Cycles	Temperature (°C)	Time (hh:mm:ss)	Ramp Rate (°C/s)
Denaturation	1	95	00:05:00	4.4
Amplification	40			
		95	00:00:10	4.4
		60	00:00:10	2.2
		72	00:00:12	4.4
Melt Curve	1			
		95	00:00:05	4.4
		60	00:01:00	2.2
		97	Continuous	0.11
Cooling	1	40	00:00:30	2.2

**Table 2.11: mRNA RT-q-PCR PrecisionPLUS SYBR Conditions.**

Programme Name	Cycles	Temperature (°C)	Time (hh:mm:ss)	Ramp Rate (°C/s)
Denaturation	1	95	00:15:00	1
Amplification	45			
		94	00:00:15	1
		55	00:00:30	1
		70	00:00:30	1
Melt Curve	1			
		95	00:00:05	4.4
		65	00:01:00	2.2
		97	Continuous	0.11
Cooling	1	40	00:00:30	2.2

**Table 2.12: miRNA q-PCR Quantitect SYBR Conditions.**

## 2.5 RNA-Seq and MicroArray Analyses

### 2.5.1 Bioinformatics Methodology

#### Exiqon RNA-Seq Analysis

RNA-Seq experiments were performed by Exiqon (Exiqon, Denmark) and Dr. David Simpson (Queens, University Belfast, QUB) details of which are outlined in Chapter 3, Chapter 4 and Chapter 5. Following RNA-Seq intensity correction and base calling (into BCL files), FASTQ files were generated using appropriate *bcl2fastq* software (Illumina Inc, UK), which includes quality scoring of each individual base in a read. Subsequently, data was separated for paired-end reads to determine whether the second read significantly differs from the first in terms of overall quality.

Data analysis was initially performed by Exiqon (Exiqon, Denmark) for Chapters 3 and 4. The components of Exiqon next generation sequencing (NGS) RNA-Seq analysis pipeline include *Bowtie2* (v2.2.2), *Tophat* (v.2.0.11) and *Cufflinks* (v2.2.1). *Tophat* is a fast splice junction mapper for RNA-Seq reads. *Tophat* was used to align the sequencing reads to the reference genome (*h.sapiens*, hg19/GRC37, UCSC Genome Browser) using the sequence aligner *Bowtie2*. *Tophat* was also utilised to identify splice junctions for both known and novel transcripts from the sequence alignments.

*Cufflinks* receives alignment results from *Tophat* and it uses them to assemble the aligned sequences into transcripts, thus constructing a map of the transcriptome. To guide the assembly process, an existing transcript annotation was used. In addition, Exiqon performed fragment bias correction which seeks to correct for sequence bias during library preparation. *Cufflinks* then assembled aligned reads into different transcript isoforms based on exon usage and also determined the transcriptional start sites (TSSs).

It is necessary to build linear model groups with samples paired by donor eye. The *limma* functionality of *edgeR* is ideal for this but requires counts of mapped reads as an input. Counts were generated using *featureCounts* and

inference of differential expression was by generalised linear model likelihood ratio test (glmLRT) implemented by *edgeR*.

### IPA RNA-Seq Analyses

Following analysis by Exiqon, further functional analysis was performed by Dr. Brian Lane (University of Liverpool), through Ingenuity Pathway Analysis (IPA). IPA v01-08 (Qiagen, UK) Core and Comparison analyses were performed with lists of differentially expressed genes (DEGs) generated from expression analyses that included gene name, false discovery rate (FDR)  $p$ -value and log<sub>2</sub> fold change. Unless indicated, FDR  $p$ -value threshold of 0.01 was used throughout experiments (chapter 3, 4, and 5) to select lists of DEGs for analysis. Core analysis output included ranked lists of Canonical Pathways (processes with biological or molecular biology significance defined by the Ingenuity Knowledge Base) and single molecule UpStream Regulators of a single DEG supplied. The canonical pathways and upstream regulators identified in two or more Core analyses were compared in Comparison analyses. Comparisons were performed by hierarchical clustering based on process enrichment score or activation z-score.

Fishers exact tests reported as a likelihood value ( $-\log(p\text{-value})$ ) were performed to assess canonical pathway enrichment. Canonical pathways and UpStream Regulators were ranked by activation z-score which is a weighted statistic that correlates measured gene expression with the expected direction of expression of the DEG list supplied. The activation score is equivalent to a zero-centred normal distribution z-score therefore only scores of  $\pm 1.96$  were regarded as significant and the sign of the z-score indicates the direction of regulation of the process.

### R/Bioconductor RNA-Seq Analyses

Analyses using named Bioconductor packages (v3.6;<http://www.bioconductor.org>) were conducted in R v 3.4.3 (<http://cran.t-project.org>), statistical programming environment. Heat maps were generated using the Bioconductor package *pheatmap*, using a Pearson Correlation distance and a complete agglomeration method, with a gene-wise scaled and centred log<sub>2</sub>

transformed data. Principal component analysis (PCA) was used to identify the main components of variation in a data set. By identifying three principal components, large data sets can be visualised to demonstrate the naturally arising sample classes based on their expression profiles. The R package, *prcomp*, was used to perform PCA on data grouped by samples in columns and genes in rows. The first principal components were visualised using the R package 3dplot.

### 2.5.2 Statistical Analyses

Large numbers of statistical tests may result in false positives regardless of the null hypothesis being true. Procedures for controlling the false positive rate are commonplace in transcriptomics, the most notable being the Bonferroni correction. Bonferroni correction is used to control for study-wide error rate. Bonferroni critical  $P$  ( $\alpha$ ) is calculated by dividing the study-wide error rate by the number of tests performed. Typically critical  $P$  level for significance is set to 0.05, however these false positives can be controlled for by setting critical  $P$  levels at a lower value. Bonferroni correction is appropriate only when a single false positive in a set of tests would arise. Bonferroni correction is limited by the problem that error rate control cannot be localised to individual tests, and this correction does not distinguish between exploratory and data-driven testing. In this thesis, the Benjamini-Hochberg method derived from limiting false discovery rates to control error rates in multiple comparisons was used.

Benjamini-Hochberg controls the false discovery rate, i.e. the portion of significant results that are actually false positives. Following next generation sequencing and microarrays the false discovery rate was set at 0.01. Benjamini-Hochberg method ranks discoveries' individual  $p$ -values from smallest to largest and ranked on a scale of  $1-\infty$  respectively. Individual  $p$ -values are compared to its Benjamini Hochberg critical value,  $(i/m)Q$ , where  $i$  is the rank,  $m$  is the total number of tests, and  $Q$  is the chosen FDR (0.01). The largest  $p$ -value that has  $p < (i/m)Q$  is significant, and all smaller  $p$ -values are also significant.

## **Chapter 3**

# **Transforming Growth Factor- $\beta$ 2 Modulates Gene Expression in the Human Trabecular Meshwork**

### 3.1 Introduction

All TGF- $\beta$  isoforms are expressed within the eye and localisation studies have identified the presence of TGF- $\beta$ 2 in the anterior segment of both healthy and diseased eyes<sup>385,386</sup>. TGF- $\beta$ 2 and related family members have been implicated in ocular disease and TGF- $\beta$ 2 signalling plays a central role in fibrotic ocular diseases and wound healing<sup>387,388</sup>. Physiologically, TGF- $\beta$  is produced by the ciliary epithelium and lens epithelium in its latent form<sup>389</sup>. Aqueous humour (AH) bathes many tissues in the anterior segment of the eye; the corneal endothelium, trabecular meshwork, and iris<sup>390</sup>. The normal physiological AH contains various cytokines and growth factors of which TGF- $\beta$  is predominant<sup>391,392</sup>.

Multiple studies have identified elevated concentrations of TGF- $\beta$ 2 in the AH of primary open angle glaucoma (POAG) patients<sup>393-396</sup>. TGF- $\beta$ 2 is a major driver of extracellular matrix (ECM) secretion and deposition<sup>220</sup>, and in POAG it has been unequivocally shown that the increased concentration of TGF- $\beta$ 2 in the AH drives ECM expression and deposition in the trabecular meshwork (TM) cells<sup>397</sup>. Alterations within the ECM can restrict the outflow across the TM, providing a physical resistance affecting the contractile properties of the TM<sup>157</sup>, which in turn results in elevated intraocular pressure (IOP)<sup>119</sup>. The specific molecular changes which lead to increased outflow resistance in the TM in POAG are unknown, however, there are two non-exclusive hypotheses or models: the ECM hypothesis and the contractility hypothesis<sup>130,397</sup>. In glaucoma the actin meshwork forms a cross-link pattern increasing the rigidity and contractility of the TM<sup>253</sup>, which leads to increased outflow resistance in the TM<sup>398-400</sup>. The alternative hypothesis proposes that changes in the ECM of the TM are related to elevated IOP<sup>397</sup>. The most characteristic structural change is an increase in ECM, with an accumulation of "plaque material"<sup>119,156,401</sup>, which correlates with the degree of axonal damage in the optic nerve<sup>130</sup>. Perfusion of normal TM in organ culture with TGF- $\beta$ 2 also induces changes in the ECM and pathological changes similar to those seen in the TM of POAG patients<sup>402</sup>.

TGF- $\beta$ 2 driven alterations in TM physiology are clinically relevant as elevated IOP is currently the only modifiable risk factor for POAG and is a key player in the disease pathogenesis<sup>52</sup>. There is overwhelming evidence from several prospective randomised multi-centre studies showing that reduction of IOP is neuro-protective, in the sense that it delays or even prevents the structural and functional damage of optic nerve axons in glaucoma<sup>403,404</sup>. Understanding the role of TGF- $\beta$ 2 in driving structural and functional alterations in the outflow pathway is essential to develop new therapies based on the modulation of TGF- $\beta$ 2 signalling in the trabecular meshwork<sup>164</sup>.

Gene expression studies are essential in further developing our understanding of the role TGF- $\beta$ 2 may play in POAG. Three microarray studies have analysed alterations in gene expression in the TM induced by TGF- $\beta$ 2 in cultured human TM cells<sup>405,406</sup>; none of these studies made the complete datasets publicly available. Oligonucleotide Human Genome U133A arrays (Affymetrix) were used to study alterations in gene expression of 22,215 genes in cultured human TM cells from 5 donors treated for 72hrs with 1ng/mL of TGF- $\beta$ 2<sup>405</sup>. Significant differential gene expression was based on a twofold fold change: 19 genes were up-regulated, and 2 genes down-regulated. Proteomic analysis of the same cells was performed with two-dimensional electrophoresis and mass spectrometry. This initial microarray and proteomics study identified alterations in ECM components and cell cytoskeletal proteins<sup>405</sup>.

Using the same U133A Affymetrix array, and RNA extracted from cultured TM cells treated with 300pM TGF- $\beta$ 2 for 72hrs, alterations in several genes involved in growth factor signalling, ECM homeostasis and cell cytoskeleton were identified<sup>407</sup>. 16 genes were found to be differentially expressed following treatment with TGF- $\beta$ 2; these included; vascular endothelial growth factor (VEGF), follistatin-like 3 (FSTL3), fibroblast growth factor 5 (FGF5), latent binding protein-1 and -2 (LTBP1 and 2), and SMAD7<sup>407</sup>. Subsequently, using a more comprehensive array (Affymetrix GeneChip® Human Genome U133 Plus 2.0 Array) containing 54K probe sets, on RNA from cultured TM cells from donors with glaucoma (n=3) treated with 5ng/mL of TGF- $\beta$ 2 for 16 hours, a twofold or greater up-regulation in

ECM-related genes compared to untreated control cells was detected<sup>406</sup>. The full dataset was not made publicly available, however examples of the altered genes included thrombospondin 1, plasminogen activator inhibitor (PAI) – 1, collagen 4A1 (COL4A1) and ADAM metallopeptidase with thrombospondin type 1 motif 5 (ADAMTS5)<sup>406</sup>.

Across all three microarray studies common genes were limited to v-maf musculoaponeurotic fibrosarcoma oncogene homolog (MAF), PAI-1 and LTBP1<sup>244,405,406</sup>. Several key genes previously identified using q-PCR in prioritised targets were not detected in these microarray studies, although there is significant evidence they are regulated by TGF- $\beta$  in the human TM. Among these were, thrombospondin-1, fibronectin, collagen type VI, tissue transglutaminase,  $\alpha\beta$ -crystallin, myocillin, connective tissue growth factor (CTGF) and TGF- $\beta$ 1<sup>408–413</sup>.

At their core, microarrays are simple devices to simultaneously measure the relative concentration of many different DNA or RNA sequences and they are not without their limitations. Firstly, arrays provide indirect measures of relative concentration. Due to kinetics of hybridisation, the signal level at a given location on the array is not linearly proportional to concentration of the species hybridising to the array. Secondly, especially with respect to complex mammalian genomes, it is often difficult to design arrays in which multiple DNA/RNA sequences will not bind to the same probe on the array. This is particularly problematic for gene families and genes with splice variants<sup>414</sup>. Finally, microarrays can only detect sequences that they have been designed to detect; novel and unknown transcripts cannot be identified through microarrays. This is highlighted in the data obtained for fibronectin expression obtained in the microarray studies<sup>244,405,407</sup>. All three studies failed to detect more than a two-fold upregulation in fibronectin<sup>244,405,407</sup> despite multiple previous studies reporting a significant increase in fibronectin expression and protein levels in response to TGF- $\beta$ 2 treatment of human cultured TM cells<sup>415</sup>. Fibronectin undergoes high levels of alternative splicing generating up to 20 protein isoforms and limited probe coverage in the microarray design<sup>244</sup>.

RNA-Seq technology offers significant benefits over previous microarray technologies. In RNA-Seq millions of RNAs are randomly sampled and sequenced

simultaneously. The sequence identifies each 'read' and a digital expression value is obtained for each gene by counting the number of reads assigned to it. Both known and novel transcripts and splicing events can be detected. This technology offers increased specificity and sensitivity, for enhanced detection of genes, transcripts, and differential expression. With array hybridisation technology, gene expression measurement is limited by background at the low end and signal saturation at the high end. RNA-Seq technology quantifies discrete, digital sequencing read counts, offering a broader dynamic range. RNA-Seq provides unbiased detection of novel transcripts and the sequencing coverage depth allows for easier detection of rare and low-abundance transcripts<sup>416</sup>.

### 3.2 Aim

The aim of this study was to employ RNA-seq to investigate genome-wide alterations in the transcriptome of normal trabecular meshwork cells in the presence or absence of TGF- $\beta$ 2 and detect pathophysiological mechanisms underlying glaucoma.

## 3.3 Materials and Methods

### 3.3.1 Sample Collection, Preparation, and Tissue Culture Establishment

Cadaveric eyes were provided by the Liverpool Research Eye Bank and handled in accordance to the tenets of the Declaration of Helsinki (Ethics Code; RETH000833). Globes were excluded if the maximum post-mortem time exceeded 48hours. Human trabecular meshwork cells were cultured directly from the anterior segment using the explant method described previously (2.1.3). Cells were maintained in DMEM-low glucose (Sigma, UK) supplemented with 10% fetal calf serum (Bio Sera, UK), 2mM L-glutamine (Sigma, UK), Pen/Step (Sigma, UK), and 2.5ug/mL Fungizone (Amphotericin B, Sigma, UK). Samples were incubated at 37°C (5%CO<sub>2</sub> and 95% humidity) for 7-14 days with a medium changed every 2 days ensuring not to disturb the explant. Glaucomatous TM samples (n=3) were also used in this experiment and cultured as above. Specific culture techniques are outlined in Chapter 2 (2.3).

<b>Donor I.D</b>	<b>Age</b>	<b>Sex</b>	<b>Medical History</b>
LGP-1	57	Male	No Glaucoma History
LGP-2	65	Male	No Glaucoma History
NTM002	57	Male	No Glaucoma History
NTM009	57	Male	No Glaucoma History
NTM720	64	Male	No Glaucoma History
NTM020	88	Female	No Glaucoma History
GTM 304-04	74	Female	POAG
GTM 730-03	88	Male	POAG
GTM 034	86	Male	POAG

**Table 3.1: Human TM Cell Donor Information**

### 3.3.2 Characterisation of Human Trabecular Meshwork Cells

The phenotype of the cultured cells was assessed on the basis of the distinctive morphology of human TM cells and positive immunofluorescence (IF) staining of caveolin1 (CAV1), caveolin2 (CAV2), aquaporin 1 (AQP1), and myocilin (MYOC). Experimental details are highlighted in section 2.2.1.

### 3.3.3 TGF- $\beta$ 2 Stimulations

All confluent cells were mycoplasma tested as described previously (2.1.5) prior to experimentation. Human TM cells between passages 5 and 7 were grown to 80% confluence and growth arrested using serum free medium prior to stimulation. Cells were stimulated with recombinant human TGF- $\beta$ 2 (R&D Systems, UK) at a concentration of 5ng/mL for 4 hours or 24hours. Vehicle control cells were stimulated with equal volumes of 4mM HCl and 0.1%tv BSA solution. Treatment time points and concentration were determined based on preliminary experiments which evaluated the activation of the TGF- $\beta$  signalling pathway with 1ng/mL, 5ng/mL and 10ng/mL TGF- $\beta$ 2 over a time period of 0-72 hours. Following 4 and 24 hours of stimulation total RNA was extracted (2.4.1).

### 3.3.4 Total RNA Extraction and QC

Total RNA from human cultured trabecular meshwork cells was isolated using the Qiagen Universal All Prep kit (Qiagen, UK) as per manufacturers' specifications, described in (2.4.1). Total RNA was quantified initially on the Nanodrop-2000, and quality was determined by the Bioanalyser 2100 as described in (2.4.2 and 2.4.3 respectively).

### 3.3.5 RNA-Seq of Cultured Normal Human Trabecular Meshwork Cells

#### 3.3.5.1 Template Preparation, rRNA Depletion, and cDNA Library Construction, Purification and QC

All mRNA sequencing experiments were conducted at Exiqon Services, Denmark. Two groups of mRNA libraries were prepared: a group of 5 control human trabecular meshwork samples (referred to as 'CK'\_group in the remainder of Chapter 3) and a group of 5 treated samples (referred to as 'TK'\_group in the remainder of Chapter 3). The starting material of total RNA (100ug) was enriched for mRNA using the oligodT bead system and the isolated mRNA was enzymatically fragmented. First and second strand synthesis were performed and the double stranded cDNA was purified (AMPure XP, Beckman Coulter, Denmark). The cDNA was end repaired, 3' adenylated and Illumina sequencing adaptors ligated onto the fragments ends. Following this the mRNA stranded libraries were pre-amplified with PCR and purified (AMPure XP).

Libraries size distribution was validated and quality was inspected on a Bioanalyser high sensitivity DNA chip (Agilent Technologies, UK). High quality libraries were quantified using q-PCR, the concentration normalised and the samples pooled according to the project specification (number of reads).

The library pools were re-quantified with q-PCR and optimal concentration of the library pool was used to generate the clusters on the surface of a flowcell before sequencing on an instrument using Nextseq 500, High Output sequencing kit (51 cycles) according to the manufacturer instructions (Illumina Inc., USA).

#### 3.3.6 RNA-Seq Data Analysis

Following sequencing, intensity correction and base calling (into BCL files), FASTQ files were generated using appropriate bcl2fastq software (Illumina Inc.) which includes quality scoring of each individual base in a read. At this stage the data was separated for paired-end reads to determine whether the second read significantly differs from the first in terms of overall quality.

Data analysis was performed by Exiqon (Exiqon, Denmark). The components of Exiqon NGS RNA-Seq analysis pipeline include *Bowtie2* (v.2.2.2), *Tophat* (v2.0.11) and *Cufflinks* (v2.2.1) as described in Chapter 2 (2.5.1).

As we were comparing groups, *Cuffdiff*, normally used for unpaired samples to calculate FPKM (number of fragments per kilobase per million mapped fragments) was replaced with featureCounts.

featureCounts was used to calculate the counts of mapped reads in specific genes when groups with paired samples were compared, and generalised linear model likelihood ratio test (glmLRT) implemented by edgeR was used to test differential expression across submitted samples using featureCounts input.

Post processing of *Cufflinks* and *Cuffdiff* was performed using *CummeRbund* and Bioconductor software to generate visual representations of sequencing results.

### 3.3.7 mRNA-Seq Data Validation

Validation of RNA samples (CK\_group and TK\_group) was performed using Primer Design Ltd primer assays (Primer Design Ltd, UK). Specific q-PCR conditions are outlined in Chapter 2 (2.47). q-PCR was performed for selected significantly altered differentially expressed genes. 1ug of total RNA was reverse transcribed into cDNA using miScript II RT (Qiagen, UK) kit according to manufacturers' specifications (2.4.5). Real time analysis was performed using Primer Design Ltd. custom primers for target genes (see Table 3.2 below). q-PCR was performed on a LightCycler®480 real-time PCR system (Roche Diagnostics, Switzerland). All mRNA were measured at  $C_T$  threshold levels and normalised with the average  $C_T$  values of a reference gene; GAPDH. Values were expressed as fold increase over the corresponding values for control by the  $2^{-\Delta\Delta CT}$  method. Two independent experiments were performed and the average ( $\pm$ SEM) results were calculated using GraphPad software (GraphPad Software, San Diego, USA). Data were expressed as the mean values  $\pm$  SEM and analysed using student t-test. Statistical differences in the mean were considered statistically significant as  $p < 0.05$ .

<b>Primer Name</b>	<b>Sequence</b>
EDN1	<b>F</b> 5'-CCAGGAGCTCCAGAAACAG-3' <b>R</b> 5'-GAGCAGGAGCAGCGCTT-3'
NOX4	<b>F</b> 5'-CACAGACTTGGCTTTGGATTTC-3' <b>R</b> 5'-GGATGACTTATGACCGAAATGATG-3'
FSTL3	<b>F</b> 5'-GACTTCATCAGGAACAAGTGGTC-3' <b>R</b> 5'-AGGTCCGTAGCCATGAGGAT-3'
FNDC1	<b>F</b> 5'-GACTTCATCAGGAACAAGTGGTC-3' <b>R</b> 5'-AGGTCCGTAGCCATGAGGAT-3'
KANK4	<b>F</b> 5'-CATCTTCAGCCTTGAATTCCTCAT-3' <b>R</b> 5'-TTCTAATGTGCTAATGTGCTCCTG-3'
ATP10A	<b>F</b> 5'-TCGGCATTGTCATCTACGCA-3' <b>R</b> 5'-AGGAGCAGGACACACCAGA-3'
WNT2B	<b>F</b> 5'-TTGGAGTGGTAGCCATAAGCAT-3' <b>R</b> 5'-TTGAACGCTGACTGTGTAGGT-3'
LDLRAD4	<b>F</b> 5'-AAGAGTTGGAGCACAGGCTT-3' <b>R</b> 5'-TTACAGACCAGCGAACCAAGA-3'
PMEPA1	<b>F</b> 5'-TTAGACTCCGCTCTTGTTCTCC-3' <b>R</b> 5'-ATGCTCTCCTCTGGTCACCT-3'
CDKN2B	<b>F</b> 5'-GCAAGCCTGTCTGAGACTCA-3' <b>R</b> 5'-ACACACTCCTAAATATCCCTGGAA-3'
CDKN2B-AS1	<b>F</b> 5'-CCACATCAATGATGAAGCCAGAA-3' <b>R</b> 5'-TTGATCTCTGCTGTTGAATCAGAAT-3'
RASL11B	<b>F</b> 5'-CCTCACCAAACGATTCATCGG-3' <b>R</b> 5'-ACCTGGAGTGTCTTGAACCTG-3'

OSR2	<b>F</b> 5'-TCTCCACACAAATGTCCCACA-3' <b>R</b> 5'-TTTCGCCTGAACACTTTGCC-3'
LEFTY2	<b>F</b> 5'- GGTGGTCTTAATGTAGGTCTTAACTT-3' <b>R</b> 5'-AGACAGGAAATGGAAGGACACA-3'
DACT1	<b>F</b> 5'-CTTCATGCTGTGGCTGTGC-3' <b>R</b> 5'-GGACGGTAAGGAACTGTCTGT-3'
GAPDH	<b>F</b> 5'-CGAGCCACATCGCTCAGACACC-3' <b>R</b> 5'- GGTCAATGAAGGGGTCATTGATGGCAAC- 3'

**Table 3.2: Primer Design Ltd Primer Assays and Custom GAPDH Primer Pair Sequence.** Custom primer assays were designed by Primer Design Ltd. for RNA-Seq validation. GAPDH reference primer was designed in-house.

## 3.4 Results

### 3.4.1 Characterisation of Human Trabecular Meshwork Cells

Human TM cells were cultured directly from human cadaver eyes collected from donor patients (n=6). The phenotype of the cells was assessed based on the distinctive morphology of human TM cells (Figure 3.1) and positive IF staining of caveolin 1, caveolin 2, aquaporin 1, and myocilin (Figure 3.2 A-F).

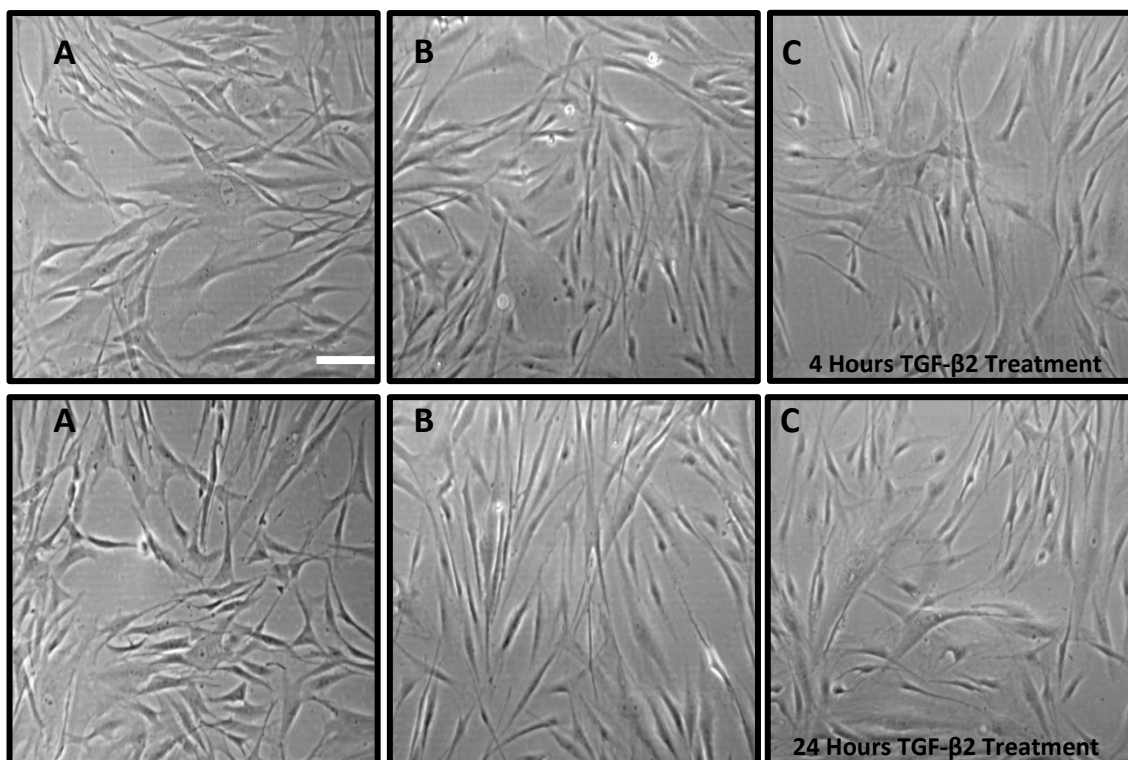


**Figure 3.1: Representative Phase Contrast Microscope Images of Human Cultured TM Cells.** (A) Before TGF- $\beta$ 2 treatment, (B) Post growth arrest, and (C) Post TGF- $\beta$ 2 treatment, at 4 and 24 hours as indicated. Donor: LGP-1; Scale Bar: 20 $\mu$ m; passage; 6. Cultured TM cells are known to grow in a monolayer with no multi-layered growth<sup>417</sup>.

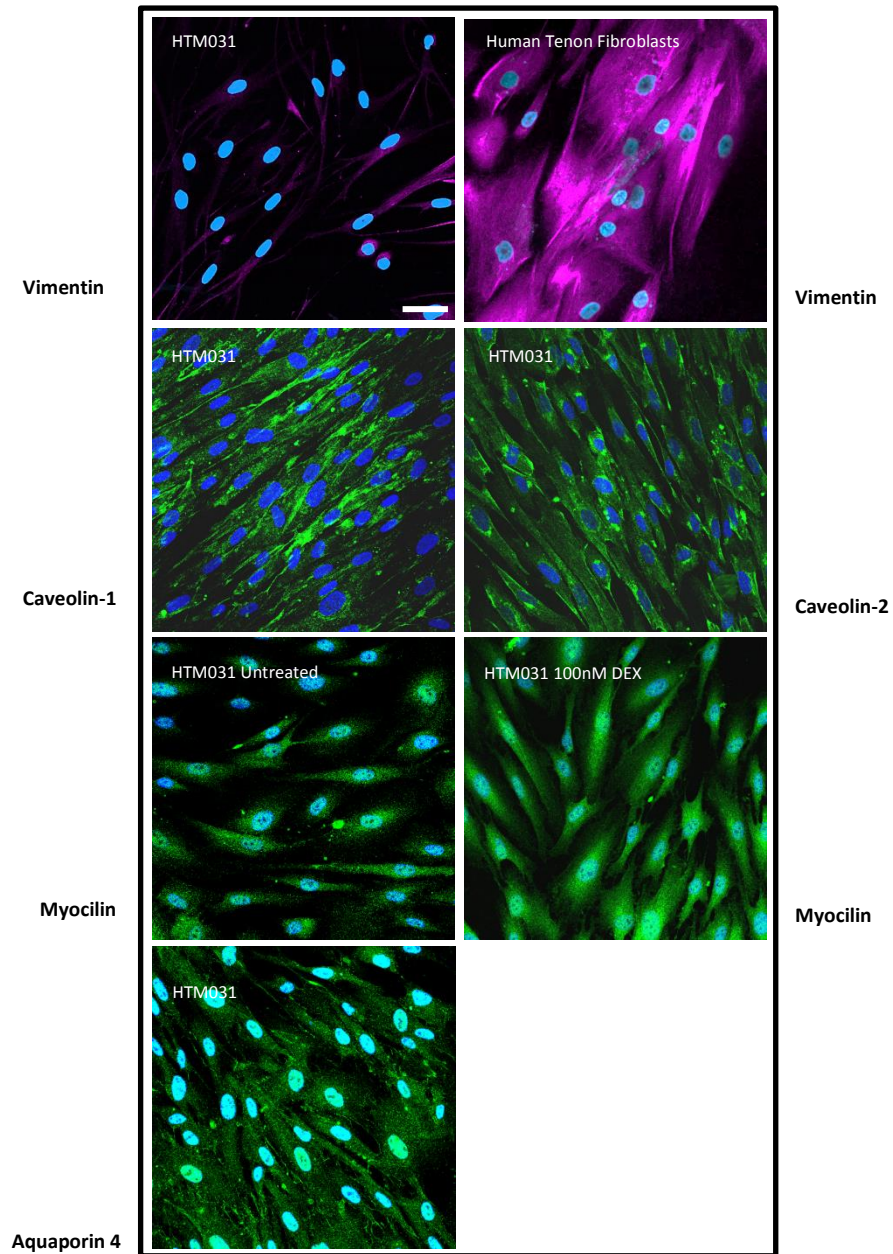


**Figure 3.2: Representative Fluorescent Confocal Microscope Images of Human TM Cells;** (A) Vimentin expression is low in human TM cells in comparison to (B) Vimentin expression in human tenon fibroblasts. (C) Caveolin 1 and (D) Caveolin 2 are expressed in human TM cells with localisation to the cytoplasm and perinuclear region. (E-F) Myocilin expression in human TM cells is induced by dexamethasone stimulation. (G) Aquaporin-4 is expressed in human TM cells, localised to the plasma membrane region. Scale Bar: 20 $\mu$ m.

## 3.4.2 RNA-Seq Analysis of Human Trabecular Meshwork Cells in the Absence or Presence of TGF- $\beta$ 2

### 3.4.2.1 RNA-Seq Summary

Two mRNA libraries (CK\_group and TK\_group) constructed using AMPure XP beads were pooled and sequenced on a flow cell using NextSeq500, High Output sequencing kit to obtain 30 million reads and 50bp paired-end reads. Paired-end reads were separated to determine whether the second read significantly differed from the first in overall quality. Majority of the data had a Q score greater than 30 (one base call in 1000 is predicted to be incorrect). Mapping of sequencing data represents a useful QC step in RNA-Seq analysis pipeline as it can help evaluate quality of samples. For this purpose reads are classified as follows;

**Unmapped Reads:** Reads that do not align to the reference genome (*H.sapiens*, hg19 / GRC37, UCSC Genome Browser), out mapped reads or high abundance reads such as polyA and polyC homopolymers.

**rRNA reads:** RNA reads of ribosomal origin.

**mtRNA reads:** RNA reads of mitochondrial origin.

**Mappable reads:** RNA reads that align to the reference genome (as above).

Table 3.3 shows the total number of reads obtained for each sample and genome mapping for each sample was on average 82%. Uniformity of the samples mapping results suggests that the samples are comparable.

Sample Name	Total Readcount	rRNA(%)	mtRNA(%)	Mapped(%)	Unmapped(%)
CK_Group1	57023686	0.71	5.51	80.13	13.65
CK_Group2	44504091	0.52	2.21	80.21	17.05
CK_Group3	40024297	0.4	2.04	83.82	13.74
CK_Group4	47803322	0.27	4.12	82.29	13.32
CK_Group5	46181400	0.23	4.67	82.07	13.01
TK_Group1	47487795	0.57	4.51	80.4	14.52
TK_Group2	40939102	0.16	1.68	84.8	13.36
TK_Group3	55439358	0.38	1.62	84.05	13.96
TK_Group4	48512081	0.18	2.27	83.66	13.89
TK_Group5	44826263	0.81	3.94	82.06	13.19

**Table 3.3: Summary of the Mapping Results for Each Sample.** Reads from each of the two libraries (CK\_Group and TK\_Group) were extracted based on their unique I.Ds. In total 40-57 million reads per sample were obtained. Based on alignment to the reference genome, *H.sapiens*, hg19 / GRC37, UCSC Genome Browser, the number of identified genes per sample was calculated. Reliability of identified genes increased with the number of identified fragments. All genes were included in statistical comparison of two groups, irrespective of how few calls have been made. Table 3.4 (below), indicates that all samples included in this study have comparable call rates.

Sample Name	Gene	Isoform
CK_Group1	17328	67943
CK_Group2	17368	65624
CK_Group3	16837	65785
CK_Group4	17111	68083
CK_Group5	16855	64011
TK_Group1	17050	65102
TK_Group2	16544	64816
TK_Group3	16146	64874
TK_Group4	16451	63755
TK_Group5	16751	63966

**Table 3.4: Number of Genes and Isoforms Identified in Each Sample.** All genes and isoforms identified in each sample have a fragment count estimation of at least 10 counts per gene.

### 3.4.2.2 Principal Component Analysis

Principal component analysis (PCA) is a method used to identify the main components of variation in a data set. By identifying three principal components, large data sets can be visualised to demonstrate the naturally arising sample classes based on their expression profiles.

The R package, `prcomp`, was used to perform PCA on FPKM transformed counts data from control (CK\_Group) and treated (TK\_Group) cells. The first principal components were visualised using the R package `3dplot`. In Figure 3.3 (below), cells are coloured while donor pairs are represented by spheres of the same size. Samples separate in different regions of the PCA plot corresponding to the principal sources of variation within the experiment. Sample groups in this experiment, CK\_Group and TK\_Group, segregate on the first and second principal component axes, but there is a clear relationship between donor pairs, indicating the need to incorporate donor source as a factor in an expression analysis of this data.

When biological differences between samples are pronounced it can be seen in the primary components of the variation of the data. Samples separate in different regions of the PCA plot corresponding to their biology. Sample groups in this experiment, CK\_group and TK\_Group, tend to cluster on the primary component and sample cluster pairs on the secondary component.

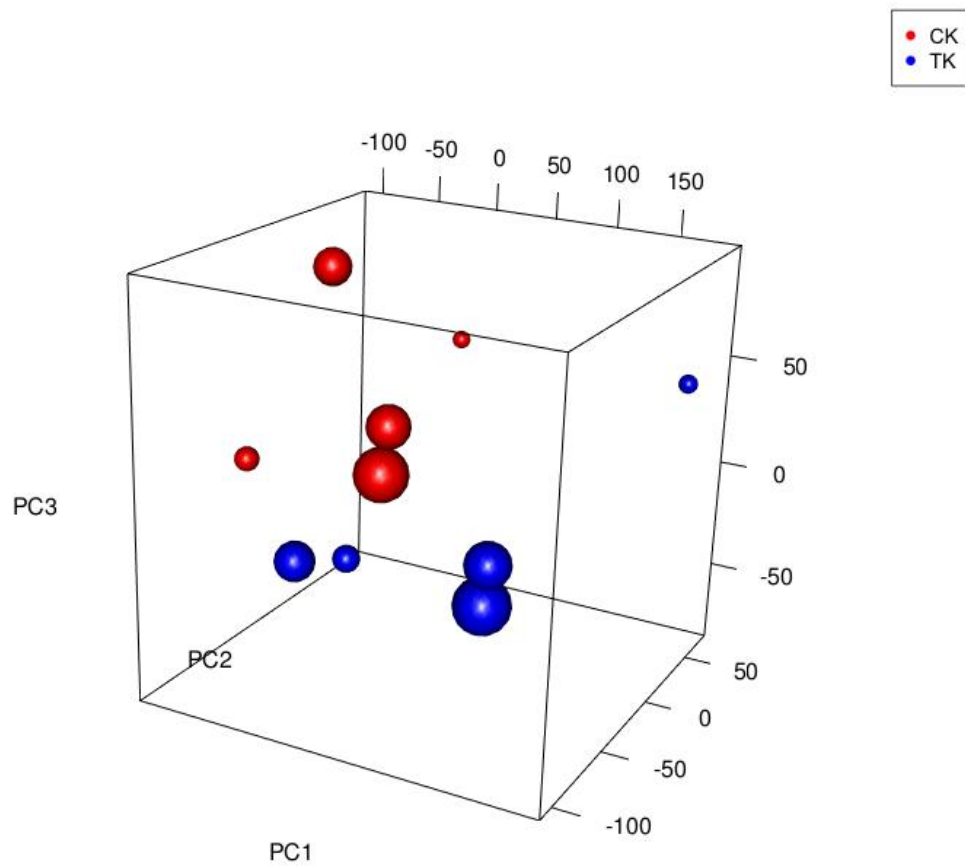


**Figure 3.3: Principal Component Analysis of RNA-Seq Data for Control Untreated TM Cells and TGF- $\beta$ 2 Treated TM Cells.** The PCA was performed on all samples passing QC using the top 500 genes that have the largest coefficient of variation based on FPKM counts. Cell treatments are coloured according to the key and donor pairs are represented by spheres of the same size. Based on normalised FPKM (abundance) for each gene for each sample.

### 3.4.2.3 Heat Map and Unsupervised Clustering

Heat maps were generated using the Bioconductor package 'pheatmap' from FPKM counts of control (CK\_Group) and treated (TK\_Group) cells, using a Pearson Correlation distance and a complete agglomeration method, with gene-wise scaled and centred log2 transformed FPKM count data.

The heat map diagram below (Figure 3.4) shows the results of the two-way hierarchical clustering of RNA transcripts and samples. It includes 500 genes based on the false discovery rate (FDR)  $p$ -value in the control (CK\_Group) vs treated (TK\_Group) expression analysis. Each row represents one gene and each column represents one donor. The colour represents relative expression level of transcript across all donors. The colour scale is shown below; orange represents an expression level above the mean; blue represents an expression level below the mean.

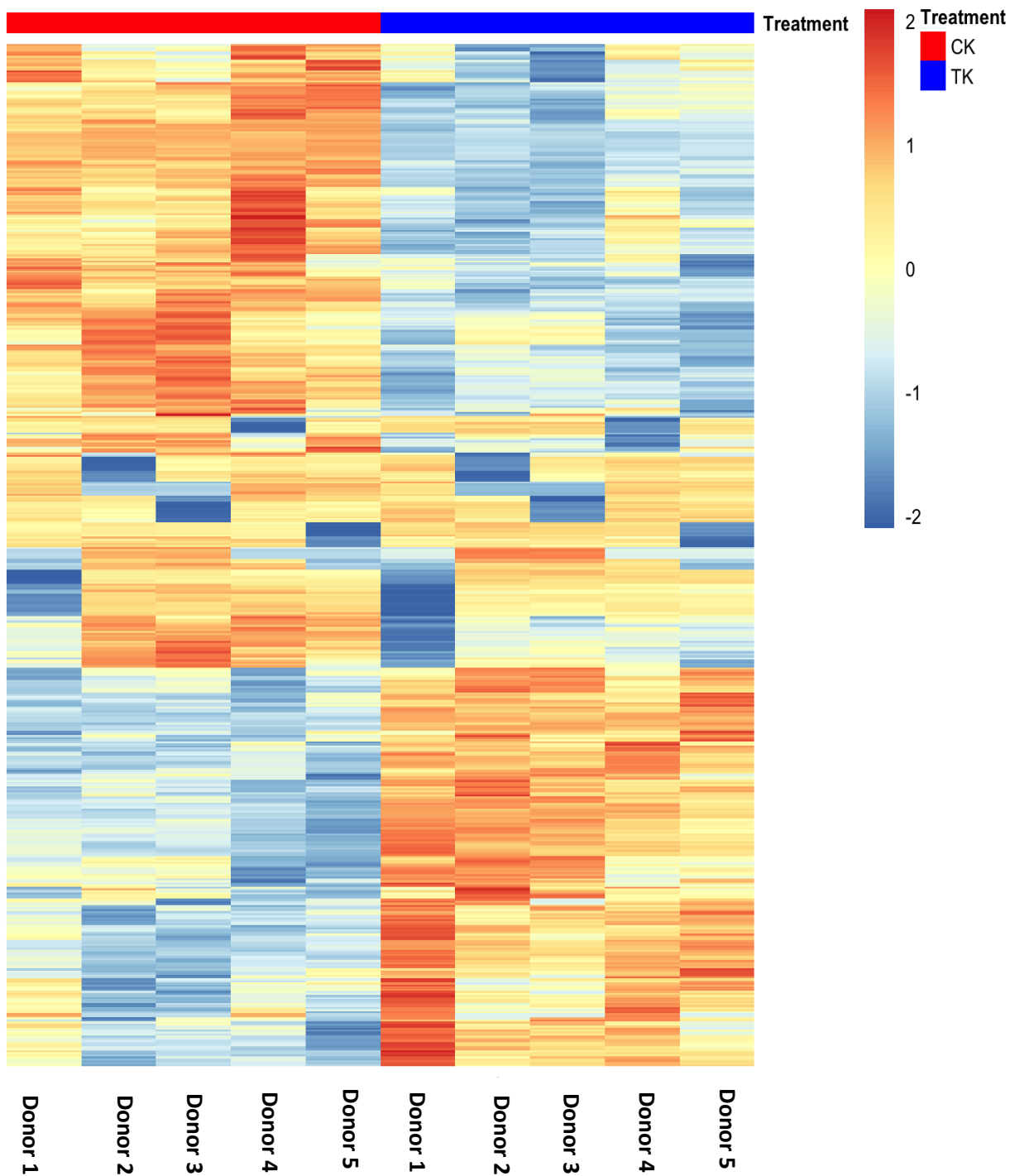


**Figure 3.4 Heat Map and Unsupervised Clustering of Human TM Cells Treated with TGF- $\beta$ 2.** Hierarchical clustering by sample and transcripts was performed on all samples passing the QC using the top 500 genes that have the largest coefficient of variation based on FPKM counts.

### 3.4.3 Functional Analysis of Gene Pathways Involved in TGF- $\beta$ 2 Stimulation of Human Trabecular Meshwork Cells

#### 3.4.3.1 Differentially Expressed Genes in Human Trabecular Meshwork Cells in the Presence or Absence of TGF- $\beta$ 2 Obtained from RNA-Seq Analysis

The top 500 differentially expressed genes were ranked by false discovery rate (FDR), the most significantly altered based on their FDR are shown in Appendix (8.4). From the top 500 DEGs based on FDR the 50 most up- and down-regulated genes were ranked by LogFC and are shown in Table 3.5 and 3.6 respectively.

Gene ID	Gene Name	LogFC
<i>Up-Regulated Genes</i>		
KANK4	KN Motif and Ankyrin Repeat	11.08
LINC00312	Long Intergenic Non-Protein Coding RNA 312	9.65
C4orf26	Chromosome 4 Open Reading Frame 26	9.39
ISLR2	Immunoglobulin Superfamily Containing Leucine	7.91
LDLRAD4	Low Density Lipoprotein Receptor Class A Domain Containing 4	7.23
RASL11B	RAS Like Family 11 Member B	7.12
IL11	Interleukin 11	7.08
LEFTY2	Left-Right Determination Factor 2	6.94
EDN1	Endothelin 1	6.58
LMCD1	LIM And Cysteine Rich Domains 1	6.35
S1PR5	Sphingosine-1-Phosphate Receptor 5	6.14
NOX4	NADPH Oxidase 4	5.87
NPPB	Natriuretic Peptide B	5.86
PMEPA1	Prostate Transmembrane Protein Androgen Induced 1	4.81
SEMA7A	Semaphorin 7A	4.61
CDKN2B	Cyclin Depended Kinase Inhibitor 2B	4.29
FSTL3	Folistatin-Like 3	4.19
MYOZ1	Myozenin 1	4.13
INHBE	Inhibin Beta E Subunit	4.12
DGKI	Diacylglycerol Kinase Iota	4.05
FNDC1	Fibronectin Type III Domain-Containing Protein 1	4.02
TLL2	Tolloid-like 2	3.92
XYLT1	Xylosyltransferase 1	3.88
COMP	Cartilage Oligomeric Matrix Protein	3.82
TSPAN13	Tetraspanin 13	3.75
NUAK1	NUAK Kinase Family Member 1	3.69
ATP10A	ATPase Phospholipid Transporting 10A	3.62
DACT1	Dishevelled Binding Agonist of Beta Catenin 1	3.58
CDH2	Cadherin 2	3.49
TENM4	Teneurin Transmembrane Protein 4	3.47
ADAMTS4	ADAM Metallopeptidase with Thrombospondin Type 1 Motif 4	3.27
SPHK1	Sphingosine Kinase 1	3.10
LANCL2	LanC-like 2	3.01
PPAPDC1A	Phosphatidic Acid Phosphatase Type 2 Domain-Containing Protein 1A	2.99
ITGA11	Integrin Subunit Alpha 11	2.96
ADAM19	ADAM Metallopeptidase Domain 19	2.89
PXDC1	PX Domain Containing 1	2.62
ENC1	Ectoderman1-Neural Cortex 1	2.50
DCBLD1	Discoidin, CUB, And LCCL Domain Containing 1	2.46
SMAD7	SMAD Family Member 7	2.45
SKIL	SKI-like Proto-Oncogene	2.19

**Table 3.5: Top 50 Up-Regulated Genes in Cultured Human TM Cells in the Presence or Absence of TGF- $\beta$ 2.** Pools of 5 donor samples for each group (control CK\_Group and TGF- $\beta$ 2 Treated TK\_Group) were used to generate the results from mRNA-Seq. LogFC = Log fold change.

Gene ID	Gene Name	LogFC
<i>Down-Regulated Genes</i>		
MOV10	MOV10 RISC Complex RNA Helicase	-1.68
CPA4	Carboxypeptidase A4	-1.83
ALDH3B1	Aldehyde Dehydrogenase 3 Family Member B1	-1.92
TENC1	Tensin Like C1 Domain Containing Phosphatase	-1.98
NABP1	Nucleic Acid Binding Protein 1	-1.98
ZFP36	Zinc Finger Protein 36	-2.13
UBE2L6	Ubiquitin Conjugating Enzyme E2 L6	-2.17
PARP14	Poly(ADP-ribose) polymerase Family Member 14	-2.231
ADM	Adrenomedullin	-2.24
S1PR3	Sphingosine-1-Phosphate Receptor 3	-2.25
ISYNA1	Inositol-3-Phosphate Synthase 1	-2.31
PHLDA1	Pleckstrin Homology Like Domain Family A Member 1	-2.42
SMAD3	Smad Family Member 3	-2.46
GMPR	Guanosine Monophosphate Reductase	-2.47
DUSP6	Dual Specificity Phosphatase 6	-2.49
PARP10	Poly(ADP-ribose) polymerase Family Member 10	-2.62
RAB27B	RAB27B, Member RAS Oncogene Family	-2.69
CSF1	Colony Stimulating Factor 1	-2.69
SEMA3D	Semaphorin 3D	-2.71
TOP2A	DNA Topoisomerase II Alpha	-2.74
DDX60	DEXD/H-Box Helicase 60	-2.80
PTX3	Pentraxin 3	-2.93
WNT2B	Wnt Family Member 2B	-2.96
PLEKHA6	Pleckstrin Homology Domain Containing A6	-2.96
PLEKHG4	Pleckstrin Homology and RhoGEF Domain Containing G4	-3.01
AKR1C2	Also-Keto Reductase Family 1 Member C2	-3.30
LINC00341	Spectrin Repeat Containing Nuclear Envelope Family Member 3	-3.31
AKR1C3	Aldo-Keto Reductase Family 1 Member C3	-3.35
IFIT3	Interferon Induced Protein With Tetratricopeptide Repeats 3	-3.54
SLC40A1	Solute Carrier Family 40 Member 1	-3.59
COL21A1	Collagen Type XXI Alpha 1 Chain	-3.62
PSMB9	Proteasome Subunit Beta 9	-3.64
TMEM140	Transmembrane Protein 40	-3.65
AKR1C1	Aldo-Keto Reductase Family 1 Member C1	-3.67
IFIT2	Interferon Induced Protein With Tetratricopeptide Repeats 2	-3.84
SLC2A12	Solute Carrier Family 2A Member 12	-4.16
AKR1B10	Aldo-Keto Reductase Family 1 Member B10	-4.24
APOL3	Apolipoprotein L3	-4.35
OSR2	Odd-Skipped Related Transcription Factor 2	-5.37
STEAP4	STEAP Family Member 4	-5.53
ADH1B	Alcohol Dehydrogenase 1B	-7.66

**Table 3.6: Top 50 Down-Regulated Genes in Cultured Human TM Cells in the Presence or Absence of TGF- $\beta$ 2.** Pools of 5 donor samples for each group (control CK\_Group and TGF- $\beta$ 2 Treated TK\_Group) were used to generate the results from mRNA-Seq. LogFC= Logfold change.

### 3.4.3.2 Visual Identification of RNA Transcripts Obtained by RNA-Seq Analysis

Volcano plots provide a way to visualise RNA transcripts displaying large-magnitude changes which are also statistically significant. The volcano plot was constructed by plotting the expression FC on the y-axis, and the log CPM (counts-per-million) between the two experimental groups (CK\_Group and TK\_Group) on the x-axis. Two regions of interest exist on the plot; the extreme right of the plot indicates high statistical significance and the top and bottom of the plot indicates strongly up- or down-regulated genes respectively.

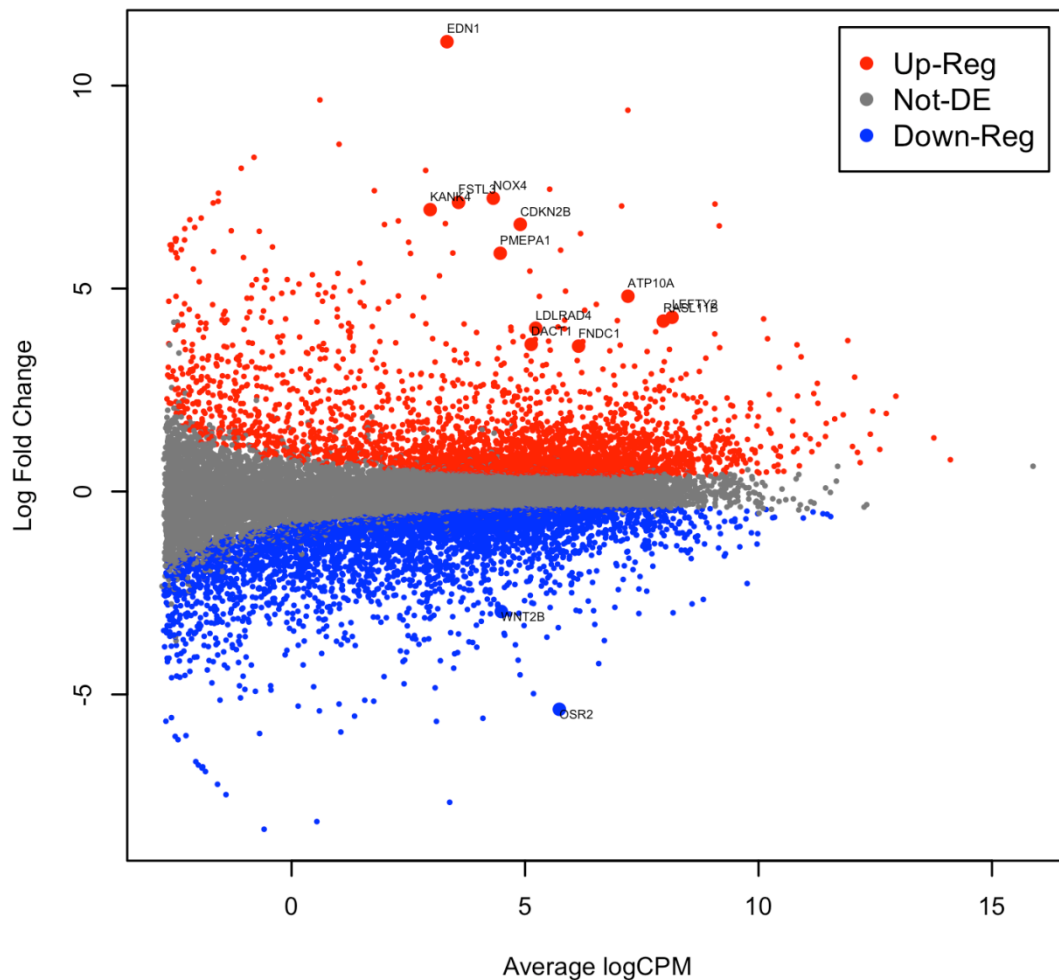


**Figure 3.5: Volcano Plot Showing the Relationship Between the LogFC and the Average Log Counts-per-Million (CPM).** The relationship between statistical significance and LogFC in normalised expression between the experimental groups, CK\_Group and TK\_Group, are shown in the plot. FC= Fold Change. **Key:** Up-Reg= Significantly up-regulated genes between the two sample groups are indicated by the red dots; Not DE= Genes were not differentially expressed between the two sample groups; Down-Reg= Genes that were significantly down-regulated between the two sample groups are indicated by blue dots.

### 3.4.3.3 TGF- $\beta$ 2 Activated Processes in Cultured Human Trabecular Meshwork Cells

Exiqon performed a gene ontology (GO) enrichment analysis with genes found to be differentially expressed in control (CK\_Group) vs treated (TK\_Group) comparison. Significance was ranked by FDR. Two different statistical tests, Fisher's test and Elim method, were used and compared to generate Table 3.7.

In house analysis of biological processes was performed on genes with an FDR  $p$ -value  $<0.025$  in the control (CK\_Group) vs treated (TK\_Group) expression analysis using Core Analysis in the Ingenuity Pathway Analysis (IPA, Qiagen, UK)<sup>418</sup>. This functional analysis of genes found to be differentially expressed includes the identification of enriched canonical pathways (functional processes defined in the Ingenuity Knowledge Base), the identification of potential up-stream regulators and potential down-stream effects of the differentially expressed gene set. Interestingly, similar processes were enriched through IPA in relation to ECM organisation, a process identified by Exiqon analysis (Table 3.7). 254 IPA canonical pathways were significantly enriched (Fishers' Exact Benjamini Hochberg (BH) adjusted  $p < 0.05$ ). The top ranked canonical pathways with an enrichment score  $>4$  (Fisher's Exact BH adjusted  $p < 0.0001$ ) are tabulated in Table 3.8 below.

Table 3.7 and Table 3.8 include several canonical pathways and processes of direct relevance to the current study; including, RhoA signalling, ECM and cytoskeletal organisation, and inflammatory-related processes. Figure 3.7 depicts a canonical pathway map for RhoA signalling, a canonical pathway found to be enriched through IPA analysis. Figure 3.6 identifies the top canonical pathways of the top 1% differentially expressed genes in TGF- $\beta$ 2 treated human TM cells compared with control TM Cells. The activation score threshold was  $\pm 1.96$  and canonical pathways enriched in this are regarded as significant. The sign of the Z-score indicates the direction of regulation of the process, and enriched canonical pathways of  $p < 0.0001$  were determined as statistically significant.

Table 3.9 identifies the significantly DEGs associated with the RhoA signalling pathway identified in TGF- $\beta$ 2 treated human TM cells.

Class of Encoded Proteins	Number Affected	
	Annotated	Significant
Extracellular matrix organization	278	196
Axon guidance	309	200
Response to toxic substance	130	92
Activation of signalling protein activity involved in unfolded protein response	67	51
Positive regulation of cell migration	217	148
Regulation of apoptotic process	1041	617
Negative regulation of multicellular organismal process	599	367
Collagen fibril organization	41	29
Cellular response to oxygen-containing compound	587	358
Neural crest cell development	42	31
G-protein coupled receptor signalling pathway	453	272
Negative regulation of apoptotic process	630	367
Signal transduction	3603	2119
Single-organism cellular process	8273	4653
Phagocytosis	130	91
Artery morphogenesis	41	29
Hair follicle development	68	49
Sprouting angiogenesis	48	39
Inflammatory response	371	232
Epithelial tube morphogenesis	258	166

**Table 3.7: Significant Biological Processes Between the TGF- $\beta$ 2 Treated TM Cells and Control Cells (TK\_Group and CK\_Group).** Significant biological processes for differentially expressed genes between CK\_Group and TK\_Group are outlined above. Of 17186 genes annotated, 10106 were significantly associated with biological processes.

Ingenuity		<b>-log(p-value)</b>	<b>Ratio</b>	<b>z-score</b>	<b>Downregulated</b>	<b>Upregulated</b>
<b>Canonical Pathways</b>						
Axonal Guidance Signalling		9.60E+00	4.20E-01	NaN	161/445 (36%)	216/445 (49%)
Epithelial Adherens Junction Signalling		9.49E+00	5.31E-01	NaN	35/143 (24%)	85/143 (59%)
Germ Sertoli Cell Junction Signalling	Cell-Cell	8.94E+00	5.03E-01	NaN	52/169 (31%)	97/169 (57%)
Molecular Mechanisms of Cancer		8.24E+00	4.22E-01	NaN	146/370 (39%)	185/370 (50%)
NRF2-mediated Oxidative Stress Response		7.41E+00	4.68E-01	-0.745	89/190 (47%)	83/190 (44%)
Integrin Signalling		7.38E+00	4.58E-01	3.109	74/212 (35%)	118/212 (56%)
Aryl Hydrocarbon Receptor Signalling		7.33E+00	5.04E-01	-1.298	75/135 (56%)	45/135 (33%)
Remodeling of Epithelial Adherens Junctions		6.78E+00	5.91E-01	3.153	8/66 (12%)	48/66 (73%)
RhoA Signalling		6.50E+00	5.00E-01	3.742	32/122 (26%)	66/122 (54%)
Hepatic Fibrosis / Hepatic Stellate Cell Activation		6.13E+00	4.53E-01	NaN	62/181 (34%)	81/181 (45%)
Regulation of the Epithelial-Mesenchymal Transition Pathway		5.75E+00	4.44E-01	NaN	69/187 (37%)	81/187 (43%)
PI3K/AKT Signalling		5.55E+00	4.80E-01	2.449	52/123 (42%)	65/123 (53%)
Gap Junction Signalling		5.49E+00	4.49E-01	NaN	57/167 (34%)	84/167 (50%)

Glioblastoma Multiform Signalling	5.45E+00	4.53E-01	1.588	60/159 (38%)	84/159 (53%)
IL-8 Signalling	5.37E+00	4.34E-01	0.333	79/196 (40%)	90/196 (46%)
Xenobiotic Metabolism Signalling	5.18E+00	4.07E-01	NaN	129/270 (48%)	83/270 (31%)
Death Receptor Signalling	5.07E+00	5.00E-01	-0.59	51/92 (55%)	34/92 (37%)
Chronic Myeloid Leukemia Signalling	4.99E+00	4.85E-01	NaN	45/103 (44%)	52/103 (50%)
Colorectal Cancer Metastasis Signalling	4.99E+00	4.12E-01	0.103	93/243 (38%)	115/243 (47%)
IGF-1 Signalling	4.94E+00	4.81E-01	1.265	42/106 (40%)	56/106 (53%)
ILK Signalling	4.90E+00	4.27E-01	1.835	64/192 (33%)	99/192 (52%)
Actin Cytoskeleton Signalling	4.88E+00	4.16E-01	4.613	64/221 (29%)	109/221 (49%)
Role of Tissue Factor in Cancer	4.86E+00	4.67E-01	NaN	45/120 (38%)	58/120 (48%)
NGF Signalling	4.63E+00	4.62E-01	1.236	49/119 (41%)	63/119 (53%)
Ephrin Receptor Signalling	4.62E+00	4.30E-01	2.429	55/172 (32%)	96/172 (56%)
B Cell Receptor Signalling	4.55E+00	4.22E-01	0.688	70/187 (37%)	88/187 (47%)
Osteoarthritis Pathway	4.48E+00	4.15E-01	-0.679	75/205 (37%)	93/205 (45%)
Interferon Signalling	4.40E+00	6.11E-01	-2.4	23/36 (64%)	8/36 (22%)
HIPPO Signalling	4.37E+00	4.88E-01	-0.756	39/86 (45%)	43/86 (50%)
UVA-Induced MAPK Signalling	4.33E+00	4.67E-01	-0.729	54/105 (51%)	42/105 (40%)
Role of Macrophages, Fibroblasts and Endothelial Cells in Rheumatoid Arthritis	4.29E+00	3.87E-01	NaN	119/302 (39%)	128/302 (42%)

Role of NFAT in Cardiac Hypertrophy	4.26E+00	4.16E-01	2.138	74/190 (39%)	94/190 (49%)
FLT3 Signalling in Hematopoietic Progenitor Cells	4.18E+00	4.88E-01	0	36/82 (44%)	41/82 (50%)
Fc $\epsilon$ Receptor-mediated Phagocytosis in Macrophages and Monocytes	4.13E+00	4.73E-01	0	37/93 (40%)	39/93 (42%)
Pancreatic Adenocarcinoma Signalling	4.07E+00	4.49E-01	-0.801	55/118 (47%)	55/118 (47%)
CD27 Signalling in Lymphocytes	4.03E+00	5.38E-01	-0.784	30/52 (58%)	20/52 (38%)

**Table 3.8: IPA Biological Processes Identified in TGF- $\beta$ 2 Treated TM Cells.**

Significant biological processes and canonical pathways for differentially expressed genes found between CK\_Group and TK\_Group are outlined above. Processes involve ECM organisation associated processes and activated canonical pathways including RhoA signalling. NaN = unrepresented value.

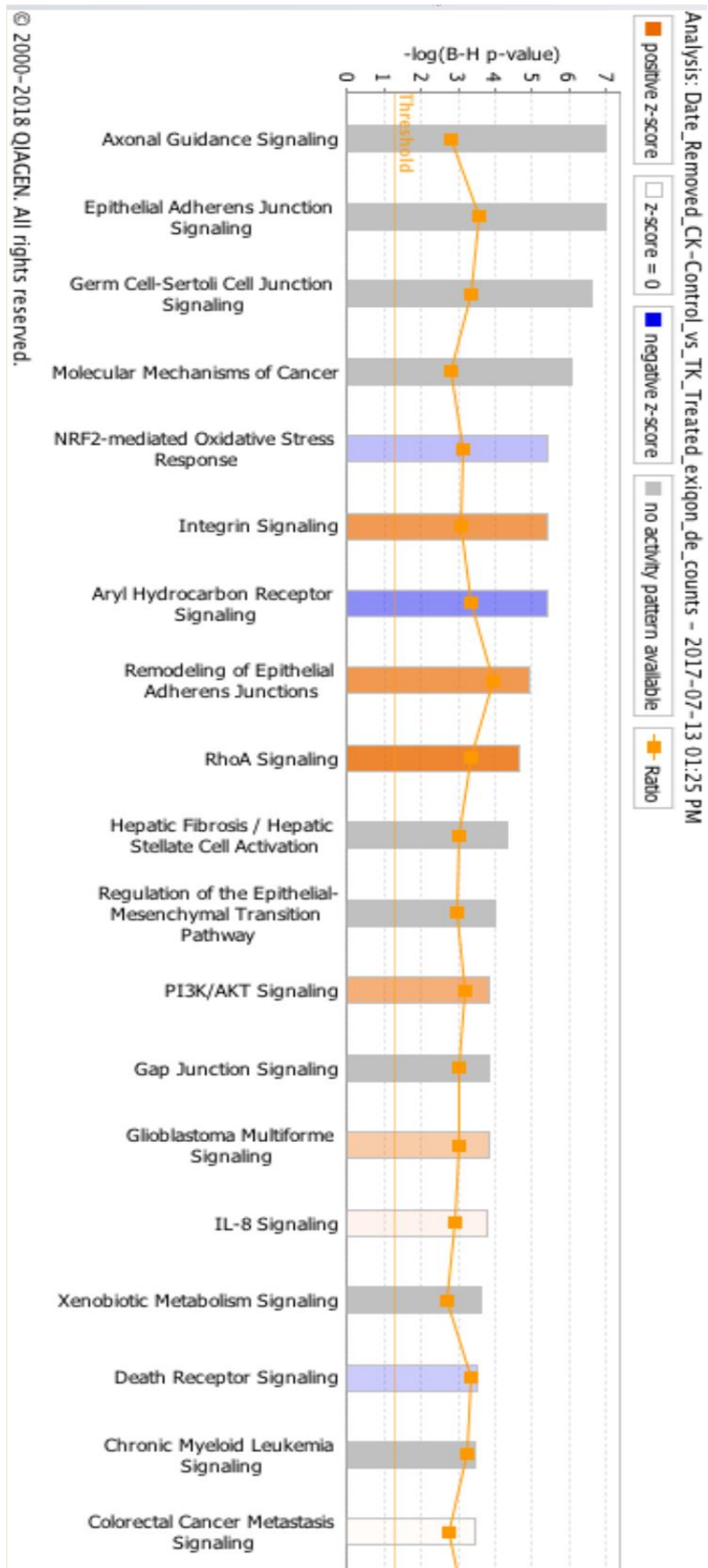


**Figure 3.6: Top Canonical Pathways of the Top 1% Differentially Expressed Genes in TGF- $\beta$ 2 Treated Human TM Cells Vs Control TM Cells.** IPA revealed the top canonical pathways of the top 1% DEGs in TGF- $\beta$ 2 TM cells vs control TM cells. Z-score threshold was  $\leq 2$ , and enriched canonical pathways of  $p < 0.0001$  were determined as significantly enriched.

RhoA Signaling : Date\_Removed\_CK-Control\_vs\_TK\_Treated\_exiqon\_de\_counts : Expr Log Ratio

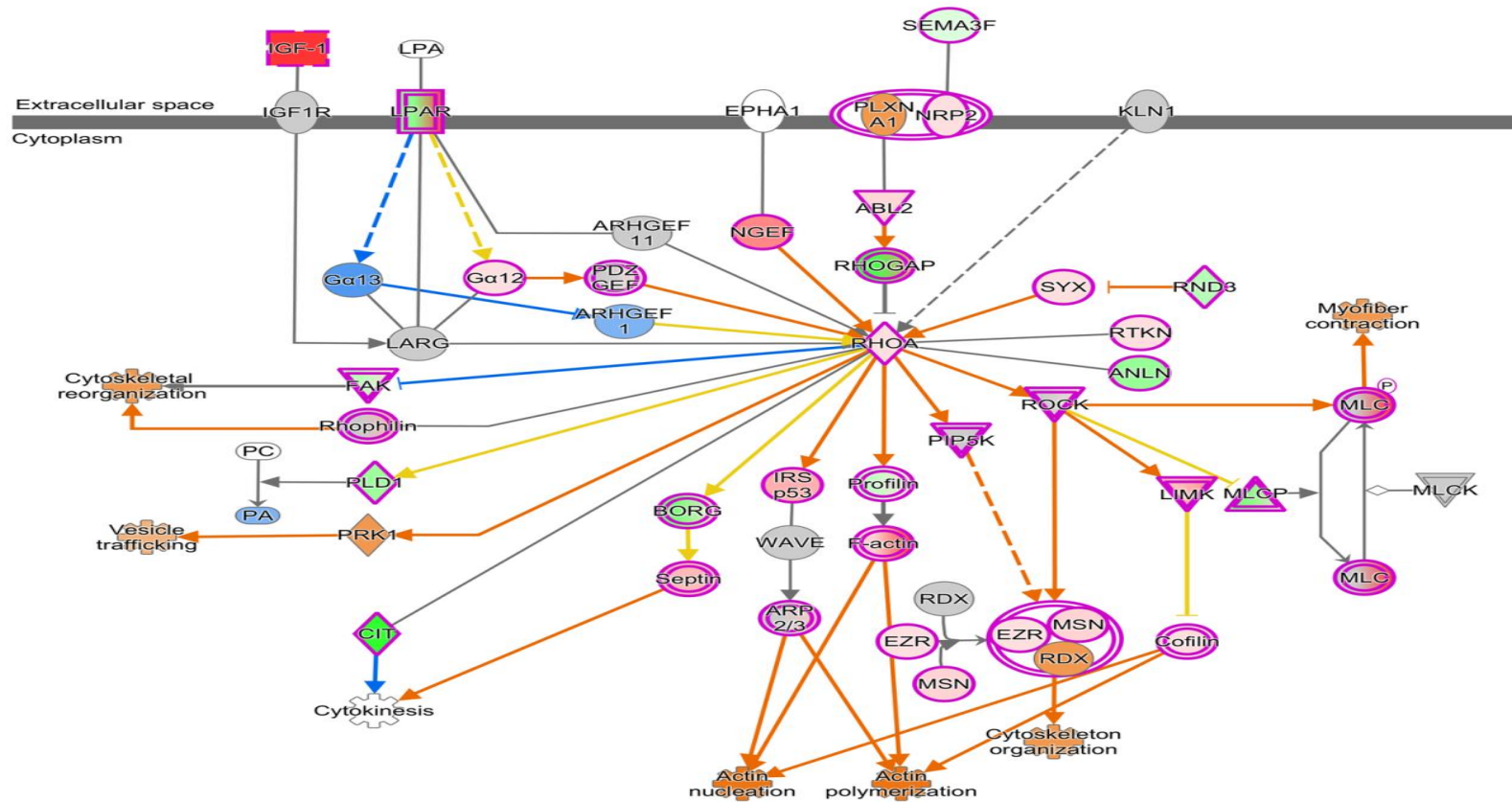


**Figure 3.7: Canonical Pathway Map for RhoA Signaling Pathway.** The highest (green) and lowest (orange/red) expressed genes derived from the RNA-Seq data set of pooled (n=5) control and treated cultured human TM cells.

<b>Symbol</b>	<b>Entrez Gene Name</b>	<b>LogFC</b>	<b>FDR (q-value)</b>
ABL2	ABL proto-oncogene 2, non-receptor tyrosine kinase	0.87	1.01E-06
ACTA2	actin, alpha 2, smooth muscle, aorta	3.058	8.65E-15
ACTB	actin beta	1.412	6.15E-08
ACTC1	actin, alpha, cardiac muscle 1	7.447	6.35E-24
ACTG1	actin gamma 1	0.963	6.72E-05
ACTG2	actin, gamma 2, smooth muscle, enteric	2.032	1.40E-10
ACTR2	ARP2 actin related protein 2 homolog	0.742	5.26E-04
ACTR3	ARP3 actin related protein 3 homolog	1.12	3.91E-07
ANLN	anillin actin binding protein	-1.73	1.64E-22
ARHGAP5	Rho GTPase activating protein 5	0.694	3.96E-05
ARHGAP6	Rho GTPase activating protein 6	-3.115	1.19E-15
ARHGAP9	Rho GTPase activating protein 9	1.613	1.85E-03
ARHGAP12	Rho GTPase activating protein 12	-0.499	1.02E-02
ARHGAP35	Rho GTPase activating protein 35	-0.726	1.66E-04
ARPC2	actin related protein 2/3 complex subunit 2	0.913	4.89E-06
ARPC3	actin related protein 2/3 complex subunit 3	0.419	1.50E-02
ARPC4	actin related protein 2/3 complex subunit 4	0.52	2.24E-03
ARPC5	actin related protein 2/3 complex subunit 5	0.935	1.52E-05
BAIAP2	BAI1 associated protein 2	1.702	8.86E-21
CDC42EP1	CDC42 effector protein 1	0.678	2.27E-04
CDC42EP3	CDC42 effector protein 3	-0.853	8.83E-05
CDC42EP4	CDC42 effector protein 4	-2.196	5.45E-18
CFL1	cofilin 1	0.866	9.51E-05
CFL2	cofilin 2	0.574	8.07E-03
CIT	citron rho-interacting serine/threonine kinase	-3.495	6.32E-23
DLC1	DLC1 Rho GTPase activating protein	2.53	4.94E-36
EZR	ezrin	0.677	6.57E-03
GNA12	G protein subunit alpha 12	0.623	2.11E-04
IGF1	insulin like growth factor 1	6.666	1.89E-09
LIMK1	LIM domain kinase 1	1.394	2.14E-17
LIMK2	LIM domain kinase 2	2.51	4.32E-30
LPAR1	lysophosphatidic acid receptor 1	-0.656	9.79E-04
LPAR3	lysophosphatidic acid receptor 3	-1.279	4.72E-03
LPAR5	lysophosphatidic acid receptor 5	4.143	2.87E-06
LPAR6	lysophosphatidic acid receptor 6	-1.918	5.77E-10
MPRIP	myosin phosphatase Rho interacting protein	0.551	2.05E-03
MSN	moesin	0.949	3.72E-06
MYL6	myosin light chain 6	1.01	1.45E-05
MYL7	myosin light chain 7	7.411	2.03E-38
MYL9	myosin light chain 9	1.284	3.24E-05
MYL12A	myosin light chain 12A	1.064	1.50E-06
MYL12B	myosin light chain 12B	0.652	9.82E-04
NEDD4	neural precursor cell expressed, developmentally down-regulated 4, E3 ubiquitin protein ligase	1.508	8.65E-18
NGEF	neuronal guanine nucleotide exchange factor	2.608	9.47E-13
NRP2	neuropilin 2	0.663	3.76E-04
PFN1	profilin 1	0.711	4.46E-04

PFN2	profilin 2	-0.954	5.74E-09
PIP5K1A	phosphatidylinositol-4-phosphate 5-kinase type 1 alpha	0.781	1.19E-03
PLD1	phospholipase D1	-1.613	4.27E-13
PLEKHG5	pleckstrin homology & RhoGEF domain containing G5	0.518	1.99E-02
PPP1R12A	protein phosphatase 1 regulatory subunit 12A	0.724	8.83E-05
PPP1R12B	protein phosphatase 1 regulatory subunit 12B	-2.167	9.65E-19
PTK2	protein tyrosine kinase 2	0.448	5.62E-03
PTK2B	protein tyrosine kinase 2 beta	-1.175	6.23E-09
RAPGEF2	Rap guanine nucleotide exchange factor 2	0.769	1.89E-06
RHOA	ras homolog family member A	0.465	2.21E-02
RHPN2	rhopilin Rho GTPase binding protein 2	1.723	1.16E-06
RND3	Rho family GTPase 3	-1.224	9.94E-08
ROCK1	Rho associated coiled-coil containing protein kinase 1	0.392	1.99E-02
RTKN	rhotekin	0.667	8.61E-04
SEMA3F	semaphorin 3F	-0.551	1.54E-02

**Table 3.9: Differentially Expressed Genes Associated with RhoA Signalling Pathway Identified by RNA-Seq.** RhoA Signalling Pathway was enriched in human TM cells treated with TGF- $\beta$ 2. Only the significantly differentially expressed genes in TGF- $\beta$ 2 treated human TM cells, associated with RhoA Signalling pathway are shown.

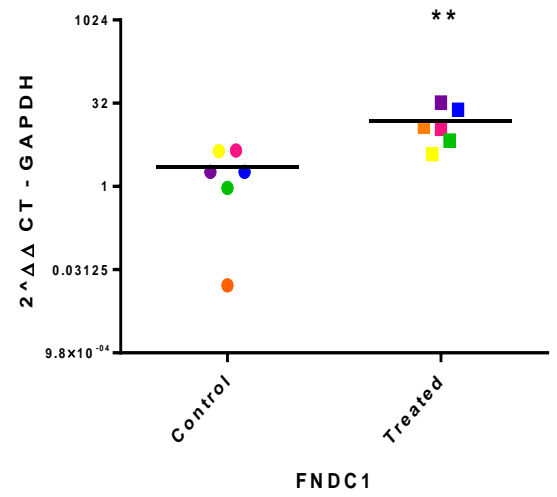
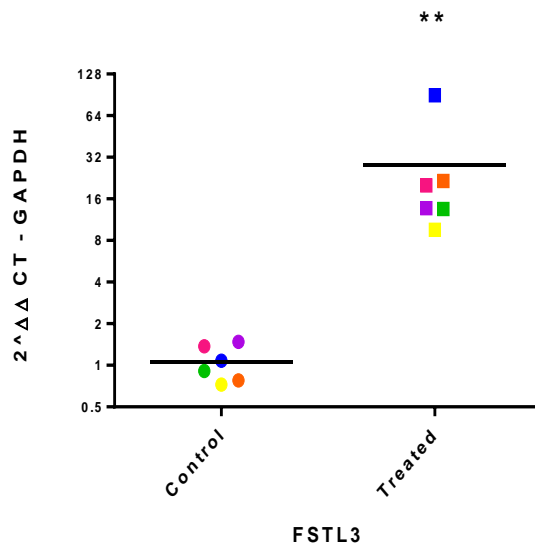
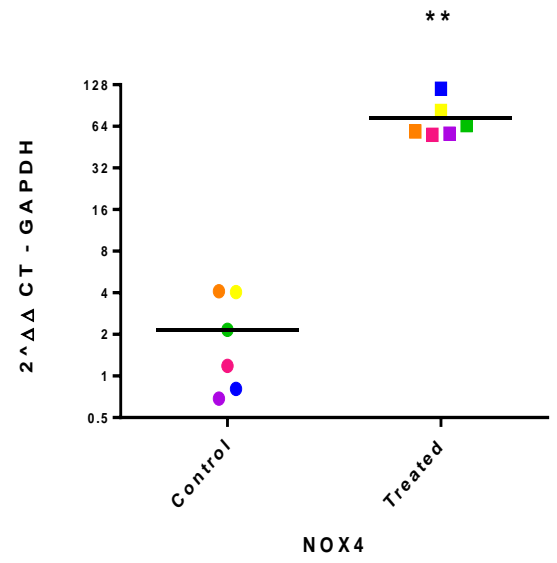
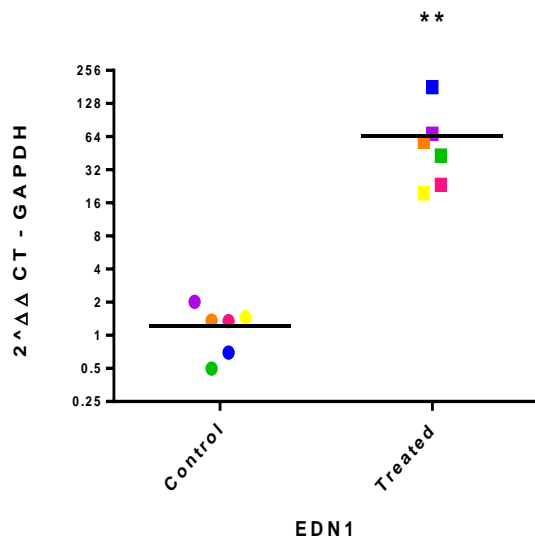
#### 3.4.4 q-PCR Assay Validation of Top Differentially Expressed Genes in Cultured Human TM in the Presence or Absence of TGF- $\beta$ 2

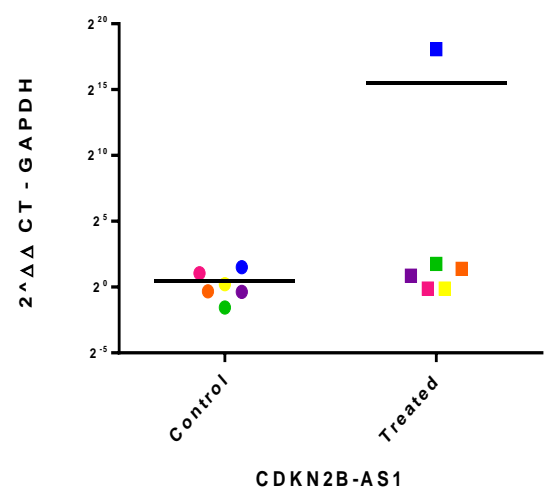
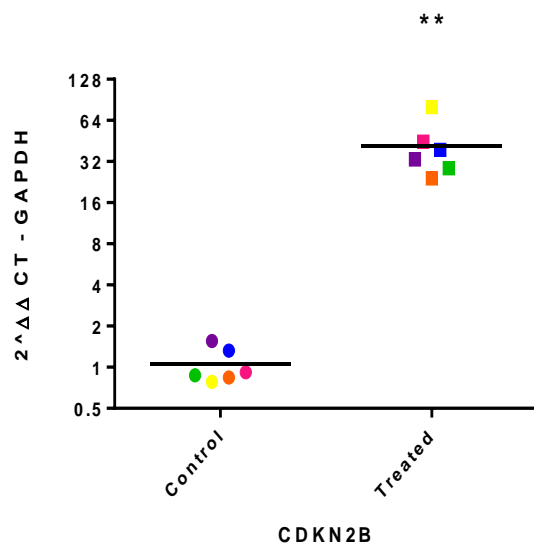
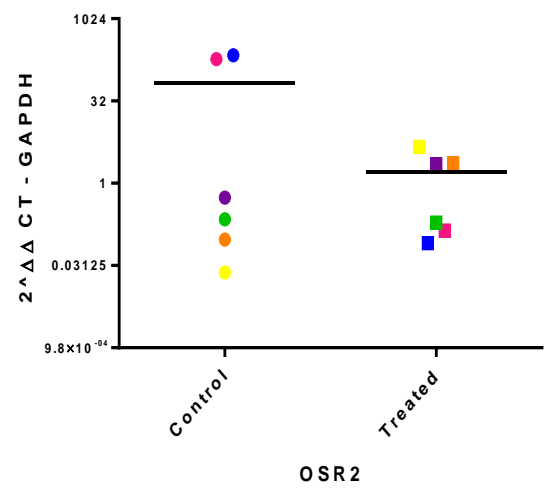
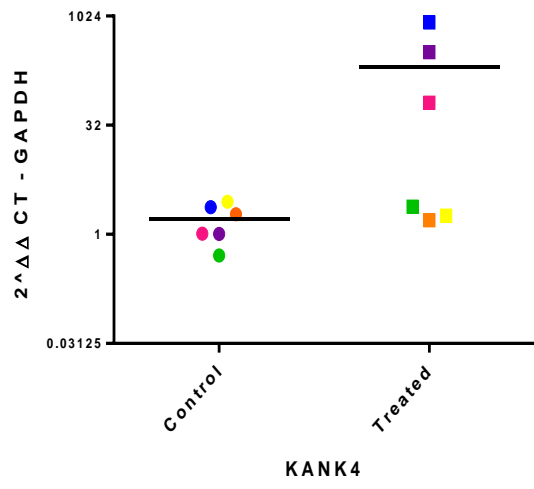
To further confirm the results obtained from the RNA-Seq analysis, a subset of the top differentially expressed genes (DEGs) between the control group, (CK\_Group) and the TGF- $\beta$ 2 group (TK\_Group) of cultured human TM cells, were analysed using q-PCR with Primer Design custom primer assays (Table 3.2). In addition, q-PCR was performed to compare alterations in gene expression between control normal TM cells (CK\_Group) with that of glaucomatous TM samples for the same subset of genes already analysed.

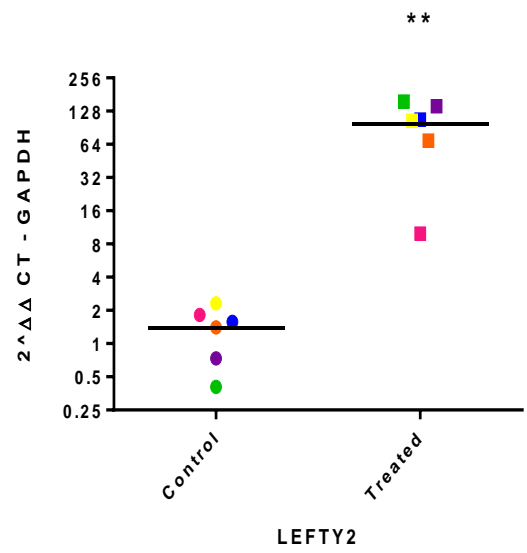
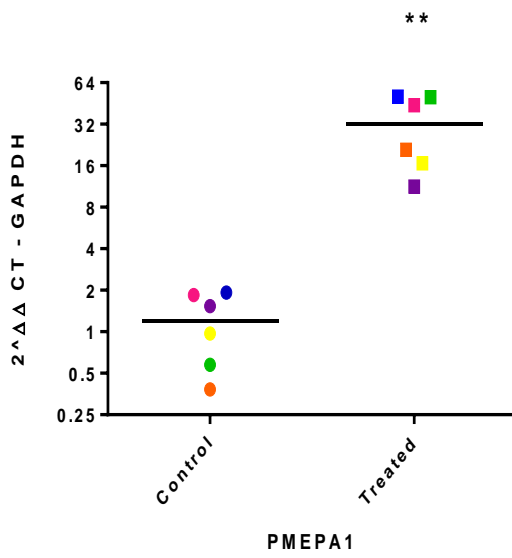
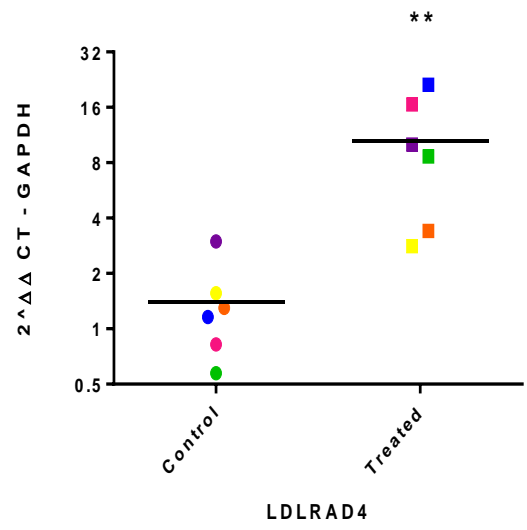
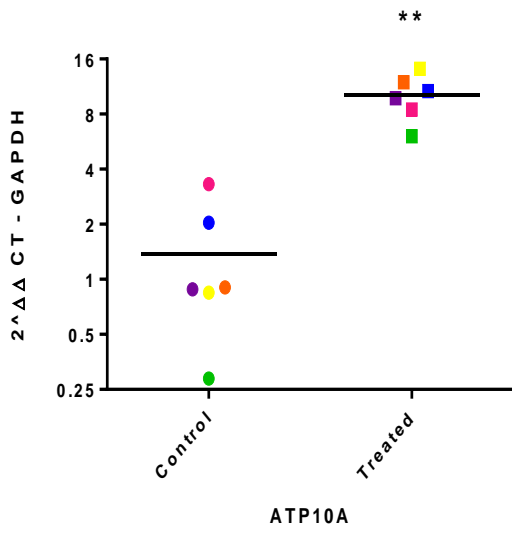
Fifteen candidate genes (Table 3.10) were selected for q-PCR analysis on the basis of their statistical significance in the RNA-Seq data set and on the basis of published literature providing evidence of their involvement in glaucoma pathophysiology. The fifteen candidate genes included; endothelin 1 (EDN1), follistatin-like protein 3 (FSTL3), KN motif and ankyrin repeat domain-containing protein4 (KANK4), ATPase phospholipid transporting 10A (ATP10A), low density lipoprotein receptor class A domain-containing 4 (LDLRAD4), fibronectin type 3 domain-containing 1 (FNDC1), Wnt family member 2B (WNT2B), RAS-like family 11 member B (RASL11B), prostate transmembrane protein, androgen induce 1 (PMEPA1), left right determination factor 2 (LEFTY2), odd-skipped related transcription factor 2 (OSR2), dishevelled binding antagonist of beta catenin 1 (DACT1), and cyclin dependent kinase inhibitor 2B (CDKN2B) and its antisense gene (CDKN2B-AS1). CDKN2B-AS1 was not identified as one of the top 500 DEGs but CDKN2B-AS1 is located in a mapped POAG locus on chr9p21 and it may be involved in the regulation of nearby genes including CDKN2B<sup>419</sup>. Thirteen of the fifteen candidate genes demonstrated consistent trends of differential expression by q-PCR. To further confirm the differential expression of candidate genes an independent sample was added to each group increasing the biological replicates to 6 (CK\_Group (n=6), TK\_Group (n=6)) as well as three glaucomatous donor samples. Statistical analysis was performed using GraphPad (Prism, version 6), and all data sets were subjected to two sample students t-tests. Results were classified as significantly significant if  $p < 0.05$ .

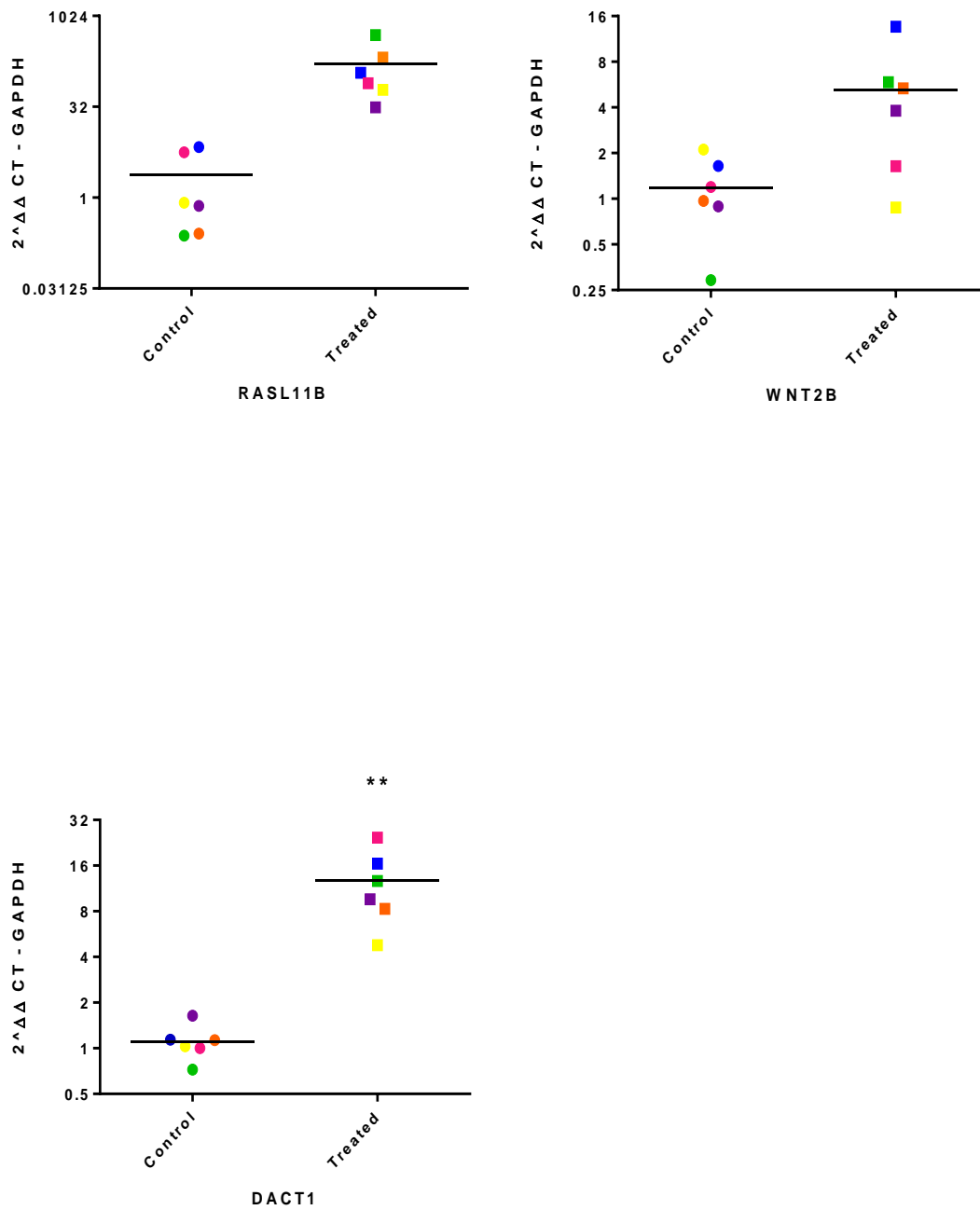
Candidate Gene	LogFC	P-Value
EDN1	6.581011	5.9E-150
NOX4	5.868904	2.1E-105
FSTL3	4.198732	3E-99
KANK4	11.08088	2.62E-95
ATP10A	3.624783	4.03E-66
LDLRAD4	7.225079	1.9E-59
FNDC1	4.023905	6.79E-57
WNT2B	-2.95701	2.93E-56
RASL11B	7.122587	2.91E-60
PMEPA1	4.810826	2.76E-84
LEFTY2	6.944008	4.88E-62
OSR2	-5.36648	4.15E-67
DACT1	3.58056	2.81E-58
CDKN2B	4.291877	1.41E-92
CDKN2B-AS1	-	-

**Table 3.10: Summary of Expression Levels of Candidate Genes Based on RNA-Seq Analysis.** FC-Fold Change. Values for CDKN2B-AS1 were unavailable as it was not sequenced as a long non-coding-RNA it does not contain a 3'UTR, therefore could not be assessed in RNA-Seq library.

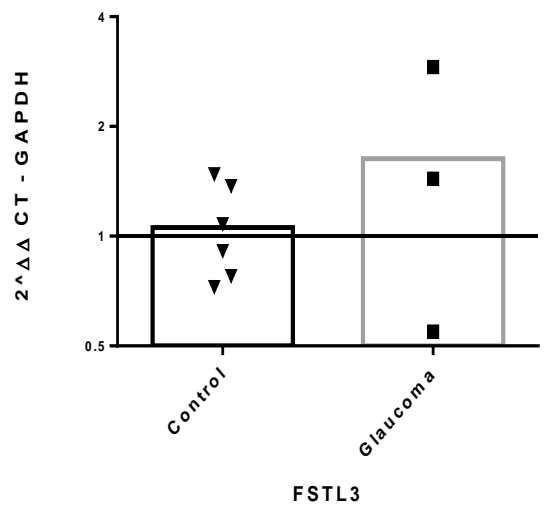
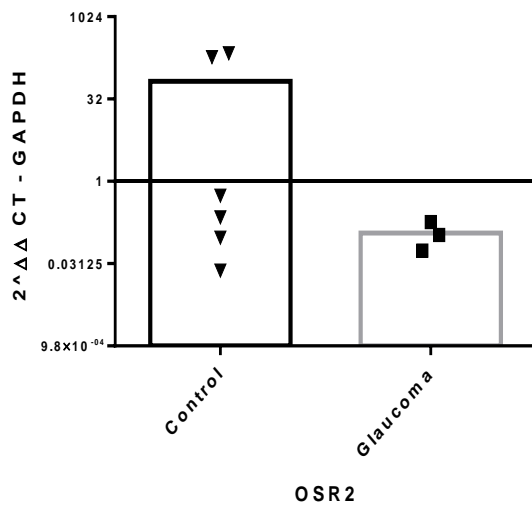
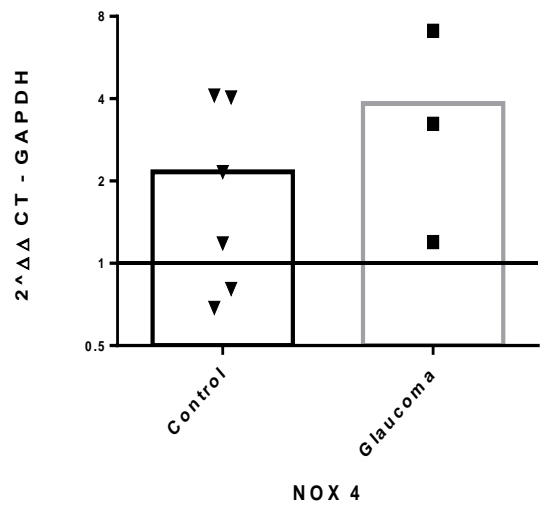
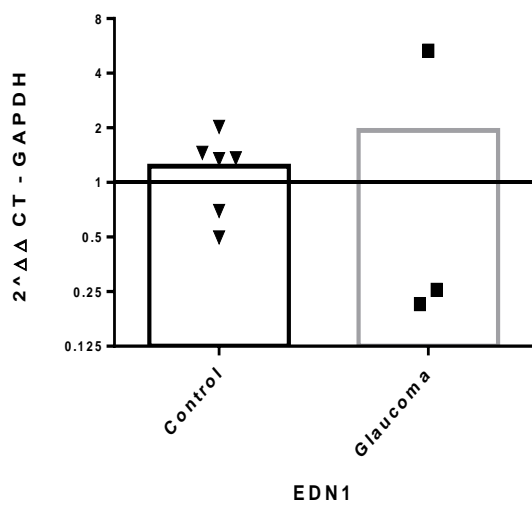


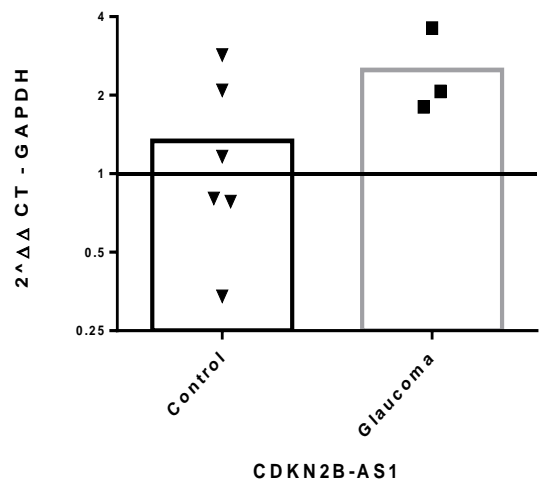
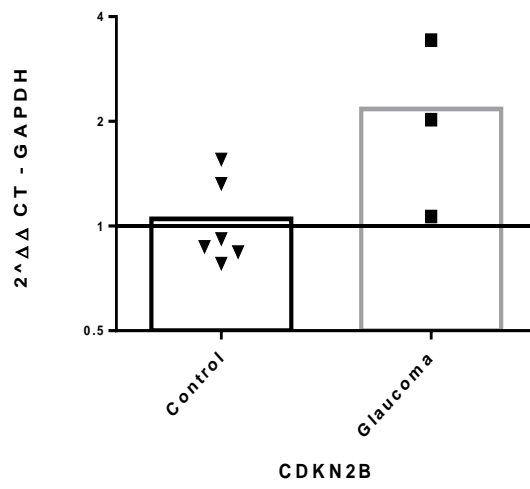
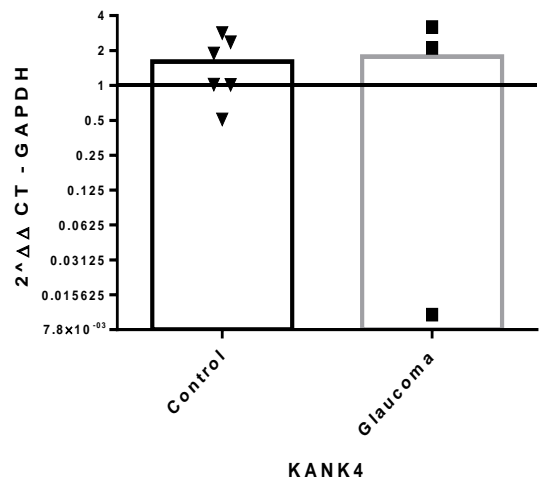
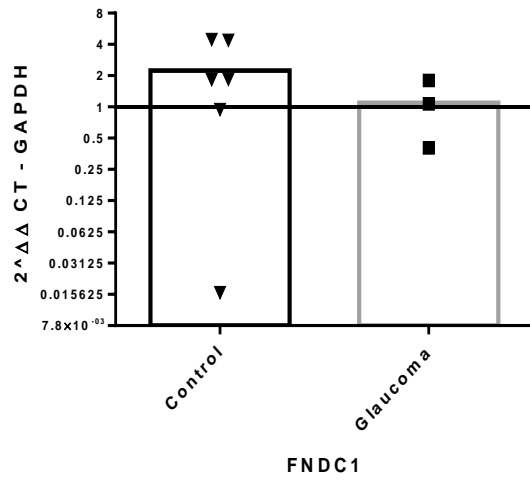


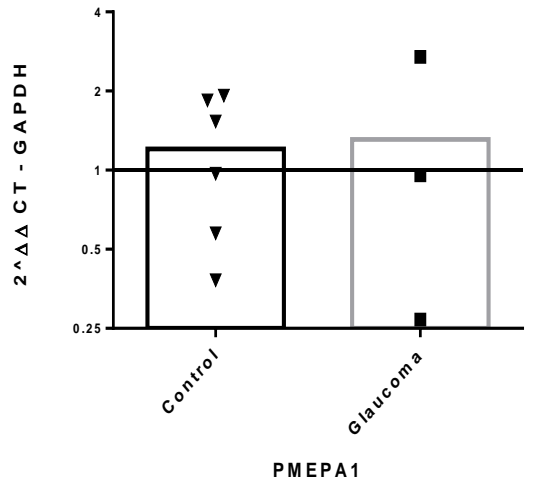
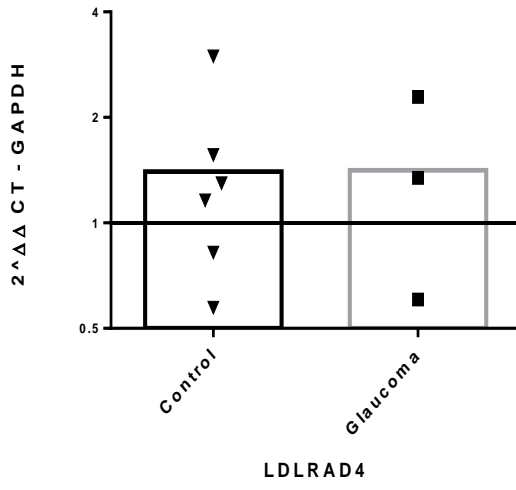
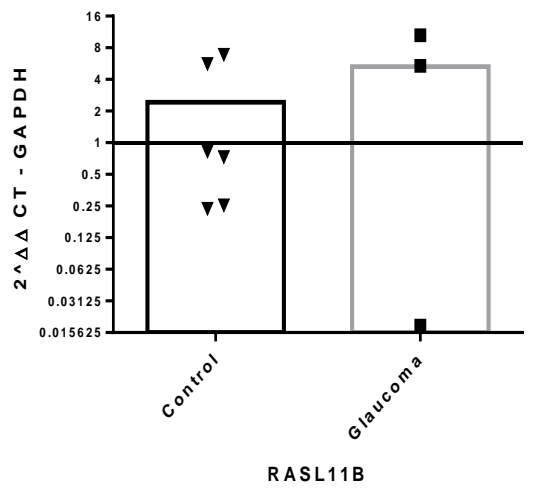
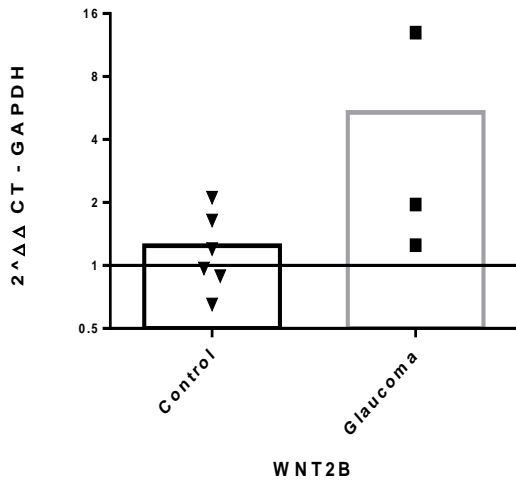




**Figure 3.8: Expression Levels of Candidate Genes in Cultured Normal Human TM Cells.** CK\_Group are denoted as “Control” on graphs and TK\_Group as “Treated”. Candidate genes were identified as significantly differentially expressed through RNA-Seq except for CDKN2B-AS1. Paired donors are colour coded. Circles represent individual donor gene without TGF- $\beta$ 2 treatment and squares represent donors with TGF- $\beta$ 2 treatment. An asterisk (\*) denotes significant differential gene expression after treatment (two-sample t-test  $p < 0.05$ ).







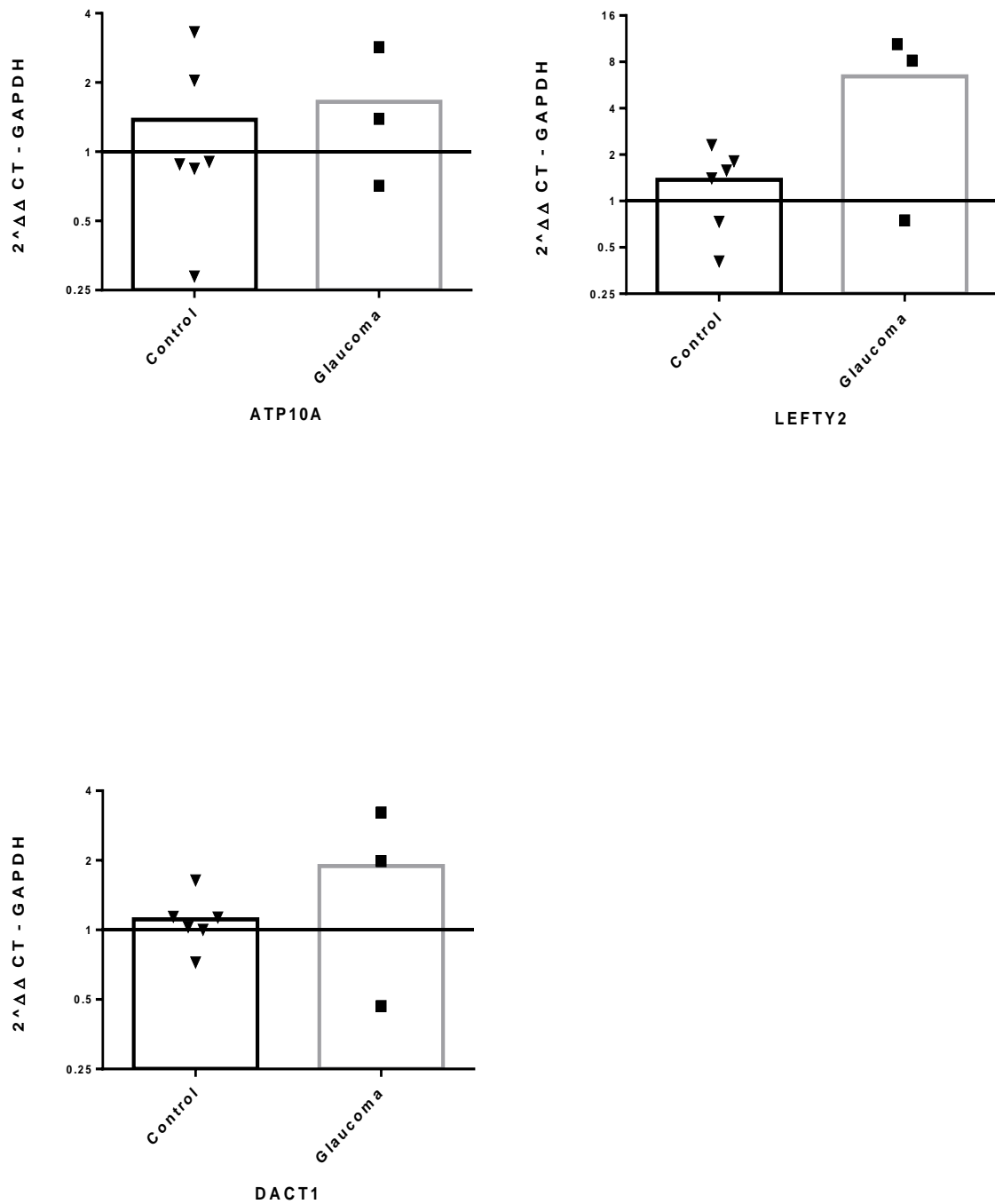


**Figure 3.9: Expression Levels of Candidate Genes in Cultured Normal Human TM Cells and Glaucomatous TM Cells.** CK\_Group are denoted as “Control” on graphs and glaucomatous samples as “Glaucoma”. Triangles represent control donor gene expression and squares represent glaucomatous donor gene expression. An asterisk (\*) denotes significant differential gene expression after treatment (two-sample t-test  $P < 0.05$ ).

## 3.5 Discussion

Primary-open angle glaucoma (POAG) has complex trait inheritance<sup>420</sup>. Forward genetics is a common approach to dissecting complex traits, like common human diseases, and our ability to identify genes for common diseases has greatly accelerated over the past several years. However, despite access to the complete genome sequence for a diverse number of species, large-scale haplotype maps for genotyping, technologies capable of screening DNA polymorphisms and gene activity on an unprecedented scale, and well-characterised human cohorts, even the largest genome-wide association studies (GWAS) have limited power to detect genes with small effects<sup>420</sup>. GWAS in glaucoma have identified a number of novel disease-predisposing genes, but progress in uncovering the mechanisms by which these genes lead to glaucoma, which is required to understand disease pathogenesis and develop new therapies, has been far slower<sup>420</sup>.

Genes and their downstream products comprise a complex regulatory machinery that sustains the delicate homeostasis of an organism in a changing environment. The transcriptome is the complete set of transcripts in a cell, and their quantity, for a specific developmental stage or physiological condition. Understanding the transcriptome is essential for interpreting the functional elements of the genome and revealing the molecular constituents of cells and tissues, and also for understanding development and disease<sup>421,422</sup>. The aim of this study was to reverse engineer glaucoma in the laboratory using a known glaucomatous stimulus in the TM, TGF- $\beta$ 2, and assess genome-wide alterations in gene expression and regulation in a holistic, hypothesis-independent and discovery-driven manner, to identify the genes and pathways dysregulated by glaucoma stimuli.

### 3.5.1 Genome-Wide Transcriptome Profiling in TGF- $\beta$ 2 Treated Human TM Cells

Using high-throughput RNA-Seq methods in cultured human TM cells treated with TGF- $\beta$ 2 (5ng/mL) for 24 hours there were several significantly differentially expressed genes (DEGs) and canonical pathways that were enriched. Dose duration and concentration are important factors which must be considered when examining gene expression studies. Individual donor characteristics such as age, sex, and previous disease history may also play a role in gene expression.

Due to a lack of model systems to study glaucoma, the use of cultured human TM cells provides a means to evaluate their biological properties in relation to conditions such as glaucoma. As discussed previously, (Chapter 2, 2.1) primary human TM cells used throughout this thesis were obtained from either whole donor eyes or from corneal rims. TM cells are inherently in close contact with other cell types, and so, it is therefore essential to ensure the correct cell population has

been isolated prior to experimentation. The most characteristic marker for human TM cells is the increased expression of myocilin following dexamethasone treatment<sup>423</sup>. In comparison to other ocular cell types this induction appears to be TM cell specific. Other proteins have been identified in the human TM however currently there is no data that differentiates between the different regions of the TM. Due to the smaller size of TM cells there is a possibility that TM cell cultures may contain contaminants such as fibroblasts<sup>424</sup>. Vimentin, a known fibroblast marker<sup>425</sup>, was used in our studies to provide assured evidence that no fibroblasts were present in our human TM cell cultures. Human tenon fibroblasts were used as a positive control in these experiments indicating the presence of vimentin. Despite the lack of a single marker for TM cells, in comparison to surrounding ocular cells, TM cells also have pronounced phagocytosis rates that can be used as a behavioural characteristic. Glucocorticoid treatment has been linked to enhanced ECM deposition in the TM, and this is due, in part, to reduced phagocytic capabilities. Data highlights phagocytosis as an important function of TM cells<sup>426,427</sup>.

Three studies have examined global changes in gene expression in cultured human TM cells treated with TGF- $\beta$  using cDNA or oligonucleotide arrays<sup>244,405,407</sup>. To our knowledge, this is the first report to use RNA-Seq analysis to investigate the human TM transcriptome profile following TGF- $\beta$ 2 treatments. None of the microarray-based studies recapitulated the duration of TGF- $\beta$ 2 treatment for 24hours, and only one of the studies utilised the same TGF- $\beta$ 2 dose (5ng/mL)<sup>244</sup>. In our study we also used 5ng/mL as this value recapitulates the concentration of TGF- $\beta$ 2 in the glaucomatous AH<sup>428</sup> and duration was decided on the basis of SMAD phosphorylation assays(Appendix 8.1). Two studies used a 1ng/mL TGF- $\beta$ 2 dose over a time course of up to 72hours<sup>405,407</sup>. Despite these experimental differences, common genes were up-regulated in the array studies and in our RNA-Seq dataset including; NADPH oxidase 4 (NOX4), SMAD7, follistatin-like 3 (FSTL3) and cyclin dependent kinase inhibitor 2b (CDKN2B); the latter two are also up-regulated in response to TGF- $\beta$ 1 treatment in cultured human TM cells<sup>405</sup>. Limited consistency in down-regulated genes in our study and the microarray studies was also observed<sup>244,405,407</sup>. However, full datasets for each of the microarray-based studies were not made publicly available, therefore, comparisons are limited.

### Rho/ROCK Signalling Pathway

The Rho/ROCK pathway has pleiotropic functions including the regulation of cellular contraction, motility, morphology, polarity, cell division, and gene expression<sup>429</sup>. In the anterior eye Rho/ROCK signalling pathways modulate the cytoskeletal integrity of cells, synthesis of ECM components, and the permeability of endothelial cells in Schlemm's canal<sup>430</sup>. Alterations in the Rho/ROCK signalling

pathway and up-regulation of its downstream targets results in the pathogenesis of multiple diseases<sup>431</sup>.

Rho is a member of Rho family of small molecular GTP binding proteins. Rho has three isomer types: RhoA, RhoB, and RhoC; and these intracellular GTPases cycle between a GTP-bound (active conformation) and a GDP-bound (inactive conformation)<sup>432</sup>. The Rho GTPases act as a molecular switch which respond to receptor binding on the plasma membrane including heterotrimeric G protein-coupled receptors, tyrosine kinase receptors, cytokine receptors, frizzled receptors, and adhesion receptors<sup>432</sup>. In TM cells RhoA GTPase activity is stimulated by TGF- $\beta$ , connective tissue growth factor (CTGF), dexamethasone, endothelin-1, ECM proteins and mechanical stretch (for review see Rao *et al* 2017<sup>433</sup>). Based on the RNA-Seq data using Ingenuity Pathway Analysis (IPA) we identified the RhoA signalling pathway as significantly enriched in our TGF- $\beta$ 2 treated samples in comparison to our untreated controls.

Rho kinase (ROCK) is a serine/threonine kinase and one of the major downstream effectors of RhoA GTPase. ROCK has two isomers; ROCK1 and ROCK2. Rho-kinase proteins are ubiquitously expressed in most tissue, however, ROCK isoforms distribute differentially according to their specific functions. ROCK1 has high specificity for non-neuronal tissues whereas ROCK2 is commonly found in the brain and muscles<sup>429</sup>. The Rho/ROCK pathway is critical in the formation of actin stress fibres and focal adhesions<sup>434</sup>, and the regulation of actomyosin cytoskeletal organisation, cell adhesion, cell morphology, and smooth muscle contraction<sup>435</sup>. Active GTP-bound Rho GTPase activates ROCK which phosphorylates various intracellular targets. Specific substrates for Rho/ROCK signalling are myosin light chain (MLC), LIM kinase and the regulatory subunit of myosin phosphatase: myosin phosphatase substrate 1 (MYPT1)<sup>429</sup> (Figure 3.10). Phosphorylation of MLC is dependent on both myosin light chain kinase (MLCK) and myosin light chain phosphatase (MLCP). MLC is phosphorylated by Ca<sup>2+</sup>/calmodulin-dependent MLCK and dephosphorylated by Ca<sup>2+</sup>-independent MLCP, and the balance between these two components is a critical determinant of MLC phosphorylation<sup>436</sup>. LIM kinase phosphorylates and inactivates the actin binding/depolymerising factor, cofilin, in turn inducing actin cytoskeleton remodelling. LIM kinase is predominantly localised to the cytoplasm and functionally associated with the cytoskeleton<sup>437</sup>. LIM kinase contains structural features of cyto-regulatory proteins and kinase specific activity for cofilin.

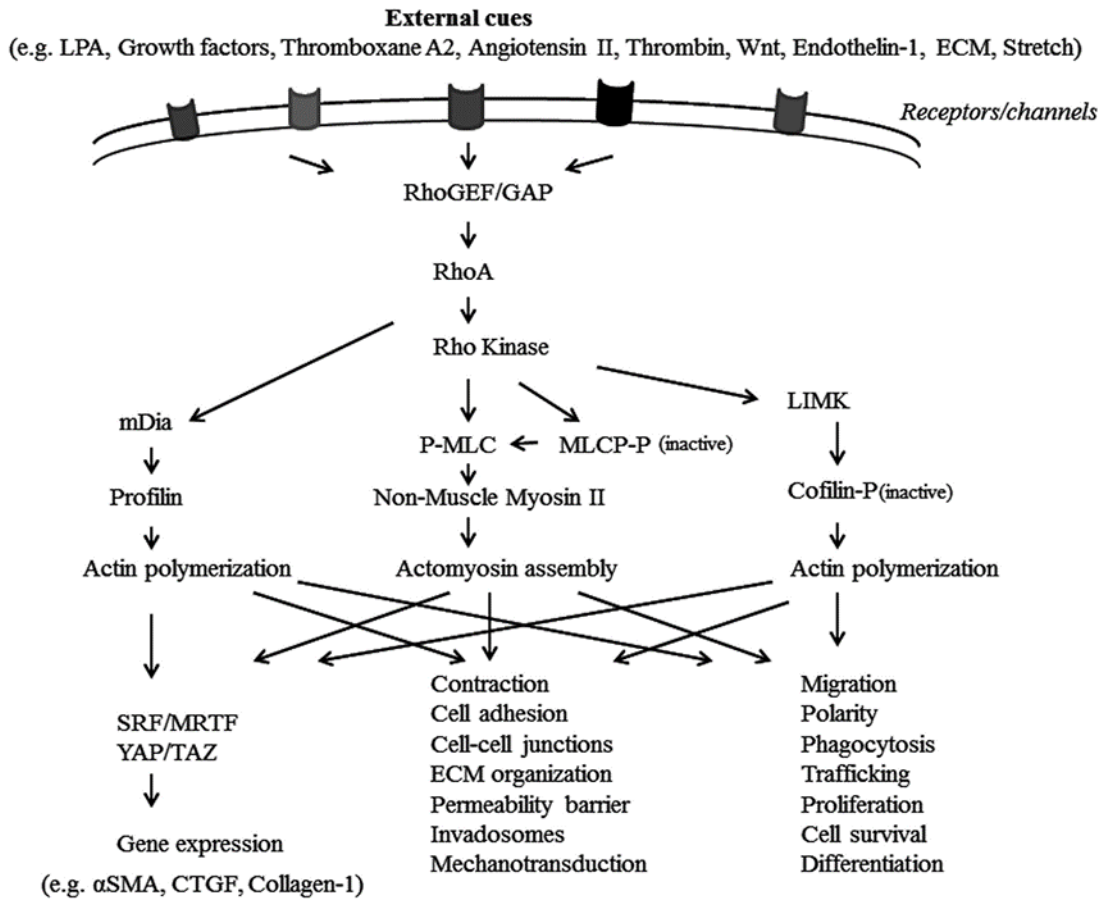


**Figure 3.10: Schematic of Rho/ROCK Signalling Pathway.** Modified from Rao *et al* 2017<sup>433</sup>. Rho/ROCK signalling cascades are implicated in cytoskeleton reorganisation and multiple cellular processes in smooth muscle and non-smooth muscle cells.

Our results do not show significant enrichment of ROCK when RhoA signalling is activated via TGF- $\beta$ 2 stimulations (ROCK1: LogFC= 0.392, FDR p= 0.019; and ROCK2: LogFC= 0.319, FDR p= 0.081). ROCK is implicated in the RhoA-mediated inhibition of MLCP as shown in Figure 3.10<sup>438</sup>. MYPT1 is the best characterised substrate for ROCK. ROCK activation by RhoA in turn activates MYPT1. Activated MYPT1 inhibits activity of MLCP resulting in enhanced MLC phosphorylation<sup>439</sup>. This phosphorylation catalyses interactions between myosin and actin which subsequently results in acto-myosin contraction<sup>440</sup>. This contractile activity is independent of contractile activity stimulated through phosphorylation of MLC by Ca<sup>2+</sup>/calmodulin dependent MLCK. Thus Rho/ROCK pathway is a master regulator of the actin cytoskeleton and cell contractility. Interestingly, increased contractility in TM cells during glaucoma pathogenesis has previously been associated with ROCK signalling<sup>441</sup>. Increased contractility leads to a reduction in outflow facilities of the drainage angle<sup>442</sup>. ROCK has previously been localised to the tissues of the AH

outflow pathway and it was found that ROCK may be implicated in increased TM contractility and ECM deposition. A number of novel therapeutics for glaucoma have emerged in recent years targeting Rho/ROCK signalling under the premise that inhibition of ROCK may reduce TM cell contractility and ECM reorganisation<sup>443</sup>. However, our results are currently contradictory to this and it is possible that ROCK may not be the best therapeutic target.

The expression of KANK4 was significantly up-regulated in TGF- $\beta$ 2 treated human TM cells by RNA-Seq when compared to control human TM cells (FC= 11.08, *p*-value= 2.62E-95). Over-expression of KANK family members, including KANK4 resulted in an overall repression of RhoA activity<sup>444</sup>. KANK proteins are predominantly distributed in the cytoplasm and KANK4 is involved in the formation of actin stress fibres. Thus, KANK proteins including KANK4 may share a common function in regulation polymerisation of actin through RhoA activity<sup>445</sup>. Cells expressing KANK family members have significantly decreased formation of actin stress fibres<sup>444</sup>. Limited data on the function of KANK4 in the TM exists but inference by analogy to its paralogues KANK2-3, would suggest a role in the maintenance of actin fibres within the TM via Rho signalling<sup>445</sup>. The polymerisation and depolymerisation cycle of stress fibres in TM cells may be implicated in glaucoma pathogenesis<sup>446</sup>. KANK4 has not yet been implicated in glaucoma pathogenesis but it may have potential role in Fuchs endothelial corneal dystrophy (FECD)<sup>447</sup>. ROCK inhibitors are used in the treatment of corneal endothelial dysfunction<sup>448</sup>.

## NADPH Oxidase Inhibitor 4 (NOX4)

TGF- $\beta$  can control reactive oxygen species (ROS) directly or indirectly by down-regulating antioxidant systems and the interplay between TGF- $\beta$  and ROS has been described in both health and disease<sup>449,450</sup>. Both TGF- $\beta$  and ROS have also been implicated in glaucoma and therefore interplay between the two may be contributing to POAG pathogenesis. Accumulating evidence suggests that NADPH oxidase 4 (NOX4) may be an important downstream effector in mediating TGF- $\beta$ -induced fibrosis in the heart, lungs and kidneys via the production of ROS<sup>451</sup>. RNA-Seq analysis in this study identified NOX4 expression as significantly up-regulated in TGF- $\beta$ 2 treated cells (FC= 5.87, *p*-value= 2.1E-105) and confirmed up-regulation of NOX4 by q-PCR (FC= 73.12, *p*-value= 0.002 Figure 3.8).

The NADPH oxidase family are widely known for their biological function of catalysing oxygen to produce ROS. To date the family includes seven members, NOX1-5 and DIOX1-2. NOX4 contributes to the pathogenesis of other ocular diseases relating to tissues of the anterior segment<sup>452-454</sup>. A recent study demonstrated that TGF $\beta$ 1-mediated production of collagen by rabbit conjunctival fibroblasts involves a NOX4-derived H<sub>2</sub>O<sub>2</sub> pathway<sup>452</sup>. NOX4 is the only isoform of the NOX family to constitutively produce hydrogen peroxide (H<sub>2</sub>O<sub>2</sub>)<sup>455</sup> and the pro-fibrotic response by fibroblasts is implemented via the generation of superoxides and H<sub>2</sub>O<sub>2</sub> by NOX4<sup>456</sup>.

To date, NOX4 has not been implicated in the TM pathology of POAG. NOX4 drives TGF- $\beta$  mediated ECM production in fibrotic diseases<sup>451</sup> (Figure 3.11). Alterations in the extracellular matrix of the TM is a hallmark of POAG pathogenesis<sup>457</sup>. Increased ECM production and decreased turnover is thought to contribute to resistance in outflow facilities thus elevating IOP<sup>119,155</sup>. Our findings suggest that the interplay between TGF- $\beta$  and NOX4 may be contributing to POAG pathogenesis via ROS driven increased ECM production within the TM. Patients with POAG have a total reactive anti-oxidant potential of 60%<sup>458</sup>. Reduction in reactive anti-oxidant potential exposes POAG patients to increased risk of oxidative damage. Oxidative stress results in damage to the mitochondrial DNA of TM cells, as well as proteins and other membranes<sup>459</sup>. Increased H<sub>2</sub>O<sub>2</sub> also causes remodelling of the TM cytoskeleton leading to TM enlargement and decreased outflow abilities<sup>460</sup>. Despite the need for acute NOX4 expression in wound healing chronic NOX4 activation is likely to result in fibrosis and organ dysfunction<sup>461</sup>. The exact mechanisms through which the TM undergoes ECM remodelling and eventual cell death are unknown, however, it may be attributed to increased H<sub>2</sub>O<sub>2</sub> levels caused by enduring NOX4 expression, driven by TGF- $\beta$ .

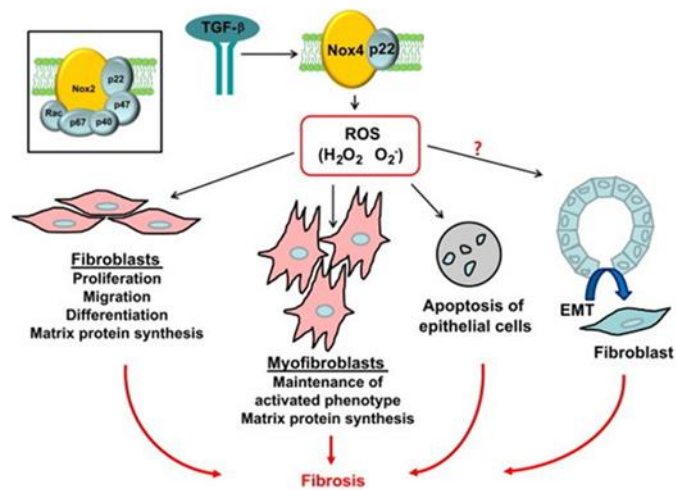


**Figure 3.11: NOX4 Mediated TGF- $\beta$ -Induced Pro-Fibrotic Responses.** Modified From Jiang *et al* 2014<sup>451</sup>. NOX4 derived ROS aid TGF- $\beta$ -induced synthesis of ECM, fibroblast differentiation. ROS also promote apoptosis.

## Endothelin 1 (EDN1)

Endothelin 1 (EDN1) is a potent vasoactive peptide that exerts its actions through two receptors endothelin A and endothelin B<sup>462,463</sup>. EDN1 has a unique profile as an endothelium-derived vasoactive factor with powerful and characteristically long-lasting vasopressor activity. Elevated expression of EDN1 in response to TGF- $\beta$ 2 has previously been shown in cultured trabecular meshwork cells and both EDN1 mRNA content and secretion from TM cells were elevated<sup>464</sup>. Our RNA-Seq identified EDN1 expression was significantly up-regulated in human TM cells exposed to TGF- $\beta$ 2 (FC= 6.58,  $p$ -value= 5.9E-150), which was confirmed by q-PCR (FC= 65.39,  $p$ -value= 0.0022, Figure 3.8).

EDN1 is expressed in all ocular tissues except the cornea<sup>465</sup> and the levels in the AH are 2-3 times higher than in plasma<sup>466</sup>. POAG patients have elevated levels of EDN1 in their AH and animal models of glaucoma have supported a role of EDN1 in glaucoma pathogenesis<sup>467,468</sup>. Endothelin A receptor is expressed in TM cells<sup>469</sup> and *in-vitro* studies identified increased TM cell contractility in response to elevated EDN1 expression<sup>470</sup>. Increased contractility of TM cells is a hallmark of glaucoma<sup>471</sup>. Contraction of TM cells decreases intracellular space resulting in increased resistance to AH outflow. There is accumulating evidence for the role of EDN1 in glaucoma pathogenesis<sup>472-475</sup>. The main risk factor for developing POAG is elevated IOP. Normal tension glaucoma, in which glaucomatous optic neuropathy occurs at normal IOP, suggests that other factors may be involved in the disease pathogenesis, for example, reduced ocular blood flow<sup>476,477</sup>. Both IOP and ocular blood flow are affected by EDN1<sup>467</sup>. Differential experimental approaches identified elevated EDN1 in AH increased IOP<sup>478-480</sup>. Animal models show a dose dependent rise in IOP after intracameral injection of EDN1<sup>478</sup>. In the bovine eye, EDN1 induced the reduction of AH outflow cause by increased TM contraction<sup>401</sup>. Contractility could be blocked by inhibition of the Rho kinase signalling pathway<sup>481</sup>.

In addition to the biochemical and morphological changes in the TM during glaucoma pathogenesis, the optic nerve head (ONH) is subjected to structural loss of RGCs. Physiologically EDN1 helps to maintain IOP by strict control of TM contractility. Pathological levels of EDN1 reduce ocular blood flow and increase TM cell contractility<sup>482</sup>. Intravitreal injections of EDN1 reduced ocular blood flow to the ONH in healthy volunteers<sup>483</sup>. Perfusion of EDN1 in animal models also induced similar optic neuropathies<sup>472</sup>. Thus, ischaemic insult to the ONH occurs and subsequent RGC death. An antagonism of EDN1 in both pressure dependent and independent pathways provides a promising approach for treatment of glaucoma by several mechanisms: (1) reduction of IOP; (2) enhanced ocular blood flow; and (3) increased survival of RGCs.

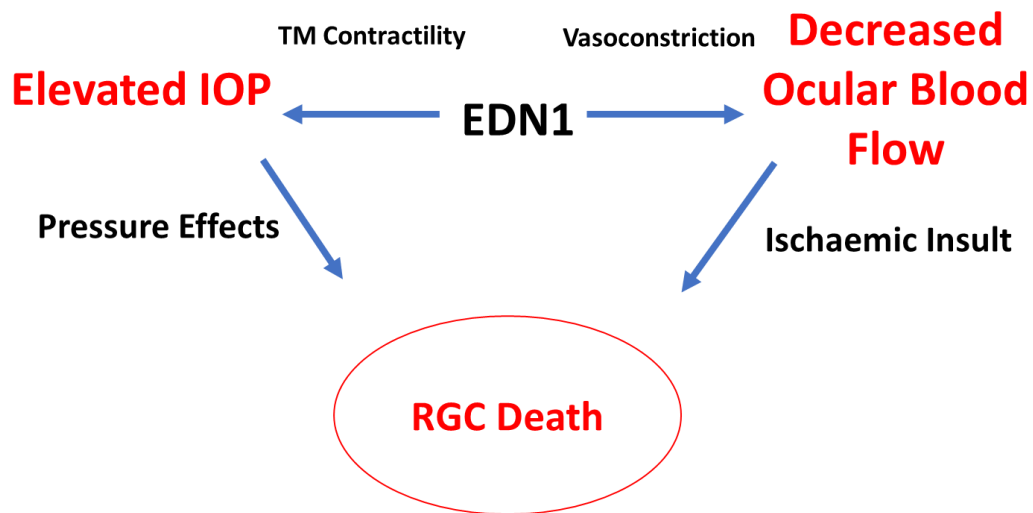


**Figure 3.12: Pathological Role of EDN1 in Glaucoma.** Disruption of physiological EDN1 levels results in decreased ocular blood flow and elevated IOP. Pressure and ischaemic insults lead to subsequent RGC death i.e. ONH structural loss.

## Cyclin Dependent Kinase Inhibitor 2B and Cyclin Dependent Kinase Inhibitor 2B Antisense Gene (CDKN2B and CDKN2B-AS1)

Cyclin-dependent kinase inhibitor-2B (CDKN2B) gene and its antisense gene CDKN2B-AS1 are located on chr9p21. CDKN2B encodes a cyclin-dependent kinase inhibitor, p15<sup>INK4b</sup>, which plays an important role in the regulation of the cell cycle through the inhibition of cyclin-dependent kinase 4 (CDK4)<sup>484</sup>. The expression of CDKN2B is significantly induced by TGF- $\beta$ <sup>485</sup> and plays a role in the mediation of TGF- $\beta$ -induced cell cycle arrest<sup>485,486</sup>. TGF- $\beta$  inhibits cell proliferation by producing G1 phase cell cycle arrest<sup>485</sup> and CDKN2B, which forms a complex with either CDK4 or CDK6 preventing their activation, acts as an effector of TGF- $\beta$  cell cycle arrest<sup>487</sup>.

In human TM cells stimulated with TGF- $\beta$ 2, CDKN2B was up-regulated as shown by RNA-Seq (FC= 4.29,  $p$ -value= 1.41E-92), and confirmed by q-PCR (FC= 41.57,  $p$ -value= 0.0022 Figure 3.8). POAG associated single nucleotide polymorphisms (SNPs) have been identified by GWAS and candidate gene investigations within the 9p21 locus<sup>488-490</sup>. The relationship between CDKN2B-AS1 genetic variants and specific glaucoma features is unknown<sup>491</sup>. CDKN2B-AS1 is a long non-coding RNA which is likely have a functional effect on a target mRNA through complementary binding to induce RNA degradation or translational inhibition. It has been proposed that CDKN2B-AS1 may influence the nearby genes: CDKN2A and CDKN2B; both of which are essential in cell proliferation and senescence<sup>492</sup>. SNPs within or close to CDKN2B-AS1 are associated with a number of diseases including glaucoma, coronary artery disease, diabetes and cancer<sup>490,492-497</sup>. There is some evidence that CDKN2B-AS1 can regulate the expression of CDKN2B and that this relationship may be reciprocal<sup>498,499</sup>. Given the induction of CDKN2B by TGF- $\beta$ 2 in our study we investigated the expression profile of CDKN2B-AS1 in the same TGF- $\beta$ 2 treated human TM cells and in the glaucomatous samples. Only one of six donors exhibited an increase in expression of CDKN2B-AS1 in the presence of TGF- $\beta$ 2 (Figure 3.8). However, there was an overall increase in expression of CDKN2B-AS1 in the glaucomatous TM; this was not statistically significant given the small sample size (Figure 3.9). Further studies are required to dissect the role and interplay of CDKN2B and CDKN2B-AS1 in the TM and in POAG<sup>490</sup>.

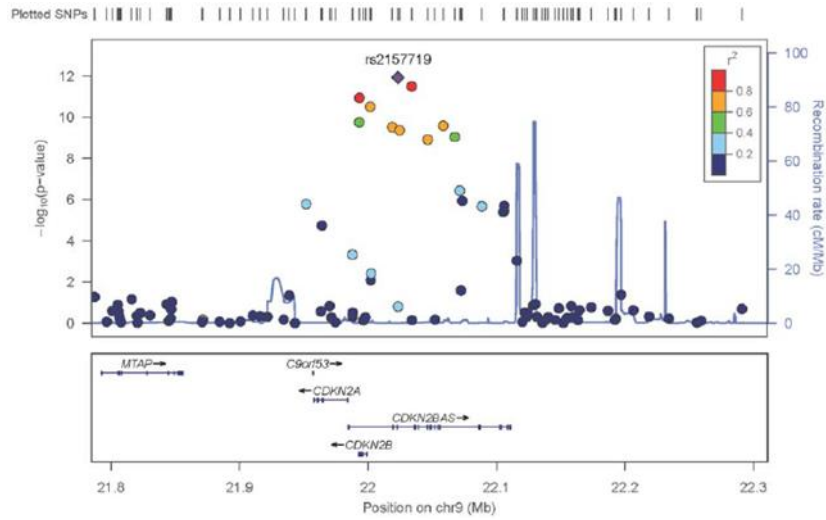


**Figure 3.13: Localisation of CDKN2B and CDKN2B-AS1 on Chr9p21.** Figure from Wiggs *et al* 2015<sup>500</sup>.

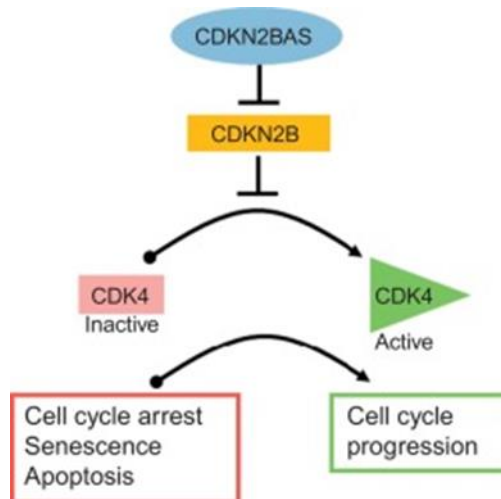


**Figure 3.14: Effects of CDKN2B and CDKN2B-AS1 on Cell Cycle via CDK4 Inhibition.** Modified from Wiggs *et al* 2015<sup>500</sup>. CDKN2B inhibits CDK4 to regulate cell cycle. Disruption of cell cycle in disease leads to cellular loss in the TM.

## WNT Signalling Pathway

Wnt signalling plays multiple roles in embryogenesis and development, including cell proliferation, differentiation, migration, cell polarity, and cell survival and apoptosis<sup>501</sup>. In the eye, Wnt signalling pathways are associated with different stages of ocular development and growth, cell differentiation, connectivity and proliferation<sup>502</sup>. Alterations in Wnt signalling, due to mutations or external cues, result in multiple ocular diseases including, retinal degeneration, cataract, congenital ocular malformations, and exudative vitreoretinopathies<sup>503</sup>. More recently, studies have demonstrated a potential role for Wnt signalling in POAG pathogenesis<sup>504</sup>.

Wnt proteins are a highly conserved family of secreted glycoproteins that signal two types of receptors; seven-pass transmembrane receptors known as frizzled proteins (FZD), and single-pass transmembrane co-receptors lipo-protein receptor related proteins (LRPs)<sup>505,506</sup>. Wnt signalling can occur via the canonical and non-canonical pathway. The canonical pathway is  $\beta$ -catenin dependent, whereas the non-canonical pathway is  $\beta$ -catenin independent<sup>507</sup>. Several extracellular secreted factors regulate Wnt signalling. Secreted frizzled-related proteins (SFRPs) and Wnt-inhibitory factor 1 (WIF-1) prevent Wnt binding with FZD receptors resulting in inhibition of both canonical and non-canonical pathways<sup>508</sup>. Dickkopf proteins (DKKs) also inhibit Wnt signalling by binding LRP5/6<sup>509</sup>.

WNT2B expression was significantly repressed in our RNA-Seq data (FC= -2.96,  $p$ -value= 2.93E-56), however further validation of this down-regulation could not be achieved by q-PCR (Figure 3.8). The WNT2B gene encodes a member of the wingless-type MMTV integration site (WNT) family of secreted signalling factors. A possible role of Wnt signalling in the ocular outflow system has been previously suggested<sup>510</sup> and WNT2B expression has been reported in the human TM<sup>511,512</sup>. Inhibition of Wnt signalling in TM cells results in persistent increases in intrinsic cell stiffness, a key hallmark of POAG pathogenesis<sup>513</sup>. The expression of secreted frizzled-related protein-1 (sFRP-1) is elevated in the glaucomatous TM<sup>511</sup>. sFRP-1 is an antagonist of Wnt signalling and murine and ex-vivo perfusion models supported a role for sFRP-1 in elevated IOP in glaucoma by inhibiting Wnt signalling<sup>511</sup>. Interestingly, sFRPs are induced by TGF- $\beta$  and may therefore drive decreased Wnt gene expression in TGF- $\beta$  treated TM cells as observed by our study and previous studies<sup>511,514</sup>. There is evidence of a cross-inhibition between TGF- $\beta$  signalling and canonical Wnt pathways<sup>515</sup>: TGF $\beta$ -2 inhibits Wnt3a-induced canonical Wnt pathway activation and Wnt3a inhibits TGF $\beta$ 2-induced Smad4 pathway activation<sup>510</sup>.

Our data confirms TGF- $\beta$ 2 inhibits Wnt signalling by repressing WNT2B but also induces the expression of Wnt antagonists. The DACT1 (dishevelled binding agonist of beta cantenin 1), encoding gene was highly represented in our RNA-Seq

data (FC= 3.58,  $p$ -value= 2.81E-58) and again in q-PCR (FC= 12.71,  $p$ -value= 0.0022 Figure 3.8). Interestingly, a trend of increased gene expression for DACT1 was also observed in glaucomatous TM cells when compared to controls (Figure 3.7.). DACT1 expression in intestinal epithelial cells is increased by TGF- $\beta$ <sup>516</sup> and mediates TGF- $\beta$  driven apoptosis in renal mesangial cells<sup>517</sup>. DACT1 has not been associated with ocular disease previously but may play a role of TGF- $\beta$ -mediated inhibition of Wnt signalling in the TM.

### Prostate Transmembrane Protein Androgen Induced 1 (PMEPA1)

Prostate transmembrane protein androgen induced 1 (PMEPA1) encodes a protein of 252 amino acids with a type 1b trans-membrane domain. PMEPA1 is a negative regulator of TGF- $\beta$  signalling in prostate cancer cells<sup>518</sup>. The ubiquitin-mediated proteosomal degradation pathway is an evolutionary conserved cascade that tightly regulates TGF- $\beta$  signalling<sup>519</sup>. Membrane bound PMEPA1 isoforms are able to interact with regulatory SMADs (SMAD2) and ubiquitin ligases, to block TGF- $\beta$  signalling independently of the proteasome-mediated degradation<sup>520</sup>. In our study PMEPA1 expression was significantly up-regulated in human TM cells treated with TGF- $\beta$ 2 by RNA-Seq (FC=4.81,  $p$ -value= 2.76E-84), and corroborated by q-PCR (FC=32.28,  $p$ -value= 0.0022 Figure 3.7). A microarray analysis of gene expression in human optic nerve head astrocytes identified differential expression of SMURF2 in response to hydrostatic pressure<sup>521</sup>. SMURF2 is a SMAD-ubiquitin ligase that induces the ubiquitination and degradation of the TGF- $\beta$ -SMAD2/3 pathway to regulate TGF- $\beta$  signalling. Interaction between SMURF2 and PMEPA1 have previously been described in prostate cancer<sup>522</sup>.

Low density lipoprotein receptor class A domain containing 4 (LDLRAD4) an important paralog of PMEPA1<sup>523</sup>, was significantly up-regulated in our RNA-Seq data (FC= 7.23,  $p$ -value= 1.9E-59). LDLRAD4, also known as C18ORF1, encodes the LDLRAD4 protein whose primary function is to negatively regulate TGF- $\beta$  signalling<sup>524</sup>. It is hypothesised that LDLRAD4 competes with inhibitory SMAD4 and prevents propagation of intracellular signals<sup>524</sup>. In our study LDLRAD4 expression was also significantly up-regulated in human TM cells exposed to TGF- $\beta$ 2 for 24 hours by q-PCR (FC= 10.46,  $p$ -value= 0.0043, Figure 3.8).

Both PMEPA1 and LDLRAD4 have not previously been implicated in glaucoma pathogenesis. It is possible that an up-regulation of PMEPA1 and LDLRAD4 in TGF- $\beta$ 2 treated human TM cells is a response to internally control the acute TGF- $\beta$ 2 insult; however further investigation would be required to implicate both genes in the pathogenesis of the disease.

### Follistatin-like 3 (FSTL3)

Follistatin-like 3 (FSTL3) is a member of the follistatin family which differs from follistatin (FST) as it lacks the third follistatin domain and a consensus heparin-binding sequence. Both FSTL3 and FST inhibit the actions of activins and bone morphogenic proteins (BMPs) which are members of the TGF- $\beta$  family that are involved in processes such as cell proliferation and differentiation, immune response, and wound repair<sup>525</sup>. In our study FSTL3 expression was significantly up-regulated in human TM cells exposed to TGF- $\beta$ 2 for 24hours using RNA-Seq (FC= 4.19,  $p$ -value= 3E-99), and confirmed by q-PCR (FC=28.07,  $p$ -value=0.0022, Figure 3.8). Previous gene expression profiling of TGF- $\beta$ 2 treated TM cells by microarray identified an up-regulation of FSTL3<sup>406</sup>.

The role of TGF- $\beta$ 2 in POAG is multifaceted and the identification of downstream effectors of TGF- $\beta$  signalling is required to understand disease pathogenesis and identify new therapeutic targets. BMPs are members of the TGF- $\beta$  superfamily which have been identified in the human TM<sup>526</sup> and BMPs can block TGF- $\beta$ 2 induction of ECM proteins in the TM. The expression of gremlin, a BMP antagonist, is elevated in glaucomatous TM cells<sup>408,527</sup>. Interestingly, FST, also a BMP antagonist, is expressed in TM cells<sup>526</sup>. The role of FSTL3 in glaucoma or following TGF- $\beta$ 2 induction is unknown. It has been proposed that the increase in FSTL3 expression following TGF- $\beta$ 2 stimulations may antagonise BMP7 and or BMP4 which therefore reduces their antagonism of TGF- $\beta$  signalling<sup>408,527</sup>.

FSTL3 attenuation of BMP antagonism of TGF- $\beta$  signalling may have pro-fibrotic effects<sup>528</sup>. In murine transgenic models FSTL3 knockout accentuated interstitial fibrosis in the heart<sup>528</sup>. Fibrosis of the TM cells due to biochemical and morphological changes during glaucoma pathogenesis and after glaucoma surgery is a driver in AH outflow resistance and associated elevated pressure<sup>529</sup>. Components of pro-fibrotic processes are ideal candidates for novel therapeutics in attempts to regain efficient AH outflow. The role of FSTL3 in the pathogenesis of POAG has not been established. However it is likely that induction of TGF- $\beta$  signalling leads to elevated FSTL3 expression as a means of BMP inhibition, thus prolonging TGF- $\beta$  insult within the TM resulting in TM fibrosis and elevated IOP.

### Odd-skipped Related Transcription Factor 2 (OSR2)

Odd-skipped related transcription factor 2 (OSR2) encodes a zinc-finger protein with extensive similarity to the *Drosophila* Odd-skipped family of putative transcription factors<sup>530</sup>. Gene expression and phenotypic analyses have indicated that the odd-skipped gene product functions to prevent inappropriate expression of other segmentation genes<sup>531,532</sup>. In our study OSR2 expression was significantly down-regulated in human TM cells treated with TGF- $\beta$ 2 (FC= -5.37,  $p$ -value= 4.15E-

67), however this could not be confirmed by q-PCR in healthy TM cells treated with TGF- $\beta$ 2 (Figure 3.8). The OSR2 promoter possesses SMAD3/4 and ATF binding elements. TGF- $\beta$ 2 down-regulates OSR2 resulting in altered cell migration and cell cycle regulation in fibroblastic mesenchymal cell lines<sup>533</sup>. To date no studies have identified OSR2 as being implicated in glaucoma.

### Left-right Determination Factor 2 (LEFTY2)

Left-right determination factor 2 (LEFTY2) encodes secreted ligands of the TGF- $\beta$  family which bind various TGF- $\beta$  receptors resulting in the recruitment of SMAD family transcription factors that are necessary for gene expression regulation<sup>534</sup>. Mutations in LEFTY2 have been implicated in left-right axis malformation particularly in the heart and lungs<sup>535</sup>. In our study LEFTY2 expression was significantly up-regulated by RNA-Seq (FC= 6.94, *p*-value= 4.88E-62) and confirmed by q-PCR (FC= 98.30, *p*-value= 0.0022, Figure 3.7). LEFTY is a known inhibitor of TGF- $\beta$  and is therefore an important component in the homeostasis of extracellular matrix (ECM)<sup>536</sup>. LEFTY2 has not previously been implicated in POAG however it is widely accepted that alterations in ECM secretion and deposition within the TM is implicated in glaucoma pathogenesis, and TGF- $\beta$ 2 is known to be a key driver in these changes<sup>537</sup>. As an inhibitor of TGF- $\beta$ 2, it is possible that LEFTY2 is involved in TGF- $\beta$  inhibition in human TM cells exposed to elevated TGF- $\beta$ 2.

### Ras-like Protein Family Member 11B (RASL11B)

Ras-like protein family member 11B (RASL11B) encodes RASL11B protein, a member of the small GTPase protein family with a high degree of similarity to RAS<sup>538</sup>. Interestingly, the RASL11B promoter contains an SRF binding site which is activated by TGF- $\beta$ <sup>539</sup>. In arterial smooth muscle cells TGF- $\beta$ 1 induces the expression of RASL11B in artery smooth muscle cells and macrophages<sup>540</sup>. Macrophages are a major source of TGF- $\beta$ 1 in atherosclerotic vessels and stimulate the smooth muscle cells in the vessel walls to produce ECM; this is not dissimilar to TGF- $\beta$  driven ECM deposition in the TM in glaucoma<sup>540</sup>. In our study RASL11B expression was identified as significantly up-regulated in human TM cells exposed to TGF- $\beta$ 2 by RNA-Seq (FC= 7.12, *p*-value= 2.91E-60) and confirmed by q-PCR (FC= 164.38, *p*-value= 0.0022, Figure 3.8). In a previous, RASL11B was significantly up-regulated (FC= 2.9) in glaucomatous human TM cells versus the normal TM; RNA was directly extracted from tissue post-surgery (glaucoma) or post-mortem and analysed on Illumina BeadChip arrays<sup>541</sup>. No further investigation of the potential role of RASL11B in glaucoma was pursued in this study<sup>541</sup>.

### Fibronectin Type II Domain Containing 1 (FNDC1)

Fibronectin type II domain containing 1 (FNDC1) encodes FNDC1 protein and contains a major component of the structural domain of fibronectin (FN)<sup>542</sup>. The biological role for FNDC1 is poorly understood. FNDC1 is reported to be involved in G protein signalling<sup>543</sup>. FNDC1 also known as MEL4B3, has previously been reported in skin tumours and is thought to be regulated by TGF- $\beta$ <sup>544</sup>. In our study, FNDC1 expression was significantly up-regulated in human TM cells treated with TGF- $\beta$ 2 by RNA-Seq, (FC= 4.02,  $p$ -value= 6.79E-57), and confirmed by q-PCR (FC= 15.17,  $p$ -value= 0.0087, Figure 3.8). Fibronectin (FN) is a major component of the TM extracellular matrix and increased secretion and deposition of FN has been shown in glaucomatous TM<sup>415</sup>. This increased deposition has been attributed to enhanced TGF- $\beta$  signalling and is thought to contribute to increased AH outflow resistance observed in POAG patients which results in elevated IOP<sup>240</sup>. In prostate cancer silencing of FNDC1 also represses the expression of FN<sup>545</sup>. Given the major role FN plays in the pathogenesis of POAG the relationship between FNDC1 and FN warrant further investigation to understand TGF- $\beta$  mediated processes in glaucoma pathogenesis.

### ATPase Phospholipid Transporting 10a (ATP10A)

ATPase Phospholipid Transporting 10a (ATP10A) encodes ATP10A enzyme and is a subfamily of aminophospholipid-transporting ATPases, required for the transmembrane transport of phosphatidylserine and phosphatidylethanolamine<sup>546,547</sup>. ATP10A is required to maintain an asymmetric distribution of phospholipids. Phospholipid translocation has been implicated in vesicle formation, in uptake of lipid signalling molecules and maintaining cell morphology<sup>546</sup>. ATP10A expression was significantly up-regulated by RNA-Seq in TGF- $\beta$ 2 treated human TM cells (FC= 3.62,  $p$ -value= 4.03E-66), and by q-PCR (FC= 10.18,  $p$ -value= 0.0022, Figure 3.8). Interestingly, the expression of ATP10A was elevated (FC= 2.92) in human cultured TM cells treated with steroid (triamcinolone 1mg/mL)<sup>548</sup> and ATP10A also lies in a POAG mapped locus (GLC1I) on chr15q11-13<sup>549</sup>. The role of ATP10A in the TM is unknown.

## Analysis of DEG in Glaucoma TM Samples

q-PCR analysis of DEGs identified by RNA-Seq in glaucomatous TM (GTM) samples compared to healthy controls (Figure 3.7) did not yield statistically significant fold changes. Availability of disease donor tissue is limited and therefore the number of biological samples (n=3) for this experiment was small. An increase in sample size may provide increased statistical power. GTM cells were also cultured prior to RNA-Seq and q-PCR analysis and RNA were not directly extracted from tissue. GTM cells were also not stimulated by TGF- $\beta$ 2. As AH of POAG patients has significantly elevated levels of TGF- $\beta$ 2, GTM had previously been exposed to chronic TGF- $\beta$ 2 stimulations which most likely impacts on their gene expression profiles. Together with sample size and previous chronic TGF- $\beta$  exposure may explain why no significant difference was observed between the two sample groups: control and glaucomatous.

### 3.6 Summary

Isolation and characterisation of primary human TM cells prior to sequencing proved difficult in the preparation for these experiments. The human TM has reduced cellularity with age, and to re-capitulate normal and disease states as effectively as possible older donors were used. This presented challenges with regards to effective TM culture growth and cell numbers. Low cell count resulted in low RNA yields and reduced quality. This aspect was time consuming and required attention to detail.

Our study provides a comprehensive characterisation of differentially expressed genes in response to TGF- $\beta$ 2. It demonstrates that among the set of differentially expressed genes, the majority are implicated in cytoskeletal and extracellular matrix remodelling of the human trabecular meshwork cells. TGF- $\beta$ 2 is implicated extensively in these processes however both TGF- $\beta$ -related and -unrelated genes were identified in the TM in association to TGF- $\beta$ 2 stimulations.

We have successfully identified candidate target genes which warrant further investigation regarding their potential role in POAG. NOX4 has not previously been implicated in POAG, however increasing evidence suggests that oxidative stress, of which NOX4 is a key player, plays a significant role in disease pathogenesis. miRNAs regulate a number of target genes, of which NOX4 is included. miR-25 regulates NOX4 expression in diabetic nephropathy<sup>550</sup> and may serve as an endogenous silencing factor and contributor to the regulation of NOX4. The potential role for this miRNA as a therapy is of interest moving forward.

The results obtained through next generation sequencing were not always corroborated by q-PCR. Both techniques have varying sensitivity and it important to note that whilst sequencing is quantitative, i.e the number of reads per gene is

established, q-PCR is in comparison qualitative. The effects of TGF- $\beta$ 2 are also robust and culturing the human TM cells prior to treatment may have had alternative effects on gene expression. These contributing factors must be considered moving forward and alternative approaches such as direct RNA isolation from tissue may provide a more comprehensive outlook on TM gene expression. TGF- $\beta$ 2 however is elevated in the aqueous humour of POAG patients, thus effects on gene expression that arise in response to this are of importance in understanding disease pathophysiology. Furthermore, manipulation of novel targets to reduce negative impacts on the aqueous humour outflow pathway is a promising step forward in developing new and therapeutics for POAG and this will be discussed in Chapter 6.

## **Chapter 4**

# **A Comparison of Global Gene Expression Profiles in Human Trabecular Meshwork Cells Treated with Dexamethasone using RNA-Sequencing**

## 4.1 Introduction

Corticosteroid use is widespread in ophthalmology and continues to be the mainstay of treatment for inflammatory eye diseases and post-surgically, when prolonged treatment is often required. The duration of steroid treatment ranges from several weeks, for controlling post-operative inflammation, to long-term (1 year+) for preventing corneal transplant (keratoplasty) rejection<sup>551</sup>. Up to 35% of patients without a prior glaucoma diagnosis, and up to 80% of those with pre-existing glaucoma experience clinically significant post-keratoplasty IOP elevation with long-term topical corticosteroid use<sup>551</sup>. The risk of IOP elevation, and the time-frame during which this occurs, is dependent on steroid potency, pharmacokinetics, duration of treatment, route of administration, as well as individual differences in responsiveness.

Steroid-induced elevated IOP results from increased AH outflow resistance, caused by several morphological and biochemical changes in the TM. The TM expresses glucocorticoid receptors which respond to steroid administration by regulating gene expression in the TM driving changes to the extracellular matrix, cell cytoskeleton and cross-linked actin networks<sup>552</sup>. The link between primary open-angle glaucoma (POAG) and steroid responsiveness was highlighted when the Trabecular Meshwork Inducible Glucocorticoid Response gene (TIGR; renamed myocilin), expressed in cultured trabecular meshwork<sup>553</sup>, was found within the GLC1A region of genomic DNA from families affected with chromosome 1q-linked open angle glaucoma<sup>554</sup>. Although TIGR/myocilin is expressed in TM, induced by corticosteroids, and linked with the glaucoma phenotype in a subset of patients<sup>553,554</sup>, there is no clear evidence for the pathogenic role of this gene in steroid-induced ocular hypertension or glaucoma.

Armaly<sup>555</sup> and Becker<sup>556</sup> reported that the general population could be divided into three groups based on their response to topical steroid administration: (1) high responders, 4–6% of the population, developed an IOP  $\geq$  31 mmHg or  $\geq$ 15 mmHg above baseline; (2) moderate responders, approximately one third of the population, had IOPs between 20-31 mmHg, or a pressure rise of 6–15 mmHg; and

(3) non-responders, the remaining two thirds, had pressure increases  $\leq 6$  mmHg and IOPs  $\leq 20$  mmHg. In addition, clinical risk factors for high IOP steroid response after glucocorticoid treatment have been described in: patients with primary open angle glaucoma (POAG) or glaucoma “suspects”, first-degree relatives with POAG, old age or aged less than 6 years, connective tissue disease, especially rheumatoid arthritis in men, high myopia and type I diabetes mellitus<sup>163,557</sup>. Interestingly, almost all POAG patients are steroid responders<sup>163,202</sup>, and steroid-responders who do not have POAG are at much higher risk of developing POAG compared to non-responders<sup>163,202</sup>. Moreover, relatives of POAG patients have higher rates of steroid responsiveness<sup>558–560</sup>. A better understanding of genetic and molecular mechanisms underlying the response to steroids could shed light on our understanding of steroid-induced glaucoma and the pathogenic mechanisms in primary open-angle glaucoma.

A number of structural and functional changes occur in the TM with glucocorticoid treatment that lead to elevated IOP due to increased outflow resistance<sup>552</sup>. These changes are associated with increased ECM material production and deposition<sup>561–563</sup>, TM actin cytoskeletal re-organisation<sup>257</sup>, decreased TM phagocytic activity<sup>195</sup>, decreased protease activity<sup>564</sup>, and changes in the synthesis of specific proteins<sup>565</sup>. Most of the effects of glucocorticoids on the TM result from altered gene expression mediated by activated glucocorticoid receptor inducing or repressing glucocorticoid response elements (GREs) in numerous genes and also through non-GRE pathways<sup>566</sup>.

Six studies have examined global changes in gene expression in the cultured TM cells treated with dexamethasone using cDNA or oligonucleotide arrays<sup>548,567–571</sup>. Some common differentially expressed genes were reported in these studies: myocilin (MYOC), growth arrest specific 1 (GAS1), insulin-like growth factor binding protein 2 (IGFBP2), serpin peptidase inhibitor clade A member 3 (SERPINA3) and serum amyloid A1 and A2 (SAA1; SAA2)<sup>548,567–571</sup>. However, overall the findings were not consistent across studies as, while the dose of dexamethasone (DEX) was consistent (100nM), the duration of treatment varied from 24 hours to 21 days and different microarray platforms were used (Table 4.1).

Study	Age of Donors	Cell Passage	DEX Duration	Genes assessed	Array Type
Ishibashi et al. 2002 <sup>567</sup>	7, 16, 21 and 28 yrs	4-5	7 days	2,400	cDNA
Lo et al. 2003 <sup>568</sup>	unknown	4-6	10 days	9,330	Oligonucleotide
Leung et al. 2003 <sup>569</sup>	unknown	8	10 days	2,400	cDNA
Rozsa et al. 2006 <sup>570</sup>	12,16,17 yrs	5	21 days	13,507	Oligonucleotide
Fan et al. 2008 <sup>548</sup>	52 yrs old	8	7 days	22,904	cDNA
Nehme et al. 2009 <sup>571</sup>	3 months old and 35 yrs	3-6	24 hours	33,000	Oligonucleotide (Agilent)

**Table 4.1: Summary Table of Previous Microarray Studies of DEX treatment of TM Cells.** Six individual microarrays examined global gene expression in TM cells with specific conditions utilised in each outlined above<sup>548,567-571</sup>.

The variability between study findings may relate to differences in the individual responsiveness to DEX treatment of each TM cell donor. Although there is a genetic basis to the steroid response, the basis for individual susceptibility to develop steroid induced ocular hypertension or glaucoma is unknown<sup>163</sup>. There is some evidence that alternative splicing in the human glucocorticoid receptor might impact on individual susceptibility to steroid-induced glaucoma or raised IOP (ocular hypertension)<sup>552,572</sup>.

Alternative splicing and differential initiation start sites for the human glucocorticoid receptor (GR) results in at least six isoforms<sup>552</sup>. The two major splice variants are GR $\alpha$  and GR $\beta$ ; both of which are expressed in TM cells<sup>572</sup>. GR $\alpha$  is the main ligand-binding physiological and pharmacological receptor for glucocorticoids, whereas GR $\beta$  acts as a natural dominant-negative inhibitor of GR $\alpha$  activation, and so glucocorticoid activity<sup>573</sup>. Increased expression of GR $\beta$  has been implicated in glucocorticoid resistance in systemic diseases<sup>574</sup> and there is evidence that GR $\beta$

expression in the TM might confer individual resistance to glucocorticoid induced ocular hypertension. There is decreased GR $\beta$  expression in glaucomatous TM cells compared to normal TM cells and a reciprocal increase reactivity of the glaucomatous TM to dexamethasone induction of myocilin expression, fibronectin production and induction of GRE-responsive luciferase constructs<sup>575</sup>. Conversely, increased expression of GR $\beta$  in normal TM cells confers a resistance to dexamethasone induced protein expression and inhibition of phagocytosis<sup>195</sup>.

The response of the TM to glucocorticoids results in large changes in gene expression but it is currently unclear which genes or pathways contribute to glucocorticoid induced IOP (ocular hypertension and glaucoma)<sup>163,552,571</sup>. RNA-Seq confers significant advantages over array-based gene expression studies and has not previously been performed to assess global alternations in gene expression in TM cells stimulated with glucocorticoids.

#### 4.2 Aim

The aim of this study was to employ RNA-Seq to investigate alterations in the transcriptome of normal trabecular meshwork cells in the presence or absence of dexamethasone to detect pathophysiological mechanisms underlying glaucoma and potential therapeutic targets.

## 4.3 Materials and Methods

### 4.3.1 Sample Collection, Preparation, and Tissue Culture Establishment

Cadaveric eyes were provided by the Liverpool Research Eye Bank and handled in accordance to the tenets of the Declaration of Helsinki (Ethics Code; RETH000833). Cells were maintained in DMEM-low glucose (Sigma, UK) supplemented with 10% fetal calf serum (Bio Sera, UK), 2mM L-glutamine (Sigma, UK), Pen/Step (Sigma, UK), and 2.5ug/mL Fungizone (Amphotericin B, Sigma, UK). Samples were incubated at 37°C (5%CO<sub>2</sub> and 95% humidity) for 7-14 days with a medium changed every 2 days ensuring not to disturb the explant. When cells had reached 80-90% confluence there were transferred into individual T25 tissue culture flasks and maintained as above with the subtraction of Fungizone for a further week. Cells were characterised as TM cells as previously described (3.2.3).

Donor I.D	Age	Sex	Medical History
LGP-1	57	Male	No Glaucoma
LGP-2	65	Male	No Glaucoma
NTM002	57	Male	No Glaucoma
NTM009	57	Male	No Glaucoma
NTM720	64	Male	No Glaucoma
NTM119	94	Male	No Glaucoma, cataract Surgery

**Table 4.2: Human TM Cell Donor Information.**

### 4.3.2 Dexamethasone Stimulations

All confluent cells were mycoplasma tested as described previously (2.1.5) prior to experimentation. Human TM cells between passages 5 and 7 were grown to 80% confluence and growth arrested using serum free medium prior to stimulation. Cells were stimulated with dexamethasone at a concentration of 100nMol for 16

hours. Vehicle control cells were stimulated with equal volumes of 0.1% ethanol. Treatment time points and concentration were determined based on previously published work outlining human TM cell stimulations<sup>195,565</sup>. Following 16 hours of stimulation total RNA was extracted (2.4.1).

#### 4.3.3 Total RNA Extraction and QC

Total RNA from human culture trabecular meshwork cells was isolated using the Qiagen Universal All Prep (Qiagen, UK) kit as per manufacturers specifications, described in (2.4.1). Total RNA was quantified initially on the Nanodrop-1000 (Thermofisher, UK), and quality was determined by the Bioanalyser 2100 (Agilent, UK) as described in (2.4.2 and 2.4.3 respectively).

#### 4.3.4 RNA-Seq of Cultured Normal Human Trabecular Meshwork Cells

All RNA-Seq experiments were conducted at Exiqon Services, Denmark as previously described (3.2.5). Two groups of mRNA libraries were prepared as before: a control group, consisting of untreated cultured human TM cells, henceforth referred to as CD\_Group, and a dexamethasone (DEX) treated group, henceforth referred to as TD\_Group. RNA-Seq data analysis was as previously described (Chapter 3, 3.35).

#### 4.3.5 RNA-Seq Data Validation

Validation of mRNA-seq results was performed as previously described (3.2.7). q-PCR analysis was performed using primers whose sequences were obtained from PrimerBank for target genes<sup>576</sup>, see Table 4.3 below. Data is expressed as the mean values  $\pm$  SEM and analysed using student t-test. Statistical differences in the mean were considered statistically significant as  $p < 0.05$ .

Gene expression analysis of glucocorticoid receptor isoforms, GR- $\alpha$  and GR $\beta$  was also performed to assess differential receptor ratios to identify potential steroid-responsive and non-responsive donors. q-PCR was performed using primers obtained from PrimerBank (GR $\alpha$  F:5'GAAGGAACTCCAGCCAGAA'3, R:5'TAAGGGGCTCTACAATCGAC'3 and GR $\beta$  F:5'TGACTCTACCCTGCATGTACGACCA'3, R:5'CTATTTTTTGAGCGCCAAGATTGTT'3).

<b>Gene Target</b>	<b>Primer Pair Sequence</b>
<b>PTK2B</b>	F:5'CCCCTGAGTCGAGTAAAGTTGG'3 R:5'GATACGCACGTCCTCCTTTTC'3
<b>RGCC</b>	F:5'CGCCACTTCCACTACGAGG'3 R:5'CAGCAATGAAGGCTTCTAGCTC'3
<b>ZBTB16</b>	F:5'CCTCAGACGACAATGACACGG'3 R:5'CTCGCTGGAATGCTTCGAGAT'3
<b>FKBP5</b>	F:5'CTCCCTAAAATTCCTCGAATGC'3 R:5'CCCTCTCCTTTCCGTTTGGTT'3
<b>PDPN</b>	F:5'AACCAGCGAAGACCGCTATAA'3 R:5'CGAATGCCTGTTACTACTGTTGA'3
<b>MMP1</b>	F:5'ACGGATACCCCAAGGACATCT'3 R:5'TCAGAAAGAGCATCGATATG'3
<b>VEGFC</b>	F:5'GAGGAGCAGTTACGGTCTGTG'3 R:5'TCCTTTCTTAGCTGACACTTGT'3
<b>SERPINB2</b>	F:5'TCCTGGGTCAAGACTCAAACC'3 R:5'CATCCTGGTATCCCCATCTACAG'3

**Table 4.3: Primer Pairs for RNA-Seq Validation.** Validated primer pairs for target genes were obtained from Primer Bank to use for RNA-Seq validation. All q-PCR conditions are outline in Chapter 2 (2.4).

## 4.4 Results

### 4.4.1 RNA-Seq Analysis of Human Trabecular Meshwork Cells in the Absence or Presence of Dexamethasone

#### 4.4.1.1 RNA-Seq Summary

CD\_group and TD\_group libraries constructed using AMPure XP beads were pooled and sequenced on a flow cell using NextSeq500, High Output sequencing kit to obtain 30 million reads and 50bp paired-end reads. Paired-end reads were separated to determine whether the second read significantly differed from the first in overall quality. The majority of the data had a Q score greater than 30 (one base call in 1000 is predicted to be incorrect). Mapping of sequencing data represents a useful QC step in NGS analysis pipeline as it can help evaluate quality of samples. Reads were classified, as before (Chapter 3, 3.4.2.1) into; unmapped reads, rRNA reads, reads of mitochondrial origin (mtRNA reads), and mappable reads.

Table 4.4 shows the total number of reads obtained for each sample and genome mapping for each sample was on average 82%. Uniformity of the samples mapping results suggests that the samples are comparable.

4793 genes were identified as differentially expressed in our DEX treated human TM cells when compared to control untreated TM cells. Of these, nine genes were assessed by q-PCR based on the literature, and their false discovery rate (FDR) and logFC.

<b>Sample Name</b>	<b>Total Readcount</b>	<b>rRNA(%)</b>	<b>mtRNA(%)</b>	<b>Mapped(%)</b>	<b>Unmapped(%)</b>
CD_Group1	49309220	0.38	2.61	78.78	18.23
CD_Group2	25088102	0.45	2.84	82.41	14.3
CD_Group3	49283932	0.26	4.9	79.7	15.13
CD_Group4	41486991	0.27	4.92	82.9	11.91
CD_Group5	42617457	0.57	4.18	81.95	13.29
TD_Group1	45590998	0.26	2.8	83.98	12.96
TD_Group2	49413658	0.35	2.74	82.09	14.8
TD_Group3	53913357	0.27	4.8	81.58	13.34
TD_Group4	53576647	0.25	4.53	81.75	13.46
TD_Group5	42474195	0.38	3.84	80.89	14.88

**Table 4.4: Mapping Results for Each Sample from Control Untreated TM Cells and DEX Treated TM Cells.** Reads from each of the two libraries (CD\_Group and TD\_Group) were extracted based on their unique I.Ds. In total 40-57 million reads per sample were obtained.

Based on alignment to the reference genome, *H.sapiens*, hg19 / GRC37, UCSC Genome Browser, the number of identified genes per sample was calculated. Reliability of identified genes increased with the number of identified fragments. All genes were included in statistical comparison of two groups, irrespective of how few calls have been made. Table 4.5 (below), indicates that all samples included in this study have comparable call rates.

Sample Name	Gene	Isoform
CD_Group1	16396	63558
CD_Group2	16154	61603
CD_Group3	16859	66163
CD_Group4	17087	67603
CD_Group5	16558	64825
TD_Group1	16196	64856
TD_Group2	16213	64271
TD_Group3	16539	66574
TD_Group4	17002	66298
TD_Group5	16592	65245

**Table 4.5: Number of Genes and Isoforms Identified in Each Sample from Control Untreated TM cells (CD\_Group) and DEX Treated TM Cells (TD\_Group).** All genes and isoforms identified in each sample have a fragment count estimation of at least 10 counts per gene.

#### 4.4.1.2 Principal Component Analysis (PCA)

As described in Chapter 3 (3.3.3.2) the R package `prcomp` was used to perform PCA on FPKM transformed counts data from control (CD\_Group) and treated (TD\_Group) TM cells. The first three principal components were visualised using the R package `3dplot`. In Figure 4.1 (below), cells are coloured according to their treatment (red denotes the control (CD\_Group), blue denotes the treated group (TD\_Group)), and spheres of the same size represent donor pairs. Samples separate in different regions of the PCA plot corresponding to the principal sources of variation within the experiment. The sample groups in this experiment (CD\_group and TD\_Group) segregate on the first and second principal component axes, but there is a clear relationship between donor pairs, indicating the need to incorporate donor source as a factor in an expression analysis of this data.

When biological differences between samples are pronounced it can be seen in the primary components of the variation of the data. Samples separate in different regions of the PCA plot corresponding to their biology. Sample groups in this experiment (CD\_group and TD\_Group) tend to cluster on the primary component and sample cluster pairs on the secondary component.

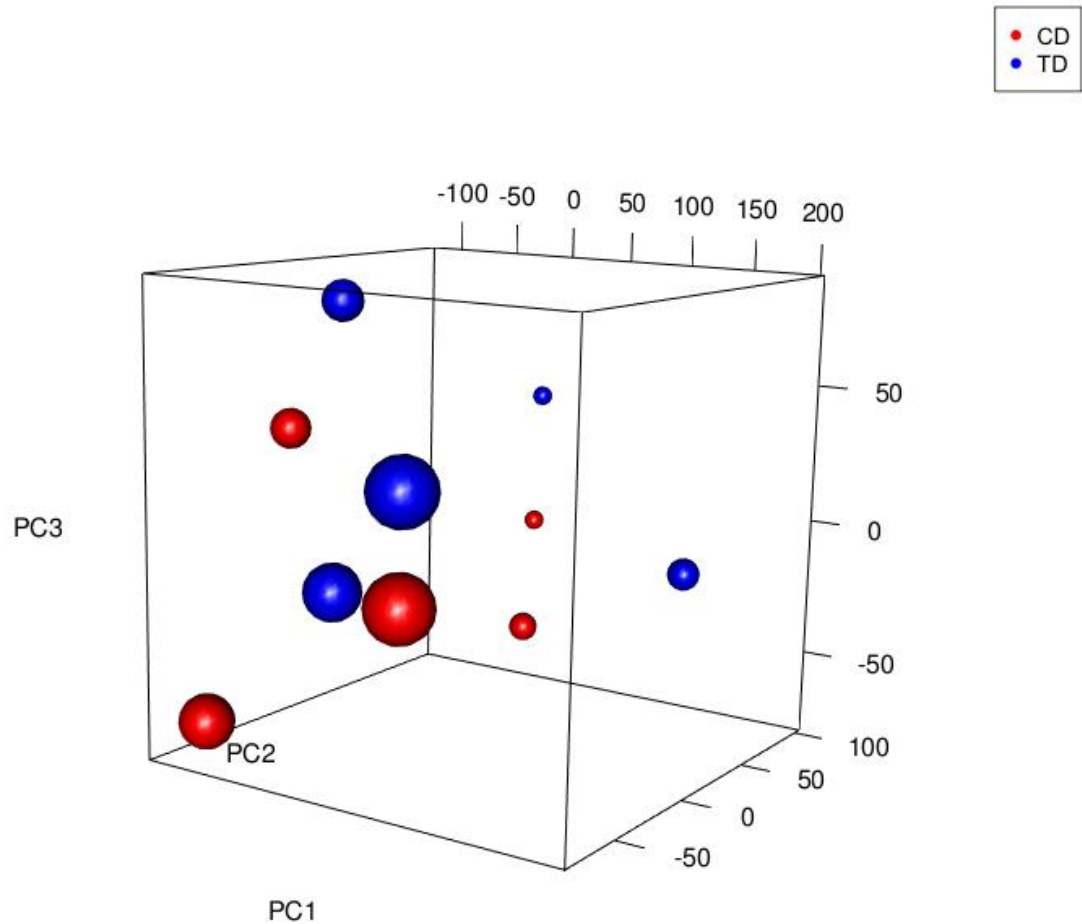


**Figure 4.1: Principal Component Analysis of RNA-Seq Data for Control Untreated TM Cells and DEX Treated TM Cells.** The PCA was performed on all samples passing QC using the top 500 genes that have the largest coefficient of variation based on FPKM counts. Cell treatments are coloured according to the key and donor pairs are represented by spheres of the same size. Based on normalised FPKM (abundance) for each gene for each sample.

#### 4.4.1.3 Heat Map and Unsupervised Clustering

Heat maps were generated using the Bioconductor package 'pheatmap' from FPKM counts of control and treated cells, using a Pearson Correlation distance and a complete agglomeration method, with gene-wise scaled and centred log2 transformed FPKM count data.

The heat map diagram below (Figure 4.2) shows the results of the two-way hierarchical clustering of RNA transcripts and samples. It includes the 500 genes based on FDR  $p$ -value in the Control (CD\_Group) vs Treated (TD\_Group) expression analysis. Each row represents one gene and each column represents one sample. The colour represents relative expression level of transcript across all samples. The colour scale is shown below: orange represents an expression level above the mean; blue represents an expression level below the mean.

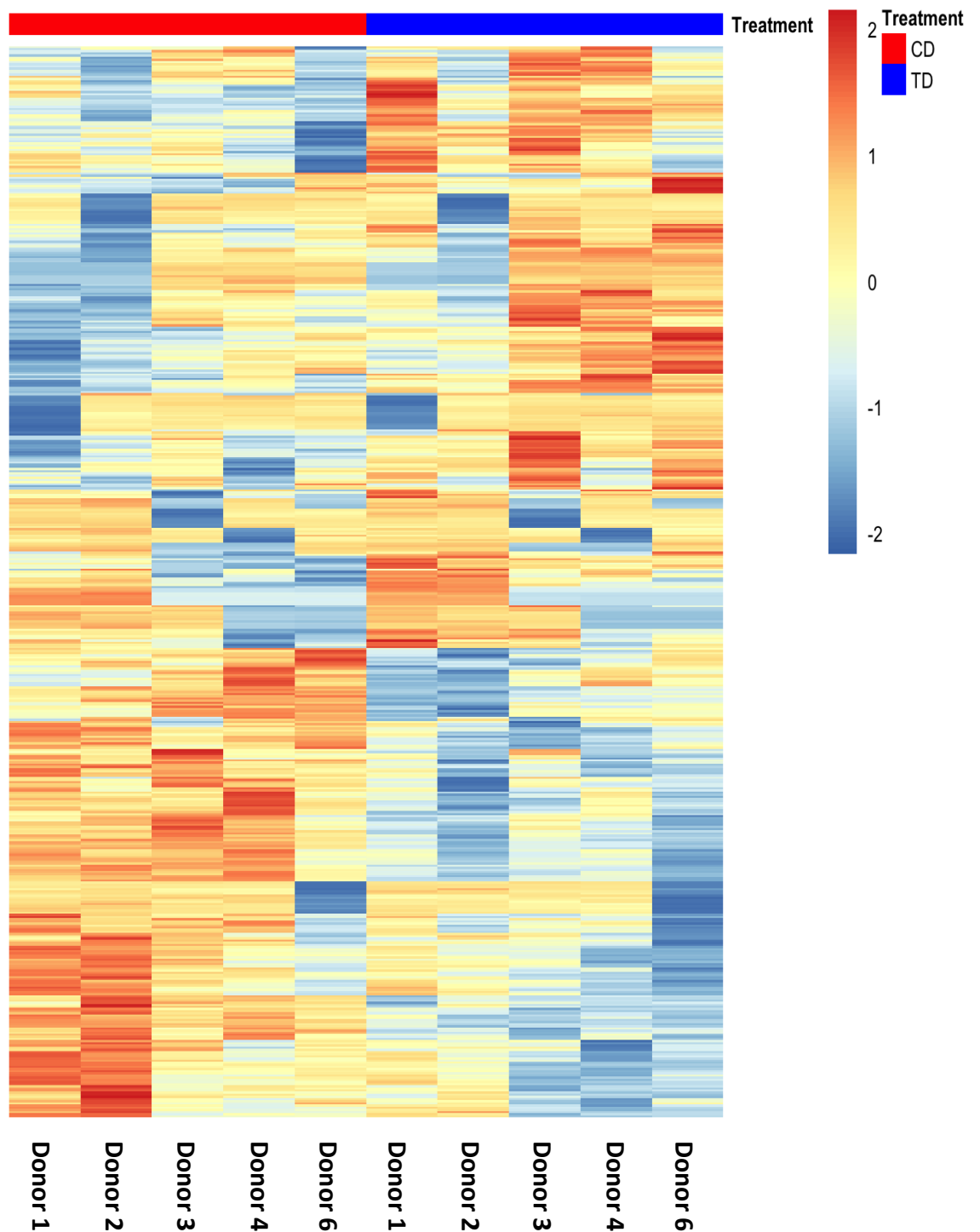


**Figure 4.2: Heat Map and Unsupervised Clustering of RNA-Seq Data from Control Untreated TM Cells and DEX Treated TM Cells.** Hierarchical clustering by sample and transcripts was performed on all samples passing the QC using the top 500 genes that have the largest coefficient of variation based on FPKM counts.

## 4.4.2 Functional Analysis of Gene Pathways Involved in Dexamethasone Stimulation of Human Trabecular Meshwork Cells

### 4.4.2.1 Differentially Expressed Genes in Human Trabecular Meshwork Cells in the Presence or Absence of Dexamethasone Obtained from RNA-Seq Analysis

The DEGs were identified based on Benjamini-Hochberg false discovery rate (FDR) corrected q-values and ranked; the most significantly altered based on their FDR are shown in Appendix (8.3). From the top 500 DEGs based on FDR the 50 most up- and down-regulated were ranked by LogFC and are shown in Table 4.6.

Gene ID	Gene Name	LogFC
<i>Up-Regulated Genes</i>		
<i>GeneName</i>		
ZBTB16	Zinc Finger and BTB Domain Containing 16	8.32
OCA2	Oculocutaneous Albinism Type 2	7.09
ALOX5AP	Arachidonate 5-Lipoxygenase Activating Protein	6.87
ALOX15B	Arachidonate 15-Lipoxygenase Type B	6.31
SAA1	Serum Amyloid A1	5.58
OLAH	Oleol-ACP Hydrolase	5.56
FAM105A	Family With Sequence Similarity 105 Member A	5.53
LGI3	Leucine Rich Repeat LGI Family Member 3	5.26
RGCC	Regulator of Cell Cycle	4.80
GPR64	Cell Surface Receptor	4.63
PDK4	Pyruvate Dehydrogenase Kinase 4	3.87
ADH1B	Alcohol Dehydrogenase 1B	3.63
IP6K3	Inositol Hexakisphosphate Kinase 3	3.62
SORBS2	Sorbin and SH3 Domain Containing 2	3.38
C10	Complement Component 10	3.05
FKBP5	FK506 Binding Protein 5	2.68
LMO3	LIM Domain Only Protein 3	2.64
NRCAM	Neuronal Cell Adhesion Molecule	2.52
IMPA2	Inositol Monophosphatase 2	2.47
AOX1	Aldehyde Oxidase 1	2.35
PTK2B	Protein Tyrosine Kinase 2Beta	2.26
METTL7A	Methyltransferase-like 7A	2.24
PER1	Period Circadian Clock 1	2.15
POM121L9P	POM121 Transmembrane Nucleoporin Like 9	2.08
SIK1	Serine/threonin-protein kinase 1	1.97
KIAA0040	Alcohol Dependence Related Gene	1.95
CRISPLD2	Cysteine Rich Secretory Protein LCCL Domain Containing 2	1.93
DUSP5	Dual Specificity Phosphatase 5	1.93
PISD	Phosphatidylserine Decarboxylase	1.76
ACSL1	Acyl-CoA Synthetase Long Chain Family Member 1	1.75
DTX4	Deltex E3 Ubiquitin Ligase 4	1.66
GLUL	Glutamate-Ammonia Ligase	1.61
FBN2	Fibrillin 2	1.58
AKR1C2	Aldo-keto reductase Family 1 Member C2	1.54
GGT5	Gamma-Glutamyltransferase 5	1.54
SSB	Sjogren Syndrome Antigen B	1.41
RPS6KA2	Ribosomal Protein S6 Kinase A2	1.40
TRNP1	TMF1-Regulated Nuclear Protein 1	1.39

SLC44A1	Solute Carrier Family 44 Member 1	1.36
PDPN	Podoplanin	1.36
AR	Androgen Receptor Gene	1.27
KLF9	Kruppel-like Factor 9	1.24
UGP2	UDP-Glucose Pyrophosphorylase 2	1.18
ERRF1	ERBB Receptor Feedback Inhibitor 1	1.14
FAT4	FAT Atypical Cadherin 4	1.11
GLRX	Glutaredoxin	1.06
TMEM164	Transmembrane Protein 164	1.04
SQRDL	Sulfide:Quinon Oxireductase	1.01
ID1	Inhibitor of DNA Binding 1	0.97
KCNE4	Potassium Voltage-Gated Channel Subfamily E Regulatory Subunit 4	0.92

**Table 4.6: Top 50 Up-Regulated Genes in Cultured Human TM Cells +/- Dexamethasone.** FC= Fold Change.

Gene ID	Gene Name	LogFC
<i>Down-Regulated Genes</i>		
SERPINB2	Plasminogen Activator Inhibitor Type 2 (aka PAI)	-3.59
NR1D1	Nuclear Receptor Subfamily 1 Group D Member 1	-3.17
ESM1	Endothelial Cell Specific Molecule 1	-2.89
GRPR	Gastrin Releasing Peptide Receptor	-2.69
PTH1H	Parathyroid Hormone-like hormone	-2.54
FST	Follistatin	-2.53
CDCP1	CUB Domain Containing Protein 1	-2.49
ALDH1A3	Aldehyde Dehydrogenase 1 Family Member A3	-2.45
NR1D2	Nuclear Receptor Subfamily 1 Group D Member 2	-2.41
NRG1	Neuregulin 1	-2.41
PER3	Period Circadian Clock 3	-2.32
C4	Complement Component 4	-2.28
IL33	Interleukin 33	-2.16
FAM180A	Family With Sequence Similarity 180 Member A	-2.12
LRRN3	Leucine Rich Repeat Neuronal 3	-2.11
ARL4C	ADP-ribosylation Factor-like 4C	-2.11
CXCL12	C-X-C Motif Chemokine Ligand 12	-2.05
FGF5	Fibroblast Growth Factor 5	-1.91
HAS2	Hyaluronan Synthase 2	-1.88
TMEM200A	Transmembrane Protein 200A	-1.87
DPF3	Double PHD fingers 3	-1.84
RGMB	Repulsive Guidance Molecule Family Member	-1.84
MMP1	Matrix Metalloproteinase 1	-1.81
VEGFC	Vascular Endothelial Growth Factor C	-1.32
CD274	Receptor PD1 ligand	-1.78
MIR2682	microRNA 2682	-1.77
IL6	Interleukin 6	-1.74
POU2F2	POU Class 2 Homeobox 2	-1.68
HBEGF	Heparin Binding EGF-like Growth Factor	-1.6
PLAT	Plasminogen Activator Tissue Type	-1.56
IL11	Interleukin 11	-1.53
TNFRSF11B	TNF Receptor Subfamily Member 11b	-1.48
ATP8B1	ATPase Phospholipid Transporting 8B1	-1.40
CLDN11	Claudin 11	-1.38
SMURF2	SMAD Specific E3 Ubiquitin Protein Ligase 2	-1.32
CORO2B	Coronin 2B	-1.29
GREM2	Gremlin 2 DAN Family BMP Antagonist	-1.25

KRT18	Keratin 18	-1.24
CHRM3	cholinergic Receptor Muscarinic 3	-1.20
UACA	Uveal Autoantigen With Coiled-Coil Domains and Ankyrin Repeats	-1.19
AMIGO2	Adhesion Molecule with Ig-like Domain 2	-1.19
KCNQ5	Potassium Voltage-Gated Channel Subfamily Q Member 5	-1.18
SYNJ2	Synaptojanin 2	-1.16
LACC1	Laccase Domain Containing 1	-1.10
MYBL1	MYB Proto-Oncogene Like 1	-1.14
DOPEY2	Dopey Family Member 2	-1.17
ARHGAP22	Rho GTPase Activating Protein 22	-1.05
FAM107B	Family With Sequence Similarity 107 Member B	-1.02
RAB3B	RAS Oncogene Family Member 3B	-1.01
SLC4A7	Solute Carrier Family 4 Member 7	-0.97
CDC25B	CDC25 Family Member B	-0.96

**Table 4.7: Top 50 Down-Regulated Genes in Cultured Human TM Cells +/- Dexamethasone. FC= Fold Change.**

#### 4.4.2.2 Visual Identification of RNA Transcripts Obtained by RNA-Seq Analysis

Volcano plots provide a way to visualise RNA transcripts displaying large-magnitude changes which are also statistically significant. The volcano plot (Figure 4.3) was constructed by plotting the expression FC on the y-axis, and the log CPM (counts-per-million) between control (CD\_Group) and DEX treated (TD\_Group) TM cells on the x-axis. Two regions of interest exist on the plot; extreme right along the x-axis indicated high statistical significance, and extreme above or below indicated strongly up- and down-regulated genes respectively.

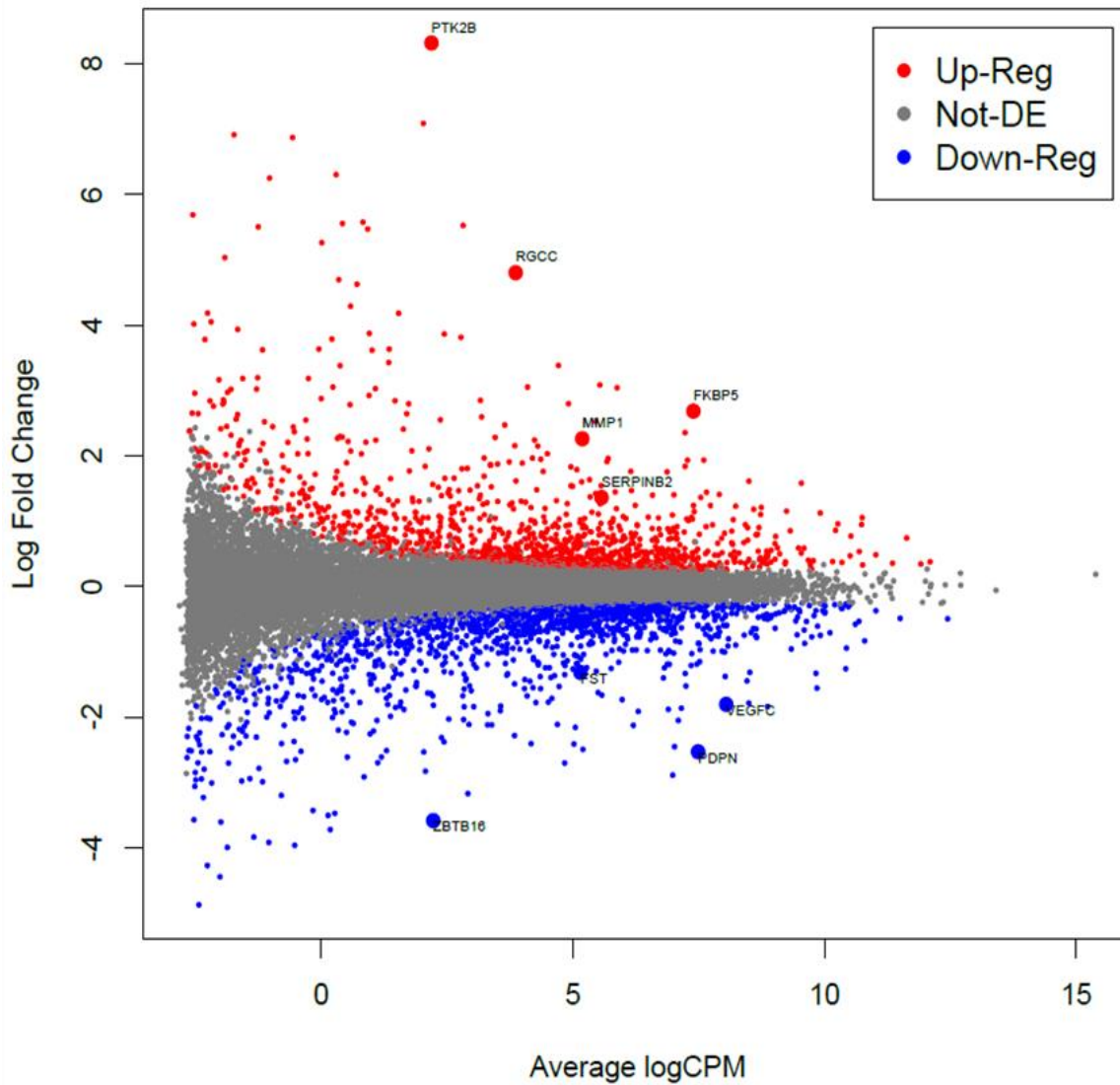


**Figure 4.3: Volcano Plot of the Relationship Between the LogFC and the Average Log Counts-per-Million (CPM) in Control Untreated TM Cells Compared to DEX Treated TM Cells.** The relationship between statistical significance and logFC in normalised expression between the experimental groups, CD\_Group (control, untreated TM cells) and TD\_Group (DEX) treated TM cells), are shown in the plot. FC= Fold Change. **Key:** Up-Reg = significantly up-regulated genes between the two sample groups are indicated by the red dots; Not DE = genes that were not differentially expressed between the two sample groups are indicated in grey; Down-Reg = genes that were significantly down-regulated between the two sample groups are indicated by blue markers.

#### 4.4.2.3 Dexamethasone Activated Processes in Cultured Human Trabecular Meshwork Cells

Biological processes significantly associated with differentially expressed protein coding genes identified through RNA-Seq are outlined in Table 4.8 below. As before (3.3.3.3) two different statistical tests were utilised to achieve these results. The analyses identified several functional groups among the candidate genes obtained from RNA-Seq data, of which angiogenesis, axonal guidance signalling and p38 MAPK signalling were represented.

Class of Encoded Proteins	Number	
	Annotated	Affected
Angiogenesis	318	159
Positive regulation of osteoblast differentiation	52	32
Circadian rhythm	69	41
Negative regulation of cell proliferation	452	199
Response to mechanical stimulus	140	64
Wound healing	496	214
Positive regulation of transcription from RNA polymerase II promoter	613	244
Signal transduction	3522	1318
Negative regulation of epithelial cell proliferation	79	43
Response to glucocorticoid	88	44
Positive regulation of DNA replication	50	28
Response to hypoxia	205	95
Negative regulation of transcription from RNA polymerase II promoter	467	187
Chemotaxis	483	213
Inflammatory response	366	159
Cell proliferation	1303	567
Cell division	545	240
Negative regulation of cytokine-mediated signalling pathway	26	18
Cellular response to ionizing radiation	46	28
Positive regulation of protein kinase B signalling	63	33

**Table 4.8: Significantly Altered Biological Processes Found to be Differentially Expressed Between DEX Treated and Untreated Control TM Cells.** Significant biological processes for differentially expressed genes found between the untreated control TM cells (CD\_Group) and TM cells treated with DEX (TD\_Group) are outlined above. Of 9383 genes annotated, 3926 were significantly associated with biological processes identified.

IPA v 01-08 (Qiagen) Core and Comparison analyses were performed with lists of DEGs generated from expression analyses that included gene name, FDR  $p$ -value and log<sub>2</sub> fold change. An FDR  $p$ -value cut off of 0.01 was used to select lists of DEGs for analysis. Core analysis output included ranked lists of Canonical Pathways (processes with biological or molecular biology significance defined by the Ingenuity Knowledge Base). The canonical pathways identified in two or more Core analyses were compared in Comparison analyses. Comparisons were performed by hierarchical clustering based on process enrichment score or activation z-score.

Fishers exact tests reported as a likelihood value ( $-\log(p\text{-value})$ ) were performed to test canonical pathway enrichment. Canonical pathways were ranked by activation z-score. The activation score threshold was  $\pm 1.96$  and canonical pathways enriched in this are regarded as significant. The sign of the Z-score indicates the direction of regulation of the process (Figure 4.4). A comparison analysis was then performed on IPA to determine the most significantly altered canonical pathways in TM cells treated with known glaucoma stimuli, TGF- $\beta$ 2 (Chapter 3) and dexamethasone. The top 76 processes that over-lap between the two treatment groups are outlined below (Figure 4.5) in which Rho signalling, inflammatory processes, and actin cytoskeleton signalling are all represented.

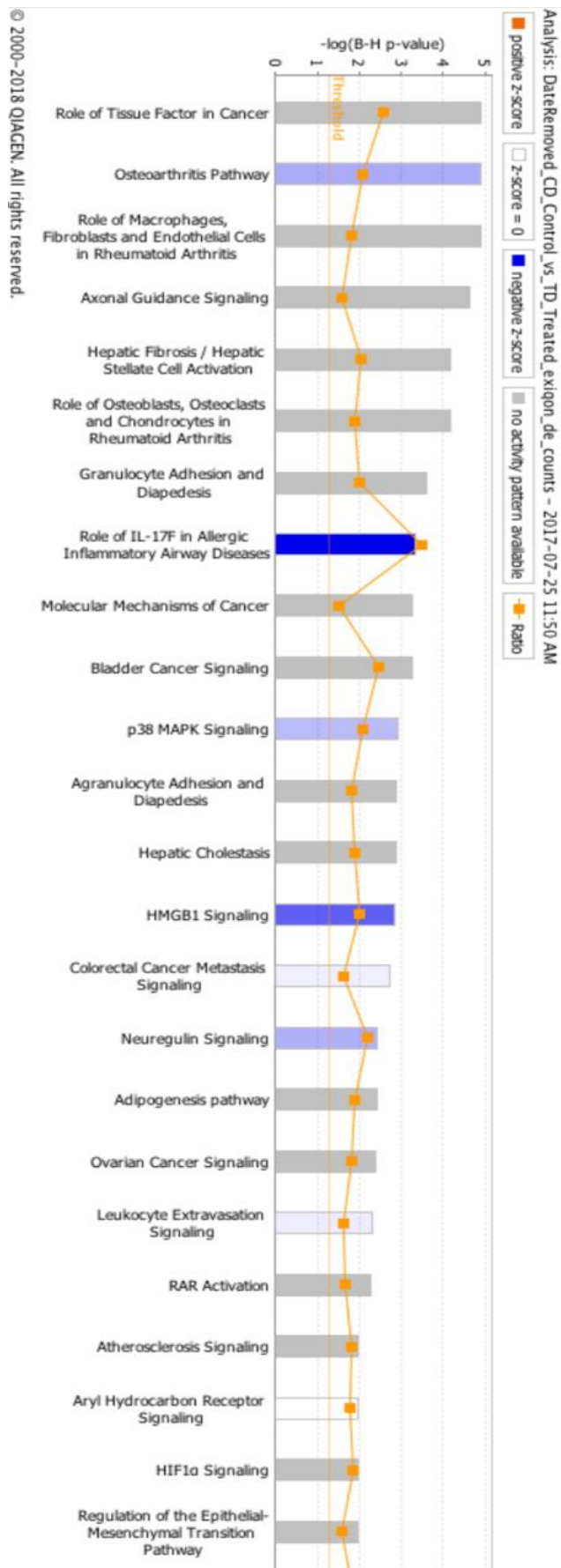


**Figure 4.4: Top Canonical Pathways of the Top 1% Differentially Expressed Genes in Human TM Cells +/- Dexamethasone.** I.P.A was used to generate the top 24 canonical pathways associated with differentially expressed genes identified by RNA-Seq in cultured human TM cells +/- DEX.

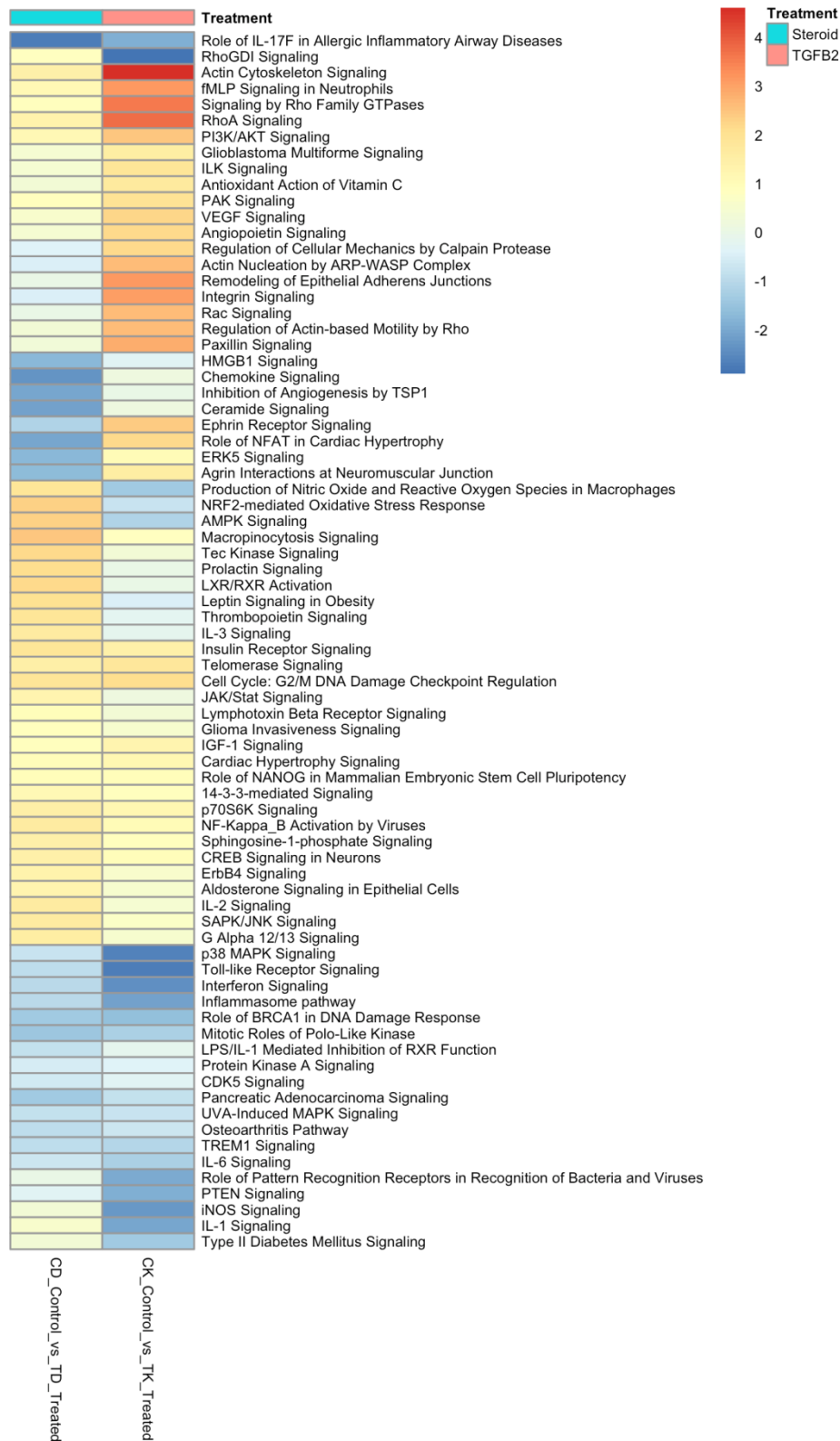


**Figure 4.5: Heat Map of Highest Ranked Over-Lapping Canonical Pathways between TGF- $\beta$ 2 Treated Human TM Cells and DEX Treated Human TM Cells.** TGF- $\beta$ 2 and DEX are known glaucoma stimuli and several processes are enriched when human TM cells are exposed to both stimuli independently.

#### 4.4.3 q-PCR Assay Assessment of Glucocorticoid Receptor Isoforms Expressed in Cultured Human TM +/- Dexamethasone

Both glucocorticoid receptor isoforms, GR $\alpha$  and GR $\beta$  are present in the normal and glaucomatous human TM<sup>572</sup>. TM cells isolated from glaucomatous patients express lower levels of GR $\beta$  compared to normal TM cells. Lower GR $\beta$  expression has been attributed to increased steroid responsiveness, therefore, it was in our interest to identify potential steroid responders within our samples based on their GR $\alpha$  to GR $\beta$  expression levels. In control, untreated samples, 50% of our TM samples had lower GR $\beta$  expression levels compared to GR $\alpha$ . Post DEX stimulation, five out of six samples had higher GR- $\beta$  expression levels in comparison to GR- $\alpha$ .

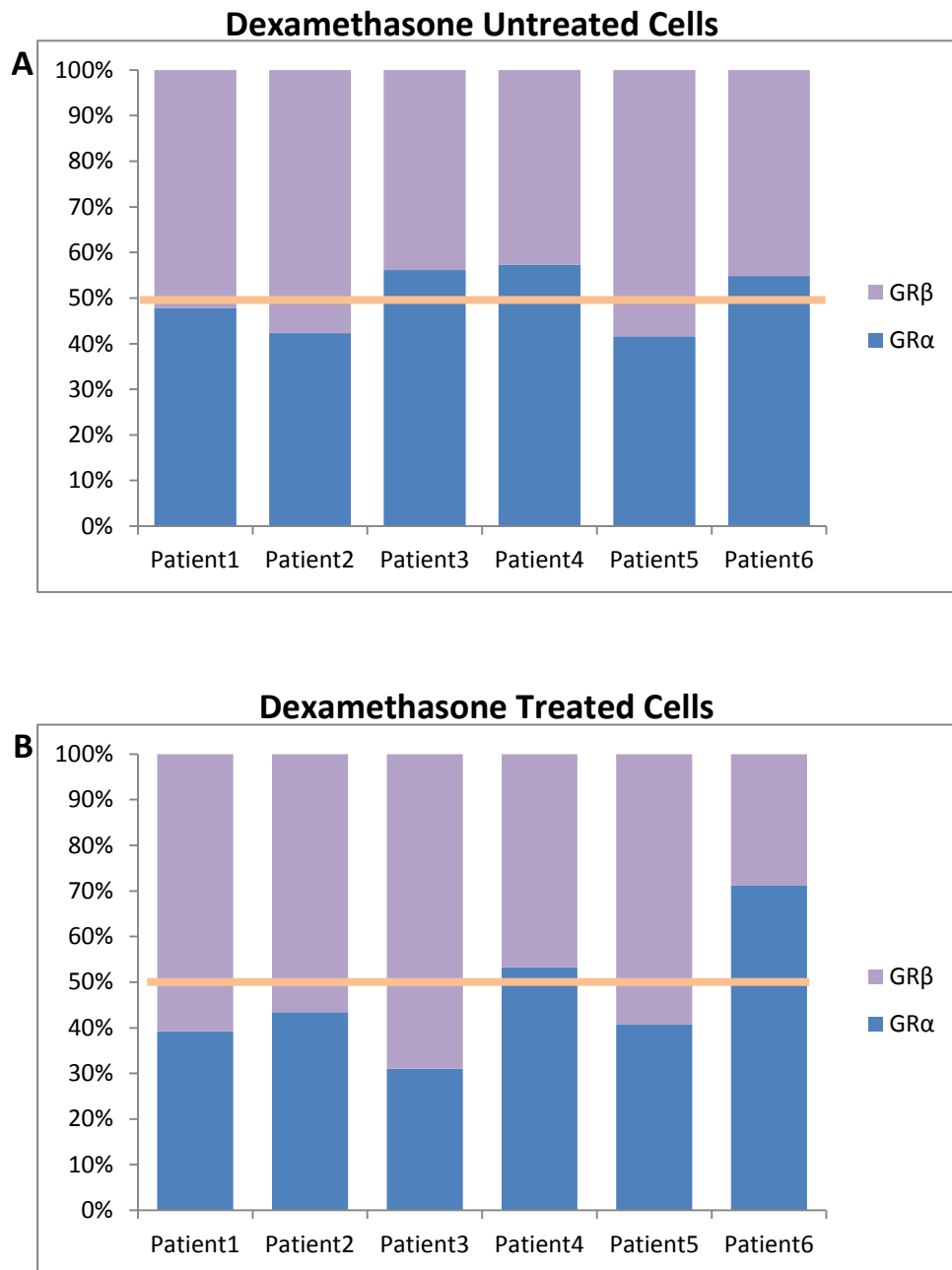


**Figure 4.6: Expression Levels of Glucocorticoid Receptor (GR $\alpha$  and  $\beta$ ) in Paired Human TM Cells +/- DEX Treatments.** (A) Untreated TM cells from 6 donors exhibit differential GR $\alpha$  and GR $\beta$  expression. 50% of the donors (Donors 3, 4, and 6) show lower GR $\beta$  expression favouring GR $\alpha$  expression in normal cell states. (B) DEX treated TM cells continue to exhibit differential GR $\alpha$  to GR $\beta$  expression. A switch in ratio was observed in only one donor (Donor 3) in response to DEX stimulations. Horizontal line represents 50% receptor expression. Ratios above and below this are represented by specific receptor keys. GR $\alpha$  is represented by blue bar, GR $\beta$  is represented by the purple bar.

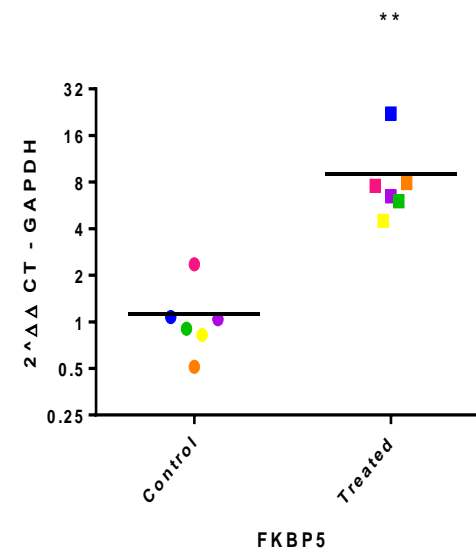
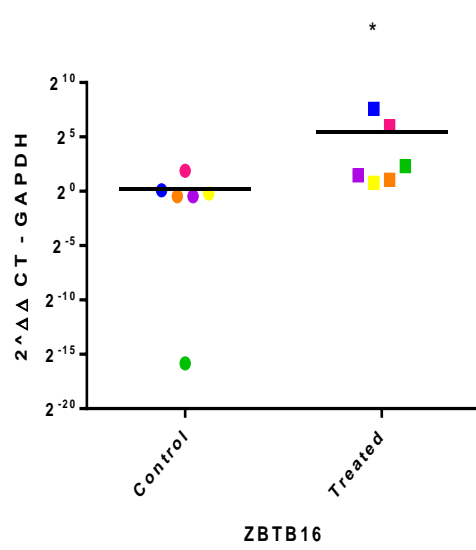
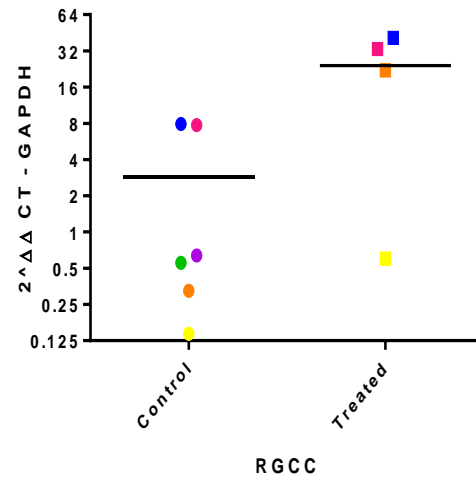
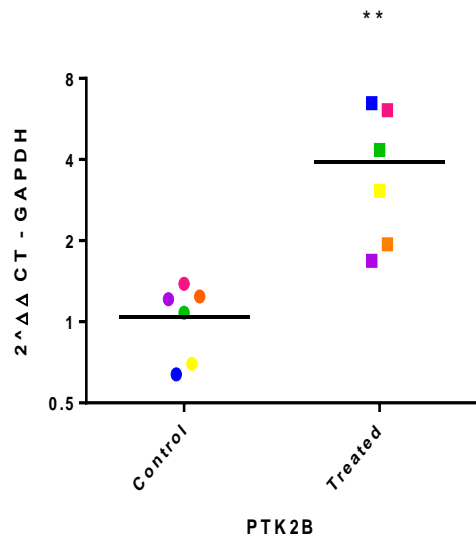
#### 4.4.3.1 q-PCR Assay Validation of Top Differentially Expressed Genes in Cultured Human TM in the Presence or Absence of Dexamethasone

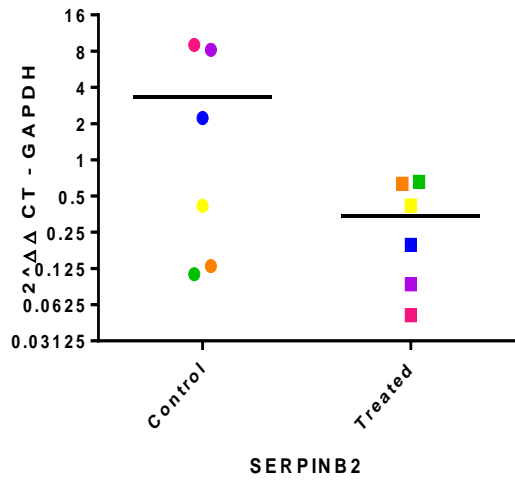
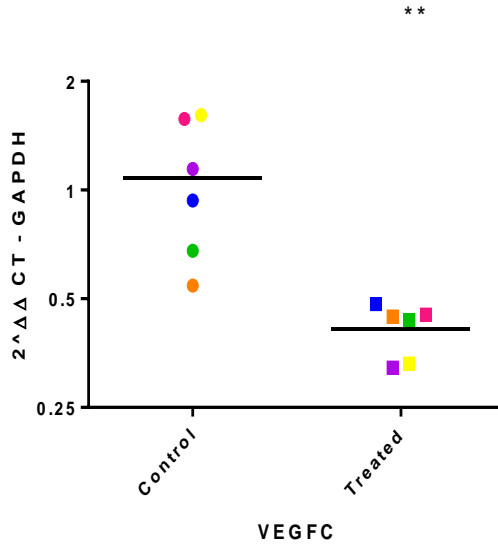
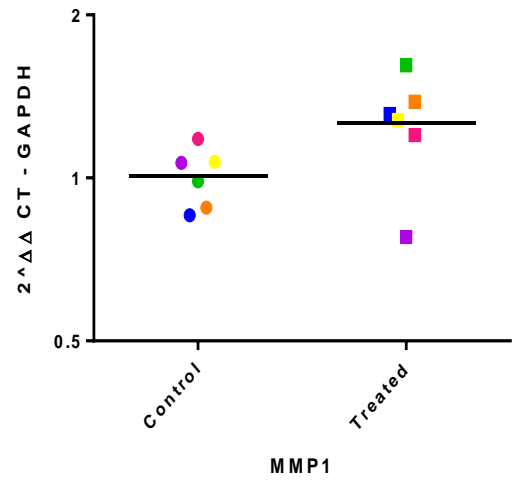
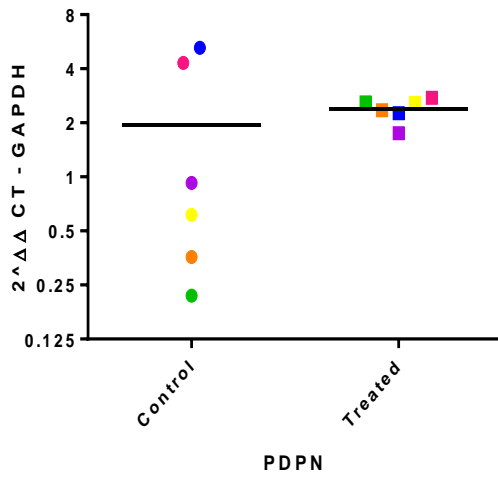
To validate results obtained from the RNA-Seq analysis, a subset of the top differentially expressed genes (DEGs) between the control group (CD\_Group), and the DEX treated group (TD\_Group), of cultured human TM, were analysed using q-PCR.

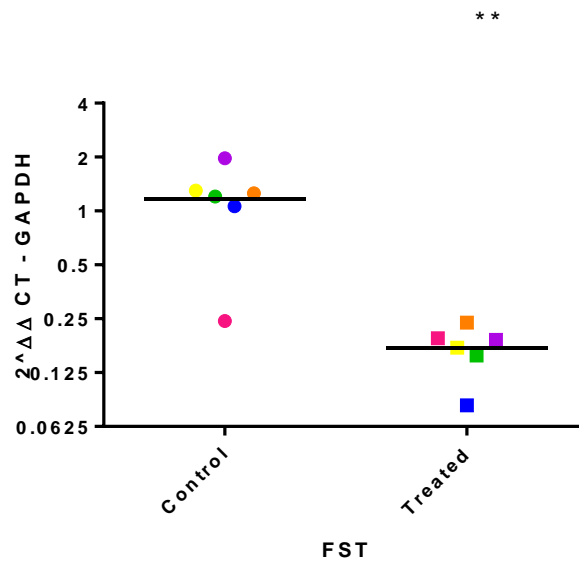
Nine candidate genes (Table 4.9) were selected for q-PCR analysis based on their statistical significance in the RNA-Seq data set and on the basis of published literature providing evidence of their involvement in glaucoma pathophysiology. Nine candidate genes; protein tyrosine kinase 2 beta (PTK2B), regulator of cell cycle (RGCC), zinc finger and BTB domain containing 16 (ZBTB16), FK 506 binding protein (FKB5), podoplanin (PDPN), matrix metalloproteinase 1 (MMP-1), vascular endothelial growth factor C (VEGFC), serpin family B member 2 (SERPINB2), follistatin (FST). Eight of the nine candidate genes demonstrated consistent trends of differential expression by q-PCR. MMP-1 expression though decreased in the RNA-Seq data was increased when quantified by q-PCR (but not statistically significant). To further confirm the differential expression of candidate genes an independent sample was added to each group increasing the number of biological replicates to 6 in each experimental group; CD\_Group (n=6) and TD\_Group (n=6). Statistical analysis was carried out using Graphpad (Prism, version 6), and all data sets were subjected to two sample students t-tests. Results were classified as significantly significant if  $p < 0.05$ .

Candidate Gene	LogFC	p-value
PTK2B	2.261071	5.73E-103
RGCC	4.804257	2.43E-88
ZBTB16	8.322036	1.85E-77
FKBP5	2.684064	5.35E-55
PDPN	1.359751	9.12E-36
MMP1	-1.80683	8.05E-44
VEGFC	-1.31898	2.3E-47
SERPINB2	-3.58675	6.65E-50
FST	-2.5333	2.97E-57

**Table 4.9: Summary of Expression Levels of Candidate Genes based on RNA-Seq Analysis.**







Donor 1 Control=●; and Treated=■

Donor 2 Control=●; and Treated=■

Donor 3 Control=●; and Treated=■

Donor 4 Control=●; and Treated=■

Donor 5 Control=●; and Treated=■

Donor 6 Control=●; and Treated=■

**Figure 4.7: Expression Levels of Candidate Genes in Cultured Human TM Cells.** CD\_Group are denoted as “Control” on graphs and TD\_Group as “Treated”. Candidate genes were identified as significantly differentially expressed through RNA-Seq. Paired donors are colour coded as per legend above. Circles represent individual donor gene expression without treatment and squares represent donors with DEX treatment. An asterisk (\*) denotes significant differential gene expression after treatment (two-sample t-test  $p < 0.05$ ).

## 4.5 Discussion

Glucocorticoids are a group consisting of natural and synthetic (dexamethasone) ligands that have been exploited for anti-immune, anti-allergic, and immunosuppressive properties<sup>577</sup>. The physiological and pharmacological actions of glucocorticoids are mediated through the cytoplasmic glucocorticoid receptor (GR), which belongs to a nuclear receptor subfamily<sup>578</sup>. The glucocorticoid receptor is a ligand activated transcription factor, involved in mediating numerous physiological functions including maintaining homeostasis, normal metabolism and immune regulation<sup>185</sup>.

Prolonged exposure to GCs can lead to a number of serious systemic, and local adverse side effects<sup>193</sup>. Ocular side effects of GCs include cataract and ocular hypertension which can lead to glaucoma<sup>579,580</sup>. The mechanism of raised IOP in glucocorticoid-induced ocular hypertension resembles POAG in that there is impaired aqueous humour outflow in the TM and both *ex vivo* and *in vivo* studies have established direct roles of glucocorticoids in the TM<sup>207,581</sup>. Specifically, glucocorticoids increase ECM proteins, decrease MMP activity, and increase TIMP metalloproteinase 1 (TIMP1) resulting in increased deposition of ECM in the TM<sup>562,563</sup>. Glucocorticoids also reduce the phagocytic activity of the TM cells which may lead to further AH outflow resistance and raised IOP<sup>427</sup>. In addition, glucocorticoids are involved in the re-organisation of the TM cytoskeleton, affecting TM migration, proliferation and function<sup>257,582</sup>.

### Glucocorticoid Receptor Isoforms in Steroid Responsiveness in Glaucoma

Glucocorticoids are widely used in ophthalmology to suppress inflammation, reduce symptoms and minimise post-surgical scarring<sup>187</sup>. Individual responses to glucocorticoid therapy in systemic diseases (asthma, cancer, and arthritis) can demonstrate variability, and, glucocorticoid resistance or enhanced responsiveness between individuals has been reported<sup>583–585</sup>. Similarly, there are individual differences to the susceptibility to develop glucocorticoid-induced ocular hypertension<sup>208,556</sup>. Almost all POAG patients are steroid responders<sup>556</sup> and non-glaucomatous steroid responders are at a higher risk for developing POAG than non-glaucomatous non-responders<sup>202</sup>. Approximately 40% of the normal population are considered steroid responders, whereas, in contrast, nearly all POAG patients are steroid responders<sup>556</sup>. A better understanding of genetic and molecular mechanisms underlying individual variation in the response to steroids could shed light on our understanding of steroid-induced ocular hypertension and ocular hypertension leading to POAG.

Differential GC responsiveness at the molecular level has been attributed to the relative expression levels of the two alternatively spliced glucocorticoid

receptor isoforms, GR $\alpha$  and GR $\beta$ <sup>575,586,587</sup> (Figure 4.8). However, a number of mechanisms regulate glucocorticoid activity; GC ligand potency, nuclear import of GC receptors, as well as alternative splicing and regulation of GR $\alpha$  and GR $\beta$  levels<sup>572</sup>. GR $\alpha$  is the biological receptor for GCs and binding of its ligands induces a conformational change and release of accessory proteins, followed by translocation to the nucleus. Glucocorticoid response elements (GREs) found on GC regulated genes facilitate homodimerization of the GR-GC complex. Interaction between GR-GC complex with GREs drives transcription of genes, whereas binding to negative GREs suppresses transcription<sup>572</sup>.

In addition to GREs, GR activity is also regulated by the different ratios of the alternatively spliced GR $\alpha$  and GR $\beta$  receptor isoforms. The GR encoding gene, NR3C1, consists of 9 exons and alternative splicing of the terminal exon generates the GR $\alpha$  and GR $\beta$  isoforms. Incorporation of exon 9 $\alpha$  gives rise to GR $\alpha$  and conversely incorporation of 9 $\beta$  gives rise to GR $\beta$ <sup>588</sup>. Exon 9 encodes the ligand binding domain; therefore, the resultant isoforms differ greatly in their ligand binding properties. GR $\beta$  can form heterodimers with GR $\alpha$  however this complex has significantly diminished transcriptional activity when compared to GR $\alpha$  homodimers<sup>588</sup>. In this way GR $\beta$  acts as a dominant negative inhibitor of GR $\alpha$  transcriptional activity and provides enhanced resistance to glucocorticoids.

Both GR $\alpha$  and GR $\beta$  are expressed in the TM<sup>575,589</sup>, and the GR $\alpha$ /GR $\beta$  ratio in the TM may play a role in an individual person's susceptibility to steroid-induced ocular hypertension and glaucoma<sup>572</sup>. The expression of GR $\beta$  is lower in TM cells isolated from glaucoma patients compared with normal individuals<sup>575,590</sup>, which may explain the high levels of steroid-responsiveness in terms of IOP elevation in glaucoma patients. Lower GR $\beta$  expression in glaucomatous TM cells results in great susceptibility to GCs, leading to ECM and cytoskeletal changes in the TM, increased outflow resistance and ultimately raised IOP and glaucoma<sup>575,590</sup>. In our study we investigated the steroid responsiveness of our human TM samples using q-PCR to quantify expression levels of GR $\alpha$  and GR $\beta$  in control and steroid stimulated TM cells. Our results identified slight differential GR expression among patients: 50% of our samples were identified as expressing a higher ratio of GR $\alpha$  to GR $\beta$  without DEX stimulations (Figure 4.6). This may indicate that these samples are part of the 40% of the normal population that are steroid responders. Interestingly, after DEX stimulations, two of the steroid responders exhibited an increase in GR $\beta$  expression, whereas only one remained to show GR $\alpha$  expression preferences.

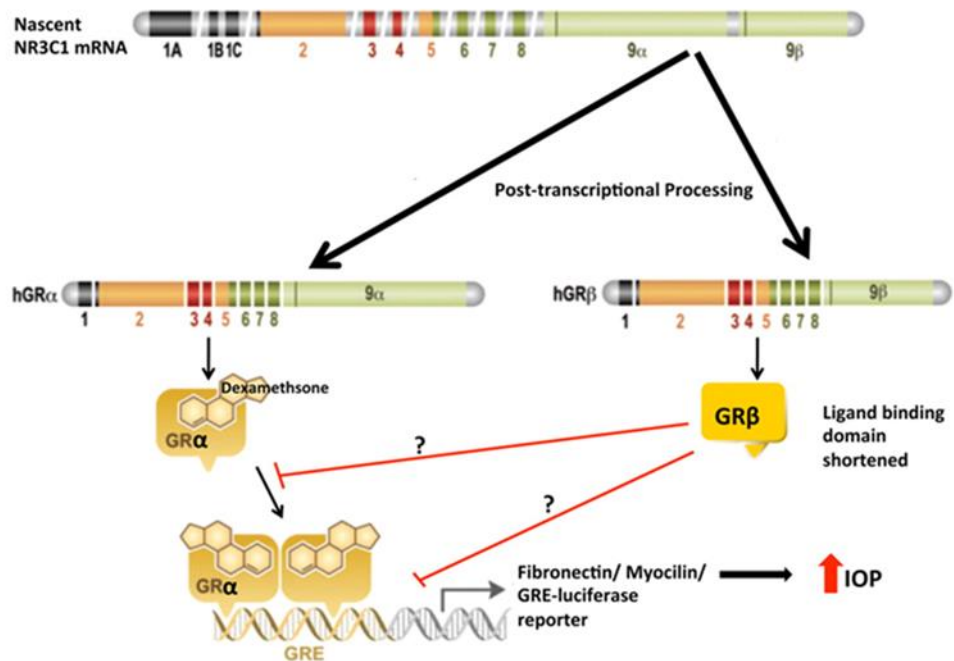


**Figure 4.8: Alternate Splicing of Glucocorticoid Receptor Generates Two Functionally Distinct Splice Isoforms: GR $\alpha$  and GR $\beta$ .** The ratio between GR $\alpha$  and GR $\beta$  regulates steroid responsiveness, with lower levels of GR $\beta$  related to increased steroid responsiveness due to reduced dominant negative inhibition of GR $\alpha$  by GR $\beta$  and increased ECM expression and elevated IOP. Modified from Revello and Cidlowski 2009<sup>591</sup>.

## Genome-Wide Transcriptome Profiling in Dexamethasone Treated Human TM Cells

Using high-throughput RNA-Seq in cultured human TM cells treated with dexamethasone (DEX; 100nM) for 16hrs there were several significantly DEGs and networks/canonical pathways that were enriched. Responses to DEX treatment are dose and duration sensitive. 16hrs was chosen to monitor acute changes in GC-induced gene expression rather than alteration induced by chronic GC exposure. Ultimately time-dependent responses require assessment but given the resource implications a short exposure was chosen as (i) we wanted to assess acute and initiating alterations in gene expression, (ii) early events maybe more relevant for the identification of potential therapeutic targets, (iii) miRNA expression was assessed in parallel and (iv) microarray studies in epidermal keratinocytes show consistent responses to 24hr, 48hr and 72hr. Donor characteristics can also play a role in gene expression responses. Experiments were limited to male donors to reduce variability related to gender and potential oestrogen-GC interactions. As glaucoma more commonly affects the ageing population, young donors were also excluded from this study. All donors were aged between 57-65 years.

Six studies have examined global changes in gene expression in cultured TM cells treated with dexamethasone using cDNA or oligonucleotide arrays<sup>548,567-571</sup>. This is the first study to use RNA-Seq to interrogate alterations in gene expression in the TM in response to glucocorticoid treatment. Only one of the microarray-based studies recapitulated the dose and duration of DEX treatment for 24 hrs and utilised two human eye donors aged 3 months and 35-years old<sup>571</sup>. A common number of genes were up-regulated in the array study<sup>571</sup> and in our dataset including response gene to complement 32 (RGC32), oculocutaneous albinism II (OCA2), serum amyloid A1 (SAA1), angiopoietin-like 4 (ANGPTL4), integrin, alpha 10 (ITGA10), FK506 binding protein 5 (*FKBP51*), Kruppel-like factor 15 (KLF15), myocilin (MYOC) and zinc finger and BTB domain containing 16 (ZBTB16)<sup>571</sup>. There was less consistency in down-regulated genes in this study and the array study<sup>571</sup>: Kallmann syndrome 1 sequence (KAL1), gamma-aminobutyric acid (GABA) A receptor, beta 1 (GABRB1) and matrix-remodelling associated 5 (MXRA5). Matrix remodelling-associated protein 5 (MXRA5, adlcan) is a TGF- $\beta$ 1 regulated anti-inflammatory and anti-fibrotic protein<sup>592</sup>.

### Protein Tyrosine Kinase 2 Beta (PTK2B)

Elevated expression of protein tyrosine kinase 2 beta (PTK2B) in response to DEX has previously been seen in cultured epidermal keratinocytes treated with 100nM DEX<sup>593</sup>. RNA-seq data identified PTK2B was significantly up-regulated in human TM cells stimulated with DEX (FC= 2.26,  $p$ -value= 5.7E-103) and this was

confirmed by q-PCR (FC= 3.933,  $p$ -value= 0.0022; Figure 4.7). Protein tyrosine kinase 2 beta (PTK2B), also known as focal adhesion kinase 2, is a member of a family of non-receptor protein tyrosine kinases, which includes focal adhesion kinase 1 (FAK) or protein tyrosine kinase 2. PTK2B is highly conserved with FAK with nearly 50% sequence identity and have a similar domain structure<sup>594</sup>. FAK is ubiquitously expressed whereas PTK2B is expressed mainly in the CNS and haematopoietic tissue<sup>595</sup> with retinal expression reported in *Drosophila*<sup>596</sup>.

Both PTK2B and FAK are phosphorylated in response to integrin-mediated cell adhesion to the ECM. PTK2B is also activated in response to a broad range of external stimuli which elevate intracellular  $Ca^{2+}$  concentration or via Src dependent pathways<sup>597</sup>. PTK2B acts in concert with Src to link Gi- or Gq-coupled receptors with the mitogen-activated protein (MAP) kinase signalling pathway and/or PI3K pathway<sup>597,598</sup>. Auto-phosphorylation of PTK2B in response to integrin-mediated cell adhesion triggers cell migration.

Both PTK2B and FAK are known to bind to proteins that interact with the cytoskeleton (e.g. paxillin<sup>599</sup>, the Rho-GAP protein Graf, and a LIM domain-containing protein) suggesting a role in cytoskeletal organisation and alteration in cellular morphology in response to extracellular stimuli<sup>600-602</sup> (Figure 4.9). There is evidence from PTK2B knockout mice that PTK2B is essential to RhoA activation in macrophages which show impaired migration when stimulated with chemokines due to reduced cell contractility and polarity<sup>603</sup>.

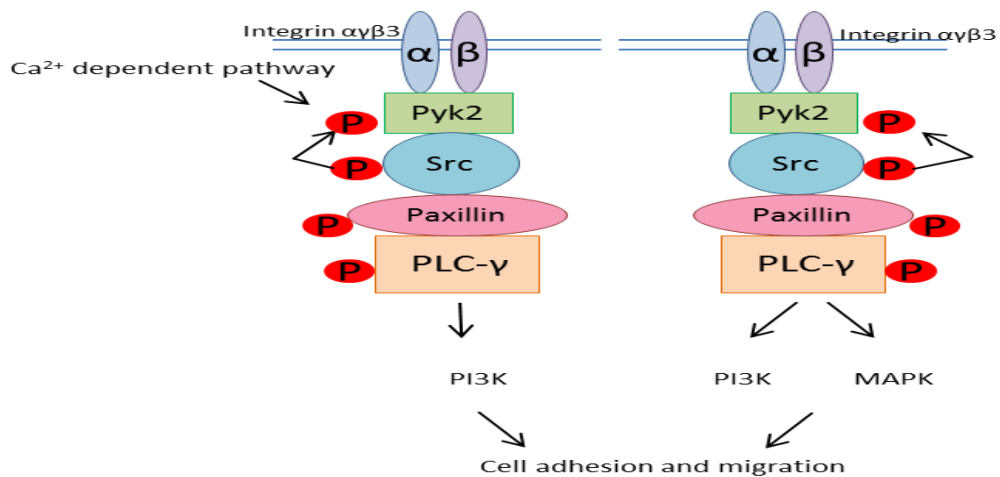


**Figure 4.9: Putative Integrin Signalling Pathways Through PYK2 or FAK (Modified from Koch *et al* 2007<sup>597</sup>).** In response to integrin  $\alpha\beta3$  activation, PYK2 and/or FAK are recruited to a signalling complex that consists of Src, paxillin and PLC $\gamma$ . PYK2 may be phosphorylated through Src or other  $Ca^{2+}$  dependent pathways whereas FAK is phosphorylated through Src. Both PYK2 and FAK can result in activation of PI3K and/or MAPK that may lead to cell adhesion and migration.

Rho and Rho-associated protein kinases, have been implicated in glaucoma pathogenesis (Ch3.4), therefore PTK2B regulation of components of this signalling pathway in the TM may also be involved in steroid-induced glaucoma. The organization of the actin cytoskeleton is critical for TM cell contractility, motility and phagocytosis. Myocilin is highly-inducible in the TM by corticosteroids and there is evidence that myocilin increases cell migration via the integrin-FAK-AKT signalling pathway<sup>604</sup>.

FAK plays a role in TM cell phagocytosis, a central function of the TM, which is reduced with dexamethasone treatment and this decline in TM phagocytosis is proposed to explain steroid-induced ocular hypertension and glaucoma<sup>195</sup>. There is evidence that phagocytosis in TM cells is regulated by opposing  $\alpha\beta3$  and  $\alpha\beta5$  integrin-mediated FAK signalling pathways<sup>605</sup>. Phagocytosis is mediated via the actin-cytoskeleton, and, FAK (and its family member PTK2B) are important signalling molecules which regulate actin cytoskeleton remodelling<sup>600-602</sup>. In parallel with the role of  $\alpha\beta5$  integrin-FAK in RPE cell phagocytosis a similar system has been proposed to be active in TM cells<sup>606</sup>. Elevated PTK2B expression within the TM has not been described before and further work is required to investigate the role of PTK2B in actin remodelling and phagocytosis<sup>606</sup> in the TM and in relation to glaucoma pathogenesis<sup>605,607</sup>.

### Regulator of Cell Cycle (RGCC)

Regulator of cell cycle (RGCC) encodes response gene to complement 3 (RGC-32) in humans. RGCC regulates cell cycle progression and it is induced by p53 in response to DNA damage<sup>608</sup> or by sublytic levels of complement system proteins (sublytic C5b-9 specifically), that result in activation of the cell cycle<sup>609</sup>. RGCC expression is also induced in response to complement activation, growth factors, and steroid hormones<sup>610-612</sup>. In our study RGCC expression was significantly up-regulated in human TM cells stimulated with DEX over 16 hours using RNA-Seq (FC= 4.80,  $p$ -value = 2.43E-88) in comparison to control cells. Statistical significance could not be achieved in q-PCR validation. Significant glucocorticoid inducible expression of RGCC in the TM was also reported after 24 hours<sup>571</sup> and 21 days<sup>570</sup> of DEX treatment. Based on the responses of rat kidney cells to methylprednisolone, RGCC was proposed to be a “corticosteroid-enhanced gene”<sup>613</sup>. The expression of RGCC is also induced in lens epithelial cells in response to corticosteroids<sup>614</sup> and may play a role in steroid-induced cataract.

The exact role of RGCC in response to corticosteroids has not been identified, nor has a role for RGCC in glaucoma been determined. In human aortic endothelial cells there was evidence RGCC mediates cell migration by regulating RhoA and ROCK1 expression and actin cytoskeletal organisation<sup>615</sup>. Overexpression of RGCC in lung cancer cell lines promotes cell migration and invasion and induces

EMT via the NF- $\kappa$ B signalling pathway<sup>616</sup>; responses which are inhibited by RGCC silencing<sup>617</sup>. A role for RGCC up-regulation in fibrotic diseases has been reported in hepatic fibrosis<sup>618</sup> and scarring following glaucoma surgery in rodent models<sup>619</sup>. These studies suggest RGCC may have a role in fibrotic responses which could contribute to a reduce outflow facility in the TM and elevated IOP. Overexpression of RGCC results in downregulation of E-cadherin, and upregulation of vimentin, fibronectin, snail and slug in the human lung cancer A549<sup>616</sup>. RGCC also plays a central role in TGF- $\beta$ 1-induced EMT of human renal proximal tubular cells inducing the expression of smooth muscle  $\alpha$ -actin ( $\alpha$ -SMA) and extracellular matrix proteins (collagen I and fibronectin)<sup>620</sup>.

### Promyelocytic Leukemia Zinc Finger (ZBTB16)

ZBTB16, also known as promyelocytic leukemia zinc finger (PLZF), is a member of the Krueppel C2H2-type zinc-finger protein family and encodes a zinc finger transcription factor. ZBTB16 is located in the nucleus and is involved in cell cycle progression. In our study ZBTB16 expression was significantly up-regulated in human TM cells stimulated with DEX via RNA-Seq (FC= 8.32,  $p$ -value = 1.85E-77). q-PCR validation of ZBTB16 expression in TM samples further corroborated the RNA-Seq findings (FC= 52.6,  $p$ -value = 0.01520). Similarly after 21 days of DEX stimulation demethylated cytosine-phosphate-guanine (CpG) sites within the ZBTB16 gene promoter regions were detected and there were corresponding increases in ZBTB16 gene expression<sup>621</sup>. ZBTB16 has been previously reported as a corticosteroid responsive transcription factor in other tissues<sup>622-624</sup>. ZBTB16 is a transcriptional repressor involved in cell cycle control and is known to suppress the expression of several genes that regulate cell proliferation<sup>625</sup>. Studies in the corneal endothelium support a role for ZBTB16 in the suppression of corneal endothelial cell proliferation<sup>626</sup>. The corneal endothelium and TM cells are derived from the neural crest and share similar characteristics<sup>627</sup>. Further work on the role of ZBTB16 in TM cell physiology is required.

## FK506 Binding Protein (FKBP51)

FK506 binding protein 5 (FKBP5 or FKBP51) encodes FKBP51 a member of the immunophilin protein family which is a novel steroid receptor-associated protein<sup>628</sup>, and a strong inhibitor of glucocorticoid receptor (GR) function<sup>629–631</sup>. In addition to its GR modulatory properties, FKBP51 interacts with several other co-chaperones to regulate steroid receptor splicing protein function and modulates a number of pathways related to immune function, cell growth and metabolism, cytoskeletal organisation, autophagy and DNA methylation<sup>632</sup>.

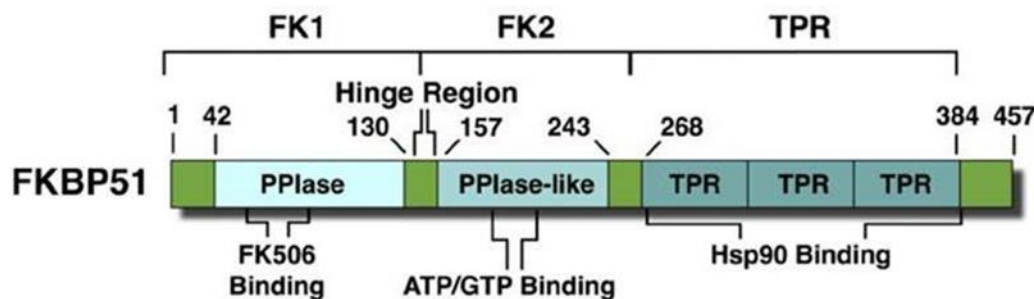


**Figure 4.10: FKBP51/FKBP5 Structure.** FKBP51 consists of three domains- an FK1 domain which has PPlase activity and bind immunosuppressants, an FK2 domain which is FK1-like but does not bind immunosuppressants, and a C terminal domain which has a 3 TPR domain which can bind to Hsp90. FKBP51 is up-regulated in response to steroids. Modified from Online Resource (FKBP5 Pharma Ltd)<sup>633</sup>.

Glucocorticoid action requires binding of GC ligand to GR $\alpha$  inducing nuclear translocation, to regulate gene expression. In the absence of a ligand, GR $\alpha$  remains in the cytoplasm as a multiprotein heterocomplex that contains heat shock protein (Hsp)90, Hsp70, and an immunophilin, such as FKBP51<sup>634</sup>. FKBP51 contains a peptidyl-prolyl *cis/trans* isomerase (PPlase) domain and a C terminal tetratricopeptide repeat (TPR) domains (Figure 4.10). TPR domains bind Hsp90 and aids chaperoning of GR in nuclear translocation<sup>630</sup>. FKBP51 is bound to mature GR $\alpha$  and it has been shown that GC ligand binding induces the release of FKBP51 bound to GR $\alpha$ . This allows the incorporation of FKBP family member, FKBP52, to GR $\alpha$ <sup>635</sup>. FKBP52 binds dynein which shuttles the complex from the cytoplasm, via microtubules, to the nucleus where it can then exert effects on gene expression (Figure 4.11).

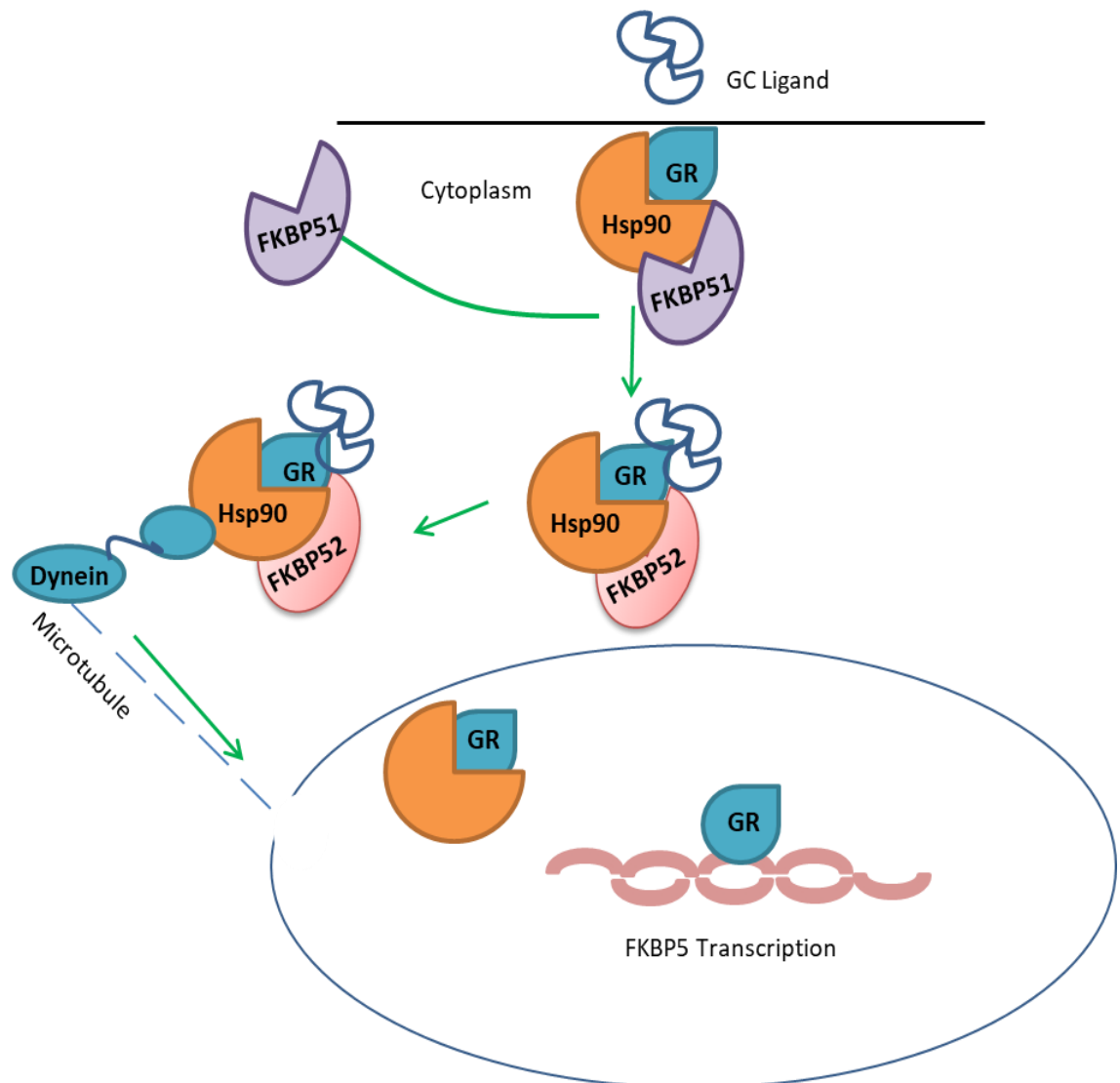


**Figure 4.11: The FKBP51 and FKBP52 Genes Regulate Glucocorticoid Receptor Nuclear Translocation. Modified from Trebble 2013<sup>636</sup>.** FKBP51 is released from GR $\alpha$  upon binding of GC ligand. FKBP family member FKBP52 is incorporated and induces the binding of Dynein, a protein required for nuclear translocation via microtubules.

Lower GR $\beta$  expression compared to GR $\alpha$  expression is thought to contribute to enhanced GC sensitivity in glaucomatous patients as well as non-glaucomatous steroid responders<sup>590</sup>. Interestingly, FKBP51 expression patterns in glaucomatous TM is not uniform which may be disruptive of GR $\beta$  nuclear import thus contributing to the low nuclear GR $\beta$  expression and increased glucocorticoid sensitivity observed in POAG patients<sup>637</sup>.

Our study identified FKBP51 expression was significantly up-regulated in human TM cells in the presence of DEX (FC= 2.68,  $p$ -value= 3.3E-52). Up-regulation

of FKBP51 was further validated in TM cells by q-PCR (FC= 9.09,  $p$ -value= 0.0313, Figure 4.7). Significant glucocorticoid inducible expression of FKBP51 in the TM was previously reported after 24hours<sup>571</sup> and 21 days<sup>570</sup> of DEX treatment. In C57BL/6J mice, treated with topical 0.1% dexamethasone sodium phosphate ophthalmic solution 3 times daily for up to 5 weeks, all mice showed increased FKBP51 expression at weeks 3 and 5<sup>638</sup>. DNA methylation of the FKBP51 promoter is lost with GC treatment with a concomitant increase in FKBP51 expression in murine studies<sup>639</sup>; similar methylation changes have been reported in the human TM treated with 100nM DEX for 21 days<sup>640</sup>. This data suggests FKBP51 plays a significant role in steroid-induced glaucoma, but the mechanism is currently unknown. A candidate gene association study typed SNPs in FKBP51 in POAG patients but no significant risk alleles were identified<sup>641</sup>.

Similar to GR $\alpha$ , GR $\beta$  can also complex with Hsp90, and it has previously been reported that Hsp90 is essential for GR $\beta$  nuclear transportation<sup>642</sup>. FKBP51, but not FKBP52, is involved in GR $\alpha$  and  $-\beta$  nuclear translocation independent of ligand-binding<sup>637</sup>. Further work identified overexpression of FKBP51 enhanced the nuclear transport of GR- $\beta$  in trabecular meshwork cells<sup>637</sup>. FKBP51 involvement in chaperoning GR $\beta$  nuclear translocation may represent a novel therapeutic target through which FKBP5 induces glucocorticoid resistance.

It is of note that previous reports have stated that FKBP51 have caused glucocorticoid resistance in a number primates<sup>629</sup>. In addition, FKBP51 is known to be increased by glucocorticoids<sup>570,571</sup>, suggesting that regulation of FKBP51 levels represents a potential feedback mechanism for inhibiting glucocorticoid responses. Recently several miRNAs (miR-124, miR-15a, miR-142, and miR-511) have been identified with target sites on the FKBP51 mRNA<sup>643-645</sup>. Although all miRNAs have been shown to regulate FKBP51 mRNA, only miR-511 was found to robustly regulate FKBP51 at the protein level<sup>108</sup>. miR-511 suppresses the GC-induced up-regulation of FKBP51 in cells and primary neurons also, suggesting its role in FKBP51s modulatory action on GRs<sup>645,646</sup>. Our study further confirms FKBP51 expression is enhanced by glucocorticoids (DEX specifically), further strengthening the premise that FKBP51 is a potential therapeutic target and may be a candidate for miRNA therapeutics.

## Podoplanin (PDPN) and Vascular Endothelin Growth Factor C (VEGFC)

Podoplanin (PDPN) has been localised to the TM of the human anterior segment<sup>647</sup>. PDPN is a mucin-type transmembrane glycoprotein which is reported to be a specific lymphatic endothelial cell marker<sup>648</sup>. A microarray study based on perfused non-glaucomatous human donor anterior segments to identify pressure-related gene expression was the first to identify PDPN in the human TM<sup>649</sup>. The expression of PDPN was consistently up-regulated in response to elevated IOP/perfusion pressure in all donors and immunohistochemical staining localised expression to the trabecular meshwork and inner wall of Schlemm's canal. The authors proposed that PDPN represents a novel candidate for pressure regulation in the human trabecular meshwork<sup>649</sup>. In our study PDPN expression was significantly up-regulated by RNA-Seq (FC= 1.36, *p*-value = 3.39E-33) but not in the q-PCR validation (FC= 2.38, *p*-value = 0.384 Figure 4.7).

Pronounced expression of PDPN in the conventional outflow pathway and TM in the normal human eye was confirmed in an immunohistochemical study<sup>647</sup> and expression is altered in POAG<sup>650</sup>. The trabecular meshwork cells have some properties consistent with lymphatic endothelial cells and the aqueous humour parallels lymphatic fluid in interstitial spaces<sup>650</sup>. The aqueous humour ultimately drains into Schlemm's canal (SC) which has some of the structural, molecular and functional properties of lymphatic vasculature<sup>651</sup>. The SC expresses some lymphatic markers: prospero-related homeobox 1 transcription factor (PROX1), vascular endothelial growth factor receptor 3 (VEGFR3) and integrin  $\alpha$ 9; but not lymphatic vessel endothelial hyaluronan receptor 1 (LYVE1) and podoplanin<sup>651</sup>. VEGFC/VEGFR3 signalling is an important regulator of the SC<sup>652</sup>. VEGFC drives the proliferation of SC endothelial cells and in adult mice a single injection of recombinant VEGFC into the adult eye resulted in sprouting, proliferation, and growth of SC endothelial cells, whereas VEGFA obliterated the aqueous outflow system<sup>653</sup>. Furthermore, in an adult mouse a single intracameral injection of recombinant VEGFC induced SC growth and resulted in a sustained reduction in IOP<sup>652</sup>. VEGFC expression was downregulated in human TM cells in response to DEX treatment using RNA-Seq (FC= -1.32, *p*-value= 1.44E-44) and with q-PCR validation (FC= 0.412, *p*-value = 0.0022). The role of VEGFC in SC physiology in humans and primates is unknown but murine studies<sup>652,653</sup> suggest increasing VEGFC reduces IOP and the reduction in VEGFC in the TM in response to DEX in this study warrants further study. VEGFC may be a therapeutic option in POAG<sup>652</sup> and steroid-induced glaucoma.

## Plasminogen Activator Inhibitor 2 (SERPINB2)

Plasminogen activator inhibitor 2 (PAI-2) or serpinB2 (SERPINB2) is a serine protease inhibitor of the serpin superfamily which acts as a coagulation factor (Figure 4.12) inactivating tissue plasminogen activator (tPA) and urokinase plasminogen activator<sup>654</sup>. SERPINB2 is induced during inflammatory processes and infections in many cell types: macrophages, fibroblasts, endothelial cells, and differentiating keratinocytes<sup>655-657</sup>. SERPINB2 non-expressing cells exhibit differences in cellular protrusion dynamics in comparison to SERPINB2 expressing cells, suggesting that SERPINB2 has an effect on matrix remodelling primarily through a novel role in regulation of motility and interactions with the surrounding ECM<sup>658</sup>.

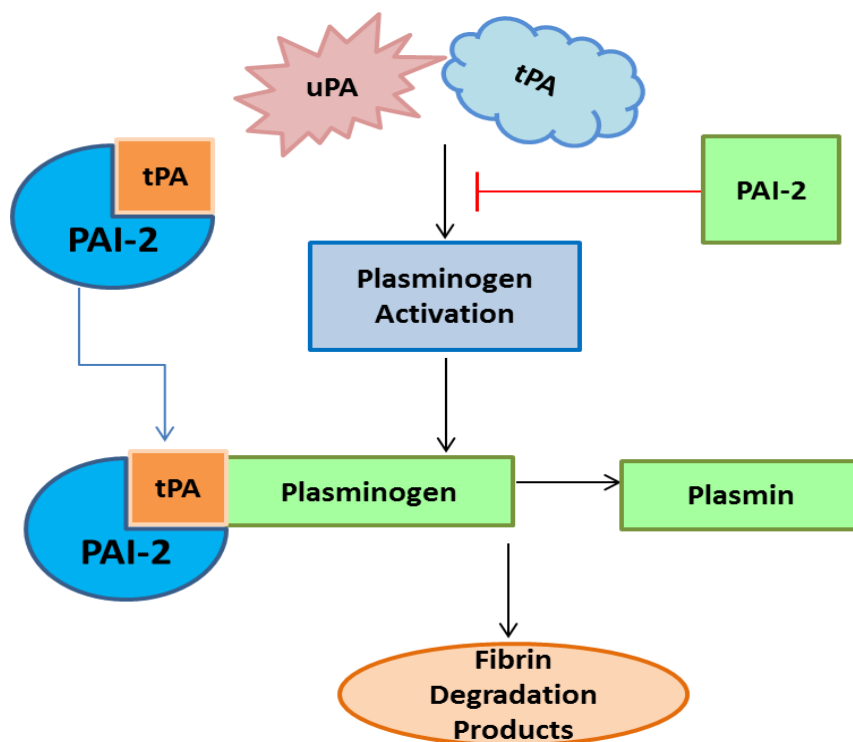


**Figure 4.12: PAI-2 Inhibits tPA Activity.** Modified from Kohler *et al* 2000<sup>659</sup>.

SERPINB2 expression was significantly down-regulated in human TM cells stimulated by DEX in our study (FC= -3.59,  $p$ -value= 4.66E-47). Validation of SERPINB2 decreased expression could not be achieved by q-PCR (FC= 0.34,  $p$ -value = 0.3052). Significant glucocorticoid down-regulation SERPINB2 expression in the TM was also reported after 6-8 days of DEX treatment<sup>568</sup>. The role of SERPINB2 in the TM is not known. The extracellular function of SERPINB2 is to regulate fibrinolysis but as SERPINB2 is mainly intracellular its role within the cell is not well understood<sup>654</sup>. SERPINB2 is a direct downstream target of p53 and intracellular

SERPINB2 has a direct role in cellular senescence through the stabilisation of p21<sup>660</sup>. SERPINB2 also plays a role in matrix remodelling and carcinogenesis by regulating fibroblast motility and interactions with the ECM<sup>658</sup>. Interestingly, plasminogen activator inhibitor 1 (PAI-1), a phylogenetically distinct but regulated coagulation factor, is induced in the TM when treated with TGF- $\beta$ 2 which is proposed to inhibit ECM degradation via MMP regulation<sup>244</sup>. This alternative relationship between PAI-1 and PAI-2 has previously been described<sup>661</sup>. The ratio of PAI-1/PAI-2 may be a useful biomarker in differentiating normal and glaucomatous patients.

### Matrix Metalloproteinase 1 (MMP-1)

Matrix metalloproteinase 1 (MMP-1) is an interstitial collagenase and fibroblast collagenase in humans, part of the MMP enzyme family which exhibit different substrate specificities, which together are capable of degrading all components of the ECM<sup>662,663</sup>. A number of studies and experimental findings have implicated a role for MMP-1 in glaucoma<sup>664-667</sup>. Previous studies have shown that DEX treatment of cultured human TM cells (100nM for 3-6 days) decreases the expression of MMP-1 using q-PCR and collagen degradation assays<sup>666</sup>. In our RNA-Seq data MMP-1 expression was decreased in human TM cells treated with DEX (FC= -1.81, p-value= 4.4E-41); q-PCR did not confirm this, (FC= 1.26, p-value= 0.0649 Figure 4.7). Protein, functional studies and time course studies including collagen degradation assays and ELISA are required to fully validate this finding but previous studies support the down-regulation of MMP-1 with DEX treatment in the human TM<sup>666</sup>. This reduction in MMP-1 may relate to the decreased ECM turnover seen in the outflow pathway with corticosteroid treatment<sup>552</sup>. The DEX induced decrease in the expression and activity of MMPs in the TM is likely to contribute to the increased outflow resistance observed in steroid responders<sup>666</sup>.

MMP-1 reduction in response to DEX has garnered great interest in recent years and researchers have begun to investigate the potential of MMP-1 glucocorticoid-inducible gene virus therapy as a novel treatment of glaucoma<sup>666</sup>. Research so far has investigated the effects of a glucocorticoid-inducible virus vector overexpressing recombinant MMP-1 on both human TM cells and perfused human anterior segments<sup>666</sup>. Transfected cells and anterior segments showed increased MMP-1 expression in a cyclic manner with the addition and removal of DEX<sup>666</sup>.

## Follistatin (FST)

Follistatin (FST) is an autocrine glycoprotein that is expressed in most tissues<sup>668,669</sup>. The essential biological function of FST is binding and neutralising transforming growth factor beta (TGF- $\beta$ ) superfamily, including activin, myostatin, and bone morphogenic protein (BMP)<sup>670-672</sup>. FST is a stress responsive protein exerting protective effects by neutralising TGF- $\beta$ 2 signalling by antagonising BMP and activin<sup>669</sup>. FST is expressed in the normal and glaucomatous TM<sup>526,673</sup> and this expression is increased in a dose-dependent manner with TGF- $\beta$ 2 treatment<sup>673</sup>.

Our RNA-Seq data indicated that FST expression was significantly down-regulated in TM cells stimulated with DEX in comparison to normal cells (FC= -2.53,  $p$ -value= 2.36E-54); down-regulation was further corroborated by q-PCR (FC= -0.168,  $p$ -value = 0.0022). Significant glucocorticoid inducible expression of FST in the TM was also reported after 21 days<sup>570</sup> of DEX treatment. The biological activities and underlying mechanisms for FST involvement in the TM have yet to be explored fully<sup>673</sup>.

As well as its role in neutralising members of the TGF- $\beta$  superfamily, FST has been shown to be a stress responsive protein. TM cells undergo oxidative stress as a result of an imbalance between reactive oxygen species (ROS) and anti-oxidants. Studies have shown that FST reduces ROS production and is thought to interact with members of the NADPH oxidase inhibitor (NOX) family<sup>674</sup>. Interestingly, FST can be regulated at both transcriptional and post-transcriptional levels<sup>675,676</sup>, which allows an opportunity to manipulate FST expression therapeutically.

## Comparison of Key Enriched Canonical Pathways Following Dexamethasone Treatment and TGF- $\beta$ 2 in TM Cells

Using IPA Comparison Analysis the enriched canonical pathways were compared (Figure 4.5) between TGF- $\beta$ 2 treatment (5ng/mL for 24 hours) and DEX treatment (100nM for 16 hours). TGF- $\beta$ 2 results in a greater alteration in gene expression but common canonical pathways are either up- or down-regulated when compared to DEX treatment. The degree and timing of the TGF- $\beta$ 2 stimulation reflects human *ex-vivo* perfusion models in which TGF- $\beta$ 2 induces raised IOP within 24 hours<sup>244</sup> whereas DEX treatment in the same model system takes at least 7-14 days<sup>207</sup>. However, common canonical pathways were activated including actin cytoskeleton, RhoA signalling and signalling by Rho family GTPases (Figure 4.5). Both DEX and TGF- $\beta$ 2 induce the formation of cross-linked actin networks (CLANs) which are believed to stiffen the TM leading to increased aqueous humour outflow resistance and increased IOP<sup>253</sup>. Understanding the molecular mechanisms triggered by TGF- $\beta$ 2 and steroid treatments not only improves our understanding of the pathogenesis of POAG but also steroid-induced OHT and glaucoma. Given that

common pathways like RhoA signalling are activated by TGF- $\beta$ 2 and steroids, this supports the use and development of common therapeutic agents. A dual inhibitor of LIM and Rho kinase (LX7101) lowered IOP in mice with steroid-induced OHT (dexamethasone), this will be discussed further in Chapter 6. Our data supports the concept that inhibition of RhoA signalling is a therapeutic option for both POAG and steroid-induced OHT/glaucoma.

#### 4.6 Summary

Our study characterises differentially expressed genes in human TM cells in response to dexamethasone through RNA-Seq for the first time. This involved the isolation of RNA from glucocorticoid treated primary human TM cells in addition to healthy normal TM cells. 40% of the normal population are steroid responders and this presents an obstacle when investigating a general gene expression profile of normal cells in response to a known glaucoma stimulus, dexamethasone. Differential expression between different donors is expected, however this is further enhanced by individual donor steroid responsiveness. This steroid response was considered and an attempt was made to identify the potential steroid responsive individuals in the data-set. Alternative methods in the future may require a better screening process for steroid responsive samples which will provide a more disease appropriate cohort for examining global gene expression and aid in potential novel target identification.

Among a robust data-set the majority of differentially expressed genes are implicated in extracellular matrix remodelling and glucocorticoid receptor activation and translocation. A number of differentially expressed genes have the potential to be manipulated for therapeutic gain in steroid-induced glaucoma. Of particular interest is FKBP51, a member of the immunophilin family. FKBP51 is involved in the translocation of GR $\beta$  to the nucleus and has already been shown to directly regulated by miRNAs, a promising future therapeutic technique. Going forward, investigation of the roles of miRNAs in the human TM particularly in relation to FKBP51 would be of interest. Elucidating the outcome of enhanced FKBP51 expression in the TM in order to enhance GR $\beta$  expression thus enhancing steroid sensitivity may play a pivotal role in reducing steroid-inducible pathological effects observed frequently in glaucoma. The potential role of miRNA therapies and FKBP51 as a novel therapeutic target for POAG and this will be discussed in Chapter 6.

## **Chapter 5**

### **Identification of TGF- $\beta$ 2 Inducible miRNAs in Human Trabecular Meshwork Cells**

## 5.1 Introduction

### 5.1.1 miRNAs and Glaucoma

Much of the current research on miRNAs is focused on the role of miRNAs in cellular pathology and physiology, typically using the gene expression profiling approach. miRNAs have already been shown to participate in the regulation of most cellular functions, and there is also substantial evidence implicating miRNA expression changes in multiple diseases (for review see Li *et al* 2012<sup>362</sup>). The clinical relevance of genetic mutations affecting miRNA genes or miRNA binding sites has not been thoroughly investigated. However, some functional polymorphisms in miRNA genes have been discovered that might be relevant in the progression of diseases such as acute lymphoblastic leukaemia<sup>677</sup> and diabetic retinopathy<sup>678</sup>. Due to the ability of miRNAs to modify cellular functions and their involvement in multiple pathologies, there has been emerging interest in developing new technologies for their therapeutic use including ocular diseases such as macular degeneration<sup>679</sup>.

Elevated IOP due to decreased outflow facility in the trabecular meshwork is a major risk factor for POAG<sup>680</sup>. Increased outflow resistance results from alterations in the TM cells and key components of the ECM<sup>681</sup>. A number of miRNAs have been detected in the TM in both health and disease<sup>381</sup>. miRNAs play important roles in several physiological and pathological processes including the regulation of inflammatory microenvironments, cell cycle and apoptosis, contractility, cell senescence and fibrosis<sup>368</sup>. Several of these pathways are dysregulated in the TM in glaucoma. Most studies have investigated the role of miRNAs in the biology of the TM and in relation to glaucoma pathogenesis<sup>381</sup>. There are an increasing number of studies examining extracellular miRNAs in the aqueous humour which drains through the TM. Analysis of the patients undergoing cataract surgery identified up to 264 miRNA species in AH using PCR arrays, of which miR-202, miR-193b, miR-135a, miR-365, and miR-376a were the most abundant<sup>682</sup>. Three studies have reported differentially expressed miRNAs in glaucomatous AH using microarray systems and PCR arrays<sup>379,683,684</sup>. However, these studies failed to detect any

common differentially expressed miRNAs; among the significantly differentially expressed miRNAs were; miR-92a, miR-1587, miR-143, miR-518, miR-122, and miR-451<sup>379,683,684</sup>.

Regulation of ECM synthesis and degradation is important for outflow physiology and in the pathogenesis of the outflow pathway in glaucoma<sup>685</sup>. ECM dynamics are central to TM function in health and disease and the miR-29 family are amongst the best characterised miRNAs regulating the ECM<sup>686</sup>. The miR-29 family consists of three members: miR-29a, miR-29b, and miR-29c; they share a common seed region and are predicted to target overlapping sets of genes involved in ECM regulation and homeostasis<sup>686</sup>. The miR-29 family have potent anti-fibrotic effects in multiple organs<sup>365</sup> and in the TM<sup>381</sup>. Both TGF- $\beta$ 2 and chronic oxidative stress alter the expression of the miR-29 family in TM cells<sup>687</sup>. Transfection of normal human TM cells with a miR-29b mimic results in a down-regulation of ECM components including collagens, fibronectin, and laminin (LAMC1) and SPARC/osteonectin<sup>687</sup>. Treatment of human TM cells with TGF- $\beta$ 2 results in down-regulation of miR-29b expression and the activation of pro-fibrotic pathways and ECM deposition<sup>688</sup>. Similarly, oxidative stress in human TM cells down-regulates miR-483-3p expression which has an inhibitory effect in ECM production by repressing SMAD4 expression. Oxidative stress and TGF- $\beta$ 2 drive ECM deposition in the TM by down-regulating anti-fibrotic miRNAs which may contribute to outflow resistance and raised IOP in POAG<sup>380,687,689,690</sup>.

The cytoskeleton and actomyosin system in the TM plays a central role in cell contractility and the pathogenesis of glaucoma<sup>433</sup>. Rho-associated protein kinase (ROCK) inhibitors are entering the clinical realm in glaucoma treatment<sup>691</sup>. A number of miRNAs regulate RhoA signalling pathway in multiple disease states<sup>692</sup>. The miR-200 family is one of the best studied families which can regulate epithelial to mesenchymal transitions (EMT) by repressing the ZEB1/2 transcription factors and cell contractility<sup>693</sup>. miR-200c is highly expressed in the TM where it is involved in the regulation of TM cell contraction and IOP<sup>469</sup>. Luciferase reporter assays provide evidence that miR-200c directly represses key components of the RhoA pathway including RhoA kinase, and, human TM cells transfected with miR-200c

mimic inhibits collagen gel contraction assays<sup>469</sup>. Intracameral injection of the miR-200c mimic in the rat eye decreased IOP while an adenoviral driven miR-200c sponge elevated IOP<sup>694</sup>. In the kidney the miR-200 family and miR-205 were markedly down-regulated in response to TGF- $\beta$ . There is an interplay between TGF- $\beta$ , ZEB1/2 and the miR-200 family which regulates EMT, cell contractility and motility and the ECM (Figure 5.1)<sup>695</sup>. Further work is required to dissect this pathway in the TM and the development of raised IOP.

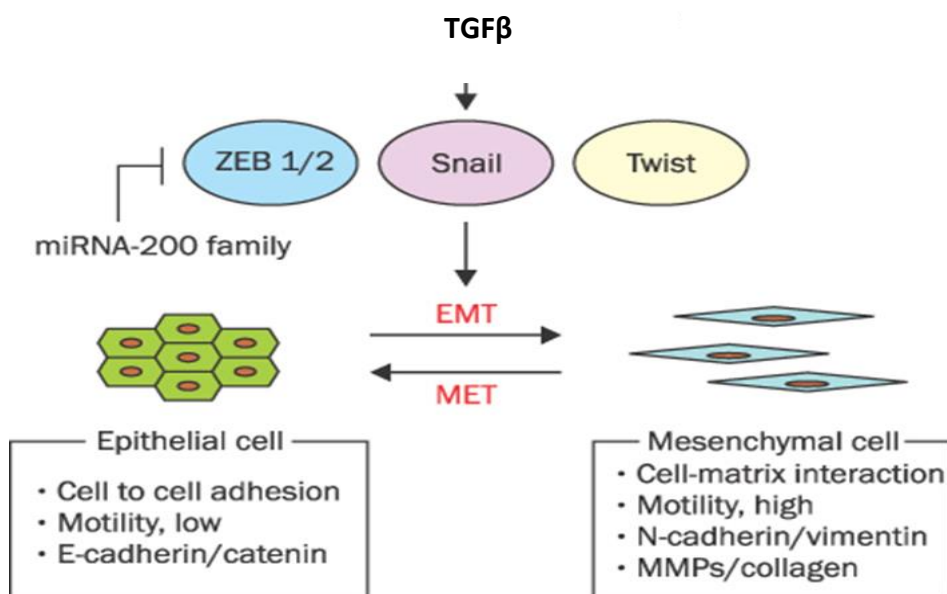


**Figure 5.1: Interplay Between miR-200 Family, TGF- $\beta$ , and ZEB1/2 in EMT Regulation.** Modified from Sabbah *et al* 2008. miRNAs regulate the expression of critical EMT signalling elements.

The TM is subject to mechanical and cyclical stress due to fluctuations in IOP and blood pressure. Laboratory studies modelling mechanical stress and alterations in miRNA expression have identified an up-regulation in several miRNAs implicated in fibrosis including miR-27b, miR-16, miR-26 and let-7<sup>381</sup>. TGF- $\beta$ 1 release in human alveolar cells is inhibited by miR-16<sup>696</sup>. Similarly, miR-24 in human TM cells targets components involved in TGF- $\beta$ 1 processing<sup>697</sup>.

TGF- $\beta$  is a multifunctional cytokine that plays a central role in wound healing and tissue repair. Following tissue wounding or inflammation, the tissue is a source of TGF- $\beta$  and in many diseases excessive TGF- $\beta$  contributes to the pathological excess of tissue fibrosis and inflammation that compromises normal organ function<sup>698</sup>. Most components of the TGF- $\beta$  signalling pathway are known to be targeted by one or more miRNA, and the regulation of TGF- $\beta$  signalling molecules by miRNAs influences the pathogenesis of fibrotic diseases<sup>699</sup>. In addition to regulating the fibrotic response in cells TGF- $\beta$  can also regulate expression of miRNAs through enhancing maturation of miRNAs<sup>700</sup>. Following TGF- $\beta$  treatment direct changes in the expression of several miRNAs have been detected in different cells<sup>701</sup>. TGF- $\beta$  treatment also induces the up-regulation of pre-miRNAs and mature miRNAs but not pri-miRNAs<sup>702</sup>. These miRNAs are regulated post-transcriptionally by a genome-independent mechanism; these miRNAs are termed TGF- $\beta$ /BMP-regulated miRNAs<sup>320,702</sup>. TGF- $\beta$ -regulated miRNAs contain R-SMAD binding elements (R-SBE) in their primary transcript. SMAD proteins directly associate with R-SBE and drive TGF- $\beta$ -mediated miRNA processing. Mutations to the R-SBE abolished TGF- $\beta$ -mediated processing<sup>703</sup>. Similar to SMAD proteins, RNA helicases p68 interact with other transcription factors including p53 and the association of p68 and p53 facilitates Drosha processing of a subset of miRNAs<sup>704</sup>.

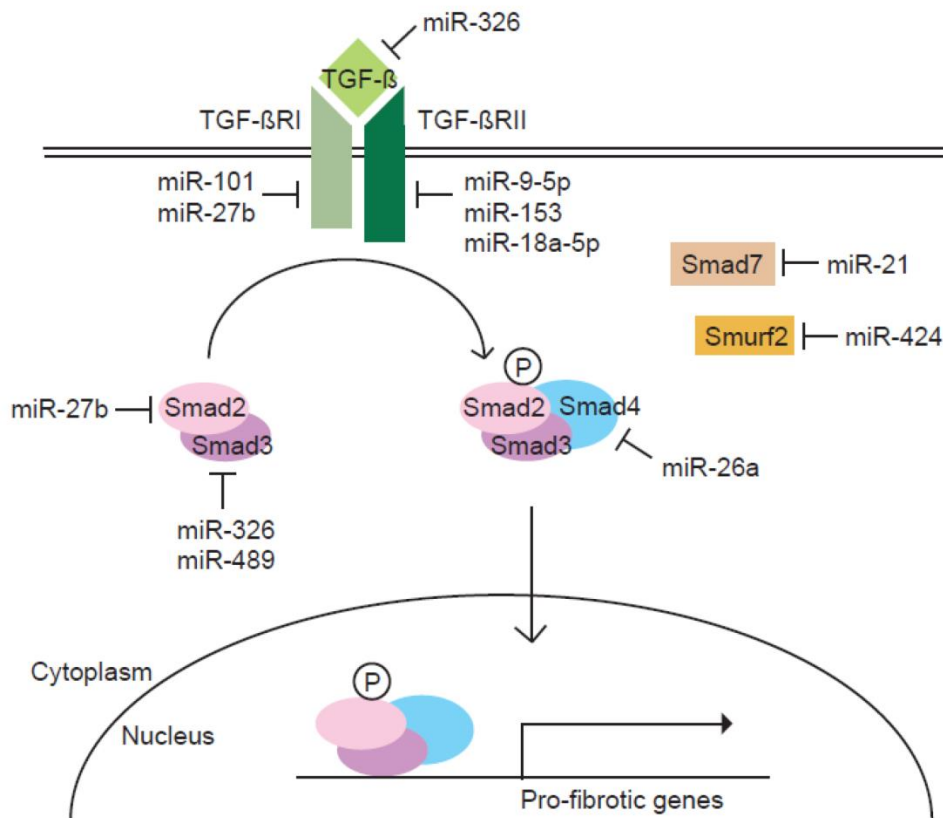


**Figure 5.2: Cross-talk Between TGF- $\beta$  and miRNAs.** TGF- $\beta$  can regulate the expression of miRNAs via their target SMAD proteins. SMAD3 binds to gene promoters inducing transcription of fibrotic genes in addition to pro-fibrotic miRNAs. Additionally, numerous miRNAs modulate components of the TGF- $\beta$  signalling pathway and drive the TGF- $\beta$ -induced fibrotic response. Modified from Kang *et al* 2016<sup>699</sup>.

### 5.2 Aim

The aim of this study was to employ both microarray-based techniques and RNA-sequencing to investigate alterations in the non-coding genome of human trabecular meshwork cells stimulated with TGF- $\beta$ 2. The overall outcome was to identify and functionally characterise TGF- $\beta$ -inducible miRNAs.

## 5.3 Materials and Methods

### 5.3.1 Tissue Culture and TGF- $\beta$ 2 Stimulations

TGF- $\beta$ 2 stimulated cultured human TM cells were prepared as previously described (Chapter 3, Table 3.1). Human TM cells were treated for an additional time-point (4hours) during this experiment due to miRNA turnover rates. Two time-points allowed for a wider range of coverage during the microarray experiments. For the most part miRNAs are stable, however, subsets of miRNAs, more commonly miRNA\*s have much faster turnover rates<sup>705</sup> and therefore earlier time points allow a broader range to be detected in an array setting. All human TM cells were used between passages 5-7. In this study two donor glaucomatous TM cells were also cultured as before but not stimulated with TGF- $\beta$ 2. In total normal human TM cells from 5 donors (+/- TGF- $\beta$ 2) and untreated glaucomatous TM cells (n=2 cadaveric donors) were studied. Table 5.1 contains all human TM donor information for samples used the miRNA array experiments in this chapter. In addition, normal human TM cells from 3 further donors were used in the miRNA manipulation experiments and Table 5.2 contains their information.

<b>Donor I.D</b>	<b>Age</b>	<b>Sex</b>	<b>Medical History</b>
LGP-1	57	Male	No Glaucoma History
LGP-2	65	Male	No Glaucoma History
NTM002	57	Male	No Glaucoma History
NTM009	57	Male	No Glaucoma History
NTM720	64	Male	No Glaucoma History
NTM020	88	Female	No Glaucoma History
GTM 304-04	74	Female	POAG
GTM 730-03	88	Male	POAG

**Table 5.1: Human TM Donor Information for miRNA Array Experiments.**

<b>Donor I.D</b>	<b>Seq I.D</b>	<b>Age</b>	<b>Sex</b>	<b>Medical history</b>
NTM012	Group 1	71	Unavailable	No Glaucoma History
NTM013	Group 2	85	Unavailable	No Glaucoma History
NTM029	Group 3	65	Unavailable	No Glaucoma History

**Table 5.2: Human TM Donor Information for miRNA Manipulation Experiments.**

### 5.3.2 miRNA Isolation and QC

The Qiagen Universal All Prep kit (as per manufacturers' specifications) was used to isolate miRNA from human trabecular meshwork cells (normal and glaucomatous) as described in (Chapter 2, 2.4.1). Total RNA including miRNA was quantified using the NanoDrop-2000, and quality determined by the Bioanalyser 2100 as described in Chapter 2 (2.4.2 and 2.4.3 respectively). Samples with R.I.N below 8 were discounted.

### 5.3.3 Microarray Analysis of Human TM Cells

All microRNA array aspects of this study were carried out by Exiqon services, Denmark. The quality of total RNA was verified by an Agilent 2100 Bioanalyser profile upon arrival at Exiqon. 750ng total RNA from both treatment group (TK\_group as it will be henceforth referred to) and reference group (CK\_group as it will be henceforth referred to) was labelled with Hy3™ and Hy5™ fluorescent label, respectively, using miRCURY LNA™ microRNA Hi-Power Labelling kit, Hy3™/Hy5™ (Exiqon, Denmark), following manufacturers' specifications. The Hy3™-labelled samples and a Hy5™ labelled reference RNA sample were mixed pair-wise and hybridised to the miRCURY LNA™ microRNA Array 7<sup>th</sup> Gen (Exiqon, Denmark), which contains capture probes targeting all microRNAs for human, mouse or rat registered in the miRBase V18.0. Hybridisation was performed according to the miRCURY LNA™ microRNA Array instruction manual using a Tecan HS4800™ hybridisation station (Tecan, Austria). After hybridisation the microarray slides were scanned and stored in an ozone free environment (ozone level below 2.0ppb) in order to prevent potential bleaching of fluorescent dyes. The miRCURY LNA™ microRNA Array slides were scanned using the Agilent G2565BA Microarray Scanner System (Agilent Technologies, INC., USA) and the image analysis was carried out using the IMAGene® 9 (miRCURY LNA™ microRNA Array Analysis software, Exiqon, Denmark). The quantified signals were background corrected (Normexp with offset value 10, see Ritchie *et al.* 2007) and normalised using the global LOWESS (Locally Weighted Scatterplot Smoothing) regression algorithm. Due to the high number of miRNAs that were tested in parallel, microarrays are prone to give false positive results, i.e. miRNAs are found to be statistically different between two conditions,

but in reality, are not. The false positive rate was controlled for in this experiment by multiple testing correction that adjusted  $p$ -values derived from multiple statistical tests. For this expression analysis, the calculated  $p$ -values were based on moderated  $t$ -statistics. Furthermore, the Benjamini and Hochberg multiple testing adjustment method has been applied to the  $p$ -values. Samples have been paired according to donor pair. An expression analysis for glaucoma diseased group (GTM) compared to the control CK\_Group was also performed using simple comparison methods.

#### 5.3.4 microRNA Array Data Validation

To validate the most significantly altered miRNAs identified by microRNA array analysis in the sample and control groups (TK\_group and CK\_group), miScript SYBR® Quantitect (Qiagen, UK) q-PCR assays were performed (see Table 5.3 below). Briefly, 1ug of total RNA (including miRNA) was reverse transcribed to cDNA using miScript II RT kit (Qiagen, UK) according to manufacturers' specifications outlined in Chapter 2 (2.4.5). q-PCR was performed on a Lightcycler® 480 real-time PCR system (Roche Diagnostics, Switzerland). All miRNA levels were measured at  $C_T$  threshold levels and normalised with the average  $C_T$  values of reference targets; SNORD61 and SNORD68. Values were expressed as fold increase over the corresponding values for control by the  $2^{-\Delta\Delta CT}$  method. Two independent experiments were performed and the average ( $\pm$ SEM) results were calculated using GraphPad software (GraphPad Software, San Diego, USA). Data were expressed as the mean values  $\pm$  SEM and analysed using student  $t$ -test. Statistical differences in the mean were considered statistically significant as  $p < 0.05$ .

### 5.3.5 Human Trabecular Meshwork Transfection Optimization

Two miRNAs (hsa-miR-145-5p and hsa-miR-143-3p) were significantly up-regulated in the miRNA array experiment and validated by q-PCR. Primary human trabecular meshwork cells were transfected with mimic and inhibitors for two candidate miRNAs as detailed in Table 5.3 below to investigate their involvement in target gene regulation.

The amount of miRNA mimic or inhibitor needed to efficiently down-regulate or up-regulate a target gene can vary widely, depending on the miRNA, cell type, and chosen analysis method. To determine the concentration that provides optimal results, optimisation experiments using varying mimic and inhibitor concentrations as well as varying amounts of transfection reagent, HiPerfect Transfection Reagent (Qiagen, UK), were performed.

Primary human TM cells between passages 5-7, were seeded at a density of 20,000 cells per cm<sup>2</sup> for transfection experiments. At 50% confluence cell growth was arrested by the addition of serum free DMEM-low glucose for 24 hours as before (Chapter 2, 2.1.4). There were four experimental conditions optimised for each human donor TM cells (n=2): TGF- $\beta$ 2 treatment-only control cells, scrambled oligonucleotide control and TGF- $\beta$ 2 cells, TGF- $\beta$ 2 TM cells and miR-143 mimic and inhibitor, and TGF- $\beta$ 2 TM cells and miR-145 mimic and inhibitor (Table 5.3) for 24 hours. Scrambled control, mimics and inhibitors were used at three different doses, (50nM, 75nM, and 100nM) and the HiPerfect volumes ranged from 9 $\mu$ L/mL to 18 $\mu$ L/mL final volume. Both a scrambled negative control and an Ambion A fluorescently (FAM) labelled siRNA (AM 4611, Thermo Fisher Scientific, UK) negative controls were used to aid in correct interpretation of results, and to determine transfection efficiency respectively.

Transfection efficiency was determined by the FAM labelled siRNA control 24hours after transfection using fluorescent microscopy. The effect of mimic and inhibitor transfections (hsa-miR-145-5p and hsa-miR-143-3p) on target mRNAs was measured by q-PCR (Table 5.4). Briefly, total RNA was isolated as above and 1 $\mu$ g total was reverse transcribed using miScript RT II kit (Qiagen, UK) as before (5.2.2

and 5.2.3 respectively). q-PCR was performed using Primer Design Ltd. SYBR green (UK) on a LightCycler480® real-time PCR system (Roche Diagnostics, Switzerland). All mRNA levels were measured at  $C_T$  threshold levels and normalised with the average  $C_T$  values of a reference gene; GAPDH. Independent experiments were performed and statistically analysed as before (Chapter 3, 3.2.7).

Candidate miRNA	Sequence
hsa-miR-145-5p Mimic (miR-145m)	5'GUCCAGUUUCCCAGGAAUCCCU3'
hsa-miR-145-5p Inhibitor (miR-145i)	5'GUCCAGUUUCCCAGGAAUCCCU3'
hsa-miR-143-3p Mimic (miR-143m)	5'UGAGAUGAAGCACUGUAGCUC3'
hsa-miR-143-3p Inhibitor (miR-143i)	5'UGAGAUGAAGCACUGUAGCUC3'
Scrambled Negative Control (SNC)	ID: 1027271

**Table 5.3: miScript miRNA Mimic and Inhibitors.** Synthesised miScript miRNA mimics and inhibitors for both hsa-miR-143-3p and hsa-miR-145-5p were supplied by Qiagen, UK. A scrambled negative control (Qiagen, UK) was used throughout experiments.

### 5.3.5.1 q-PCR Assessment of miRNA Mimics and Inhibitors of miR-145-5p on Target Genes and EMT-related Genes

A literature and bioinformatics search was used to identify validated targets of miR-145-5p; validated targets have been confirmed experimentally and not solely based on *in silico* predictions<sup>706</sup>. Many bioinformatics tools have been developed to predict miRNA:miRNA and miRNA:mRNA interactions. Bioinformatic tools are useful for accurate and rapid identification of miRNA targets with potential cellular roles to enable functional characterisation and validation in a biological model. Web based tools provide multiple search options, two of which we utilised; the target gene symbol, and the species-specific miRNA name. Displayed results for gene symbol searches provide multiple miRNA targets associated with a given mRNA. Conversely miRNA specie-specific searched provide

miRNA targeted mRNAs whose 3' UTR contain a seed region associated with the miRNA of interest. Two validated miRNA target interaction web-interfaces were employed: miRTarBase(v8) (<http://mirtarbase.mbc.nctu.edu.tw/php/index.php>) and Validated Target Module of miRWalk 2.0 (<http://zmf.umm.uni-heidelberg.de/apps/zmf/mirwalk2/>)<sup>707,708</sup>. Using the specie-specific search option three experimentally validated mRNA targets were identified as regulated by miR-145-5p and miR-143-3p: TGF- $\beta$ 2 (miR145)<sup>709</sup>, CTGF<sup>710</sup> (miR-145 and miR-143) and SMAD2<sup>711</sup> (miR-145). CTGF is involved in glaucoma pathogenesis via remodelling of the actin cytoskeleton of the TM, which results in increased resistance to AH outflow and in turn elevated IOP<sup>712</sup>. In addition, there was significant evidence miR-145-5p is a major repressor of EMT<sup>713</sup> and TM cells can undergo an EMT-like phenomena resulting in an increased fibrotic phenotype<sup>599</sup>. Therefore, the impact of miRNA inhibitors on TGF- $\beta$ 2 induced alterations in E-cadherin, N-cadherin, and vimentin were assessed; and the EMT transcriptional regulators: zinc finger protein SNAI1 (SNAIL) and zinc finger protein SNAI2 (SLUG). Primer sequences for miRNA validated gene targets (TGF- $\beta$ 2, SMAD2, CTGF) and EMT-related genes are given in Table 5.4 below.

<b>Gene</b>	<b>Primer Sequence</b>
<b>TGF-<math>\beta</math>2</b>	F:5' –TCCTGTGGACGCGTATCG-3' R: 5' –TGTCAGTGACTATCATGTGCGTTATTAACC-3'
<b>SMAD2</b>	F: 5'-AGATCCATAATGAATCCAGAACTTC-3' R: 5'-GAAGAAAAATCTAAAAGCCCTCTATG-3'
<b>CTGF</b>	F: 5'-GCTTACCGACTGGAAGACACG-3' R; 5'-CGGATGCACTTTTTGCCCTT-3'
<b>E-Cadherin</b>	F: 5'-TCATGAGTGTCCCCGGTAT-3' R: 5'-GTCAGTATCAGCCGCTTCAGAT-3'
<b>N-Cadherin</b>	F; 5'-CCACAG CTCCACCATATGACT-3' R: 5'-CCCCAGTCGTTTCAGGTAATC-3'
<b>SLUG</b>	F: 5'-CGCCTCCAAAAAGCCAAAC-3' R: 5'-CGGTAGTCCACACAGTGATG-3'
<b>SNAIL</b>	F: 5'-ACCCAATCGGAAGCCTAACT-3' R:5'-GGTCGTAGGGCTGCTGGAA-3'
<b>Vimentin</b>	F: 5'-AGAACCTGCAGGAGGCAGAAGAAT-3' R: 5'-TTCCATTCACGCATCTGGCGTT-3'

**Table 5.4: Primer Sequences used for q-PCR of Validated mRNA Targets of miR-145 and miR-143 and EMT-related Genes.** Primer sequences were obtained from Primer Bank and primers were synthesised by Eurogentec (TGF- $\beta$ 2, SMAD2 and CTGF) and Eurofins (E-cadherin, N-cadherin, SLUG, SNAIL and vimentin).

### 5.3.6 RNA-Seq Analysis of Genome-wide Transcriptional Effects of miRNA Inhibitors of miR-145-5p and miR-143-3p to Identify Target Genes

The experimental identification and validation of miRNA:mRNA interactions can be performed using a number of approaches. Gene:miRNA interactions can be cell and disease context specific; and given the conflicting results of q-PCR based validation, an RNA-Seq approach was applied to provide indirect evidence of miRNA:mRNA targets. As miR-145-5p and miR-143-3p were up-regulated in the TGF- $\beta$ 2 treated human TM cells specific miR-143 and miR-145 inhibitors (143i and 145i respectively) were transfected and genome-wide alterations in mRNA expression was measured by RNA-Seq.

Human TM cells (n=3) were grown to 50% confluence as before (5.2.5) and growth arrested for 24hours. TM cells were co-transfected with 5ng/mL TGF- $\beta$ 2 and 100nM miRNA inhibitor for either 143i, 145i or both (143i and 145i). Control cells were TGF- $\beta$ 2 treated only and TGF- $\beta$ 2 treated plus scrambled negative control. TM cells were transfected for 24hours. 100nM was chosen as inhibitor dose to ensure complete inhibition of the target miRNA as per manufacturers' instructions.

Total RNA was extracted as before and subjected to QC analysis using the Agilent Bioanalyser 2100. 1 $\mu$ g total RNA was used for RNA-Seq at the Core Facility at Queens University Belfast (QUB; Dr. David Simpson).

### 5.3.7 RNA-Seq of TGF- $\beta$ 2 Positive Cells Co-Transfected with miRNA Inhibitors (miR-143i and miR-145i)

There were five experimental conditions for each of the donor TM cells/biological replicates (n=3): TGF- $\beta$ 2 treatment only control TM cells (TC\_Group), scrambled oligonucleotide control and TGF- $\beta$ 2 TM cells (SNC\_Group), TGF- $\beta$ 2 TM cells and miR-143 inhibitor (143i\_Group), TGF- $\beta$ 2 TM cells and miR-145 inhibitor (145i\_Group), and TGF- $\beta$ 2 TM cells transfected with miR-143 inhibitor and miR-145 inhibitor (143i/145i\_Group).

#### 5.3.7.1 cDNA Library Construction, Purification and QC

RNA sequencing experiments were conducted at Queens University, Belfast. The starting material, 500ng RNA, was enriched for mRNA using the oligodT bead system and the isolated mRNA was enzymatically fragmented. Library preparation was achieved using TruSeq RNA Library kit (Illumina, USA). Library quantification was assessed using NanoDrop 2000 (Thermo Fisher Scientific, UK) and diluted based on NanoDrop values to produce average fragment sizes up to 20nM. Libraries were then quantified by q-PCR and diluted to 4nM. Optimal concentration of the library pool was used to generate clusters on the surface of a flowcell before sequencing using Nextseq 500, High Output sequencing kit (Illumina, USA) for 75 cycles single end reads.

#### 5.3.7.2 RNA-Seq Data Analysis of TGF- $\beta$ 2 Positive Cells Co-Transfected with miRNA Inhibitors (143i and 145i)

Expression analysis was performed on the following treatment groups, SNC\_Group, 143i\_Group, and 145i\_Group, compared to the TGF- $\beta$ 2 treatment only group, TC\_Group. NGS analysis was performed using Partek Flow (6.017) running on 64-bit linux machine with a Safari 11 browser. FASTQ files were filtered to remove sequences with a Phred score<30 and adaptors were removed. Sequence alignment was achieved using *TopHat* (4.1) running *Bowtie* (1.0). Alignment quality statistics were calculated. Raw gene counts data were generated by quantification to the Partek E/M annotation model (based on Xing *et al* 2006) using hg19-Ensembl Transcripts Release 75.

Counts were imported into edgeR. A linear model of gene expression was constructed comparing gene expression in pairs of cells treated with inhibitors or scrambled control, with TGF- $\beta$ 2 treatment used as a common reference. Inference of differential expression was by log ratio test using glmLRT.

### 5.3.8 RNA-Seq Validation

#### 5.3.8.1 ACTA2 Differential Gene Expression Validation by q-PCR

Validation of RNA samples (TC\_Group, SNC\_Group, 143i\_Group, and 145i\_Group) was performed using q-PCR for selected significantly differentially expressed genes. 1µg of total RNA was reverse transcribed using miScript II RT kit according to manufacturer's specification, outlined in Chapter 2 (2.4.5). Real time analysis was performed using primer pairs for ACTA2 (Actin, Alpha 2, Smooth Mucle, Aorta; smooth muscle actin) obtained from Primer Bank (ACTA2; F:5'-GTGTTGCCCTGAAGAGCAT-3',R:5'-GCTGGGACATTGAAAGTCTCA-3' and GAPDH; F:5'-CGAGCCACATCGCTCAGACACC-3', R:5'-GGTCAATGAAGGGGTCATTGATGGCAAC-3'). q-PCR was performed on a LightCycler® 480 real-time PCR system (Roche Diagnostics, Switzerland) according to conditions outlined in Chapter 2 (2.5.4). All mRNA levels were measured at C<sub>T</sub> threshold levels and normalised with the average C<sub>T</sub> values of a reference gene; GAPDH. Values were expressed as fold increase over the corresponding values for control by the  $2^{-\Delta\Delta CT}$  method. Two independent experiments were performed and the average ( $\pm$ SEM) results were calculated using GraphPad software (Graphpad Software, San Diego, USA). Data is expressed as the mean values  $\pm$ SEM and analysed using student t-test. Statistical significance was  $p < 0.05$ .

#### 5.3.8.2 ACTA2 Differential Protein Expression Validation by Western Blot Analysis

Protein lysates were isolated from groups (TC\_Group, SNC\_Group, 143i\_Group, and 145i\_Group) as described in Chapter 2 (2.3.1). Protein lysates were separated by SDS-PAGE and transferred to nitrocellulose membranes by semi-dry Bio-Rad TurboBlot transfer system (Bio-Rad, UK). Membranes were blocked for 1 hour at room temperature in Odyssey® TBS-Blocking Buffer (Li-Cor Biosciences, USA). Primary ACTA2 antibody was used at a concentration of 1µg/mL and primary GAPDH antibody at a concentration of 0.1µg/mL, and membranes were probed overnight at 4°C. Membranes were probed for 90 minutes, following membrane washes (3X5minute washes), with IRDye® 800CW and IRDye®680RD conjugated

fluorescent secondary antibodies (Li-Cor) diluted in blocking buffer at a concentration of 60ng/mL. Membranes were washed and imaged using Odyssey® CLx9120 Infrared Imaging System (Li-Cor Biosciences, USA).

## 5.4 Results

### 5.4.1 miRNA Array Data Analyses

#### 5.4.1.1 Calls and Threshold Filtering

The threshold of detection was calculated for each individual microarray slide as 1.2 times the 25<sup>th</sup> percentile of the overall signal intensity across the array slide. miRNAs with intensities above the threshold in less than 20% (or 2) of the samples were removed from the final dataset used for expression analysis. For this experimental data set a total of 1609 probes were discarded by the filtering procedure. Figure 5.3 (below), indicates a summary of present calls for each sample, i.e. the number of miRNAs above the background threshold. Biologically identical samples should have present call numbers within the same range. All obtained numbers of present calls were within the expected range, and comparable for all samples.

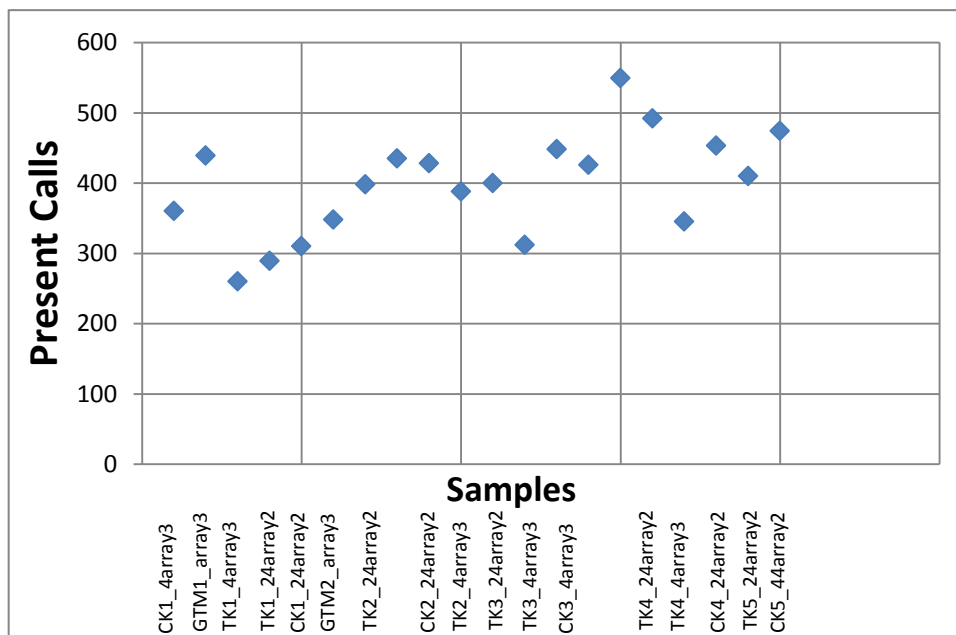


**Figure 5.3: Present Calls and Threshold Filtering Plot.** Plot above shows number of miRNAs detectable above background threshold for each sample out of a possible 2102 possible miRNAs. CK=control group, TK=treatment group. GTM=glaucomatous sample; 4 and 24 respectively refer to TGF- $\beta$ 2 stimulation time period (hrs).

#### 5.4.1.2 miRNA Expression Analysis of TGF- $\beta$ 2 Treated TM Cells

A miRNA expression analysis for TK\_24 vs. CK\_24 was performed. The miRNA profiling identified 3 miRNAs from a total number of miRNAs analysed (447) by the miRCURY LNA™ microRNA Array that were significantly expressed between the control (CK\_Group) and TGF- $\beta$ 2 treated (TK\_Group) groups ( $p < 0.05$ ). 11 miRNAs from a pool of 425 were significantly expressed between the control (CK\_Group) and glaucomatous samples (GTM). Both sets of results were obtained from the 24hour time-point. No statistically significant differential expression was reported from the CK\_Group and TK\_Group exposed to TGF- $\beta$ 2 for 4 hours. Significantly differentially expressed miRNAs for each analysis are shown in Table 5.6 and Table 5.7 respectively.

Probe ID	Annotation	Average Hy3	logFC	<i>p</i> -value
147771	hsa-miR-4328	7253	0.0665	2.99E-02
42641	hsa-miR-145-5p	7462	0.605	2.99E-02
13177	hsa-miR-143-3p	8101	0.957	2.99E-02

**Table 5.6: Differentially Expressed miRNA Genes in the TGF- $\beta$ 2 Treated TM.** Table 5.6 denotes statistically significant differentially expressed miRNA candidates ranked according to *p*-value. Results were obtained from comparing control CK\_Group against treated TK\_Group at a 24hour time point (n=5).

Probe ID	Annotation	Average Hy3	CK_Group	GTM	logFC
42629	hsa-miR-376c-3p	6518	-0.449	-1.866	-1.417
11091	hsa-miR-377-3p	6929	-0.224	-1.632	-1.408
10943	hsa-miR-136-5p	7886	-0.368	-1.676	-1.308
10995	hsa-miR-199a-3p /hsa-miR199b-3p	8366	-0.251	-1.426	-1.175
29562	hsa-miR-199a-5p	8204	-0.186	-1.352	-1.166
146086	hsa-miR-30a-5p	6839	-0.166	0.957	1.123
13177	hsa-miR-143-3p	8101	-0.759	0.346	1.105
13140	hsa-miR-138-5p	8016	-0.274	0.800	1.074
11041	hsa-miR-29c-3p	8939	-0.521	0.526	1.047
147771	hsa-miR-4328	7253	-0.633	0.396	1.028
28191	hsa-miR-30e-5p	6914	-0.149	0.864	1.013

**Table 5.7: Differentially Expressed miRNA in the Normal and Glaucomatous TM.**

Significantly differentially expressed miRNAs ranked according to absolute value of log fold change (logFC) when the normal TM miRNA population (CK\_Group n=5) was compared to the glaucomatous TM (GTM; n=2).

#### 5.4.1.2.1 Volcano Plot Analysis of Untreated and TGF- $\beta$ 2 Treated Human TM Cells

A volcano plot analysis of the data obtained between untreated, control (CK\_Group) and TGF- $\beta$ 2 treated (TK\_Group) provides a visual representation of those miRNAs that display large-magnitude changes that are statistically significant. The volcano plot was constructed by plotting the negative log of the  $p$ -value on the y-axis (base 10); this results in data points with low  $p$ -values appearing towards the bottom of the plot. The log fold-change (logFC) between the two experimental groups is plotted on the x-axis; the logFC is used so that up and down-regulated miRNAs appear equidistant from the centre of the plot. Plotting points in this manner resulted in two regions of interest in the plot; those points that are found towards the top of the plot that are either far right or far left. These points represent values that display large magnitude fold changes as well as high statistical significance. Three differentially expressed miRNAs are shown on the volcano plot as significantly up-regulated in TGF- $\beta$ 2 treated human TM cells.

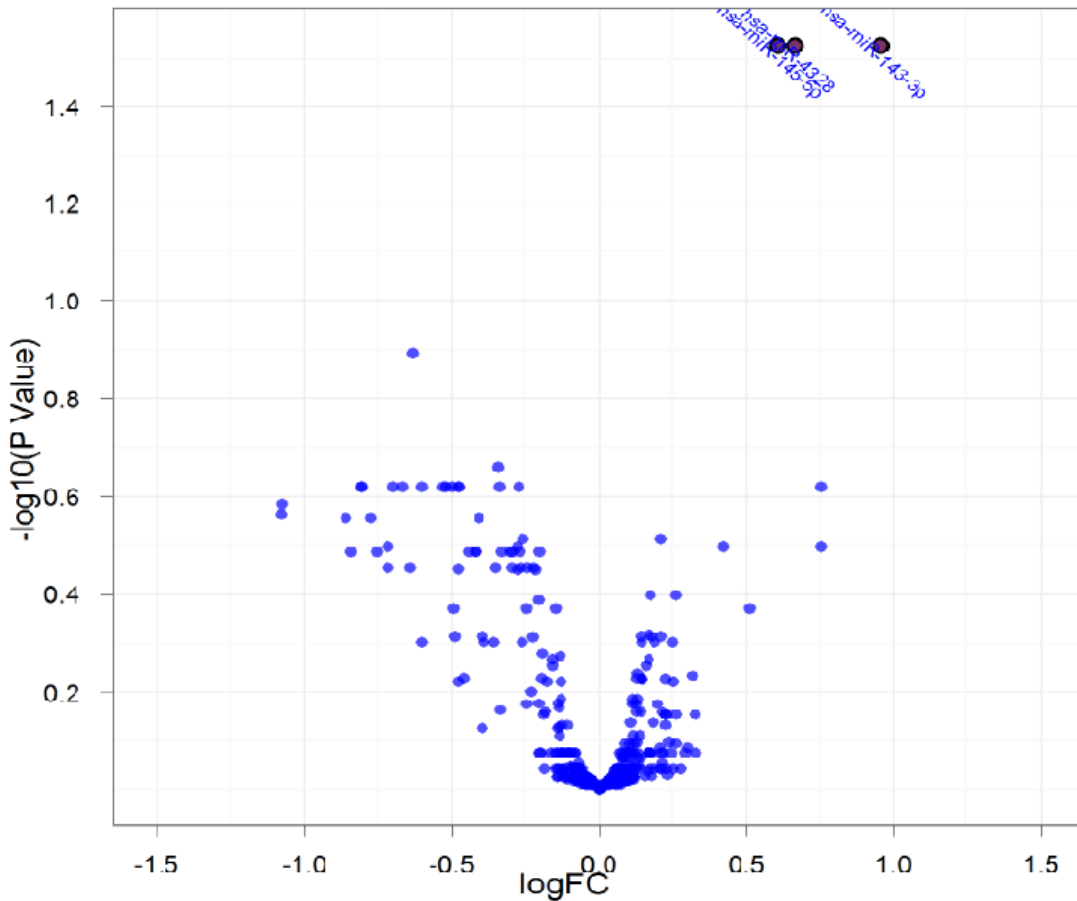


**Figure 5.4: Volcano Plot Analysis of Untreated and TGF- $\beta$ 2 Treated Human TM Cells miRNA Expression.** The above volcano plot shows the relationship between the logarithm of the  $p$ -values and the log fold-change (logFC) between untreated control (CK\_Group) and TGF- $\beta$ 2 treated TM cells (TK\_Group). The top statistically significant differentially expressed miRNAs are marked with an annotation: hsa-miR-4328, has-miR145-5p, and hsa-miR-143-3p (n=5).

#### 5.4.2 q-PCR Assay Validation of Top Differentially Expressed miRNAs in Cultured Human TM +/- TGF- $\beta$ 2

To validate the results obtained from the miRNA array, all three candidate miRNAs identified between the control CK\_Group and treated TK\_Group, were analysed using q-PCR with miScript primer assays (Qiagen, UK): hsa-miR-4328, hsa-miR-145-5p and hsa-miR-143-3p. Differential expression of the top three candidates was also validated in glaucomatous samples (GTM). Expression profiles were analysed by q-PCR with two reference targets used as controls, small nucleolar RNA, C/D box 68 (SNORD68) and Small nucleolar RNA, C/D box 61 (SNORD61). All three candidates demonstrated consistent trends of differential expression by q-PCR. There was no statistical significance observed when results were subjected to two sample students t-tests. Results were only classified as statistically significant when  $p < 0.05$ .

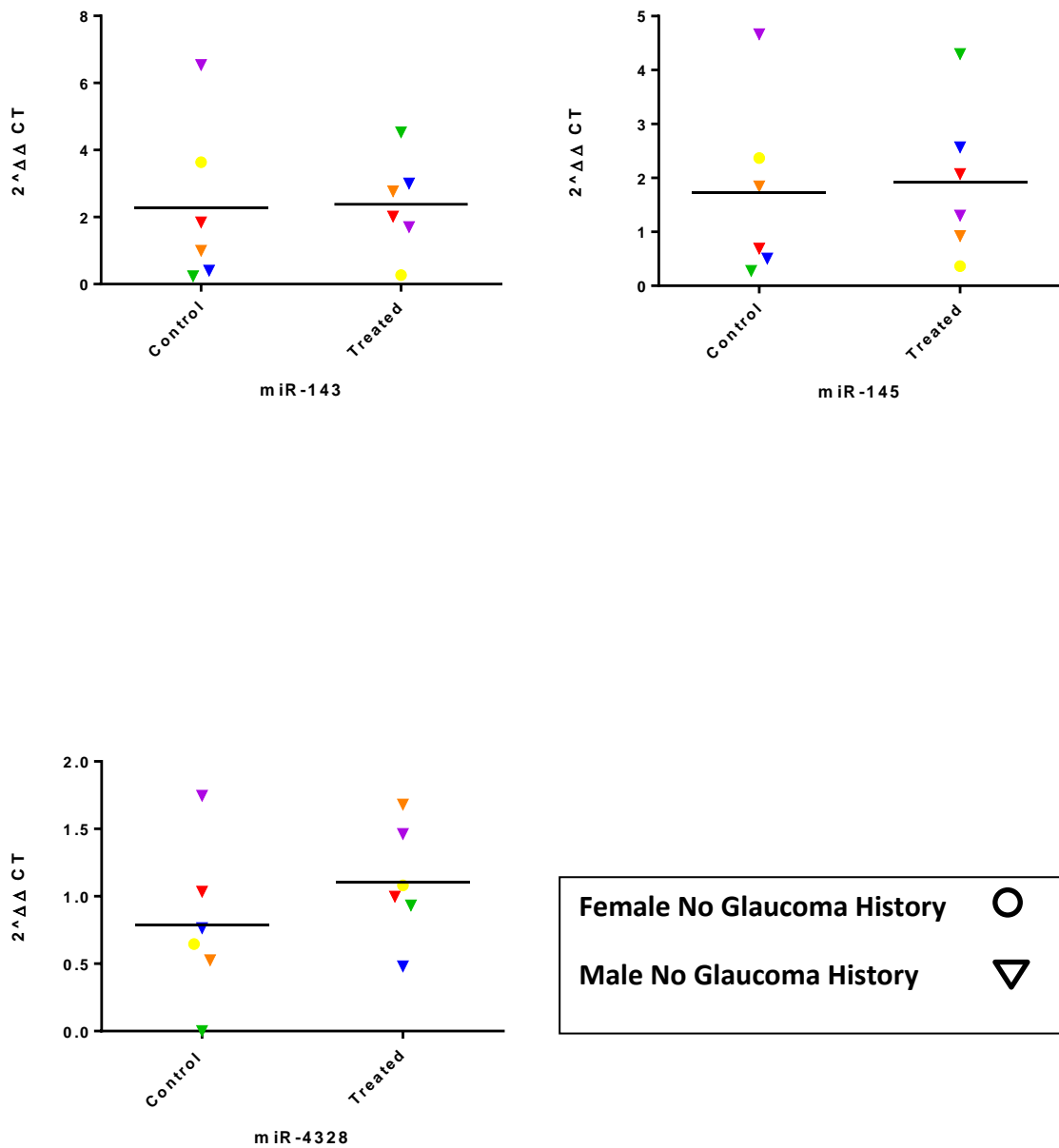


**Figure 5.5: q-PCR Validation of Significantly Up-regulated miRNAs from Microarray Data of TGF- $\beta$ 2 Cultured Human TM Cells.** CK\_Group are denoted as “Control” on graphs and TK\_Group as “Treated” represent miRNAs from untreated control and TGF- $\beta$ 2 treated TM cells. The miRNAs, miR-143, miR-145 and miR-4328 were identified as significantly differentially expressed in the microarray. Individual human TM donor pairs are indicated by same coloured symbols on the graphs (n=6). Female donors are indicated by circle markers, whilst male donors are indicated by triangles. All donors have no previous glaucoma history.

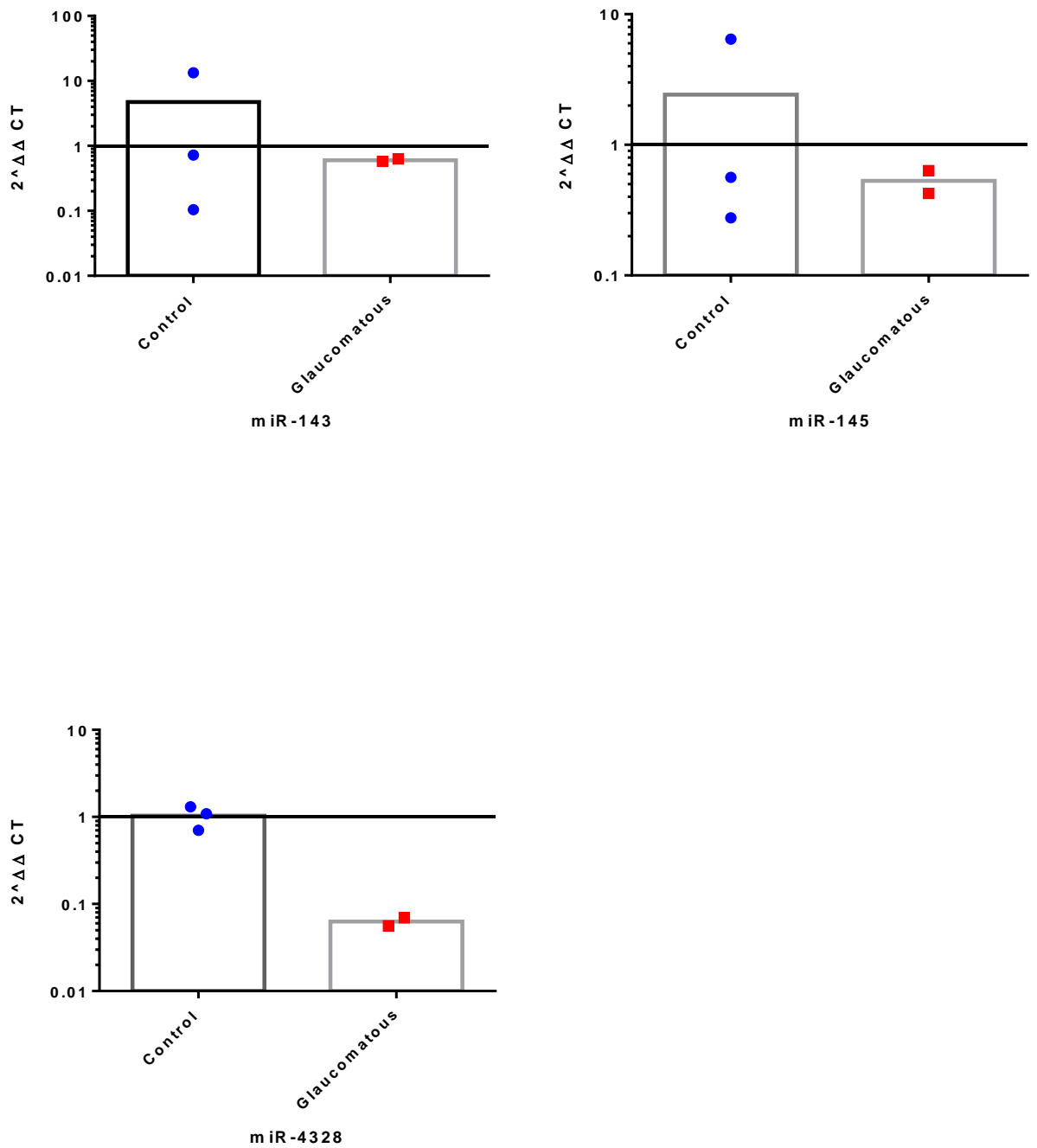


**Figure 5.6: Expression Levels of miR-143, miR-145 and miR-14328 in Cultured Human Glaucomatous TM Cells.** The CK\_Group are denoted as “Control” on graphs representing untreated TM cells and glaucomatous cells (GTM) as “glaucomatous”. The expression of miR-143 and miR-4328 were identified as up-regulated in the GTM compared to controls in the microarray data (see Table 5.7).

### 5.4.3 Human Trabecular Meshwork Transfection Optimisation

#### 5.4.3.1 Human TM Cell Viability with Varying Volumes of HiPerfect Reagent

Human TM cells were subjected to increasing volumes of HiPerfect Transfection Reagent (Qiagen, UK) to assess cell death and viability prior to transfection. Cells were transfected with a FAM labelled siRNA with varying volumes of HiPerfect reagent from 0 $\mu$ L to 18 $\mu$ L. Bright-field images of the TM cells were obtained to assess cell death rates under varying volumes of transfection reagent and fluorescent images were obtained as a means of monitoring transfection success rates.

Figure 5.7 (below) shows that with the highest volumes of HiPerfect Transfection reagent, 15 $\mu$ L and 18 $\mu$ L, no cell death occurred over the proposed transfection time-frame; 24hours. This can be seen from the healthy morphology of the human TM cells and lack of any apparent cellular debris.

FAM labelled siRNA uptake was shown to be successful with both volumes of reagent (15 $\mu$ L and 18 $\mu$ L) for 24 hours also through fluorescent imaging. TM cells exposed only to HiPerfect Reagent and no siRNA were used as a negative control. Transfection efficiency of TM cells is typically very low, with efficiency rates of approximately 10%<sup>714</sup>. Possible explanations for this observation include TM decreased capacity to take up exogenous DNA due to their phagocytic phenotype<sup>714</sup>.

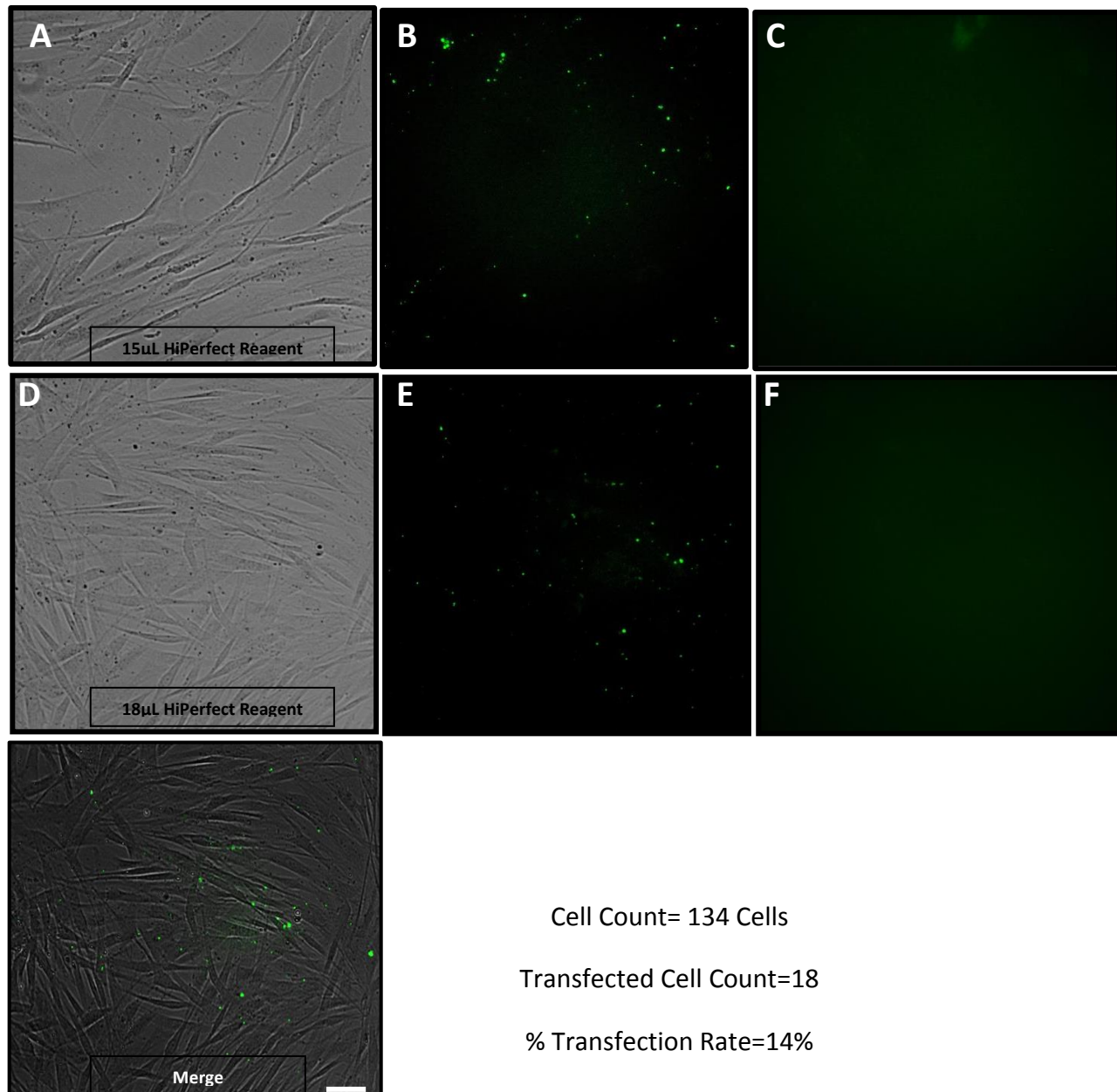


**Figure 5.7: Transfection Optimisation; Cell Viability Assessment.** Human TM cells were transfected with FAM labelled siRNA and varying volumes of HiPerfect Transfection Reagent. Figure 5.7 is representative images of human TM cells after 24hours transfection with siRNA and 15µL and 18µL HiPerfect Transfection reagent. (A) and (D): Brightfield images of human TM cells after transfection with 15µL and 18µL respectively; (B) and (E): Fluorescent imaging of human TM cells after 24hours highlighting uptake of FAM labelled siRNA; (C) and (F): Control fluorescent images were taken of cells exposed only to HiPerfect Reagent and no siRNA; and (G) Composite of brightfield imaging and fluorescent imaging indicating areas of siRNA uptake. Scale bar = 20µM.

#### 5.4.3.2 Effects of miRNA Inhibitors (miR-143i and miR-145i) on Target Gene and EMT-related Gene Expression

To investigate key miRNA:mRNA relationships in TGF- $\beta$ 2 treated TM cells of miR-145-5p and miR-143-3p the effects of miRNA inhibitors (143i and 145i) were assessed by q-PCR in three experimentally validated mRNA targets: TGF- $\beta$ 2, SMAD2 and CTGF. Predicted target genes for miR-145-5p mimics and inhibitors were not statistically altered in this experiment. Limited sample size and transfection efficiency may be causative of this. Increasing sample number may be beneficial for identification of key target genes and this will require some more experimental work. At mRNA level EMT-related genes and validated targets for miR-143 and miR-145 were unaffected by q-PCR.

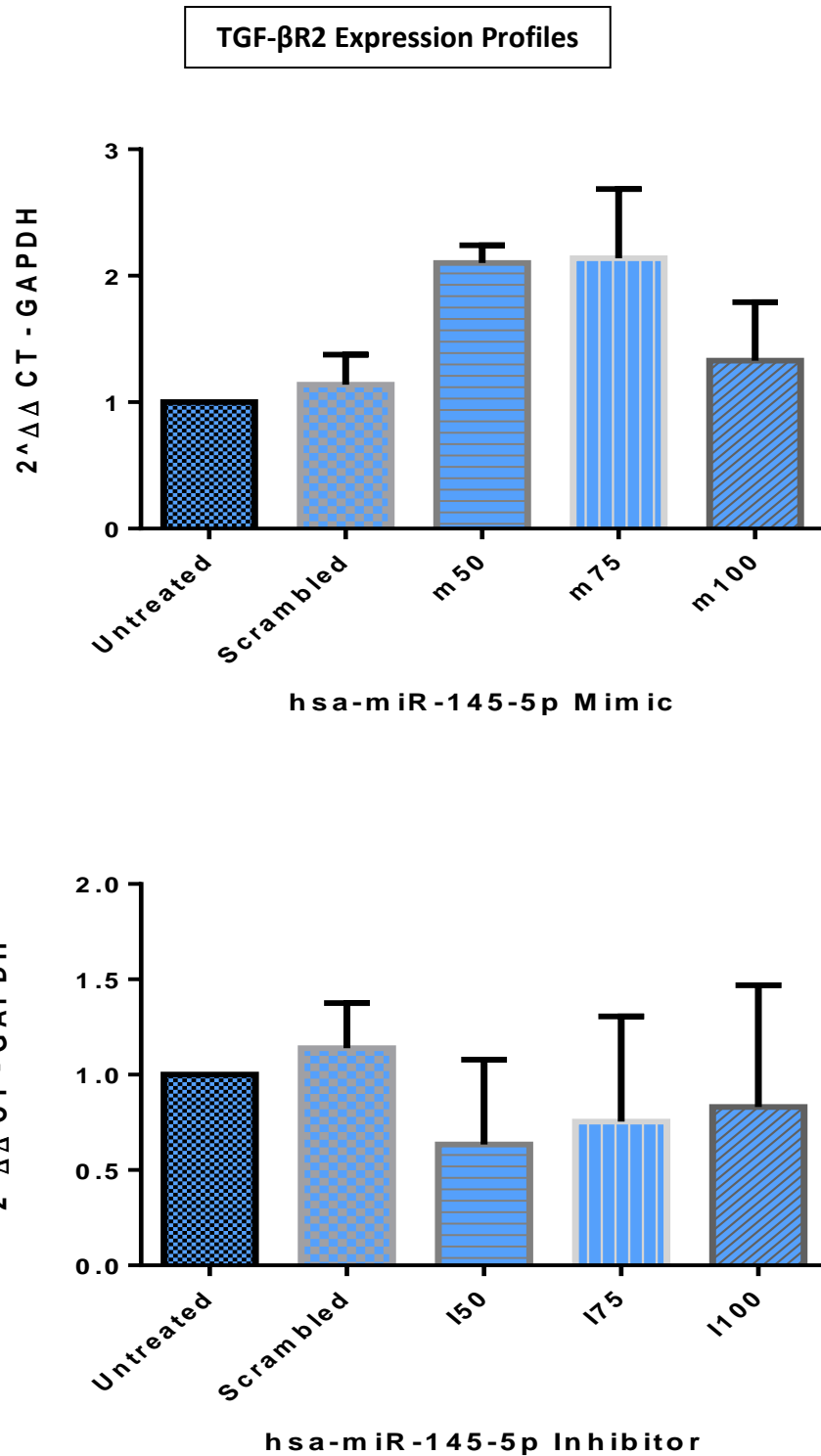


**Figure 5.8: TGF- $\beta$ 2 Expression Profiles in TGF- $\beta$ 2 TM Cells Treated with a miR-145-5p Mimic and Inhibitor.** q-PCR shows a trend that miR-145 mimic increases TGF- $\beta$ 2 expression and miR-145i decreases expression. Untreated; human TM donor cells without TGF- $\beta$ 2 stimulation. Scrambled; TGF- $\beta$ 2 treated human TM donor cells transfected with scrambled negative control. I50-I100; Concentrations of synthesised inhibitor, 50nM to 100nM. (n=2) (Error Bars S.E.M).

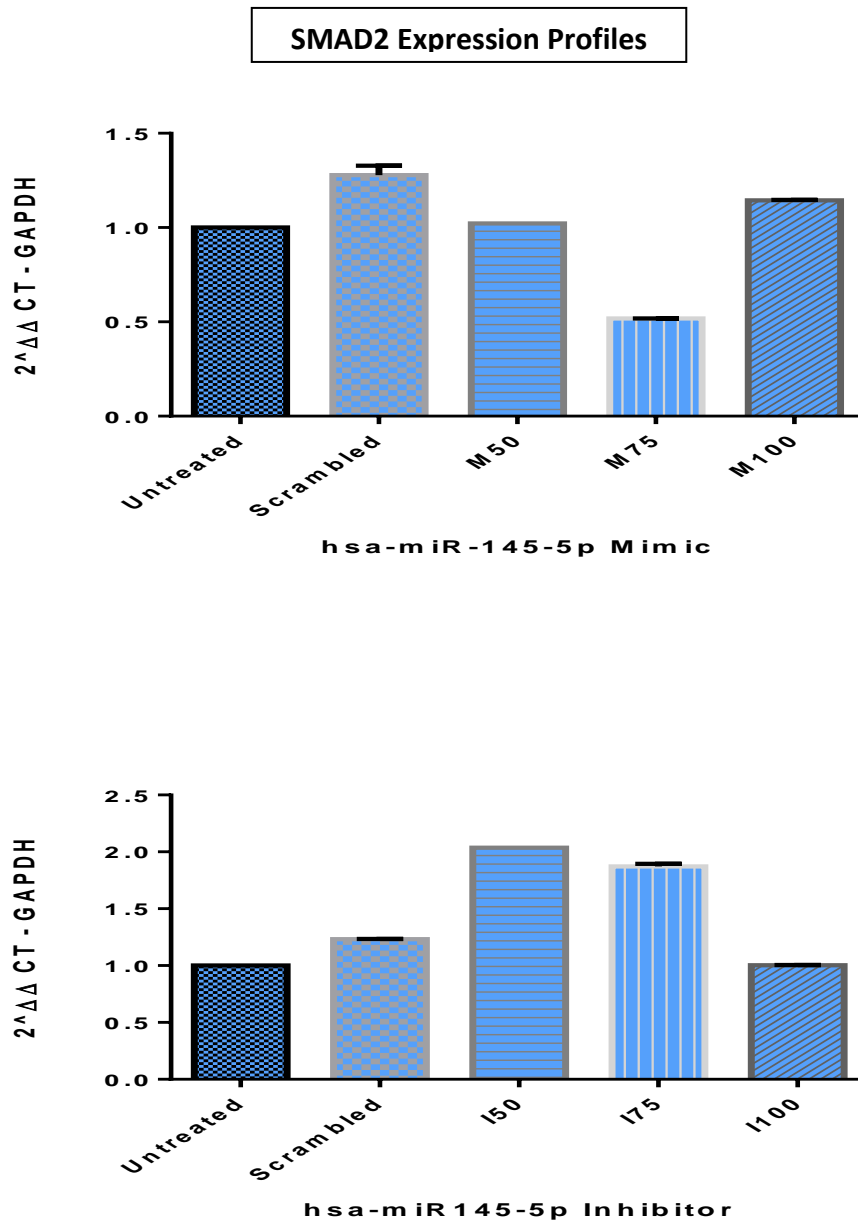


**Figure 5.9: SMAD2 Expression Profiles in the Presence of Synthesised Mimics and Inhibitors for miR-145-5p.** SMAD2 expression profiles normalised to GAPDH. hsa-miR-145-5p synthesised mimic does not stably regulate SMAD2 expression .. 75nM concentration decreases expression whilst 100nM concentration appears to return to stable expression levels similar to the controls. The hsa-miR-145-5p synthesised inhibitor however has distinct effects on SMAD2 expression levels with expression seen to decrease as concentration of inhibitor increases from 50nM to 100nM. Untreated; human TM donor cells without TGF-β2 stimulation. Scrambled; TGF-β2 treated human TM donor cells transfected with scrambled negative control. 150-1100; Concentrations of synthesised inhibitor, 50nM to 100nM. (n=2).

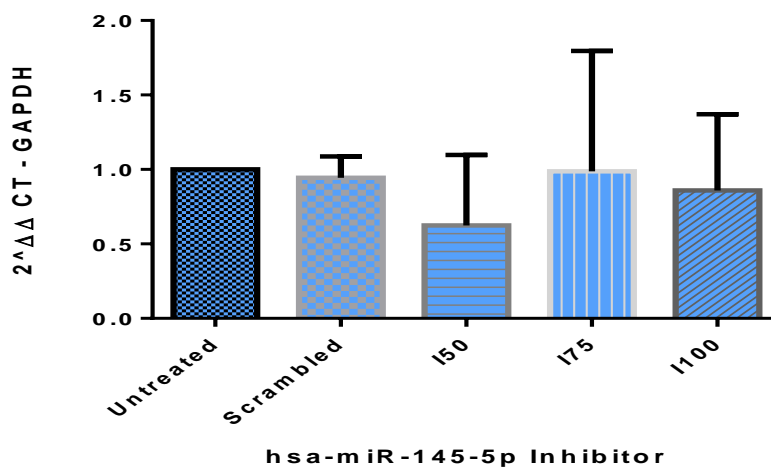
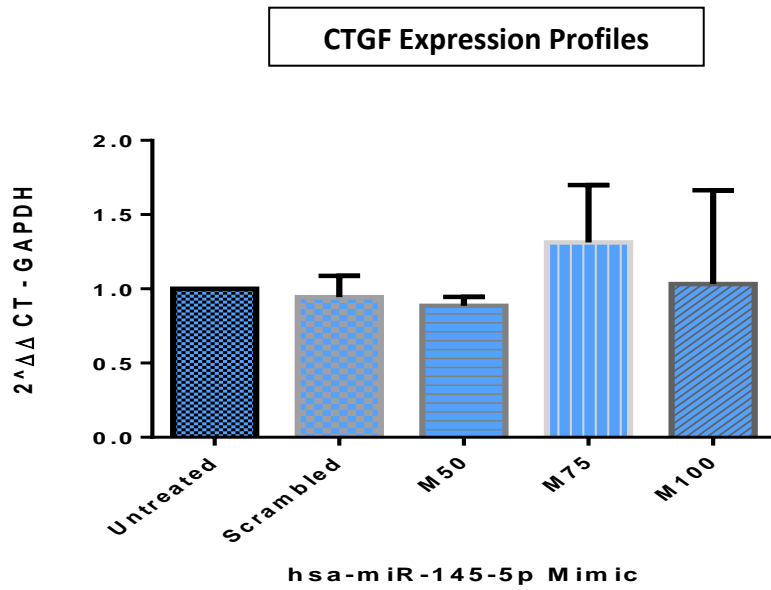


**Figure 5.10: CTGF Expression Profiles in the Presence of Synthesised Mimics and Inhibitors for miR-145-5p.** q-PCR shows no obvious regulation of CTGF gene expression in the presence of synthesised mimics or inhibitors for hsa-miR-145-5p. Untreated; human TM donor cells without TGF- $\beta$ 2 stimulation. Scrambled; TGF- $\beta$ 2 treated human TM donor cells transfected with scrambled negative control. I50-I100; Concentrations of synthesised inhibitor, 50nM to 100nM. (n=2) (Error Bars S.E.M).

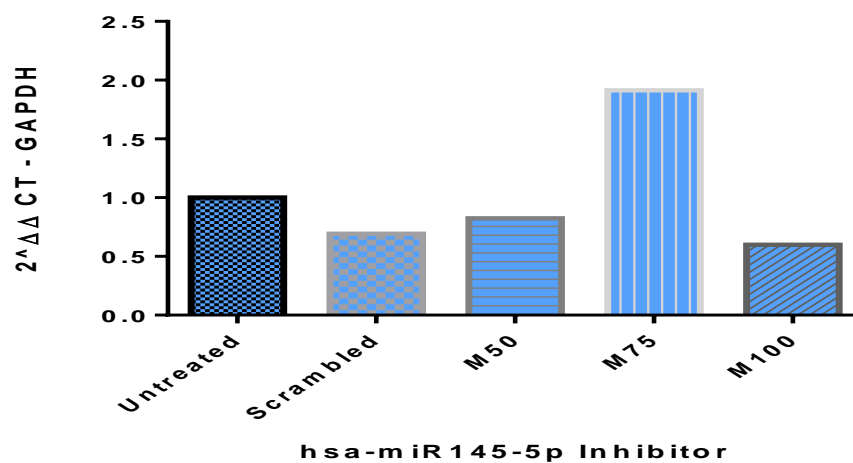
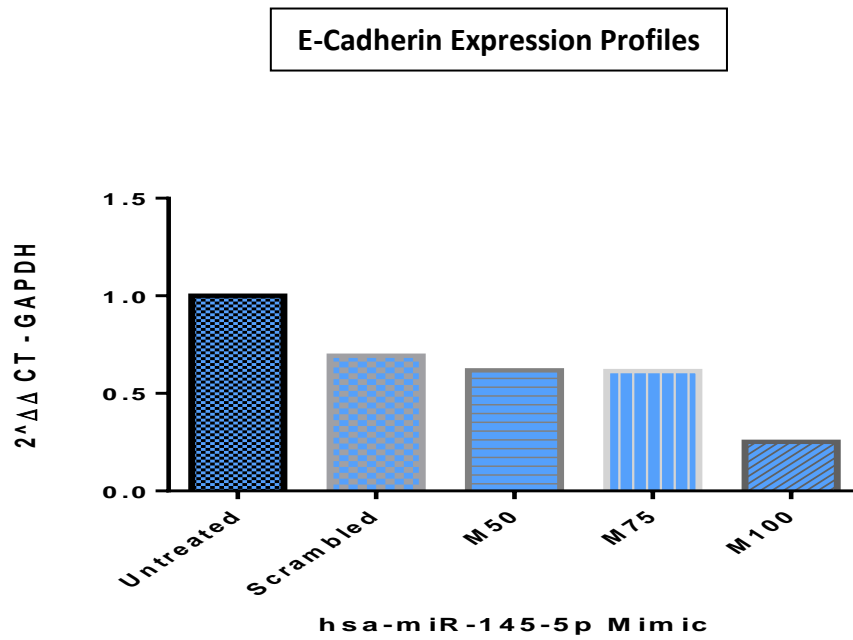


**Figure 5.11: E-Cadherin Expression Profiles in the Presence of Synthesised Mimics and Inhibitors for miR-145-5p.** q-PCR shows no obvious regulation of E-Cadherin gene expression in the presence of synthesised mimics and inhibitors for hsa-miR-145-5p. Untreated; human TM donor cells without TGF- $\beta$ 2 stimulation. Scrambled; TGF- $\beta$ 2 treated human TM donor cells transfected with scrambled negative control. I50-I100; Concentrations of synthesised inhibitor, 50nM to 100nM. (n=2).

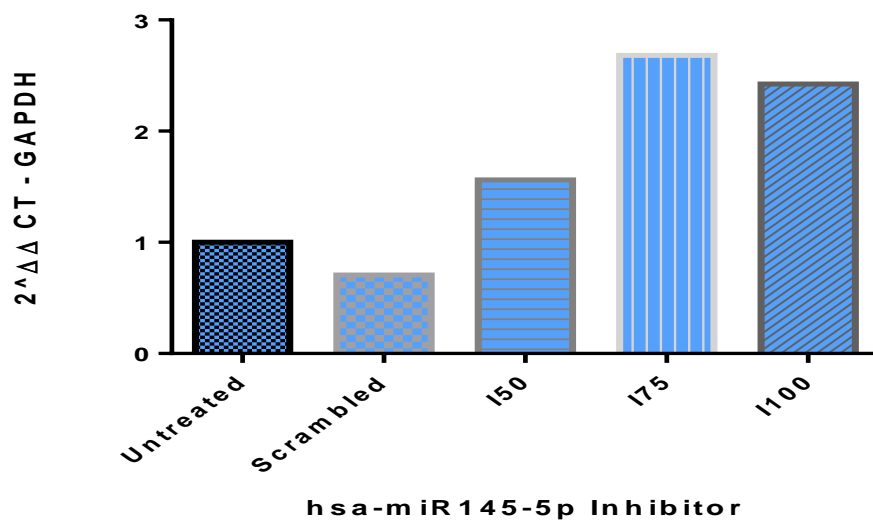
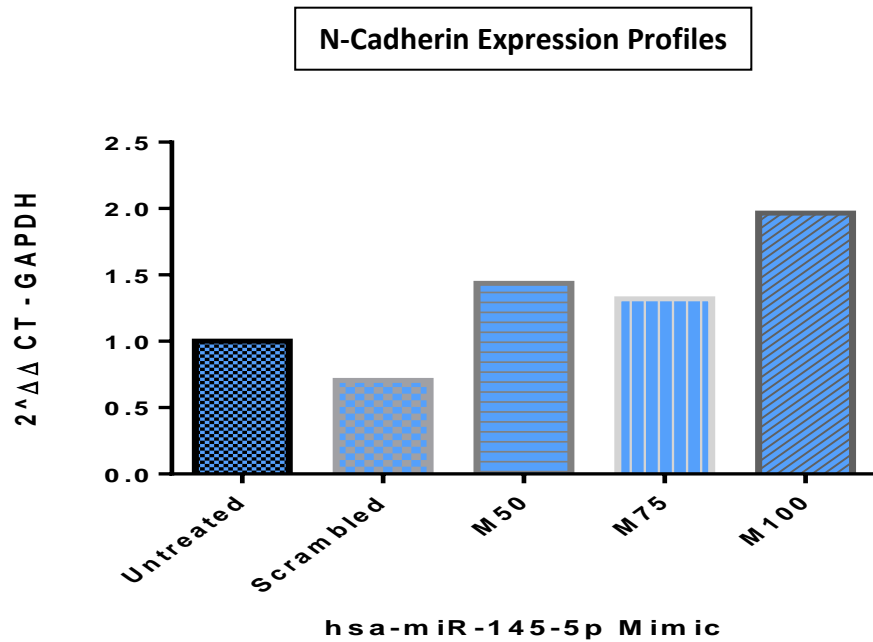


**Figure 5.12: N-cadherin Expression Profiles in the Presence of Synthesised Mimics and Inhibitors for miR-145-5p and miR-143-3p.** q-PCR shows no obvious regulation of N-cadherin gene expression in the presence of synthesised mimics or inhibitors for hsa-miR-145-5p. Untreated; human TM donor cells without TGF-β2 stimulation. Scrambled; TGF-β2 treated human TM donor cells transfected with scrambled negative control. I50-I100; Concentrations of synthesised inhibitor, 50nM to 100nM. (n=2).

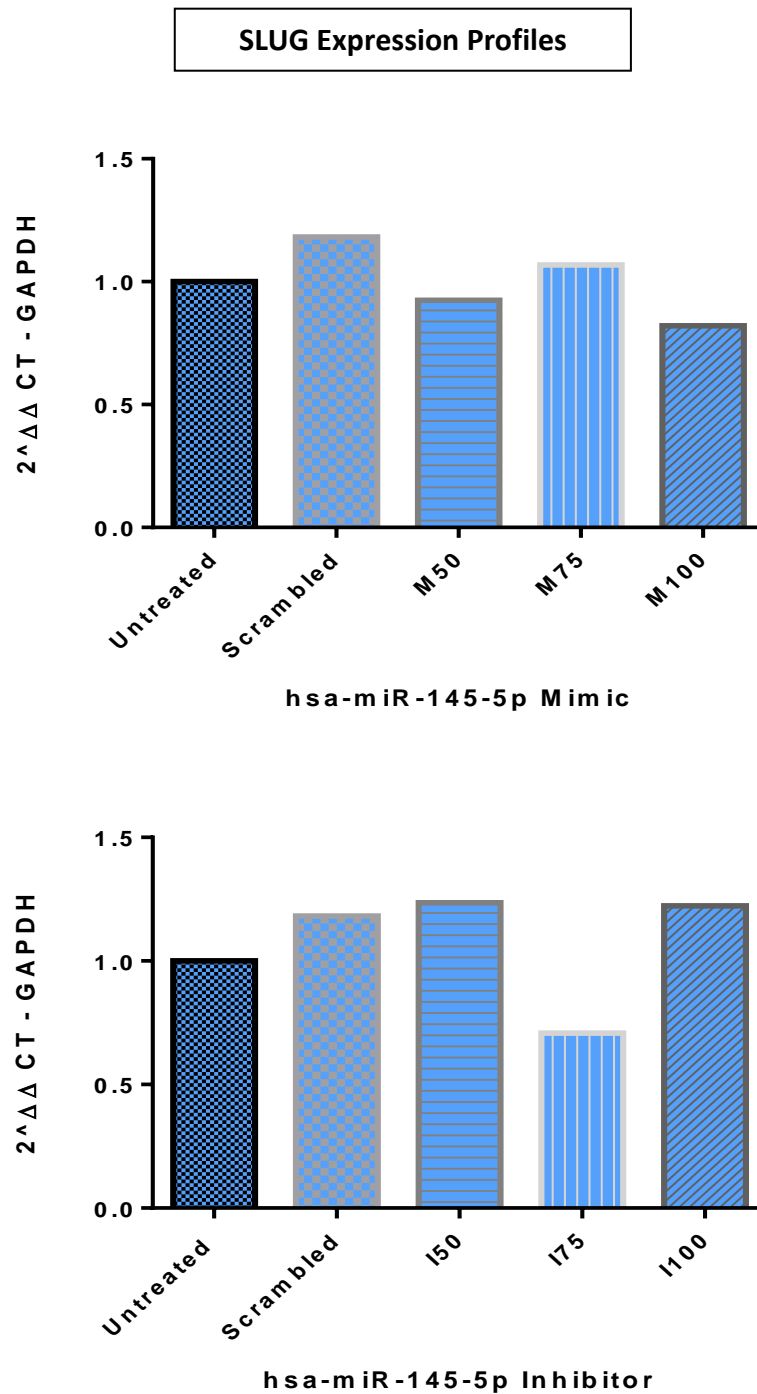


**Figure 5.13: SLUG Expression Profiles in the Presence of Synthesised Mimics and Inhibitors for miR-145-5p.** q-PCR shows no obvious regulation of SLUG gene expression in the presence of synthesised mimics or inhibitors for hsa-miR-145-5p. Untreated; human TM donor cells without TGF-β2 stimulation. Scrambled; TGF-β2 treated human TM donor cells transfected with scrambled negative control. I50-I100; Concentrations of synthesised inhibitor, 50nM to 100nM. (n=2).

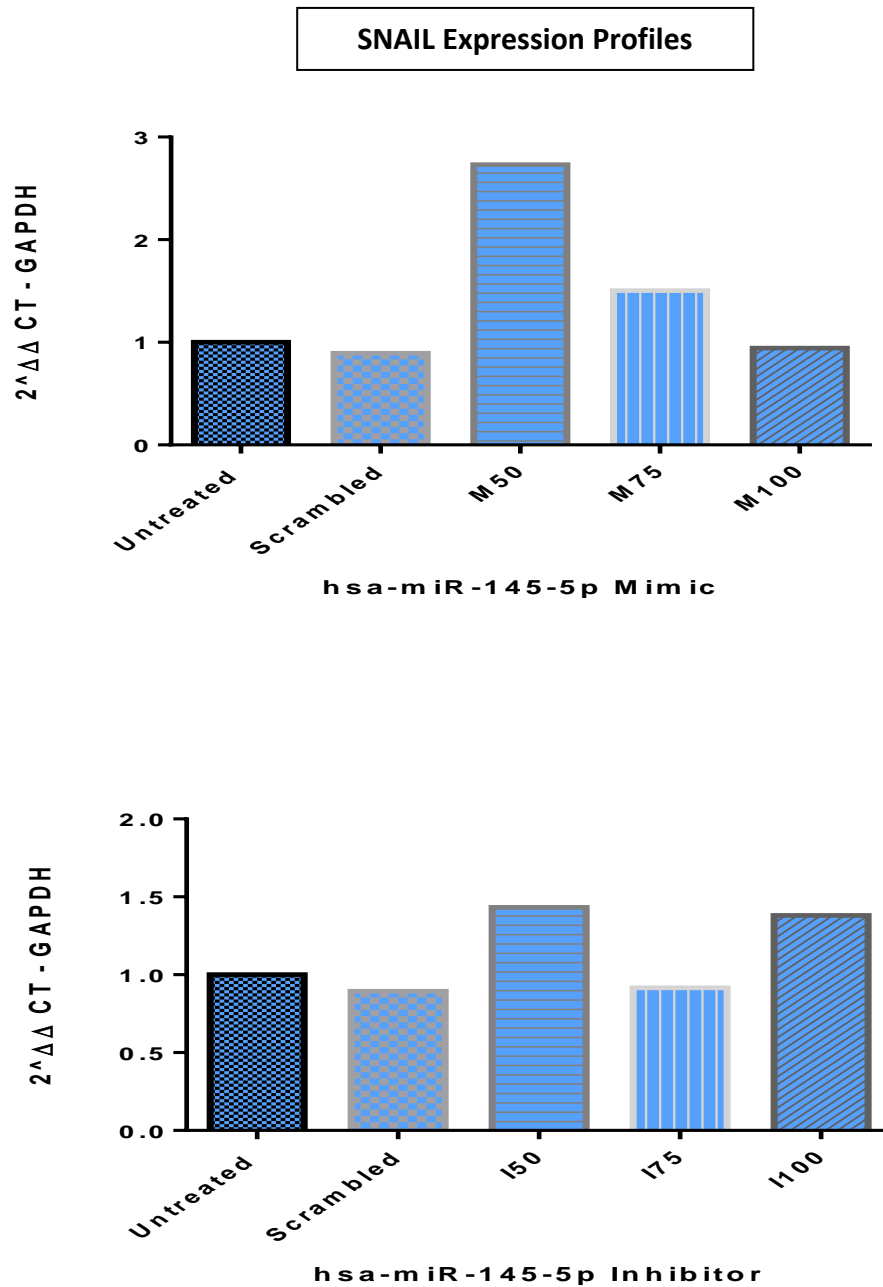


**Figure 5.14: SNAIL Expression Profiles in the Presence of Synthesised Mimics and Inhibitors for miR-145-5p and miR-143-3p.** q-PCR shows no obvious regulation of SNAIL gene expression in the presence of synthesised inhibitors for either hsa-miR-145-5p however there is a trend of down-regulation of gene expression in the presence of hsa-miR-145-5p mimic. Untreated; human TM donor cells without TGF- $\beta$ 2 stimulation. Scrambled; TGF- $\beta$ 2 treated human TM donor cells transfected with scrambled negative control. I50-I100; Concentrations of synthesised inhibitor, 50nM to 100nM. (n=2).

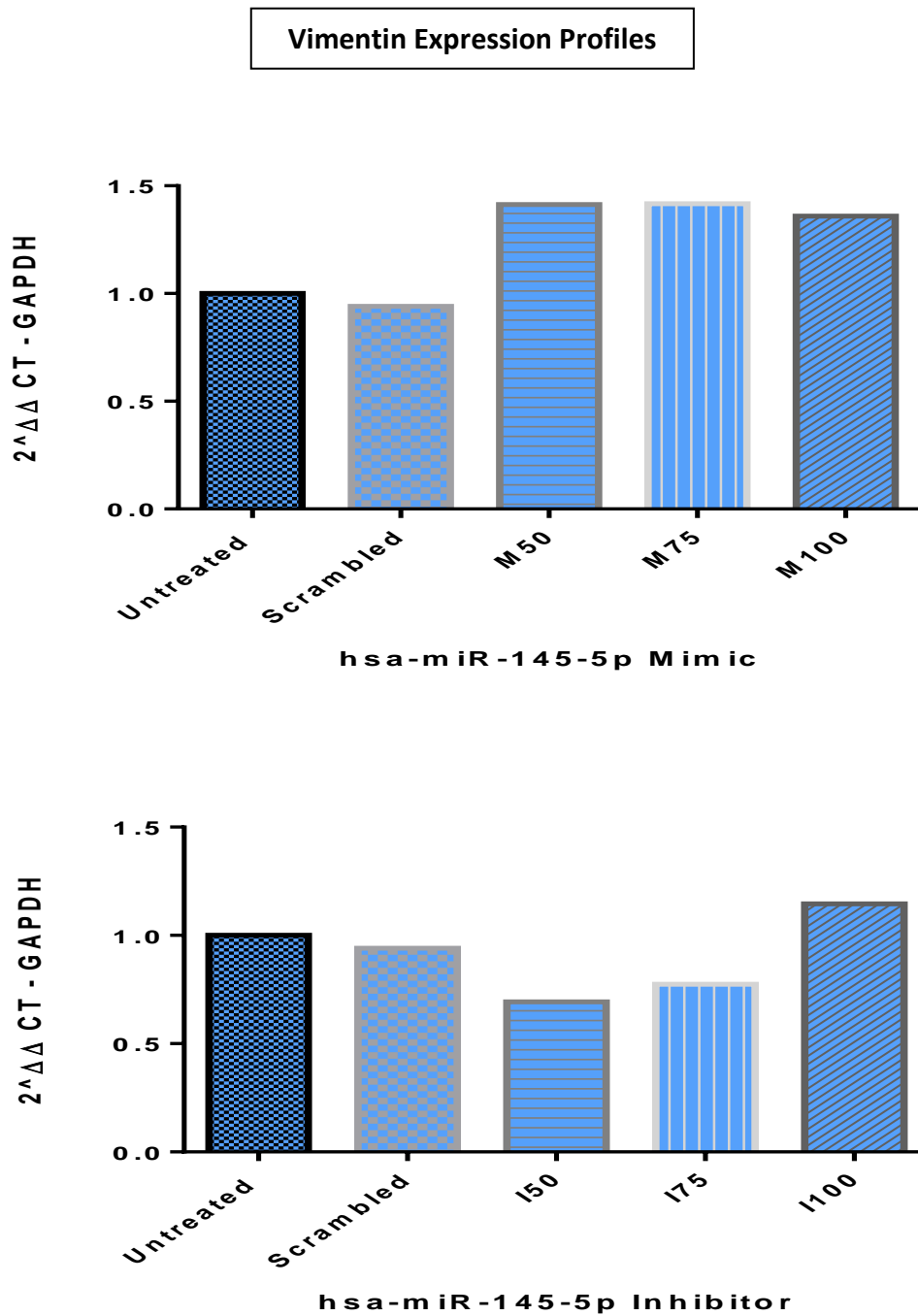


**Figure 5.15: Vimentin Expression Profiles in the Presence of Synthesised Mimics and Inhibitors for miR-145-5p.** q-PCR shows no obvious regulation of vimentin gene expression in the presence of synthesised hsa-miR-145-5p mimic, and up-regulation of gene expression in the presence of hsa-miR-145-5p inhibitor. Untreated; human TM donor cells without TGF- $\beta$ 2 stimulation. Scrambled; TGF- $\beta$ 2 treated human TM donor cells transfected with scrambled negative control. I50-I100; Concentrations of synthesised inhibitor, 50nM to 100nM. (n=2).

#### 5.4.4 RNA-Seq Analysis of hsa-miR-145-5p and hsa-miR-143-3p Inhibitor Target Expression Profiles

mRNA-Seq of human TM cells co-transfected with miR-143 and miR-145 inhibitors in addition to TGF- $\beta$ 2 treatment was performed to identify putative mRNA targets for miR-143-3p and miR-145-5p in human TM cells in the presence of TGF- $\beta$ 2.

##### 5.4.4.1 mRNA-Seq Summary

mRNA libraries were produced to include the four sample groups, (TC\_Group, SNC\_Group, 143i\_Group, and 145i\_Group) using TrueSeq Stranded mRNA Library Prep and sequenced on a flow cell using NextSeq500, High Output sequencing kit to obtain between 22-32 million reads per sample. Library quantification was achieved using the KAPA Library Quantification kit for Illumina Platforms. The majority of runs had a Q score greater than 30 (1 base call in 1000 is predicted to be incorrect).

Sample Name	Total Readcount	Aligned	Unaligned	Unique	Non-Unique
TC_Group 1	26257923	27415156	1031217	23861788	1364918
TC_Group 2	28747199	30041559	1094412	26152220	1500567
TC_Group 3	27965304	29173068	1090187	25450977	1424140
SNC_Group 1	26045301	27448597	956619	23601077	1487605
SNC_Group 2	26783023	28128363	1131127	24092400	1559496
SNC_Group 3	26914107	28128802	1057954	24419986	1436167
143i_Group 1	28176784	29633954	1084492	25460369	1631923
143i_Group 2	26158969	27394637	1142051	23507945	1508973
143i_Group 3	24479616	25500634	1039169	22143908	1296539
145i_Group 1	27996179	29481077	1008993	25382838	1604348
145i_Group 2	27603982	28854358	1057198	25072821	1473963
145i_Group 3	25474624	26723828	1007477	23029942	1437205
143i/145i_Group 1	26731699	27805408	1136038	24216487	1379174
143i/145i_Group 2	26568459	27864475	1041491	24018138	1508830
143i/145i_Group 3	28751348	30034351	1165728	26019018	1566602

**Table 5.9: Summary of Mapping Reads For Each Sample.** Reads for each sample across all five groups (TC\_Group, SNC\_Group, 143i\_Group, 145i\_Group, and 143i/145i\_Group), were extracted based on their unique I.Ds. In total 22-32 million reads per sample were obtained. Based on alignment to the reference genome, *H.sapiens*, hg19/GRC37, UCSC Genome Browser, the number of identified genes per sample was calculated.

#### 5.4.4.2 Principal Component Analysis

PCA reduces the dimension of a large data set and allows biological differences between samples to be observed in the primary components of the variation of the data. Figure 5.16 shows a PCA plot of the raw counts data. While the effect of TGF- $\beta$ 2 treatment is segregated, the effect of the miRNA inhibitors are not clearly resolved. This could be a result of mixed cell populations and low transfection efficiencies. There is some association of samples from the same donor eye. Different treatments are represented by different colours on the plot as shown by the key. Donors are shown as spheres of the same size.

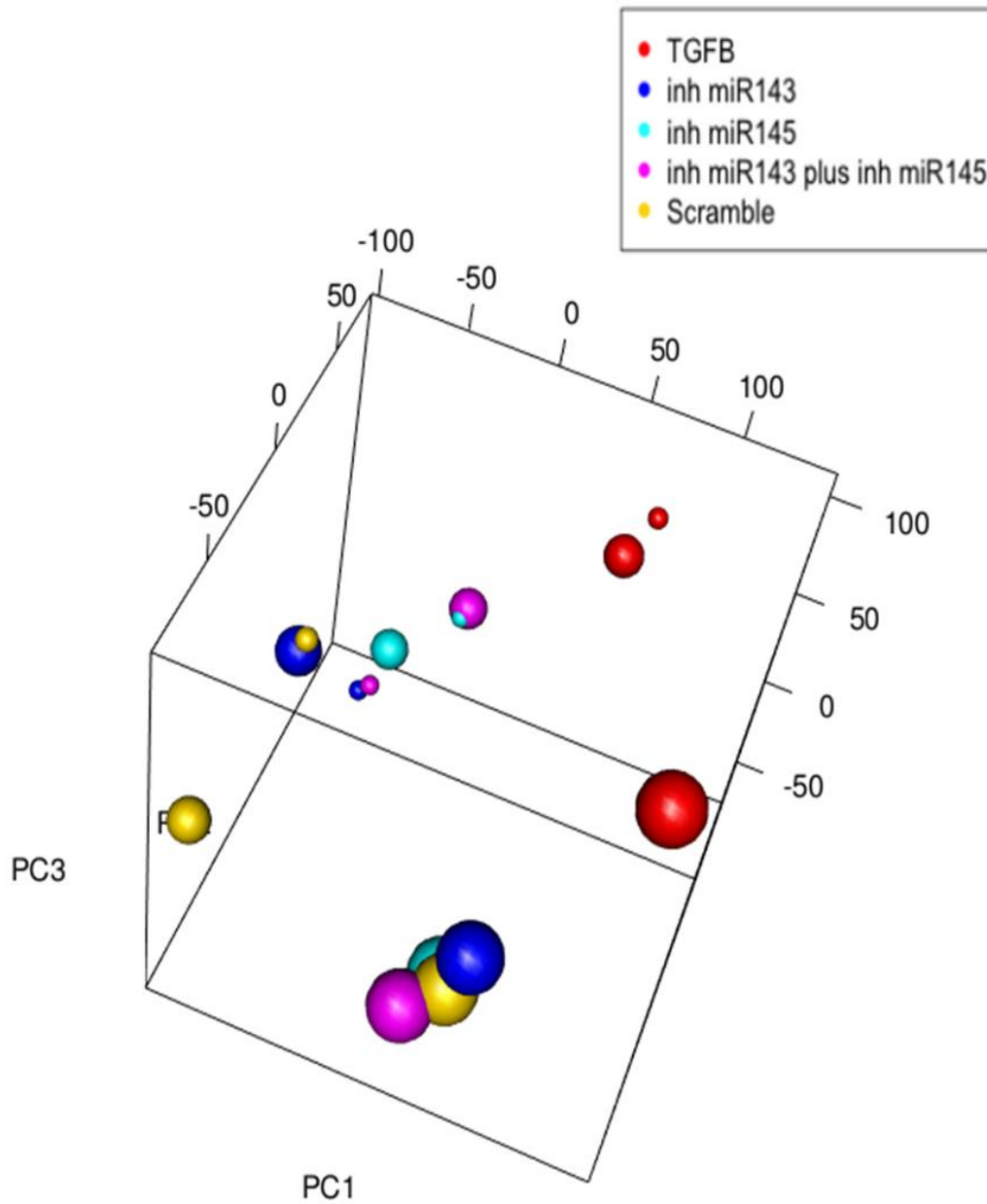


**Figure 5.16: Principal Component Analysis Across All Sample Groups.** TGF- $\beta$ 2 treatments tend to segregate however little segregation is observed between individual inhibitor and scrambled control treatment groups.

## 5.4.5 Functional Analysis of Genes Associated With miR-143 and miR-145 Inhibition Following TGF- $\beta$ 2 Treatment

### 5.4.5.1 Differentially Expressed Genes in Human Trabecular Meshwork Cells Post miR-143/miR145 Inhibition Following TGF- $\beta$ 2 Treatment

The top 500 differentially expressed genes were ranked by FDR, available in Appendix (8.6). From this list we isolated the top 50 DEGs based on FDR and ranked them according to Log fold change (LogFC). LogFC for the top up- and down-regulated genes was obtained from mRNA-Seq data analysed using Partek Flow (6.017) software. For this experiment differentially expressed genes have been divided between two sample groups and details are outlined in tables below. Differential gene expression was calculated using the control TGF- $\beta$ 2 only group (TC\_Group) and the miR inhibitor groups (143i\_group and 145i\_Group).

The 50 most significantly up-regulated genes and down-regulated in human TM cells treated with TGF- $\beta$ 2 and transfected with miR-143 inhibitor (143i) are shown in Table 5.10 and 5.11 respectively. Similarly, the 50 most significantly up-regulated genes and down-regulated genes in human TM cells treated with TGF- $\beta$ 2 and transfected with miR-145 inhibitor (145i) are shown in Table 5.12 and 5.13 respectively. These genes were filtered by their FDR then subsequently by logFC. Targets of miRNA inhibitors that are directly affected usually have increased expression profiles while the converse is true of indirectly affected genes.

Gene Name	LogFC	p-value
<i>Up-Regulated Genes</i>		
TPPP3	4.94	1.09E-08
FAM111B	4.73	4.81E-09
NFATC2	4.38	4.95E-15
PKMYT1	4.34	1.78E-09
PTHLH	4.24	1.38E-13
FOSB	4.13	1.34E-15
RRM2	4.06	1.01E-11
RRAD	4.02	3.31E-19
DTL	3.97	1.27E-08
CLSPN	3.87	1.46E-07
MKI67	3.79	6.91E-12
TOP2A	3.64	1.12E-10
WDR76	3.09	1.8E-07
E2F1	2.73	3.70E-09
TNFAIP3	2.56	8.14E-13
ANLN	2.54	3.30E-08
MCM5	2.51	4.27E-12
TCF19	2.47	5.69E-11
HMGA2	2.39	1.32E-14
HAS2	2.38	4.63E-08
PRC1	2.38	1.01E-07
CHAF1A	2.36	2.84E-08
MCM2	2.17	7.49E-09
RGMB	1.99	3.38E-20
TRIB1	1.88	5.55E-09
FOSL1	1.84	2.86E-08
NET1	1.81	1.11E-08
SRGAP1	1.78	4.11E-13
MCM4	1.60	3.44E-09
CD44	1.59	7.50E-15
PNP	1.58	1.29E-10
AKAP12	1.48	1.44E-08
ARHGAP22	1.36	7.06E-13
CDK6	1.34	5.25E-09
EFHD2	1.31	3.17E-11
TSPAN5	1.17	3.36E-12
FLNC	1.14	1.26E-08
RALA	1.09	3.61E-08
DCBLD2	1.08	4.61E-08
UGCG	1.06	7.49E-08
PIK3CD	1.03	3.92E-09
WNT5A	1.01	1.74E-09

FHOD1	1.00	1.84E-08
S100A10	0.99	1.18E-13
POU2F2	0.98	2.93E-09
FRMD6	0.98	6.61E-13
LMNA	0.91	2.69E-08
ZFP36L1	0.72	8.48E-08
TUBA1C	0.60	3.50E-09
VIM	0.56	1.14E-08

**Table 5.10: Top 50 Uniquely Up-Regulated Genes in Human TGF- $\beta$ 2 Treated Cells Exposed to miR143 Inhibitor (143i). LogFC= Log fold change.**

Gene Name	LogFC	p-value
<i>Down-Regulated Genes</i>		
GAL3ST3	-4.02	6.67E-12
LEFTY2	-3.64	8.13E-09
TMEM119	-2.74	2.56E-09
NXPH3	-2.64	1.72E-20
PKP2	-2.42	9.86E-19
SLC7A14	-2.31	2.44E-11
THBD	-2.22	3.54E-09
CLIC3	-2.12	6.03E-09
PPFIBP2	-2.08	6.98E-12
SLC6A6	-2.07	3.60E-28
FRY	-2.06	1.52E-10
PPM1H	-2.06	2.05E-12
SYNPO2	-2.02	2.67E-12
ARL4D	-1.99	2.70E-10
PTGIS	-1.94	1.54E-13
GPC4	-1.90	8.73E-14
SGK223	-1.87	6.91E-17
DAPK1	-1.76	2.42E-12
PCDH7	-1.76	1.06E-09
COL4A4	-1.76	3.06E-10
OPN3	-1.74	5.29E-14
COL8A1	-1.62	7.52E-12
SLC22A23	-1.58	7.48E-09
C10orf54	-1.53	2.46E-10
CLDN11	-1.49	1.06E-09
SORT1	-1.48	4.39E-10
FILIP1L	-1.45	7.39E-10
AMACR	-1.43	8.02E-09
SVEP1	-1.42	5.10E-15
PRSS12	-1.42	7.59E-18
C1orf198	-1.42	7.46E-15
SERAC1	-1.40	5.88E-09
IQCJ-SCHIP1	-1.39	9.55E-10
PPAP2A	-1.37	4.46E-16
KIAA0355	-1.36	7.15E-10
ACTA2-AS1	-1.36	4.03E-09
MEGF6	-1.29	1.54E-11
SNX30	-1.29	1.12E-10
SESN3	-1.27	2.20E-14
ATXN1	-1.21	1.76E-10
RUSC2	-1.14	1.40E-14

C2CD3	-1.05	5.91E-09
ARMC9	-1.04	8.78E-10
CTIF	-1.01	2.65E-10
OSBPL9	-0.91	1.91E-09
NEO1	-0.78	3.45E-09
KIAA1462	-0.74	1.59E-09
DAB2	-0.73	7.93E-09
WNK1	-0.71	5.25E-09
LTBP1	-0.61	9.62E-09

**Table 5.11: Top 50 Uniquely Down-Regulated Genes in Human TGF- $\beta$ 2 Treated Cells Exposed to miR143 Inhibitor. LogFC= Log fold change.**

Gene Name	LogFC	p-value
<i>Up-Regulated Genes</i>		
TPPP3	5.17	5.56E-10
MCM10	4.96	6.16E-08
FAM111B	4.81	2.14E-09
FOSB	4.41	4.1E-18
PKMYT1	4.40	8.82E-10
NFATC2	4.39	4.37E-15
RRAD	4.39	1.39E-24
PTHLH	4.37	3.91E-14
RRM2	4.22	1.31E-12
DTL	4.06	5.45E-09
CLSPN	4.02	3.10E-08
MYBL2	4.01	5.86E-08
MKI67	3.97	4.45E-13
WDR76	3.23	3.16E-08
KIFC1	3.12	8.75E-08
E2F1	2.73	4.71E-09
MCM5	2.64	2.31E-13
ANLN	2.58	2.27E-08
TNFAIP3	2.55	1.12E-12
HAS2	2.51	7.46E-09
CHAF1A	2.46	5.32E-09
LRRC8C	2.43	3.81E-09
MCM2	2.33	3.68E-10
HMGA2	2.31	4.04E-13
DDX60L	2.19	2.60E-09
UHRF1	2.18	6.47E-09
SRGAP1	2.11	1.36E-18
MCM7	2.07	7.58E-08
TRIB1	1.97	9.42E-10
RGMB	1.97	1.11E-19
SIK1	1.88	9.90E-09
FOSL1	1.80	6.12E-08
MCM4	1.72	1.79E-10
CD44	1.50	2.06E-13
MCM3	1.48	6.25E-08
AKAP12	1.48	1.55E-08
EGR1	1.45	3.84E-08
CDK6	1.42	5.60E-10
MYO10	1.28	1.77E-08
CRIP2	1.23	5.90E-08
ARHGAP22	1.20	3.47E-10

UGCG	1.19	8.15E-10
S100A10	1.17	2.26E-18
FLNC	1.11	3.17E-08
FRMD6	1.11	3.2E-16
POLR2B	1.07	2.73E-08
FHOD1	0.97	6.41E-08
ZFP36L1	0.76	1.67E-08
SERPINE1	0.69	2.67E-08
PLEC	0.67	3.47E-08

**Table 5.12: Top 50 Uniquely Up-Regulated Genes in Human TGF- $\beta$ 2 Treated Cells Exposed to miR145 Inhibitor (145i). LogFC= Log fold change.**

Gene Name	LogFC	p-value
<i>Down-Regulated Genes</i>		
GAL3ST3	-4.42	2.23E-12
NXPH3	-2.94	1.73E-22
PALMD	-2.93	6.23E-10
MYH11	-2.67	4.09E-16
COL11A1	-2.65	8.49E-14
THBD	-2.54	1.68E-10
PKP2	-2.53	2.15E-19
PTGIS	-2.42	1.85E-17
PPFIBP2	-2.36	1.73E-13
CLIC3	-2.35	6.47E-10
GPC4	-2.27	8.59E-17
PPM1H	-2.26	1.26E-13
COL4A4	-2.18	5.25E-13
SLC7A14	-2.12	3.66E-10
SLC6A6	-2.06	1.03E-27
SYNPO2	-2.03	2.82E-12
CDKN2B	-2.03	5.59E-09
SLC22A23	-2.00	1.39E-12
C10orf54	-2.01	2.04E-14
DAPK1	-1.95	9.41E-14
SGK223	-1.89	5.98E-17
FRY	-1.83	3.93E-09
CLDN11	-1.81	1.84E-12
COL8A1	-1.81	3.35E-14
PIK3IP1	-1.81	2.89E-09
ARL4D	-1.79	4.78E-09
FILIP1L	-1.73	2.84E-12
OPN3	-1.73	1.21E-13
PPAP2A	-1.58	1.73E-19
SORT1	-1.55	6.57E-11
ACTA2	-1.54	3.42E-10
SESN3	-1.54	1.3E-18
AMACR	-1.53	1.63E-09
SVEP1	-1.52	1.13E-16
PRSS12	-1.48	3.11E-19
ACTA2-AS1	-1.48	4.07E-10
C1orf198	-1.42	8.3E-15
SLC25A4	-1.39	2.67E-09
ANKH	-1.37	5.27E-10
PDE5A	-1.33	2.88E-09
SNX30	-1.23	6.56E-10
MEGF6	-1.22	1.56E-10
RUSC2	-1.18	2.1E-15

ARMC9	-1.01	2.95E-09
SNX25	-0.97	7.70E-10
CTIF	-0.96	1.60E-09
TINAGL1	-0.93	3.53E-09
NEO1	-0.82	6.39E-10
WNK1	-0.77	4.06E-10
KIAA1462	-0.75	1.17E-09

**Table 5.13: Top 50 Uniquely Down-Regulated Genes in Human TGF- $\beta$ 2 Treated Cells Exposed to miR145 Inhibitor. LogFC= Log fold change.**

The scrambled negative control group (SNC\_Group) was used to identify genes that were differentially expressed independently of transfection effects. Figure 5.17, Venn diagram below illustrates the overlap in DEGs between miRNA inhibitor groups 143i\_Group, 145i\_Group, and the scrambled control group SNC\_Group. While many genes were differentially expressed by the scrambled control and the two individual inhibitors, there are uniquely expressed genes by inhibitor treatments.

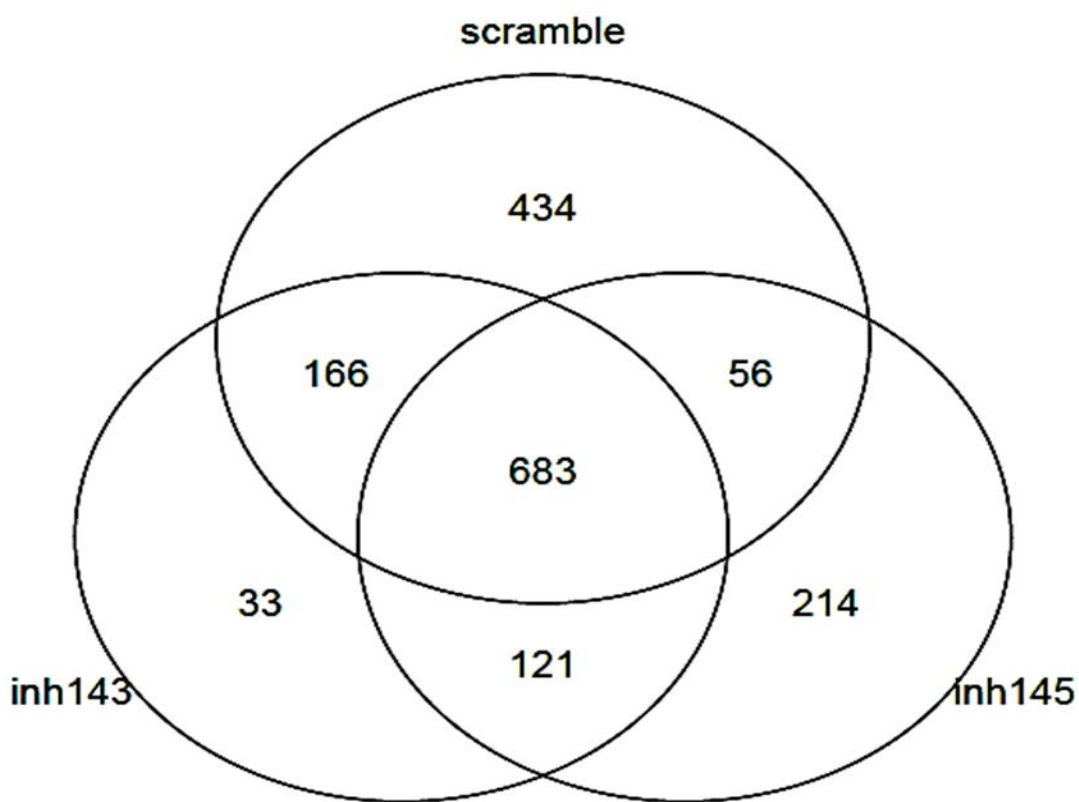


**Figure 5.17: Venn Diagram of Overlap of Differentially Expressed Genes Between Scrambled Negative Control, 143i, or 145i Transfected TM Cells Treated with TGF- $\beta$ 2.** There is an overlap of differentially expressed cells between the SNC\_Group and 143i- or 145i\_Group. However, there are unique DEGs for both the 143i\_Group and 145i\_Group that are independent to the scrambled control. The unique genes for 143i and 145i and both 143i/145i are given in Table 8.4 (Appendix).

Uniquely expressed genes in 143i\_Group and 145i\_Group outlined in Table 5.14 and Table 5.15, were filtered on FDR and subsequently on LogFC investigated for validated targets that have been confirmed experimentally using two validated miRNA target interaction web-interfaces: miRTarBase (v8) and the Validated Target Module of miRWalk 2.0. Sixteen experimentally validated targets were identified as regulated by miR-145-5p and miR-143-3p (Table 5.16).

Gene	LogFC
<b>Up-Regulated Genes</b>	
PBK	3.665
CCNE2	3.62
RRM2P3	3.58
ESCO2	3.50
PLK4	3.49
DEPDC1	3.44
KIF15	3.41
KIAA0101	3.37
BLM	3.28
KIF14	3.18
KIF2C	3.15
RAD54L	3.14
DLGAP5	3.02
RAD51AP1	2.92
HMMR	2.89
TTK	2.82
C11orf82	2.70
HELLS	2.56
RAD51	2.42
WDR62	2.42
LMNB1	2.39
FANCD2	2.38
GINS1	2.35
PSMC3IP	2.32
PPP1R14C	2.29
CCNA2	2.25
CDCA2	2.17
MAD2L1	2.13
CHAF1B	2.09
WNT7B	2.08
FANCA	2.06
CDC6	2.05
CDC25A	2.05
GINS4	2.01
RFC3	2.00
CENPE	1.99
FBXO5	1.97
PLK1	1.97
EZH2	1.93
RP11-424C20.2	1.91
RECQL4	1.88
GINS3	1.88

ZWINT	1.83
MELK	1.82
KIF20B	1.78
TIMELESS	1.69
RNASEH2A	1.66
FANCG	1.59
APCDD1L	1.57
NCAPG2	1.52
HMGB2	1.51

**Table 5.14: Top 50 Unique Up-Regulated Genes Identified in TGF- $\beta$ 2 Treated TM Cells Transfected with 143i and 145i by RNA-Seq.** Top 50 Unique up-regulated genes for 143i and 145i independent of the SNC\_Group were identified.

Gene	LogFC
<b>Down-Regulated Genes</b>	
EXTL1	-2.16
LYPD6	-2.01
LMOD1	-1.86
KCNE4	-1.84
MYOZ1	-1.79
ANK1	-1.72
VSTM2L	-1.65
WFDC1	-1.58
GLIS1	-1.48
PALM	-1.47
IL12A	-1.46
PIEZO2	-1.44
HSD17B6	-1.41
RP11-379K17.5	-1.31
SHOX	-1.30
PRELP	-1.25
PRUNE2	-1.24
DDR1	-1.24
ARSI	-1.21
ANGPT1	-1.20
FAM115B	-1.19
KLHL24	-1.19
DIO2	-1.18
FOXF2	-1.18
SLIT2	-1.17
SH3RF2	-1.09
ARNT2	-1.07
YPEL2	-1.06
CNN1	-1.01
KIF26B	-0.98
STON1	-0.98
LDLRAP1	-0.95
GTF2IP1	-0.95
YPEL3	-0.94
FAM198B	-0.94
LIMK1	-0.94
PDK2	-0.94
PPP1R3C	-0.93
AHR	-0.92
BDNF	-0.92
HDAC5	-0.92
TP53INP1	-0.91

TAPT1	-0.90
MSRB1	-0.90
COL4A5	-0.89
ACSS2	-0.87
CDKN2A	-0.87
CXCR5	-0.87
PRICKLE1	-0.87
PGPEP1	-0.85
CCDC107	-0.85

**Table 5.15: Top 50 Unique Down-Regulated Genes Identified in TGF- $\beta$ 2 Treated TM Cells Transfected with 143i and 145i by RNA-Seq.** Top 50 Unique down-regulated genes for 143i and 145i independent of the SNC\_Group were identified.

Gene	Gene Name	logFC	miRNA Target
LMNB1	Lamin B1	2.397	miR-145
PODXL	Podocalyxin-like	2.101	miR-145
ARHGAP11A	Rho GTPase Activating Protein 11A	1.092	miR-145
ZWILCH	Zwilch kinetochore protein	0.915	miR-143
SH2B3	SH2B adaptor protein 3	0.908	miR-145
ZEB1	Zinc finger e-box binding homeobox 1	0.779	miR-143/ miR-145
U2SURP	U2 SnRNP associated SURP domain containing	0.764	miR-145
CSE1L	Chromosome segregation 1-like	0.758	miR-145
ABCE1	ATP binding cassette subfamily E member 1	0.757	miR-145
EPT1	Selanoprotein 1	0.704	miR-145
HSPH1	Heat shock protein family H Member1	0.67	miR-143
JMJD1C	Jumonji domain containing protein	0.663	miR-145
BCCIP	BRCA1 and CDKN1A interacting protein	0.643	miR-143
TUBA1B	Tubulin alpha 1B	0.442	miR-143
SRSF1	Serine and arginine rich splicing factor 1	0.416	miR-145
MSN	Moesin	0.359	miR-143

**Table 5.16: Unique Differentially Expressed Genes Identified in TGF- $\beta$ 2-Treated TM Cells Transfected with 143i and 145i by RNA-Seq which are Validated miR-145 and miR-143 Targets.** Unique DEGs for 143i and 145i independent of the SNC\_Group were identified. Validated targets of both miR-145 and miR-143 were identified using miRTarbase (v8) and miRWalk 2.0 and cross-referenced against DEGs identified by RNA-Seq.

#### 5.4.5.2 Comparison Analysis of 143i and 145i in Human TM Cells +/- TGF- $\beta$ 2

A comparison analysis was performed on IPA between 143i, 145i and SNC to determine the most significantly altered genes in the TGF- $\beta$  signalling pathway, in addition to significantly differentially expressed genes upstream of miR-145-5p and ZEB1. Only genes identified as independent of SNC were considered truly differentially expressed and not a product of transfection background. Figure 5.18 identifies evidence of TGF- $\beta$  signalling pathway alterations in response to 145i but not in response to 143i or as an effect of transfection protocol. Figure 5.19 is indicative of the complexity of miRNA:mRNA modulation. miR-145 expression is affected by 143i and scrambled negative control (SNC). Figure 5.20 shows the up-regulation of ZEB1 by 143i and 145i independently of SNC.

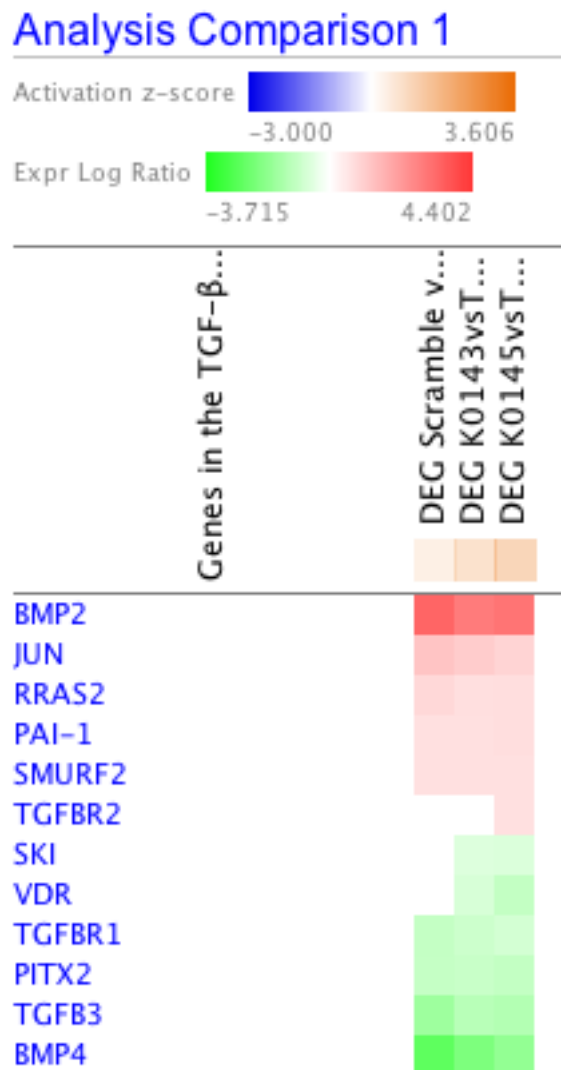


**Figure 5.18: Comparison Analysis of Canonical TGF-β Signalling Pathway Between 143i, 145i and SNC Transfected TGF-β2 Treated Human TM Cells.** TGF-β2 is significantly up-regulated in response to 145i but not 143i and SCN. Up-regulation following miRNA inhibitor transfections is indicative of a more direct effect of miRNA inhibitors. To identify true effects of 143i or 145i SNC column should have no colour change (white= unaffected), and 143i or 145i would be coloured according to up-regulation (red) or down-regulation (green).

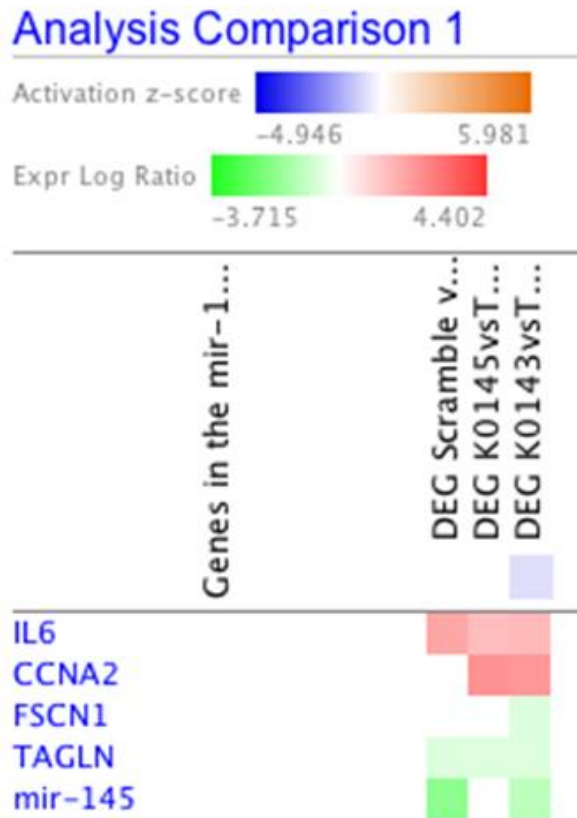


**Figure 5.19: Comparison Upstream Analysis of miR145 Between 143i, 145i and SNC Transfected TGF-β2 Treated Human TM Cells.** miRNA:mRNA modulations are complex networks which can have many off target effects. FSCN1 is down-regulated by 145i but not 143i or SNC. This is likely to be due to off target effects. CCNA2 (cyclin A2) is up-regulated by 143i and 145i. miR-145 is affected by 145i and SNC. This may indicate SNC is having undesirable off target effects which can directly and indirectly regulate genes. To identify true effects of 143i or 145i SNC column should have no colour change (white= unaffected), and 143i or 145i would be coloured according to up-regulation (red) or down-regulation (green).

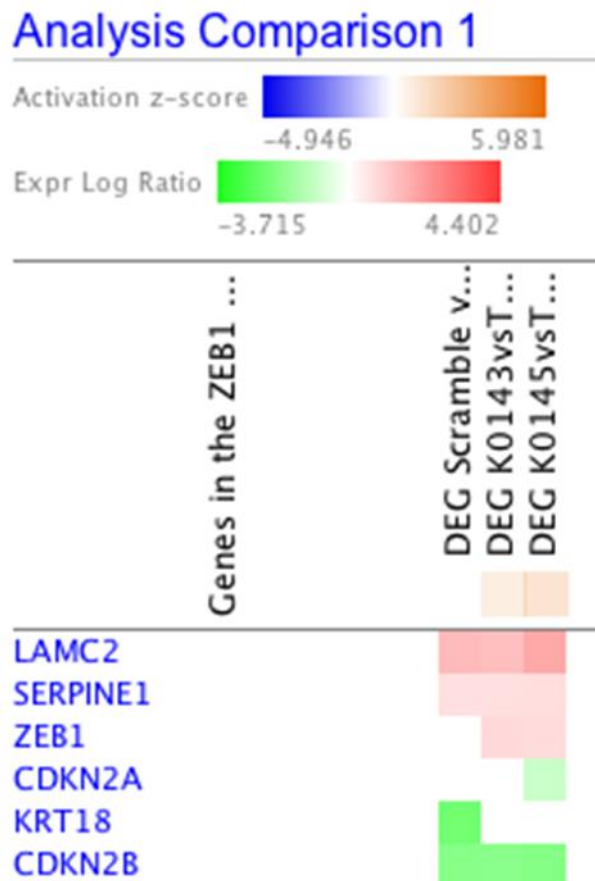
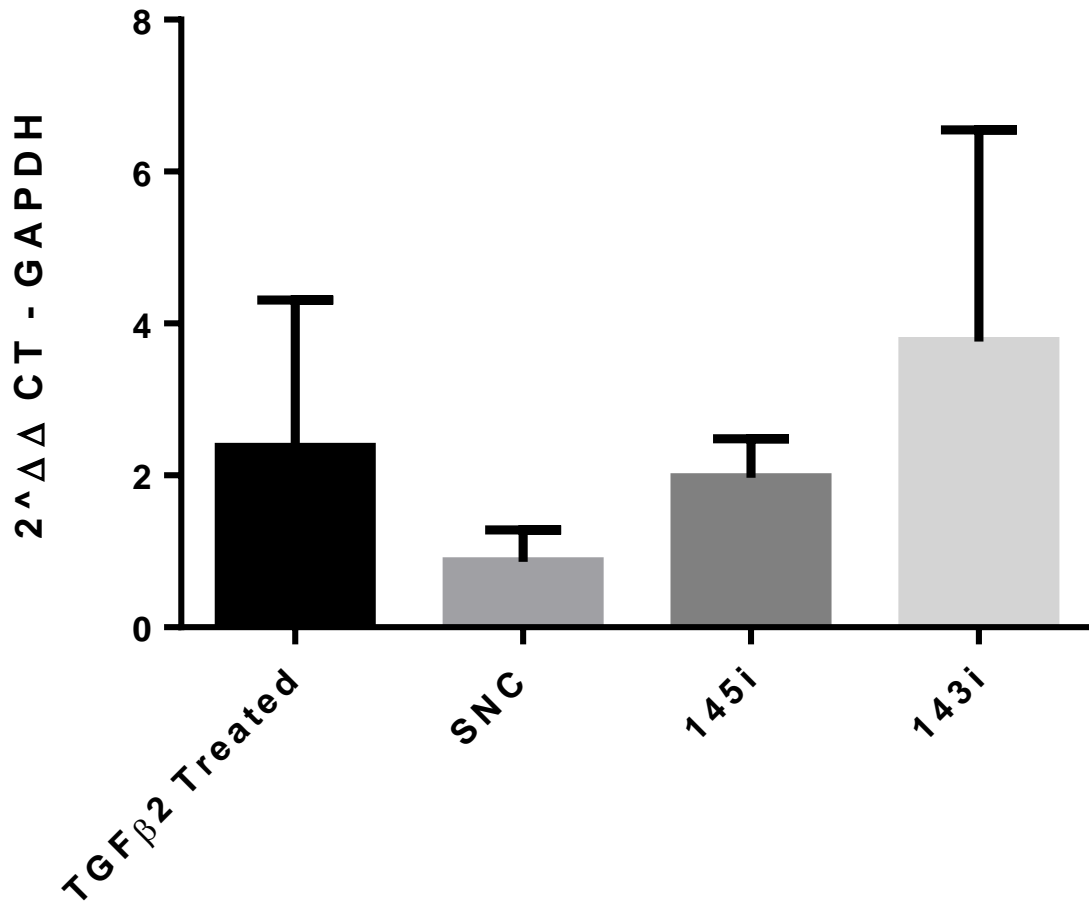


**Figure 5.20: Comparison Upstream Analysis of ZEB1 Between 143i, 145i and SNC Transfected TGF- $\beta$ 2 Treated Treated Human TM Cells.** EMT-like phenomena have been described in TM cells and miR143/145 are thought to regulate EMT. ZEB1 expression is increased by 143i and 145i but not SNC1 indicating undesirable effects of miR-145 and miR-143 transfection. To identify true effects of 143i or 145i SNC column should have no colour change (white= unaffected), and 143i or 145i would be coloured according to up-regulation (red) or down-regulation (green).

#### 5.4.5.3 Validation of hsa-miR-145-5p and hsa-miR-143-3p Inhibitor Effects of ACTA2 at mRNA Level

Human TM cells were transiently transfected with human miRNA inhibitors against hsa-miR-145-5p (145i) and hsa-miR-143-3p (143i) or a scrambled negative control (SNC). 143i did not diminish ACTA2 gene expression when compared to TGF- $\beta$ 2 treated control TM cells. Both 145i and the SNC appeared to diminish ACTA2 expression at the mRNA level when compared to the treated control. A Oneway ANOVA and Dunn's multiple comparisons test was performed on GraphPad Prism and no significant difference was found between individual treatment groups and TGF- $\beta$ 2 control cells.



### ACTA2 Gene Expression Profile

**Figure 5.21: q-PCR Analysis of ACTA2 Gene Expression in Transfected TGF-β2 Human TM Cells.** Human TM cells were treated with TGF-β2 and transfected with 143i, 145i or scrambled negative control (SNC). 145i diminish ACTA2 expression at the mRNA level compared to TGF-β2 treated cells. SNC also diminished ACTA2 mRNA expression however, ACTA expression was enhanced by 143i.

#### 5.4.5.4 Validation of hsa-miR-145-5p and hsa-miR-143-3p Inhibitor Effects ACTA2 at Protein level

Human TM cells were transiently transfected with human miRNA inhibitors against hsa-miR-145-5p (145i) and hsa-miR-143-4p (143i) or a scrambled negative control (SNC). Total protein extracts from human TM cells were probed against an anti- $\alpha$ -SMA antibody. Both hsa-miR145-5p inhibitor and hsa-miR143-3p inhibitor alone diminished  $\alpha$ -SMA expression. Expression levels were compared to a TGF- $\beta$ 2 positive protein extract.

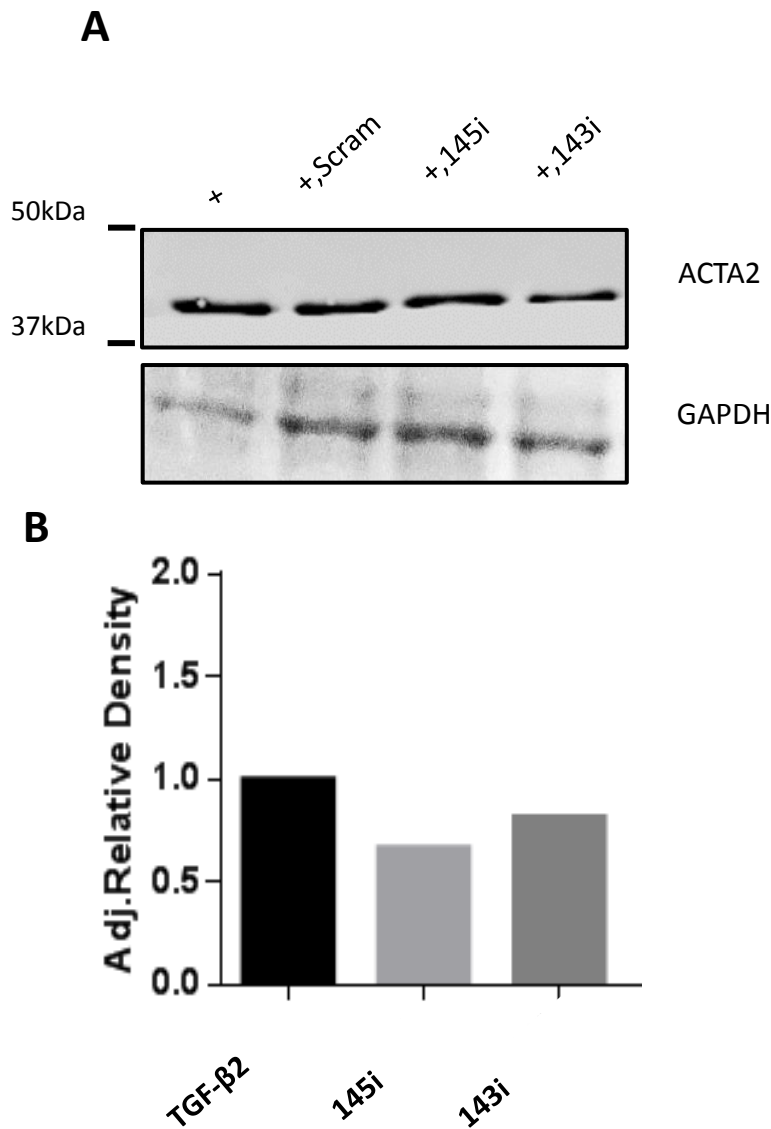


**Figure 5.22: ACTA2 Protein Expression Reduced in Presence of miRNA Inhibitors.**

(A) Human TM cells were stably transfected with synthetic miRNA inhibitors to hsa-miR-145-5p (145i) and hsa-miR143-3p (143i) or a scrambled negative control (SNC). Whole cell lysates for TGF- $\beta$  positive only cells (+), non-coding cells (+,Scram), and miR-145 inhibitor (+,145), miR-143 inhibitor (+,143). (B) Densitometric units of ACTA2 were determined using Fiji analysis software, relative to GAPDH and referred as a fold change of control, TGF- $\beta$ 2 cells.

## 5.5 Discussion

### Target miRNA Identification

TGF- $\beta$ 2 plays a central role in the pathophysiology of glaucoma in the TM affecting ECM dynamics, oxidative stress, cellular contractility, and senescence<sup>164,715</sup>. Patients with POAG have elevated levels of TGF- $\beta$ 2 in their AH and multiple *in vitro* and *in vivo* experiments have demonstrated that TGF- $\beta$ 2 plays a central role in the pathogenesis of glaucoma in the TM<sup>394,397</sup>. TGF- $\beta$ 2 dysregulates the expression of multiple genes involved in complex processes as was shown in Chapter 3. TGF- $\beta$ 2 can also influence and drive the expression of multiple miRNAs via SMAD proteins. TGF- $\beta$ 2 induced alterations in miRNA expression can provide an insight into the regulation of cellular function and dysregulated pathways in the TM in glaucoma, as well as, identifying miRNAs as potential therapeutic targets<sup>381</sup>.

In this study, global alterations in miRNA expression were investigated using a commercial microarray platform (Exiqon, Denmark) in human cultured TM cells treated with 5ng/mL TGF- $\beta$ 2 for 24 hours. Three miRNAs were significantly up-regulated following TGF- $\beta$ 2 treatment: miR-143-3p (FC= 0.957, *p*-value= 2.99E-2), miR-145-5p (FC= 0.605, *p*-value= 2.99E-2) and miR-4328 (FC=0.0665, *p*-value= 2.99E-2). In addition, using the same microarray platform glaucomatous TM cells had significantly elevated expression of miR-143-3p (FC= 1.074, *p*-value= 2.99E-2) and miR-4328 (FC= 1.028, *p*-value= 2.99E-2). Detection of miRNAs by q-PCR is technically demanding due to their small size and inherently low expression<sup>716</sup>: statistical significance could not be achieved by q-PCR analysis (Figure 5.5).

Previous literature on the physiology and targets of miR-4328 is limited. miR-4328 expression was identified in keloid scar formation<sup>717</sup>, bone formation<sup>718</sup>, mucinous cystadenocarcinoma<sup>719</sup> and steroid-induced hepatic steatosis<sup>720</sup>. Interestingly, in keloid scar formation miR-4328, miR-143-3p and miR-145-5p were significantly down-regulated<sup>721</sup>. Given the limited data regarding miR-4328 and significant literature base for miR-143-4p and miR-145-5p the subsequent experimental work focused on the latter miRNAs.

Both miR-143-3p and miR-145-5p form a bicistronic miRNA cluster 143/145 located on chr5q33 in humans (Figure 5.23)<sup>722</sup>; miR-143 is approximately 1.7kB from miR-145. It is proposed that the cluster is transcribed together but given these miRNA can have different independent cellular functions<sup>723</sup>, and cellular distributions<sup>722</sup> their regulation, targets and expression may not be inter-linked. Both miRNAs have a common promoter, but miR-145 also has a specific upstream regulatory element of approximately 1.5kB which might favour independent regulation<sup>724</sup>. The mechanism of this differential expression is not known<sup>724</sup>. TGF- $\beta$  strongly induces the expression of miR-143 and miR-145<sup>725</sup>. The majority of authors have focused on the role of the miRNA 143/145 cluster in cardiovascular disease<sup>726</sup> and cancer<sup>727</sup>.

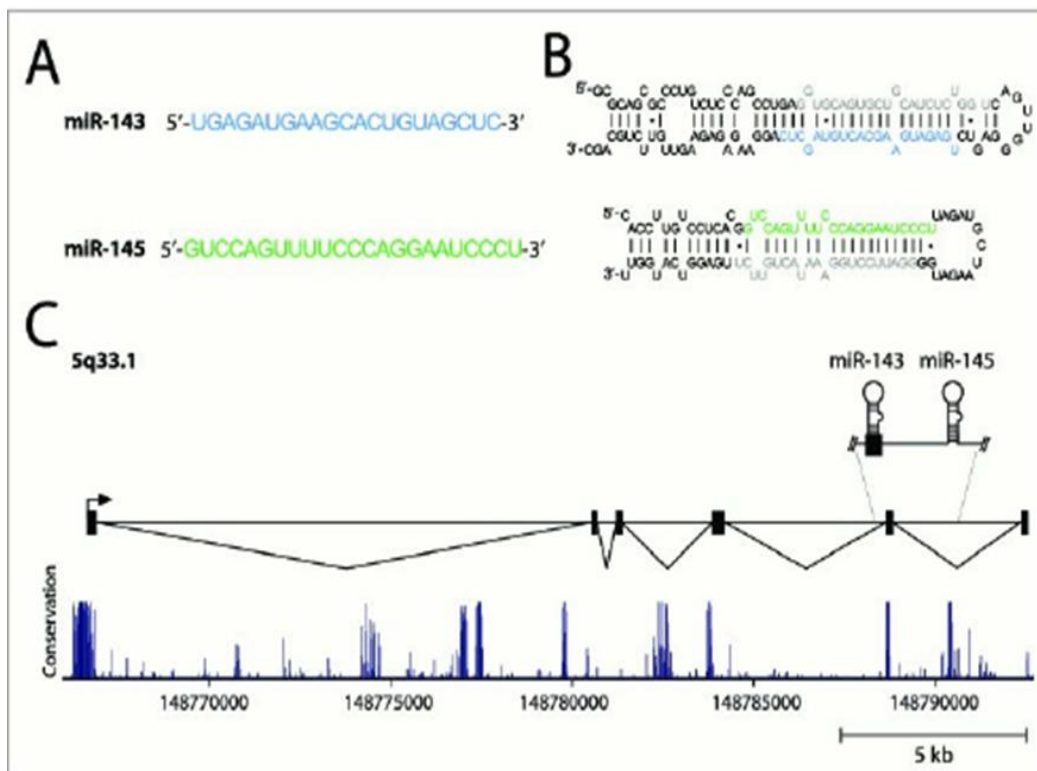


**Figure 5.23: The miR143/145 Cluster.** Modified from Kent *et al* 2014<sup>722</sup>. (A) Mature miRNA sequences of miR-143 and miR-145. (B) The secondary structures of pre-miR-143 and pre-miR145 stem loops. Mature miRNA sequences are blue (miR143) and green (miR-145). miRNA\* sequences are grey. (C) Genome organisation and major primary transcript structure of the miR-143/145 cluster.

Expression of miR-143 is highest in fibroblasts and smooth muscle cells but is also expressed in epithelial and endothelial cells. The expression of miR-145 is more restricted to mesenchymal cells (fibroblasts and smooth muscle cells). miR-143 and miR-145 are essential in the differentiation of vascular smooth muscle cells (VSMCs) during development<sup>725</sup> and their expression can induce the differentiation of neural crest stem cells into VSMCs; this effect is dependent on TGF- $\beta$  and is proposed to reflect an EMT-type process<sup>725</sup>. miR-145 alone is sufficient to differentiate stem cells into VSMCs<sup>725</sup>.

miR-143 and miR-145 are also molecular triggers of VSMC phenotypic switching<sup>728,729</sup>. VSMC retain phenotypic plasticity and can switch between a differentiated or contractile state and a de-differentiated or synthetic state (Figure 5.24)<sup>730</sup>. TGF- $\beta$  family members (TGF- $\beta$  and BMP4) promote the 'contractile phenotype' whereas PDGF stimulates the synthetic state (Figure 5.24)<sup>731</sup>. PDGF represses the expression of miR-143 and miR-145 (transcriptionally and post-transcriptionally) when VSMC de-differentiate into the synthetic state<sup>728</sup> whereas TGF- $\beta$  induces miRNA-143 and miR-145 expression and a contractile state<sup>730</sup>. Over-expression of miR-145 up-regulates the expression of VSMC differentiation markers which are the hallmark of a contractile phenotype: smooth muscle alpha actin ( $\alpha$ -SMA, ACTA2), calponin, and smooth muscle-myosin heavy chain<sup>728</sup> (SM-MHC).

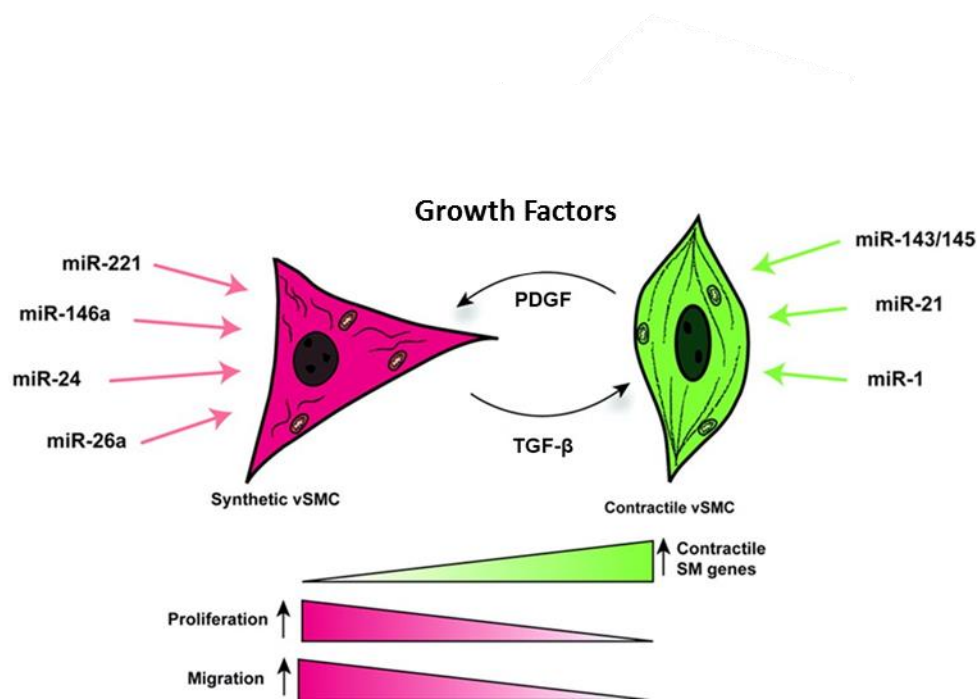


**Figure 5.24: Regulation of Vascular Smooth Muscle Cell Phenotype.** Modified from David-Dusenbery *et al* 2011<sup>730</sup>. Phenotypic plasticity and regulation of vascular smooth muscle cell (VSMC). Several stimuli can induce a switch between a de-differentiated synthetic VSMC and a differentiated contractile VSMC. The process is regulated by miRNA expression as shown and alters VSMC phenotypic behaviour.

### Target miRNAs Affect TM Cell Contractility

TGF- $\beta$ 2 increases the expression of  $\alpha$ -SMA in human TM cells altering the actin cytoskeleton and enhancing contraction of the cells<sup>252</sup>. In Chapter 3 the RhoA signalling pathway was significantly activated in human TM cells treated with TGF- $\beta$ 2 (Chapter 3, 3.4.3). RhoA signalling is involved in the regulation of  $\alpha$ -SMA expression and cell migration<sup>732</sup>.  $\alpha$ -SMA expression was significantly decreased in human TM cells co-treated with TGF- $\beta$ 2 and miRNA inhibitor miR-145-5p (FC= -1.5476,  $p$ -value= 3.42E-10). This decrease was observed by q-PCR in human TM cells for miR-145-5p inhibitor but was not statistically significant (FC= 1.96) (Figure 5.22). Protein analysis identified the diminished expression of  $\alpha$ -SMA protein in response to both miR-143-3p and miR-145-5p inhibitors when compared to a TGF- $\beta$ 2 positive control (Figure 5.23). This supports the concept that TGF- $\beta$  acting via miR-145 up-regulates  $\alpha$ -SMA expression in the TM. Actin cytoskeleton reorganisation in TM

cells results in the formation of cross-linked actin networks<sup>582,733,734</sup> (CLANs) and these are induced in human TM cells in the presence of TGF- $\beta$ 2<sup>254</sup> and corticosteroids<sup>257</sup>.  $\alpha$ -SMA is a key component of CLANs. Glaucomatous TM cells contain greater numbers of CLANs (mean= 1.03) in comparison to aged-matched normal TM cells(0.67)<sup>735,736</sup>, supporting the association between actin remodelling and POAG. CLANs are believed to increase stiffness of TM cells thus increasing AH outflow resistance, as well as disturbing TM homeostasis<sup>256</sup>.

This concept is further supported by data from the targeted deletion of miR-143/145 in mice (*miR-143/145* dKO mice)<sup>694</sup>. The deletion of miR-143 and miR-145 resulted in a 19% decrease in IOP which is equivalent to a 2 fold increase in outflow facility; the eye of the mice were microscopy and structurally normal<sup>694</sup>. AntagomiR transfections against miR-143 and miR-145 in human TM cells resulted in abnormalities in F-actin stress fibre including fibre length and variable effects on cell contraction (inter-donor variability)<sup>694</sup>. A number of genes were selected as potential predicted/validated miR-143/145 targets from the literature and others involved in actin dynamics and contractility<sup>694</sup>. Several miR-143/145 validated targets from studies in VSMCs did not show consistent results in luciferase reporter assays suggesting cell-type specific miRNA effects on mRNA regulation<sup>694</sup>. The authors proposed that an unbiased genome wide approach should be employed to investigate miR-143/145 regulated genes in human TM cells<sup>694</sup>.

### Target miRNA Manipulations

With this in mind, a combined approach was used in this study combining validated targets for miR-143/145 from the literature and a hypothesis independent genome-wide approach using RNA-Seq following miRNA inhibition. Validated targets were selected from those involved in TGF- $\beta$  signalling (TGF- $\beta$ R2: miR-145<sup>709</sup>; SMAD2:miR-145<sup>711</sup>) and glaucoma pathogenesis<sup>712</sup> (CTGF: miR-143/145)<sup>710,737,738</sup>. The transfection of miR-143/145 mimics and inhibitors did not detect a significant alteration of these targets in TM cells. This might reflect the low transfection efficiency in TM cells or cell-specific miRNA effects<sup>714</sup>. Given miR-145 is a repressor of EMT, and central role of EMT in TGF- $\beta$  driven fibrosis in the TM<sup>599</sup>, markers of

EMT were assessed following miR-145 manipulation; no significant alterations were detected by q-PCR.

The ability of a miRNA to target an mRNA is often cell specific and miRNA expression profiles can be altered when cells are taken from a tissue environment and placed in a cell culture environment<sup>739</sup>. Target prediction tools, though useful for rapid identification of validated targets for specific miRNAs, do not provide cell specific information and therefore may provide difficult to replicate when used in different model systems. In addition, human TM cells have enhanced phagocytic capabilities which results in difficult transfection conditions. Despite identifying a low transfection rate amongst cells using a FAM labelled siRNA, untransfected cells were not removed from the environment prior to protein and mRNA analyses. The presence of untransfected cells within the population may be indicated by the inability to detect significant alterations in TM cells treated with TGF- $\beta$ 2 and relative miRNA mimics and inhibitors when compared to TGF- $\beta$ 2 only controls.

### Core and Comparison Analyses

Given these findings and those of other authors investigating the role of miR-143/145 in the TM<sup>694</sup> a genome-wide RNA-Seq experiment was performed to assess differential gene expression and pathway analysis in human TM cells treated with TGF- $\beta$ 2 transfected with a scrambled negative control (SNC, inhibitors of miR-143 (143i) and miR-145 (145i). Strikingly, transfection of the SNC resulted in significant DEGs and altered pathways; many of these over-lapped with miR-143 and miR-145 inhibition. Manipulating the miR-143 and miR-145 regulatory network resulted in complex transcriptome alterations, both direct and indirect. To dissect specific alterations two approaches were taken: (1) a direct comparison of DEGs between SNC, 143i, and 145i; and (2) a 'Comparison Analysis' in Ingenuity Pathway Analysis concentrating on alterations in canonical pathways and upstream regulation between enriched processes identified in two or more Core analyses.

From the set of genes identified by the direct comparison of SNC, 143i and 145i (Table 5.14), known validated miR-143 and miR-145 targets were identified from miRTarBase v8 and miRWalk2.0 (see Table 5.16). From the direct comparison

of SNC, 143i, and 145i further evidence was found to support the relationship between miR-143/145 Rho signalling and cytoskeletal remodelling. Both moesin (MSN) and Rho GTPase activating protein 11A (ARHGAP11A) have increased expression in response to both miR-143 and miR-145 inhibitors. MSN closely regulates  $\alpha$ -SMA and inhibition of MSN reduces the expression of  $\alpha$ -SMA in the mouse cornea<sup>740</sup>. ARHGAP11A induces cell cycle arrest and apoptosis through p53 binding<sup>741</sup>. p53 has been associated with POAG whereby it induces apoptosis in response to cell death<sup>742</sup>. In addition, p53 post-transcriptionally modifies miRNAs<sup>704</sup>, therefore may be involved in a regulatory feedback loop. Up-regulation demonstrates the complexity of miRNA regulation by 143i and 145i and is indicative of a complex signalling network.

From the 'Comparison Analysis' of the TGF- $\beta$  signalling pathway in IPA (Figure 5.18), miR-145 is specifically reducing the expression of the TGF- $\beta$ R2 compared with the SNC and 143i. This has previously been shown and was evaluated by q-PCR which was not significant although there was a trend suggesting miR-145 regulated TGF- $\beta$ R2 (Figure 5.8). The finding of the RNA-Seq experiments highlight the advantages and sensitivity of RNA-Seq in terms of dynamic range and quantification compared with q-PCR<sup>743</sup>. The upstream analysis (Figure 5.20) demonstrated that ZEB1 expression was up-regulated by both 143i and 145i versus SNC. This was also seen in the direct comparison of DEGs. ZEB1 is a transcriptional repressor and an inducer of EMT<sup>744</sup>. Enhanced expression by 145i may explain the failure of miR-145 inhibitor transfection to alter the expression of EMT markers (Figures 5.11- 5.14). The up-regulation of ZEB1 by 143i and 145i demonstrates the complexity of miRNA regulation and a potentially deleterious off-target effect. Similarly, the variability seen in the data is complicated by evidence from up-stream analysis (Figure 5.20) that miR-145 expression is up-regulated by the SNC and miR-143 inhibitor; suggesting a complex regulatory system.

The phenotypic switch from a contractile and synthetic VSMC is regulated by a complex and synergistic network and similar mechanisms are likely in TM cells. Contractile smooth muscle genes ( $\alpha$ -SMA, SM-MHC, calponin and desmin) contain a converse *cis*-regulatory element: the CA<sub>6</sub>GG box (CC(A/T)<sub>6</sub>GG)<sup>725</sup>. Serum response

factor (SRF) and either myocardin or myocardin-related transcription factor (MRTF)-A/B bind to CArG box elements located within the promoter of contractile smooth muscle genes to regulate the transcription and differentiation of a contractile VSMC<sup>725</sup>. The miRNA cluster miR-143/145 promoter also contains a CArG box<sup>725</sup> and SMAD binding elements (SBE)<sup>320,702</sup>. SRF and SRF co-factors (myocardin and MRTF-A/B) activate miR-143/145 promoter<sup>725,745</sup>. TGF- $\beta$  up-regulated the expression of both myocardin and the miR-143/145 cluster via SBEs<sup>746</sup> and via the activation of RhoA signalling and ROCK1 which induces MRTF-A expression; MRTF-A also binds the CArG box in the miR-143/145 cluster (Figure 5.25)<sup>730</sup>.

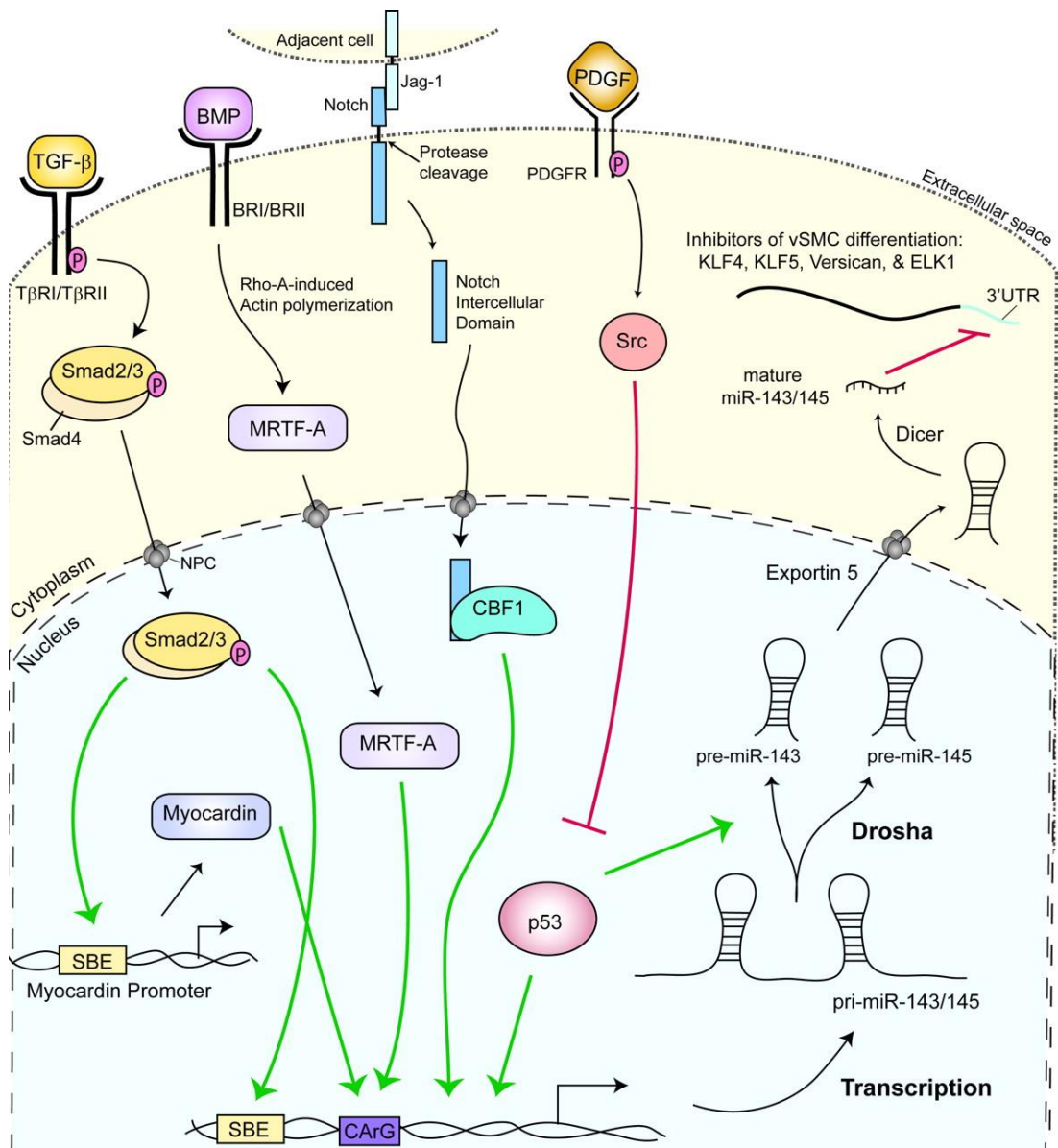


**Figure 5.25: Summary of miR143/145 Regulation.** Modified from David-Dusenbery *et al* 2011<sup>730</sup>. Multiple extracellular signals promote VSMC differentiation through the regulation of miR-143/145.

PDGF negatively regulated miR-143/145 expression indirectly via p53 to maintain a de-differentiated synthetic VSMC<sup>728</sup>. PDGF activates Src which inhibits p53 promotion of miR-143/145 expression via transcriptional and post-transcriptional mechanisms<sup>704,747</sup>. The miR-143/145 cluster is a central target of multiple signalling pathways which regulate the VSMC phenotype and are also most likely to regulate the contractile and synthetic behaviour of TM cells. Further work is required to determine the regulation of the miR-143/145 cluster and pathophysiology in the TM cell and in glaucoma. Interestingly, a recent study assessing the miRNA content of AH from normal and glaucomatous patients identified 181 differentially expressed miRNAs between both cohorts: miR-143 was significantly up-regulated in AH of glaucomatous patients<sup>684</sup>.

## 5.6 Summary

This is the first description of miRNAs expressed in human TM cells in response to TGF- $\beta$ 2 treatment. We successfully identified three miRNAs that are significantly differentially expressed in response to TGF- $\beta$ 2, miR-143, miR-145 and miR-4328. miR-4328 is relatively unexplored therefore due to time constraints we focused our remaining experiments on the potential role of miR-143 and miR-145 in the human TM, two well described miRNAs. The miR-143/145 cluster plays a fundamental role in governing VSMC and SMC-like differentiation during physiological and pathological events, and expression is enhanced in response to TGF- $\beta$ 2. Our work further demonstrates the possible effects of the miR-143/145 cluster and miR-145 independent effects on TM cytoskeleton stabilisation and remodelling in response to TGF- $\beta$ 2. This research highlights the need for further understanding of the intricate regulatory network of miR-143/145 before suitable effective therapies may be developed.

Functional relevance of miRNAs in human TM cells required stable transfection of target miRNA mimics and inhibitors. TM cells are inherently difficult to transfect and a constant low transfection yield was obtained. This proved frustrating when identification of putative targets for these miRNAs could not be effectively identified. We have hypothesised that the lack of correlation between our dataset and previously published work, in relation to miR-143 and miR-145

validated targets, may have been caused by a mixed cell population, i.e. transfected and untransfected cells. The number of untransfected cells greatly outnumbered transfected cells therefore a true evaluation of the functions of the miRNA mimics and inhibitors could not be reported. Future work would benefit from a cell sorting technique to isolate only stably transfected cells to evaluate the potential phenotypic and genotypic effects miR-143 and miR-145 are exerting on human TM cells. We have shown that  $\alpha$ -SMA is down-regulated at mRNA and protein levels and this corroborates previously published data. It is hypothesised that miR-143/miR-145 enhance TM cell contractility and to investigate this collagen contraction assays may potentially be a logical step forward. There are a number of obstacles to overcome with miRNA delivery to the TM and effective delivery must be considered prior to future work. miRNA delivery to ocular tissues is discussed further in Chapter 6.

## **Chapter 6**

### **Emerging and Novel Glaucoma Therapeutics**

## Current Therapies for Glaucoma

All treatments of glaucoma currently used in clinic target lowering IOP as a method to slow disease progression. Current therapies broadly make up five drug classes: cholinergic agonists, sympathomimetics,  $\beta$  blockers, carbonic anhydrase inhibitors, and prostaglandin analogues<sup>748</sup>. In addition to pharmaceutical therapy there are several surgical options for the treatment of POAG: glaucoma filtration surgery, shunt implants and laser trabeculoplasty<sup>749</sup>. IOP is modulated by decreasing aqueous humour production or by increased outflow facility. Current drug treatments are not selective to eye tissues and were originally developed for other diseases<sup>748</sup>. Prostaglandin analogues, and cholinergic agonists (pilocarpine), lower IOP mainly by increasing AH outflow through the conventional and uveoscleral pathways. Pilocarpine increases contractility of the ciliary body thus increasing outflow<sup>750</sup>. Prostaglandin analogues, first identified in monkeys for their IOP lowering effect<sup>751</sup>, increased the uveoscleral outflow and conventional AH outflow<sup>752,753</sup>. Sympathomimetics<sup>754</sup>,  $\beta$  blockers (timolol)<sup>755,756</sup>, and carbonic anhydrase inhibitors<sup>85,757</sup>, all decreased aqueous humour production by exerting their effects on the ciliary epithelium. When drug pharmacological intervention fails to lower IOP, invasive measures including laser treatment, surgery, or shunt implants may be used. Laser treatment mechanically increases outflow by damaging the TM tissue<sup>758</sup>. Glaucoma filtration surgery increases outflow facility through creation of a fistula for AH to bypass the non-functional TM<sup>759</sup>. Filtration surgery has a high 5-year failure rate and associated cataract complications<sup>760</sup>. Shunt implants are designed to maintain the opening made by surgery with a physical tube-like stent<sup>761</sup>.

Glaucoma-associated morphological changes include increased extracellular matrix secretion and deposition in the TM<sup>762</sup>, changes to the ECM composition of the ONH<sup>763</sup>, and increased TM cell contractility<sup>250</sup>. New therapies in development modulate the signalling pathways involved in both ECM and cytoskeletal restructuring. Adenosine receptor ligands are currently being developed. Adenosine receptors (ARs) are expressed in the ciliary body<sup>764</sup>, TM<sup>765</sup> and Schlemm's canal<sup>766</sup> and regulate the production of cAMP; AR classes, A<sub>1</sub>-A<sub>3</sub>, have differential effects on

ECM turnover<sup>767,768</sup>. A<sub>1</sub> and A<sub>3</sub> activate phospholipase C (PLC) which is part of the extracellular signal related kinase (ERK1/2) pathway. Activation of ERK1/2 leads to secretion of MMPs and accelerated ECM turnover. A<sub>2</sub> also modulates ERK1/2 pathway however, this activates connective tissue growth factor (CTGF), thus increasing ECM deposition<sup>712</sup>. Therefore, depending on the AR class, agonists or antagonists should theoretically lower IOP by enhanced ECM turnover. A<sub>1</sub> agonists enhance ERK1/2 signalling leading to specific MMP-2 and MMP-9 increase<sup>767,769,770</sup>. Consistent with this, outflow increase can be reversed by MMP inhibition<sup>769</sup>. Both A<sub>1</sub> and A<sub>3</sub> reduce TM cell volume which in turn independently increase outflow facility<sup>765</sup>. However, their molecular structures are still not well established and there is both species specificity and selectivity issues with AR agonists; this is an important area for further investigation to reverse TGF- $\beta$  driven ECM abnormalities in the TM. More recently a gene therapy for steroid-induction of MMP-1 has been described<sup>771</sup> which may circumvent issues arising with the use of AR agonists. The GRE.MMP1 gene vector successfully induced MMP one expression in the TM in response to corticosteroids<sup>771</sup>.

In addition to AR ligands, Rho-associated protein kinase (ROCK) inhibitors are also in late stage development and early clinical use<sup>772</sup>. As discussed in Chapter 3 (3.5), ROCKs are serine/threonine kinases that are downstream effectors of Rho GTPases. ROCKs phosphorylate substrates involved in the regulation of F-actin stress fibre formation, focal adhesion, and cell-cell adhesion and migration properties<sup>429,773</sup>. Downstream effects on actin cytoskeleton organisation and smooth muscle cell contractility is relevant to many cellular processes and dysregulation, and the Rho/ROCK signalling system is evident in diseases throughout the body<sup>774,775</sup>. Known substrates of ROCK are myosin light chain (MLC) kinase, LIM homeobox gene Lin11, ISL LIM Homeobox 1 (Is11) and LIM kinase<sup>776</sup>. The Rho signalling pathway is relevant for AH outflow and glaucoma<sup>777</sup>. Both ROCK1 and ROCK2 are expressed in the TM, ciliary body, and corneal epithelium. Selective roles of ROCK1 and ROCK2 in glaucoma is still unknown, however ROCK1 and ROCK2 knockout mice have lower IOP than wild type mice<sup>778</sup>.

ROCK therapies are being actively investigated to treat an array of diseases from cancer to glaucoma<sup>775,779,780</sup>. ROCK inhibitors (R1-R13) were derived from calmodulin antagonists, namely isoquinolone<sup>781</sup>. Similar to other kinase inhibitor targets, ROCK inhibitors competitively bind in the ROCK ATP binding pocket<sup>782</sup>. It is therefore difficult to ensure ROCK inhibitors selectivity over alternative kinase binding pockets, for example R-1 has been shown to inhibit protein kinase C-related protein kinase 2 (PRK2), cyclic GMP-dependent protein kinase G (PKG) and protein kinase C (PKC)<sup>783</sup>. R-1 in complex with ROCK1 and ROCK2 demonstrates differences in pocket shape and physiochemical properties compared to other kinases<sup>784</sup>, giving rise to a new generation of ROCK inhibitors, with more potent inhibition and specificity; these are currently either being evaluated in glaucoma models or in clinical trials (Table 6.1)<sup>783,785,786</sup>. Animal perfusion studies and *in vivo* studies in normal tension and ocular hypertensive rabbits have been used to test ROCK inhibitors<sup>787</sup>. Repeatedly, ROCK inhibitors decrease IOP by increased AH drainage through the TM via cytoskeletal re-structuring<sup>787-789</sup>. Bovine eyes perfused with R-3 results in cellular morphology changes of TM and Schlemm's canal cells, decreases the number of focal adhesions and widens extracellular spaces in the TM<sup>400,790</sup>. It is thought that these morphological changes are caused by the decrease in MLC kinase phosphorylation following ROCK inhibition. In addition to lowering IOP, ROCK inhibitors increase ONH blood flow, and, prevent post-operative scarring in a glaucoma surgery model by inhibiting collagen deposition and fibro-proliferation in rabbits<sup>791-793</sup>.

<b>Compound</b>	<b>Clinical Trials for IOP Reduction</b>
R-2- Ripasudil	Phase II, Approved for glaucoma and ocular hypertension treatments in Japan
R-4- RKI-983	Discontinued following Phase II
R-11- Scaffold for AMA-0076	Phase II-Completed
R-12- AR-12286	Phase II-Ongoing
R-13- AR-13324	Phase II-Ongoing

**Table 6.1: ROCK Inhibitors Approved for Clinical Trials for the Treatment of Elevated IOP<sup>794</sup>.**

## Novel Molecular Target Identification by mRNA-Seq

Glaucoma is a multi-faceted disease and with current therapies sole aim to lower IOP there is potential for advancements in this area by identification of key molecular targets involved in disease pathogenesis. We investigated the molecular changes associated with known glaucoma stimuli, TGF- $\beta$ 2 and dexamethasone and identified a range of differentially expressed genes that are likely implicated in POAG and steroid-induced glaucoma.

### LIM Kinase Inhibitors

In our study the Rho/ROCK signalling pathway was significantly enriched in response to TGF- $\beta$ 2, dexamethasone, and following the transfection of human TM cells with miR-143 and miR-145 inhibitors. Interestingly, neither ROCK1 (LogFC= 0.392, FDR  $p$ = 0.019) nor ROCK2 (LogFC= -0.319, FDR  $p$ = 0.081) were significantly differentially expressed across all three data sets. However, LIM kinase was significantly altered (LIMK1: LogFC= 1.394, FDR  $p$ = 2.14E-17 and LIMK2: LogFC= 2.51, FDR  $p$ = 4.32E-30) (Chapter 3, Table 3.9), and may be an alternative more effective target of the Rho signalling pathway in glaucoma. LIM kinases 1 and 2 (LIMK1 and LIMK2) regulate cytoskeletal dynamics by phosphorylating and deactivating cofilin, a protein required for depolymerisation of actin filaments. LIM kinases have been investigated in several diseases for their role in various cellular processes such as cell barrier integrity, axonal elongation, cell migration and cell growth arrest<sup>795</sup>. In conjunction with the growing interest in LIM kinases, LIM kinase inhibitors have also been reported (Table 6.2). A LIM kinase inhibitor, dabrafenib, has been approved for use in melanoma cancers, and is thought to inhibit tumour cell invasion through mediation of upstream signalling factors<sup>796,797</sup>.

Compound Name	Clinical Trials
Dabrafenib (Tafinlar)	Melanoma Cancer- Phase 2 and Phase 3
Dabrafenib/Panitumumab	-
Dabrafenib/Panitumumab/Trametinib	-
Dabrafenib/Trametinib	BRAF V600E Positive Cancer- Approved
Dabrafenib/Trametinib/vermuafenib	Advanced Solid Cell & Breast Cancer-Phase 1 and Phase 2

**Table 6.2: LIM Kinase Inhibitors in Clinical Trials and Approved for Use.**

### IOP Lowering Effects of LIM Kinase Inhibitors

LIMK inhibitors are thought to lower IOP through inducing depolymerisation of actin filaments in the trabecular meshwork, resulting in relaxation of the tissue<sup>794</sup>. POAG patients exhibit numerous structural changes in the TM including increased contractility which can result in decreased outflow facility and in turn elevated IOP<sup>798</sup>. Relaxation of the TM with LIMK inhibitors may counteract this effect, thus reversing a cause of elevated IOP. LIMK inhibitors offer more benefits than ROCK inhibitors as they are downstream from ROCK in the signalling cascade, their effects therefore are more specific to actin polymerisation and may offer fewer side effects than ROCK inhibitors. In a steroid induced glaucoma mouse model, LIMK2 inhibitors reduce IOP to baseline levels<sup>799</sup>. Furthermore, porcine eye perfusion with LIMK2 inhibitors increases outflow facility in the eye<sup>799</sup>. More recently an optimised LIMK2 inhibitor, LX7101, was described and has since proven to have high efficacy in a mouse model of ocular hypertension, and lowered IOP in glaucoma patients in phase I clinical trials<sup>789</sup>.

### Alternative Effects of LIM Kinase Inhibitors for Glaucoma

Reportedly, ROCK inhibitors have IOP-independent effects which are beneficial in glaucoma treatment. As a downstream molecule of the ROCK signalling pathway, LIMK inhibitors, may also have alternative uses. Reduced ocular blood flow in glaucomatous eyes causes RGC apoptosis<sup>800</sup>. ROCK inhibitors increase ocular blood flow in rabbit glaucoma models, presumably through the relaxation of vascular smooth muscle<sup>792</sup>. LIMK is a recognised regulator of vascular smooth

muscle migration<sup>801</sup> and therefore it is likely that LIMK inhibitors may increase ocular blood flow by similar mechanisms of ROCK inhibitors. Further investigation is required as a therapy to lower IOP while increasing ONH perfusion would be a major therapeutic advancement in glaucoma treatment.

### Insulin-Like Growth Factor Inhibitors

Insulin-like growth factor (IGF)-1 signalling results in the activation of the Rho/ROCK signalling pathway<sup>802</sup>. Interestingly, IGF-1 was significantly altered in our data set (LogFC= 6.666, FDR  $p= 1.89E-09$ ), and therefore may also be an alternative target of the Rho signalling pathway in glaucoma. In the IPA Comparison analysis (Chapter 4; Table 4.5) both TGF- $\beta$ 2 and DEX treatment activated IGF-1 signalling. IGF-1 receptors are widely distributed in the eye and IGF-1 receptor antagonists prevent retinal neovascularisation in murine models indicating a key role of IGF-1 in the eye<sup>803</sup>. Increased signalling for IGF-1 in the eye leads to an accumulation of vascular endothelial growth factor (VEGF)<sup>804</sup>. There is evidence that glaucoma patients have elevated levels of VEGF in the aqueous humour and additionally, there is evidence for a role of VEGF in wound healing after glaucoma filtration surgery<sup>805</sup>. The increase of IGF-1 in the eye of transgenic IGF-1 over-expressing mice causes an increase in globular cells in the iridocorneal angle which are not present in control eye<sup>806</sup>. Furthermore, mice had separation of ganglion cell nuclei indicative of ganglion cell loss which is suggestive that the mice developed glaucoma when IGF-1 is highly expressed<sup>806</sup>. IGF receptor inhibitors have been investigated for their roles in treatment of advanced cancers<sup>807</sup>. IGF has been implicated in cancer cell proliferation, survival and metastases due to its activation of downstream oncogenic proteins, phosphoinositide 3-kinase (PI3K), protein kinase B (Akt) and MAPKs.

### IGF-1 Inhibitor Potential in Glaucoma

CTGF is a primary response gene in human trabecular meshwork cells and is associated with the stabilisation of the actin cytoskeleton<sup>712</sup>. Physiological concentrations of IGF-1 induce the expression of CTGF in trabecular meshwork cells<sup>808</sup>. We investigated the response of CTGF expression to miRNA-145 inhibition

(Chapter 5, Figure 5.10) in TGF- $\beta$ 2 treated human TM cells, however no obvious regulation by miRNAs was observed. Little is known about the function of IGF-1 in the TM. Rho/ROCK signalling is a common pathway linking IGF-1 and CTGF, which is implicated in TM cell contractility<sup>809</sup>. IGF-1 inhibitors may potentially reduce the expression of CTGF in the TM of glaucoma patients resulting in increased relaxation of the outflow pathway, increasing outflow facility and lowering IOP. IGF-1 inhibitors may also be beneficial as post-surgical treatments to prevent elevated VEGF activity following glaucoma filtration surgery. Given the evidence the role of IGF-1 signalling in glaucoma warrants further investigation.

#### NADPH Oxidase (NOX) 4 Inhibitors

TGF- $\beta$ 2 is elevated in the aqueous humour of the eye and we have identified elevated expression of NADPH oxidase (NOX) 4 in TGF- $\beta$ 2 treated human TM cells by RNA-Seq experiments (Chapter 3). TGF- $\beta$ 2 can control the production of reactive oxygen species (ROS), and NOX4 is an important downstream effector of TGF- $\beta$ 2 that is significantly expressed in human TM cells in the presence of TGF- $\beta$ 2. NOX4 produces ROS as their sole function and are recognised a key modulators of signal transduction pathways and have a pathological role after excessive activation under chronic stress<sup>810</sup>. NOX4 inhibitors have been previously described in a range of models of chronic inflammatory and fibrotic diseases<sup>811</sup>. GKT137831 (NOX4/1 inhibitor) was developed following a high-throughput screen for NOX4 inhibitors<sup>812</sup>. The exact mechanism of action of NOX4 inhibitors remains unknown, however, they have been shown to have no scavenging abilities<sup>813</sup>. Clinical trials in patients with GKT137831 demonstrated excellent tolerability and reduction of various markers of chronic inflammation<sup>810</sup>.

#### Role for NOX4 Inhibitors in Glaucoma

NOX4/1 inhibitors have previously been described for their used in ischaemic retinopathies, in particular GKT137831<sup>814</sup>. GKT137831 suppresses retinal neovascularisation and neuroglial cell inflammation<sup>814</sup>, indicating a therapeutic role for NOX4 inhibitors in ocular disease. Increased H<sub>2</sub>O<sub>2</sub> by NOX4 causes remodelling of the TM cytoskeleton resulting in TM enlargement and decreased outflow

facility<sup>460</sup>. NOX4 inhibitors offer a novel therapeutic treatment for glaucoma as a reduction in NOX4 derived H<sub>2</sub>O<sub>2</sub> may result in the inhibition of pathological TM remodelling thereby maintaining outflow facilities. Interestingly GKT137831 also reduced the expression of CTGF and  $\alpha$ -SMA, two key genes associated with glaucoma pathogenesis, in dermal fibroblast wounds<sup>815</sup>. Previous studies of the actions of NOX4, in addition to our RNA-Seq data, are consistent with the hypothesis that NOX4 inhibition may be useful in blocking pro-fibrotic and TM contractile effects of TGF- $\beta$ 2 on TM cells and warrant consideration for further development as potential glaucoma therapeutic agents.

### Endothelin 1 Inhibitors

Glaucoma pathogenesis is a combination of reduced ocular blood flow and elevated IOP which ultimately leads to retinal ganglion cell death and visual loss<sup>816</sup>. Endothelin 1 (EDN1), a potent vasoconstrictor, was elevated in the TM in the presence of TGF- $\beta$ 2, as identified by our RNA-Seq experiment (Chapter 3); as well as in response to dexamethasone treatment. EDN1 is implicated in the pathogenesis of both POAG and steroid-induced glaucoma.

The heterogeneous nature of corticosteroid-induced IOP elevation indicates that other factors may also have a possible role. EDN1 is encoded for by the endothelin-1 gene and is expressed in several tissues including the non-pigmented ciliary epithelium<sup>590</sup>. EDN1 expression levels rise after 24hours exposure to DEX (100nM)<sup>195</sup>. In the TM of steroid responders, stimulation with dexamethasone results in the increased contractility of the TM as well as the decreased release of nitric oxide<sup>817</sup>. Several reports state that nitric oxide donors can relax the TM and lower IOP<sup>818,819</sup>. Endothelin receptor A activation is promoted by DEX treatment potentiating the contraction of the TM<sup>817</sup>. Glaucoma patients have elevated levels of EDN1 in both plasma and aqueous humour<sup>474</sup>. Both IOP and ocular blood flow are affected by EDN1<sup>467</sup>. Differential experimental approaches identified that elevated EDN1 levels in AH increase IOP<sup>478-480</sup>. Animal models have demonstrated a dose dependent rise in IOP after intracameral injection of EDN1<sup>478</sup>. In the bovine eye, EDN1 induced a reduction of AH outflow cause by increased TM contraction<sup>401</sup>.

Antagonism of EDN1 in both pressure dependent and independent pathways provides a promising approach for glaucoma treatment.

### EDN1 Antagonism in Glaucoma

Current endothelin (ET) receptor antagonists are classified as ET<sub>A</sub> or ET<sub>B</sub> selective depending on their relative affinity for a receptor subtype<sup>820</sup>. It has been proposed that EDN1 maintains IOP homeostasis by exerting its effects through endothelin receptor B<sup>817</sup>. Bosentan was the first mixed ET<sub>A</sub>/ET<sub>B</sub> antagonist clinically approved for the treatment of pulmonary arterial hypertension<sup>821</sup>. ET<sub>A</sub> antagonists demonstrate a dose dependent reduction in blood pressure and systemic vascular resistance<sup>822</sup>. In contrast ET<sub>B</sub> receptor antagonism produces mild vasoconstriction and pressor effect<sup>823</sup>. Therefore, it is likely ET<sub>A</sub> receptor antagonists would be beneficial for their use in glaucoma. EDN1 antagonism offers unprecedented benefits over conventional IOP lowering drugs as EDN1 can also positively regulate ocular blood flow. EDN1 antagonism offers IOP dependent and independent pathway manipulation with the overall therapeutic benefit of increased retinal ganglion cell survival. Pressure-independent pathways provide novel therapies for normal-tension glaucoma which are currently unavailable.

### SERPINB2 Agonists

SERPINB2 (PAI-2) is significantly down-regulated in TM cells in response to dexamethasone as described in Chapter 4 and elsewhere<sup>568</sup>. The exact role of PAI-2 in TM cells is unknown. It is proposed that PAI-2 is involved in ECM remodelling characteristic of steroid-induced glaucoma, and regulation of cellular senescence through p21 stabilisation<sup>660</sup>. Decreased expression of PAI-2 in glaucoma may lead to decreased outflow facility in the TM as a result of matrix remodelling and cellular senescence. TGF- $\beta$ 2 increases PAI-1 expression in TM cells<sup>661</sup> while dexamethasone down-regulates PAI-2 in the TM.

## PAI-1 and -2 Therapies in Glaucoma

The fibrinolytic system plays an important role in vascular and tissue remodelling and impaired function of both PAI1 and PAI2 has profound effects on vascular house-keeping and remodelling capacity. Two PAI-2 agonists have been developed, but only tenecteplase has been approved for clinical use in stroke patients<sup>824</sup>. Tenecteplase has a higher fibrin specificity and greater resistance to inactivation by PAI-1 (its endogenous inhibitor). PAI-2 agonists for glaucoma offer unique opportunities to regulate tPA activation and in turn ECM re-modelling in the TM. In pulmonary fibrosis PAI-1 antagonists demonstrate efficacy in preventing bleomycin-induced pulmonary fibrosis in mice<sup>825</sup>. Furthermore, a non-inhibitory PAI-1 reduces pathological accumulation of ECM through competitive antagonism of native PAI-1, thus restoring plasmin generation and increasing plasmin-dependent degradation of matrix components<sup>826</sup>. Competitive antagonism of native PAI-1 by non-inhibitory PAI-1 antagonists would be beneficial for POAG treatments where elevated TGF- $\beta$ 2 concentration in the AH is disrupting ECM turnover. Reduction of pathological ECM accumulation in the TM would alleviate elevated IOP and increase outflow facility.

## Follistatin

Follistatin (FST) is a stress responsive protein required for neutralising TGF- $\beta$ 2 by antagonising BMP and activin<sup>670</sup>. FST expression was identified in human TM cells in response to TGF- $\beta$ 2 in this study and in the literature<sup>673</sup>. Our RNA-Seq data identified FST as significantly down-regulated in response to DEX and this was also observed in alternative studies<sup>570,673</sup>. FST is required to reduce ROS and is thought to interact with NOX family members<sup>674</sup>. FST reduction in response to corticosteroid could be detrimental to RGC and TM cell health during glaucoma pathogenesis as susceptibility to ROS would increase.

FST is regulated at transcriptional and post-transcriptional levels<sup>675,676</sup> which allows for opportunity to manipulate FST expression therapeutically. FST gene therapy clinical trials have investigated the potent antagonistic effects of FST on myostatin as a treatment for Becker muscular dystrophy (BMD)<sup>827</sup>. Follistatin

gene therapy for sporadic inclusion body myositis successfully decreased fibrosis in 4 out of 6 treated subjects<sup>828</sup>. Gene therapy offers a unique targeted mechanism<sup>829</sup> to effectively induce the expression of FST in a controlled manner and may have beneficial effects on steroid-induced glaucoma pathogenesis. The inverse is true for POAG whereby FST expression is increased in response to TGF- $\beta$ 2 in a dose dependent manner. The role of elevated FST expression in response to TGF- $\beta$ 2 is unknown however it may be involved in protection of TM and retinal ganglion cells from ROS; however further studies are required. Post-transcriptional modification of FST may offer a unique gene silencing approach for FST in glaucoma therapies.

## MMP

MMP activity in the trabecular meshwork is disrupted in glaucoma patients as well as *in vitro* studies in the anterior segment and cultured TM cells. Outflow resistance is generated in the TM through continuously remodelling of the ECM governed by MMPs<sup>830</sup>. In our study MMP-1 was significantly down-regulated in human TM cells in response to dexamethasone (Chapter 4) (FC= -1.81, *p*-value= 4.4E-41). This reduction in MMP-1 may relate to the decreased ECM turnover seen in the outflow pathway with corticosteroid treatment<sup>552</sup>. An adenoviral vector containing inducible MMP-1 has been generated and extensively characterised in primary cell and organ culture systems<sup>666</sup>. Infection of the systems with the vector induced high levels of both MMP-1 mRNA and protein<sup>666</sup>. Importantly, expression of MMP-1 could be synchronised with corticosteroid treatment circumventing adverse side-effects observed during steroid-induced glaucoma<sup>666</sup>. More recently, adeno-associated viral vectors for MMP-3 secretion have been described<sup>831</sup>. Adeno-associated viral vectors overcome short-lived effects of adenovirus vectors and allow the sustained expression of MMP-3 in the AH of mice infected with the vector<sup>831</sup>. These results are promising with regards to the advent of novel gene therapies in for the treatment of POAG and steroid induced glaucoma.

## miRNA Therapeutics in Glaucoma

The expression of miRNAs is altered in various diseases and it is feasible to manipulate miRNAs *in vivo*<sup>832</sup>. There are two distinct possibilities to exploit miRNAs

for therapeutic interventions: (1) exogenous miRNAs can be applied to substitute for endogenously expressed miRNAs or (2) small molecule antagonists can be used to lower the gene regulatory effect of native miRNAs<sup>833</sup>. The latter approach allows the use of synthetic oligonucleotides for enhancing instead of silencing gene-expression in comparison to down-regulation by siRNAs<sup>833</sup>. Synthetic miRNAs can assume the regulatory role of natural miRNAs. Discovery and development of miRNA therapeutics requires the identification of signature miRNA, validation of signature miRNA by loss/gain of function studies *in vitro*, pharmacological analysis (*in vivo* miRNA delivery studies), and clinical trials<sup>834</sup>.

MRX34, a miR-34a mimic, was the first miRNA mimic to enter cancer clinical trials for its use in tumour growth and progression inhibition<sup>835</sup>. Antagonistic oligonucleotides on the other hand, which target pathology-related miRNAs are a promising therapeutic strategy for the treatment of cancer, hepatitis C and other diseases<sup>836</sup>. Antagonistic miRNAs were the first miRNA inhibitors shown to work in mammals<sup>837</sup>. The first reported use of miRNA antagonistic oligonucleotides *in vivo* was against miR-122<sup>838</sup>. miRNA-122 required structural optimisation through the use of locked nucleic acids (LNAs)<sup>839</sup> leading to the production of miravirsin for the treatment of chronic hepatitis C virus infections. Miravirsin is a phosphorothioated oligonucleotide with multiple LNA nucleosides, which binds to miR-122 and silences pathological expression effectively<sup>840</sup>. In addition to antagonistic oligonucleotides “decoy” transcripts or miRNA sponges are currently under investigation for their therapeutic abilities<sup>841</sup>. miRNA sponges bind RNA transcripts to sequester and inhibit specific miRNAs<sup>841</sup>. The first decoy described consisted of an adenoviral vector with two sites for the muscle-specific miRNA-133<sup>842</sup>. This decoy confirmed the loss of miR-133 expression in mouse and disease models to lead to cardiac hypertrophy<sup>842</sup>.

Elevated IOP is attributed in part to increased ECM deposition in the outflow pathway. A number of miRNAs have been implicated in this process and inhibition of their reduced protein expression of key genes involved in ECM turnover and deposition<sup>381</sup>. miR-29 family members in particular regulate the expression of ECM components in TM cells and this is driven by TGF- $\beta$ 2 signalling<sup>688,843</sup>. miR-24

regulates the expression of TGF- $\beta$ 1 in TM cells in response to mechanical stress<sup>697</sup>. miR-200c inhibits the contraction of TM cells and miR-200c mimic decreases IOP in rats following intracameral injections<sup>469</sup>. Conversely, inhibition of miR-200c with an adenoviral vector expressing a molecular sponge to miR-200c leads to a significant decrease in IOP<sup>469</sup>.

Three differentially expressed miRNAs were identified in our human TM cells stimulated by TGF- $\beta$ 2: miR-143, miR-145, and miR-4328. Two of these: miR-143 and miR-4328, were also significantly expressed in glaucomatous cells when compared to healthy controls. Recently, the miR-143/miR-145 miRNA cluster has been implicated in elevated IOP and deletion of the cluster resulted in up to 20% decrease in IOP in mice<sup>694</sup>. miR-143 and miR-145 mechanistically regulate actin dynamics within the TM, and so TM cell contractility. We have further shown this by the reduction of  $\alpha$ -SMA at the protein level following miR-143 and miR-145 inhibition. The RhoA/ROCK signalling pathway has been implicated in glaucoma and it is likely that miR-143 and miR-145 are involved in the regulation of key members of the signalling pathway. Evidence for both miR-143 and miR-145 regulation of components of the actin remodelling system makes them attractive future novel therapies for a more targeted glaucoma therapy. miRNAs have a wide potential therapeutic range in POAG from IOP regulation to ECM homeostasis.

In addition, we identified a novel target for miRNA regulation in human TM cells stimulated by DEX in Chapter 4. FKBP51 is a member of the immunophilin family responsible for the nuclear translocation of glucocorticoid receptor  $\beta$  (GR $\beta$ )<sup>637</sup>. Enhanced GR $\beta$  expression in glaucoma patients is attributed to decreased sensitivity to glucocorticoids and poorer prognostic outcome<sup>590</sup>. FKBP51 represents a novel target for steroid-induced glaucoma in which FKBP51 induced glucocorticoid resistance. Interestingly, a number of miRNAs<sup>643-645</sup>, in particular miR-511 robustly regulate the expression of FKBP51. miR-511 suppresses the expression of FKBP51 in primary neurons in response to glucocorticoids<sup>645,646</sup> which is indicative that FKBP51 may be a candidate for miRNA therapies in steroid glaucoma.

## Drug Delivery for Glaucoma

Controlled drug delivery to the eye is a fundamental problem in the treatment of glaucoma, due to low drug contact time and poor ocular bioavailability due to the drainage pathway and tear turnover<sup>844</sup>. Novel delivery systems have the potential to mitigate the challenges of drug delivery efficiency whilst reducing systemic side effects.

Strategies for enhanced drug delivery include drug reformulation into nanoparticles, such as nanospheres or liposomes<sup>685</sup>. Nanoparticles have large surface areas and can be composed of several materials with multifunctional surface groups, which enable the drugs to reach targeted sites and to improve bioavailability. *In vivo* examination of topically administered nanoparticles in rabbits identified no inflammatory reaction, tissue alteration or damage to the epithelial layer of the cornea in response to nanoparticles<sup>845</sup>, indicating their potential for targeted drug delivery to the eye.

Efficient gene delivery into the anterior segment of the eye is feasible through the use of adenoviral and adeno-associated viral (AAV) vectors, and lentiviruses. Viral vectors contain the transgene, a promoter and potentially a gene regulatory sequence. Adenoviral drug delivery induce high inflammatory responses at high concentrations and gene expression is relatively short (1-3 weeks)<sup>846</sup>. Adenoviruses are not recommended as a final vector for gene therapy but are useful in pre-clinical studies<sup>847</sup>. Adenoviruses for Rho signalling molecules and MMP-1 decrease TM outflow resistance in organ culture<sup>848</sup> and reduce IOP in animal models<sup>849</sup>.

AAV vectors can express the transgene for up to five years after a single dose. AAVs are not functional in the trabecular meshwork due to their inability to form double stranded DNA within the cell<sup>847</sup>. AAVs vectors carrying neuroprotective genes and injected intravitreally successfully protect RGCs in rat hypertensive models<sup>850</sup>. Additionally, AAV expressing MMP-3 in mice resulted in the secretion of MMP-3 in the AH and subsequent MMP-3 delivery to the outflow tissues facilitated targeted ECM degradation<sup>831</sup>. Lentiviruses are integrated into the host genome and

successfully transduce for long periods of time. There are however associated risks and integration can lead to undesirable side effects<sup>851</sup>. Non-viral vectors transduce in the TM and vectors carrying pigment-derived epithelium factor (PEDF) protected RGC in rats<sup>852</sup>. Non-viral vector gene delivery systems have been used to target specific tissues involved in the pathogenesis of glaucoma and effective long-term gene expression in the TM following intracameral delivery showed limited side effects on surrounding ocular tissues<sup>829</sup>.

Gene silencing with siRNAs has also been investigated for its use in glaucoma therapy. Perfusion of labelled naked siRNA to human anterior segments identified incorporation of the siRNA by the TM<sup>853</sup>. Subsequently perfusion of siRNA for glucocorticoid receptor degraded receptor RNA, and in the presence of DEX reduced the expression of glucocorticoid-induced genes (myocilin and angiopoietin-like7)<sup>853</sup>. Naked delivery of miRNAs has been described in cancer research<sup>854</sup> and therefore their use in glaucoma therapies is also feasible. However, the naked delivery of both miRNAs and siRNAs still lack efficiency; but studies coupling siRNAs to different polymers to form nanoparticles increase the efficiency of siRNA and miRNA delivery<sup>855</sup>.

## **Chapter 7**

### **Summary and Future Work**

To the best of our knowledge, this is the first identification of differentially expressed genes in the TM in response to TGF- $\beta$ 2 and dexamethasone characterised by RNA-Seq. In Chapter 3, we describe a comprehensive characterisation of differentially expressed genes in response to TGF- $\beta$ 2 in normal human TM cells, and associated gene expression in glaucomatous TM cells. TGF- $\beta$ 2 is a known glaucoma stimulus and is elevated in the aqueous humour of POAG patients<sup>856</sup>, thus effects on gene expression that arise in response to this are of importance in understanding disease pathophysiology. Through Core analysis we demonstrate that among the large data set of differentially expressed genes, the majority are implicated in cytoskeletal and extracellular matrix remodelling of the human trabecular meshwork cells. TGF- $\beta$ 2 is implicated extensively in these processes<sup>243,537</sup>, interestingly however, both TGF- $\beta$ -related and -unrelated genes were identified in the TM in association to TGF- $\beta$ 2 stimulations. Comparison analyses further implicated RhoA signalling pathway in cytoskeletal re-organisation processes in the TM following exposure to TGF- $\beta$ 2. Rho/ROCK signalling pathway is a master regulator of the actin cytoskeleton and cell contractility<sup>434</sup>. Increased contractility in TM cells during glaucoma pathogenesis has previously been associated with ROCK signalling<sup>430</sup>, and increased contractility leads to a reduction in outflow facilities of the drainage angle<sup>469</sup>. Novel therapies are currently being developed and have entered clinical trials targeting ROCK1/2 in the RhoA pathway for their involvement in glaucoma pathogenesis<sup>787</sup>. Interestingly, we did not identify ROCK as being significantly enriched in our data set, and we believe this might be indicative of alternative pathway molecules downstream of ROCK having a more significant role in cytoskeletal remodelling of the TM. Current therapies have the sole aim of lowering intraocular pressure and do not address other contributing factors of the disease such as reduced ocular blood flow which in turn leads to retinal ganglion cell death. We have identified significantly altered genes that have been implicated in reduced ocular blood flow (EDN1, FST, NOX4). This provides us with a cohort of novel targets that if manipulated may reduce negative impacts on the aqueous humour outflow pathway and ocular blood flow in a promising step forward in developing new therapeutics for POAG.

As well as identification of differentially expressed genes associated with POAG, in Chapter 4, we describe the implications corticosteroids, namely dexamethasone, have on gene expression in human TM cells. Steroid-induced glaucoma is a result of enhanced ECM deposition and decreased matrix metalloproteinases in the TM<sup>199</sup>. Core analysis of differentially expressed genes in dexamethasone stimulated TM cells, demonstrated that the majority of the data set are involved in extracellular matrix remodelling, and glucocorticoid receptor modulation. Glucocorticoid receptor isoforms have been implicated in steroid responsiveness in glaucoma<sup>857</sup>. Preferential GR $\alpha$  expression over GR $\beta$  in TM cells of glaucoma patients suggests a role of GR $\alpha$  in steroid responsiveness in terms of IOP elevation<sup>572</sup>. We have identified FKBP51 gene as significantly up-regulated in our data-set in response to dexamethasone. FKBP51 is responsible for nuclear import of GR $\alpha$  and we believe up-regulation of this gene enhances steroid-responsiveness in glaucoma patients due to the suppression of GR $\beta$  expression. In addition, we further confirm the reduction of matrix metalloproteinases in TM cells in response to corticosteroids. MMP-1, a matrix metalloproteinase essential for the regular turnover of ECM, is significantly down-regulated in our data set. Down-regulation of MMPs results in elevated IOP caused by reduced outflow facility. A number of the differentially expressed genes that we have identified in the TM in response to dexamethasone have the potential to be manipulated therapeutically (MMP-1, FKBP51, PAI-2), lending substantial new information to drug development for steroid-induced glaucoma and indeed POAG where ECM turnover is also disrupted<sup>632,771,825</sup>.

Dysregulation of gene expression in response to stimuli can be regulated by miRNAs in the TM. There is increasing evidence for the role of miRNAs in the trabecular meshwork in health and glaucoma<sup>381</sup>. In Chapter 5 we identify the differential expression of three miRNAs: miR-145-5p, miR-143-3p, and miR-4328 in human TM cells in response to TGF- $\beta$ 2. The miR-143/145 cluster plays a fundamental role in vascular smooth muscle cell-like differentiation during both physiological and pathological events<sup>724,725</sup>. miR-143 and miR-145 mRNA targets are linked to the Rho signalling pathway, and are known to regulate actin dynamics in

the TM. A miRNA microarray of human TM cells stimulated with TGF- $\beta$ 2 and further RNA-Seq of human TM cells transfected with miR-143 and miR-145 inhibitors has strengthened the association of miR143/145 with the RhoA signalling pathway in glaucoma pathogenesis. Unfortunately, a number of differentially expressed genes identified by RNA-Seq following miR-143 and miR-145 inhibition were also differentially expressed in the presence of a scrambled negative control indicating the complex nature of miRNA manipulation, and the potential for a number of off target effects that must be considered before a therapeutic target can be inferred.

Several novel drugs are currently being developed for the treatment of glaucoma which have been discussed in Chapter 6. Across all three of our studies we have identified a number of novel therapeutic candidates that if manipulated may reduce pathological effects of glaucoma. As suggested previously, alternative molecules within the Rho signalling pathway may prove more effective targets over ROCK molecules. We have identified that both Lim kinase and IGF-1 are differentially expressed in our data set and manipulation of these molecules via inhibitors may be effective in reducing TM cytoskeletal re-organisation and contraction. Furthermore, EDN1 was significantly up-regulated in our data set in the presence of TGF- $\beta$ 2 and is also up-regulated in the AH of glaucoma patients. EDN1 is a potent vaso-constrictor involved in the contraction of TM cells and ischaemic insult in the eye. We propose that antagonism of EDN1 expression via its more potent receptor, ET<sub>A</sub>, has the potential not only reduce TM contractility but also by enhancing ocular blood flow and provide significant benefit in glaucoma treatment. A range of potential novel therapies have been discussed in Chapter 6 based on differentially expressed genes we have identified in TM cells stimulated with known glaucoma stimuli; TGF- $\beta$ 2 and dexamethasone. The majority of potential drug targets we have identified are involved in ECM remodelling, cytoskeletal remodelling, and enhanced ocular blood flow to reduce pathological effects of the disease.

This comprehensive characterisation of differentially expressed genes, associated with both POAG and steroid-induced glaucoma, provide us with an extensive data-set for future study. Manipulating both RhoA signalling associated molecules and other novel targets would address the pathophysiology of glaucoma and would be a significant advance on the current pharmacological IOP-lowering drugs.

All experiments throughout this thesis were performed using cultured human trabecular meshwork cells obtained from either whole donor eyes or corneal buttons. Preferentially, direct isolation of RNA from tissue would have been utilised, as this would provide a more realistic view of global gene expression of normal TM cells and circumvent effects of tissue culture. TM cells naturally occur in a labile environment, and are only exposed to a stiffer environment in disease states, such as glaucoma. Culturing TM cells directly on tissue culture plastic is a drastic change from their natural environment and should be considered for future work. As the trabecular meshwork ages, TM cellularity decreases. The TM tissue which can be successfully extracted from whole donor eyes and corneal buttons is relatively small in size. These two factors are contributors to the decision to culture the TM cells rather than opt for direct RNA extraction. For sequencing and microarray experiments, high quality and quantity of RNA is essential, therefore culturing of human TM cells to obtain optimal RNA quantities of high quality was essential for this thesis.

## Future Work

### (i) Functional Analysis of RNA-Seq Targets

While this PhD has added to the characterisation of differentially expressed genes associated with known glaucoma stimuli, TGF- $\beta$ 2 and dexamethasone, the functional significance of these differentially expressed genes remains unclear. Gene function can often be examined by defining when and where a gene is expressed within the cell. To evaluate this, the use of a reporter gene for specific

gene targets may be useful. Replacing the coding portion of the target gene with a reporter gene will allow for monitored tracking of its protein product. Furthermore, fluorescent in situ hybridisation (FISH) would be a powerful tool for assessing the expression and localisation of RNA as a sub cellular level in donor anterior segment whole mounts or trabecular meshwork tissue specimens. Direct RNA extraction from TM tissue would yield a better understanding of differential gene expression and omitting the input cell culture may have.

Targeted mutations can also be useful in revealing specific gene functions. A number of genes we have identified are found on known glaucoma loci and functional analyses of these may be useful in elucidating a role of these genes in glaucoma pathogenesis. Reverse genetics allows for the direct manipulation of a gene target *in vitro* which can then be transferred in to a cell where integration in to the chromosome occurs. This approach is useful in highlighting the phenotypic aspects associated with a mutant gene. In the same way that cells can be engineered to express a dominant negative version of the protein providing a loss-of-function phenotype, cells can also be engineered to display a gain-of-function mutation. To assess the exact effect of the specific genes we have identified in our RNA-Seq experiments on the TM gain-of-function analyses would allow us to decipher phenotypic changes induced by genes of interest.

We would also like to assess the impact of these genes on ECM deposition through protein analyses. Western blot is a useful tool in identifying protein expression which can then be quantified by flow cytometry. ECM proteins including collagens, fibronectin and GAGs, are elevated in the glaucomatous TM. We have identified genes that are responsible for the enhanced deposition of ECM. Protein analysis following TM cell exposure to specific genes of interest may indicate specific roles of genes in ECM deposition, and preferential expression of ECM components. Protein analysis will further implicate genes in glaucoma pathogenesis as well as provide a better insight in to their specific roles.

## (ii) miRNA Manipulations and Functional Analyses

In Chapter 5 we identified significantly differentially expressed miRNAs in the human TM stimulated with TGF- $\beta$ 2. Identification of putative targets in the TM for miR-143 and miR-145 proved difficult as no significant differential expression of validate mRNA targets was observed by q-PCR. Following this RNA-Seq of TM cells treated with TGF- $\beta$ 2 and miR-143 and miR-145 inhibitors identified a subset of uniquely differentially expressed genes when compared to TGF- $\beta$ 2 TM control cells. Interestingly, the scrambled negative control was shown to have significant off target effects. For future miRNA manipulation experiments we propose the use of stable over-expression of known-down of miRNAs with viral vectors. Viral vectors incorporate well in to TM cells and exert their effects for up to 3 weeks allowing for functional assays to be performed<sup>829</sup>.

It was known that miR-143 and miR-145 effect the actin cytoskeleton of the TM via  $\alpha$ -SMA and we further identified the down-regulation of  $\alpha$ -SMA in the presence of an miR-145 inhibitor. To further validate this relationship functional assays need to be performed. TM collagen gel contraction assays will allow for the assessment of miR-145 effects on TM cell contraction *in vitro*. In addition, actin structures are easily visualised by actin antibodies and fluorescent phalloidins in fixed cells. Pronounced actin staining is present in the TM of glaucomatous human eyes<sup>736</sup>, therefore re-organisation in the presence of TGF- $\beta$ 2 and phenotypic rescues following miRNA manipulation may be visualised in TM cells.

Stable transfection of miRNAs has proven difficult thus far and future investigation may benefit from cell sorting prior to progressing with experimentation. miRNA mimics and inhibitors have the potential to be fluorescently tagged without exerting undesirable effects or affecting q-PCR outcomes. Fluorescently tagged miRNAs within the cell would provide an opportunity to sort cells using flow cytometry and by-pass the contamination by the untransfected cell population. It is worth considering however, the low number of transfected cells that will be obtained may be further reduced through the use of flow and a greater yield, or pooling technique may need to be utilised.

Further investigation of miRNA function may be achieved through the use of the human anterior segment perfusion system. miRNAs can be delivered naked to the anterior segment using the perfusion system. IOP of perfused eye can be artificially altered using TGF- $\beta$ 2 and glucocorticoids, and continuous IOP read-outs may be obtained. The effects of miRNAs on IOP can be monitored in this way following naked delivery of miRNAs to the anterior segment, to assess for fluctuations or significant changes in IOP following miRNA treatment. These experiments could provide us with a more comprehensive idea of the *in situ* effects of miRNAs in the human trabecular meshwork.

### (iii) Novel Therapies and the Organ Culture System of the Anterior Segment

Recently we have established the human and porcine organ culture system of the anterior segment (Figure 7.1). Human and porcine anterior segments can be maintained on specialised petri dishes for up to 4 weeks which provides us with the means to assess the effects of our glaucoma stimuli of interest, TGF- $\beta$ 2 and dexamethasone, on the TM *in situ* to gain better physiological insights in to the effect these stimuli are having in glaucoma pathogenesis<sup>858</sup>. Furthermore, we could benefit here from direct RNA extraction from TM tissue following perfusion as well as isolating TM cells for single cell sequencing.

In Chapter 6 we describe the potential therapeutic gains of manipulation of differentially expressed genes identified by RNA-Seq in this PhD. MMP-1 was significantly down-regulated in response to dexamethasone in our corticosteroid-induced glaucoma study. Viral gene vectors have recently been described for steroid-inducible MMP-1 expression in the TM<sup>771</sup>. Over-expression of MMP-1 would also be beneficial in POAG where excess ECM deposition decreased outflow facility. Perfusion of the organ culture system with TGF- $\beta$ 2 to enhance ECM deposition similar to those effects observed in glaucoma, following perfusion with an MMP-1-inducible vector, similar to the MMP-1 vector described<sup>771</sup>, would allow for the assessment of gene viral vectors as potential therapeutic strategies based on their effect on TM morphology *in situ*.

Perfusion of anterior segments with miR-145 and or miR-143 offers us the opportunity to assess drug concentrations, as well as, their ability to regulate TM contractility, regulate IOP, and ECM production and in a physiological environment. Furthermore, packaging of miRNAs must be considered. This model can also be employed to assess miRNA delivery using different strategies. miRNAs can be delivered naked to the eye exterior and exert desired effects on tissue locally<sup>853</sup>. Other delivery technologies including nanoparticles<sup>844</sup> and peptide-gels<sup>859</sup> can be assessed in this model, as well as, their effect *in situ* in the TM to elucidate their therapeutic potential. Perfusion systems are useful as they allow for characterisation of the same TM *in situ* both before and following and following the experiment, this is crucial in truly identifying phenotypic changes that may be occurring in the tissue in response to stimuli and drugs.

#### (iv) Target Genes and Pathways

A number of potential therapeutic targets were identified throughout this thesis in relation to both glaucoma stimuli, TGF- $\beta$ 2 and dexamethasone. A common factor across all three chapters was the potential involvement of the RhoA signalling pathway in glaucoma pathogenesis. Future work should focus on elucidating the key RhoA related proteins that are dysregulated in glaucoma pathogenesis and investigate the ability of miRNA143 and miR-145 to enhance or subdue their expression. ROCK1 and ROCK2 inhibitors have already been developed and are currently being investigated in clinical trials and through perfusion systems for the roles in decreasing IOP. We have not identified ROCK1 or ROCK2 as significantly enriched in our dataset, however we have identified LIMK as significantly enriched, another pivotal player in the RhoA signalling pathway. It would be of interest to investigate the potential role of LIMK in human TM cells particularly following TGF- $\beta$ 2 and dexamethasone treatment.

As well as investigating the RhoA signalling pathway, future work should be focused on manipulation of identified mRNA targets. NOX4 is of particular interest as it has already been shown to be successfully regulated by miRNAs and is involved in aspects of glaucoma that are not currently being treated. Oxidative stress

contributes to the loss of RGCs and this is not currently modifiable by any available drug therapy. Regulation of chronic NOX4 expression is promising and will have largely beneficial antioxidant effects within the TM. It may be of interest to induce oxidative stress in TM cells and investigate the time frame under which NOX4 chronic expression occurs. Following oxidative stress manipulations of NOX4 with miRNAs would be key experiments in order to restore normal function and prevent cellular loss.

The datasets generated throughout this thesis have provided the field with a number of potential therapeutic targets some of which have novel outcomes that have not yet been addressed in glaucoma. Alternative targets provide unprecedented benefits when tackling a multifaceted disease such as glaucoma.

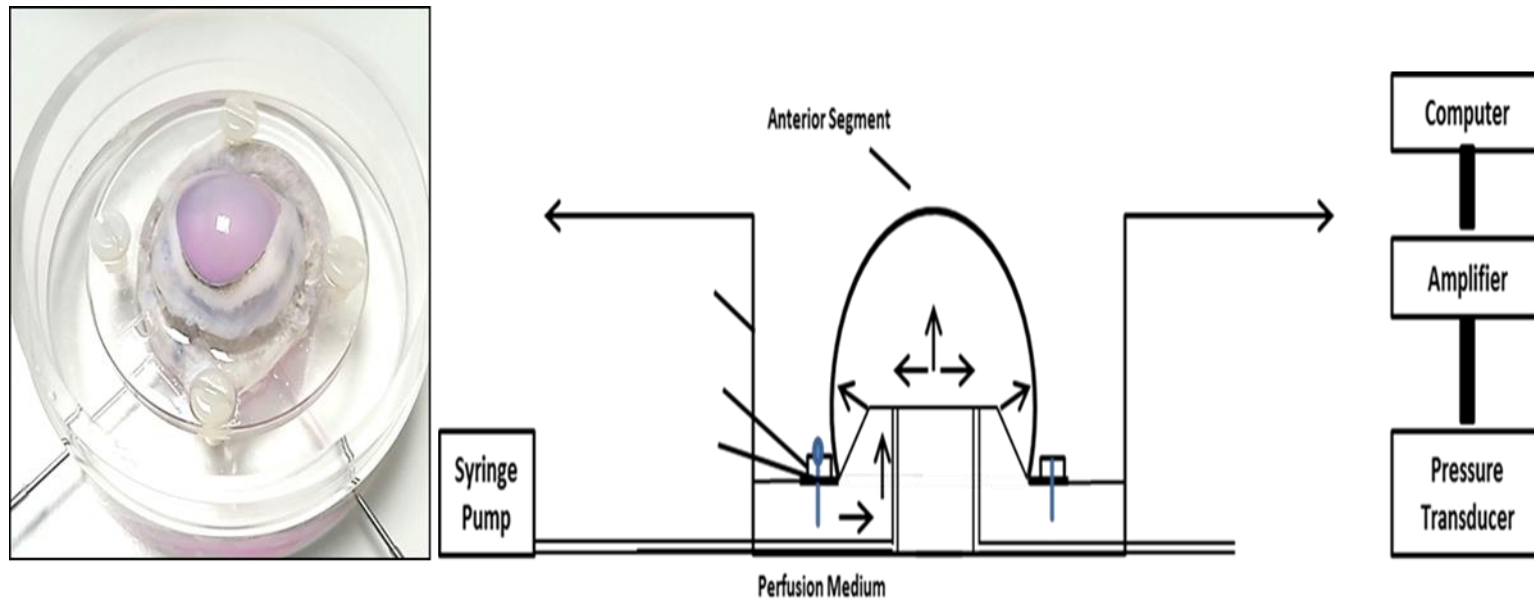


**Figure 7.1: Anterior Segment Organ Culture Perfusion Setup.** Whole globes are bisected and anterior segments are maintained in culture in a modified perfusion chamber. IOP is constantly monitored and *in situ* evaluation of drug targets can be performed following the experiment

1. Resnikoff, S. *et al.* Global data on visual impairment in the year 2002. *Bull. World Health Organ.* **82**, 844–51 (2004).
2. Giangiaco, A. & Coleman, A. L. The epidemiology of glaucoma. *J. Fr. Ophthalmol.* **28 Spec No**, 2S9-S2S12 (2005).
3. Glaucoma Research Foundation. Types of Glaucoma | . at <<https://www.glaucoma.org/glaucoma/types-of-glaucoma.php>>
4. Montana, C. L. & Bhorade, A. M. Glaucoma and quality of life. *Curr. Opin. Ophthalmol.* **29**, 1 (2017).
5. Quaranta, L. *et al.* Quality of Life in Glaucoma: A Review of the Literature. *Adv. Ther.* **33**, 959–981 (2016).
6. Foster, P. J., Buhrmann, R., Quigley, H. A. & Johnson, G. J. The definition and classification of glaucoma in prevalence surveys. *Br. J. Ophthalmol.* **86**, 238–242 (2002).
7. Chen, S.-J., Lu, P., Zhang, W.-F. & Lu, J.-H. High myopia as a risk factor in primary open angle glaucoma. *Int. J. Ophthalmol.* **5**, 750–3 (2012).
8. Mohamed-Noor, J. & Abd-Salam, D. Refractive errors and biometry of primary angle-closure disease in a mixed Malaysian population. *Int. J. Ophthalmol.* **10**, 1246–1250 (2017).
9. Kokotas, H. *et al.* Biomarkers in primary open angle glaucoma. *Clin. Chem. Lab. Med.* **50**, 2107–2119 (2012).
10. Kwon, Y. H., Fingert, J. H., Kuehn, M. H. & Alward, W. L. Primary open-angle glaucoma. *N Engl J Med* **360**, 1113–24 (2009).

11. Nickells, R. W. Apoptosis of Retinal Ganglion Cells in Glaucoma. *Surv. Ophthalmol.* **43**, S151–S161 (1999).
12. He, Z., Vingrys, A. J., Armitage, J. A. & Bui, B. V. The role of blood pressure in glaucoma. *Clin. Exp. Optom.* **94**, 133–149 (2011).
13. Managed Care Eye Institute. Coats of the Eye - Optic Disc and Nerve. at [http://teaching.pharmacy.umn.edu/courses/eyeAP/Eye\\_Anatomy/CoatsoftheEye/OpticDiscandNerve.htm](http://teaching.pharmacy.umn.edu/courses/eyeAP/Eye_Anatomy/CoatsoftheEye/OpticDiscandNerve.htm)
14. Williams, S. E. I., Bch, M. B., Sa, F. & Edin, F. Diagnosis of glaucoma. *Cme* **25**, 464–468 (2007).
15. Gupta, P. K., Asrani, S., Freedman, S. F., El-Dairi, M. & Bhatti, M. T. Differentiating glaucomatous from non-glaucomatous optic nerve cupping by optical coherence tomography. *Open Neurol. J.* **5**, 1–7 (2011).
16. Weinreb, R., Aung, T. & Medeiros, F. The pathophysiology and treatment of glaucoma. *J. Am. Med. Assoc.* **311**, 1901–1911 (2014).
17. Broadway, D. C. Visual field testing for glaucoma - a practical guide. *Community Eye Health* **25**, 66–70 (2012).
18. Drance, S. M. The glaucomatous visual field. *Br. J. Ophthalmol.* **56**, 186–200 (1972).
19. Zalta, A. H. Use of a central 10 degrees field and size V stimulus to evaluate and monitor small central islands of vision in end stage glaucoma. *Br. J. Ophthalmol.* **75**, 151–4 (1991).

20. Gloster, J. Quantitative relationship between cupping of the optic disc and visual field loss in chronic simple glaucoma. *Br. J. Ophthalmol.* **62**, 665–669 (1978).
21. Prum, B. E. *et al.* Primary Open-Angle Glaucoma. *Ophthalmology* **123**, P41–P111 (2016).
22. The Physics Classroom. The Critical Angle. at <http://www.physicsclassroom.com/class/refrn/Lesson-3/The-Critical-Angle>
23. Goldsmith, A. J. . Discussion of Gonioscopy. 1013–1025 (1950).
24. Smith, S. D. *et al.* Evaluation of the anterior chamber angle in glaucoma: A report by the American Academy of Ophthalmology. *Ophthalmology* **120**, 1985–1997 (2013).
25. Salim, S. The role of anterior segment optical coherence tomography in glaucoma. *J. Ophthalmol.* **2012**, (2012).
26. American Academy of Ophthalmology. Primary Open-Angle Glaucoma - Latin America -. at <https://www.aao.org/topic-detail/primary-openangle-glaucoma--latin-america#figure7>
27. Glaucoma Associates of Texas. Types of Glaucoma. at <http://glaucomaassociates.com/glaucoma/types-of-glaucoma/>
28. Foundation, E. G. S. *Terminology and Guidelines for Glaucoma*. (2015). at [www.unaids.org/sites/default/files/media.../2015\\_terminology\\_guidelines\\_en.](http://www.unaids.org/sites/default/files/media.../2015_terminology_guidelines_en.)
29. Powell, S. Updated glaucoma guidance raises IOP benchmark. at

<<https://www.aop.org.uk/ot/professional-support/clinical-and-regulatory/2017/11/08/updated-glaucoma-guidance-raises-iop-benchmark>>

30. American Academy of Ophthalmology. Goldmann Tonometer Remains Gold Standard for Measuring IOP - American Academy of Ophthalmology. at <<https://www.aao.org/eyenet/academy-live/detail/goldmann-tonometer-remains-gold-standard-iop>>
31. Moodie, J., Wilde, C., Rotchford, A. P., Vernon, S. A. & King, A. J. 24-Hour Versus Daytime Intraocular Pressure Phasing in the Management of Patients With Treated Glaucoma. *Br. J. Ophthalmol.* **94**, 999–1002 (2010).
32. Kim, M. S., Kim, J. M., Park, K. H. & Choi, C. Y. Asymmetry of diurnal intraocular pressure fluctuation between right and left eyes. *Acta Ophthalmol.* **89**, 352–357 (2011).
33. Agarwal, R., Gupta, S. K., Agarwal, P., Saxena, R. & Agrawal, S. S. Current concepts in the pathophysiology of glaucoma. *Indian J. Ophthalmol.* **57**, 257–66 (2009).
34. Piltz-Seymour, J. & Tania Tai, T. Y. Secondary Glaucomas. *Glaucoma Second Ed.* **1**, 434–445 (2014).
35. Foster, C. S. Secondary glaucoma. 190–194 (2000).
36. Bodh, S. A., Kumar, V., Raina, U. K., Ghosh, B. & Thakar, M. Inflammatory glaucoma. *Oman J. Ophthalmol.* **4**, 3–9 (2011).
37. Andreatta, W., Boukouvala, S. & Bansal, A. Combined Acute Haemolytic and Secondary Angle Closure Glaucoma following

- Spontaneous Intraocular Haemorrhages in a Patient on Warfarin. *Case Rep. Ophthalmol.* **7**, 233–238 (2016).
38. Barac, I. R., Pop, M. D., Gheorghe, A. I. & Taban, C. Neovascular Secondary Glaucoma, Etiology and Pathogenesis. *Rom. J. Ophthalmol.* **59**, 24–28 (2015).
  39. Thylefors, B. & Negrej, A. The global impact of glaucoma. *World Health* **72**, 323–326 (1994).
  40. Distefano, M. D. Gender and Glaucoma: what we know and what we need to know. **21**, 213–223 (2015).
  41. Quigley, H. A. & Broman, A. T. The number of people with glaucoma worldwide in 2010 and 2020. *Br. J. Ophthalmol.* **90**, 262–7 (2006).
  42. Tielsch, J. M. The Epidemiology and Control of Open Angle Glaucoma: A Population-Based Perspective. *Annu. Rev. Public Health* **17**, 121–136 (1996).
  43. Jonasson, F. *et al.* Prevalence of open- angle glaucoma in Iceland: Reykjavik Eye Study. at <https://www.nature.com/eye/journal/v17/n6/pdf/6700374a.pdf>  
>
  44. Coffey, M. *et al.* Prevalence of glaucoma in the west of Ireland Glaucoma is a major cause of irreversible. *British Journal of Ophthalmology* *BrJ Ophthalmol* **77**, 17–21 (1993).
  45. Dielemans, I. *et al.* The prevalence of primary open-angle glaucoma in a population-based study in The Netherlands. The

- Rotterdam Study. *Ophthalmology* **101**, 1851–5 (1994).
46. Mitchell, P., Smith, W., ttebo, K. A., Healey, P. R. & Sci, Bm. Prevalence of Open--angle Glaucoma in Australia The Blue Mountains Eye Study. *Ophthalmology* **103**, 1661–1669 (1996).
  47. Wensor, M. D., McCarty, C. A., Stanislaosky, Y. L., Livingston, P. M. & Taylor, H. R. The Prevalence of Glaucoma in the Melbourne Visual Impairment Project. at <[https://ac.els-cdn.com/S0161642098940313/1-s2.0-S0161642098940313-main.pdf?\\_tid=74d68dca-c08a-11e7-b42f-00000aab0f02&acdnat=1509708836\\_e732464efd86eda0eb2a589556f8f36d](https://ac.els-cdn.com/S0161642098940313/1-s2.0-S0161642098940313-main.pdf?_tid=74d68dca-c08a-11e7-b42f-00000aab0f02&acdnat=1509708836_e732464efd86eda0eb2a589556f8f36d)>
  48. Klein, Barbara; Menage, M. . Prevalence of Glaucoma: The Beaver Dam Eye Study. *Ophthalmology* **99**, 1499–1504 (1992).
  49. Leske, M. C., Connell, A. M. S., Schachat, A. P. & Hyman, L. The Barbados Eye Study. *Arch. Ophthalmol.* **112**, 821 (1994).
  50. Ramakrishnan, R. *et al.* Glaucoma in a Rural Population of Southern India The Aravind Comprehensive Eye Survey. *Ophthalmology* **110**, 1484–1490 (2003).
  51. George, R. *et al.* The Chennai glaucoma study: prevalence and risk factors for glaucoma in cataract operated eyes in urban Chennai. *Indian J. Ophthalmol.* **58**, 243–5 (2010).
  52. Jonas, J. B. *et al.* Glaucoma. *Lancet* **390**, 2183–2193 (2017).
  53. Foundation, E. G. S. in *The Guideline Project* (2014).
  54. Gordon, M. O. *et al.* The Ocular Hypertension Treatment Study:

- baseline factors that predict the onset of primary open-angle glaucoma. *Arch. Ophthalmol. (Chicago, Ill. 1960)* **120**, 714-20-30 (2002).
55. Group, T. E. G. P. S. (EGPS). The European Glaucoma Prevention Study Design and Baseline Description of the Participants. *Ophthalmology* **109**, 1612–1621 (2002).
  56. Tuck, M. W. & Crick, R. P. The age distribution of primary open angle glaucoma. *Ophthalmic Epidemiol.* **5**, 173–183 (1998).
  57. Rudnicka, A. R., Mt.-Isa, S., Owen, C. G., Cook, D. G. & Ashby, D. Variations in primary open-angle glaucoma prevalence by age, gender, and race: A Bayesian meta-analysis. *Investig. Ophthalmol. Vis. Sci.* **47**, 4254–4261 (2006).
  58. Leske, M. C., Wu, S.-Y., Hennis, A., Honkanen, R. & Nemesure, B. Risk Factors for Incident Open-angle Glaucoma The Barbados Eye Studies. *Ophthalmology* **115**, 85–93 (2008).
  59. Sommer, A. Glaucoma risk factors observed in the Baltimore Eye Survey. *Curr Opin Ophthalmol* **7**, 93–98 (1996).
  60. Leibowitz, H. M. *et al.* The Framingham Eye Study monograph: An ophthalmological and epidemiological study of cataract, glaucoma, diabetic retinopathy, macular degeneration, and visual acuity in a general population of 2631 adults, 1973-1975. *Surv. Ophthalmol.* **24**, 335–610
  61. Maunder, L. R. to the Monograph. **24**, 614–620 (1960).
  62. Hulsman, C. A. *et al.* Is open-angle glaucoma associated with early

- menopause? The Rotterdam Study. *Am. J. Epidemiol.* **154**, 138–44 (2001).
63. Ogueta, S. B., Schwartz, S. D., Yamashita, C. K. & Farber, D. B. *Estrogen Receptor in the Human Eye: Influence of Gender and Age on Gene Expression. Investigative Ophthalmology & Visual Science* **40**, (C.V. Mosby Co, 1977).
64. Higginbotham, E. J. Does sex matter in glaucoma? *Arch. Ophthalmol.* **122**, 374–5 (2004).
65. Bhopal, R. Glossary of terms relating to ethnicity and race: for reflection and debate. *J. Epidemiol. Community Heal.* **58**, 441–445 (2004).
66. Salowe, R. *et al.* Primary Open-Angle Glaucoma in Individuals of African Descent: A Review of Risk Factors. *J. Clin. Exp. Ophthalmol.* **6**, 1–13 (2015).
67. Huck, A. *et al.* Vascular considerations in glaucoma patients of African and European descent. *Acta Ophthalmol.* **92**, 1–11 (2014).
68. Kosoko-Lasaki, O., Gong, G., Haynatzki, G. & Wilson, M. R. Race, ethnicity and prevalence of primary open-angle glaucoma. *J. Natl. Med. Assoc.* **98**, 1626–1629 (2006).
69. Kosoko-Lasaki, O., Gong, G., Haynatzki, G. & Wilson, M. R. Race, ethnicity and prevalence of primary open-angle glaucoma. *J. Natl. Med. Assoc.* **98**, 1626–1629 (2006).
70. Subcommittee on Definition and Prevalence of the 1984 National Committee. Hypertension prevalence and the states of

- awareness, treatment and control in the United States. Hypertension. **7**, 457–468. (1985).
71. Moore, D., Harris, A., Wudunn, D., Kheradiya, N. & Siesky, B. Dysfunctional regulation of ocular blood flow: A risk factor for glaucoma? *Clin. Ophthalmol.* **2**, 849–61 (2008).
  72. Hayreh, S. S. Posterior Ciliary Artery Circulation in Health and Disease The Weisenfeld Lecture. *Investig. Ophthalmology Vis. Sci.* **45**, 749 (2004).
  73. Costa, V. P. *et al.* Ocular perfusion pressure in glaucoma. *Acta Ophthalmol.* **92**, 252–266 (2014).
  74. Fuchsjager-Mayrl, G. *et al.* Ocular blood flow and systemic blood pressure in patients with primary open-angle glaucoma and ocular hypertension. *Invest Ophthalmol Vis Sci* **45**, 834–839 (2004).
  75. Mitchell, P., Lee, A. J., Rochtchina, E. & Wang, J. J. Open-angle glaucoma and systemic hypertension: the blue mountains eye study. *J. Glaucoma* **13**, 319–326 (2004).
  76. Chung, H. J., Hwang, H. Bin & Lee, N. Y. The association between primary open-angle glaucoma and blood pressure: Two aspects of hypertension and hypotension. *Biomed Res. Int.* **2015**, (2015).
  77. Kim, S. W. & Kang, G. W. Diabetes mellitus as a risk factor for glaucoma outcome in Korea. *Acta Ophthalmol.* **95**, e662–e664 (2017).
  78. Lavaju, P., Shah, S., Sharma, S. & Maskey, R. Diabetes Mellitus and the risk of Primary open angle glaucoma. *Nepal. J. Ophthalmol.* **9**,

17 (2017).

79. Shen, L., Walter, S., Melles, R. B., Maria Glymour, M. & Jorgenson, E. Original Contribution Diabetes Pathology and Risk of Primary Open-Angle Glaucoma: Evaluating Causal Mechanisms by Using Genetic Information. doi:10.1093/aje/kwv204
80. Bonovas, S., Peponis, V. & Filioussi, K. Diabetes mellitus as a risk factor for primary open-angle glaucoma: a meta-analysis. *Diabet. Med.* **21**, 609–14 (2004).
81. Leffler, C. T., Schwartz, S. G., Hadi, T. M., Salman, A. & Vasuki, V. The early history of glaucoma: The glaucous eye (800 BC to 1050 AD). *Clin. Ophthalmol.* **9**, 207–215 (2015).
82. Actis, A. G., Versino, E., Brogliatti, B. & Rolle, T. Risk Factors for Primary Open Angle Glaucoma (POAG) Progression: A Study Ruled in Torino. *Open Ophthalmol. J.* **10**, 129–139 (2016).
83. van der Valk, R. *et al.* Intraocular Pressure–Lowering Effects of All Commonly Used Glaucoma Drugs: A Meta-analysis of Randomized Clinical Trials. *Ophthalmology* **112**, 1177–1185 (2005).
84. Heijl, A. *et al.* Reduction of intraocular pressure and glaucoma progression: results from the Early Manifest Glaucoma Trial. *Arch. Ophthalmol. (Chicago, Ill. 1960)* **120**, 1268–79 (2002).
85. Goel, M., Picciani, R. G., Lee, R. K. & Bhattacharya, S. K. Aqueous Humor Dynamics : A Review. 52–59 (2010).
86. To, C. H., Kong, C. W., Chan, C. Y., Shahidullah, M. & Do, C. W. The mechanism of aqueous humour formation. *Clin. Exp. Optom.* **85**,

- 335–349 (2002).
87. American Academy of Ophthalmology. Aqueous Humor Formation. at <https://www.aaopt.org/bcscsnippetdetail.aspx?id=591e80abe372-4ad3-9c49-1aed4ba74f61>
  88. Fujita\*, H., Kondo, K. & Sears, M. A New Function of Non-pigmented Epithelium of Ciliary Processes in the Formation of Aqueous Humor. *Klin. Monbl. Augenheilkd.* **185**, 28–34 (1984).
  89. Gabelt, B'Ann Kiland, Julie A. Tian, Baohe Kaufman, P. L. Aqueous Humor: Secretion and Dynamics | Ento Key. at <https://entokey.com/aqueous-humor-secretion-and-dynamics/>
  90. Uusitalo, R., Palkama, A. & Stjernschantz, J. An electron microscopical study of the blood-aqueous barrier in the ciliary body and iris of the rabbit. *Exp. Eye Res.* **17**, 49–63 (1973).
  91. Pizzirani, S. & Gong, H. Functional Anatomy of the Outflow Facilities. *Vet. Clin. North Am. - Small Anim. Pract.* **45**, 1101–1126 (2015).
  92. Mollajew, R. *et al.* Routes of epithelial water flow: aquaporins versus cotransporters. *Biophys. J.* **99**, 3647–56 (2010).
  93. Schey, K. L., Wang, Z., L Wenke, J. & Qi, Y. Aquaporins in the eye: expression, function, and roles in ocular disease. *Biochim. Biophys. Acta* **1840**, 1513–23 (2014).
  94. Dobbs, P. C., Epstein, D. L. & Anderson, P. J. Identification of isoenzyme C as the principal carbonic anhydrase in human ciliary

- processes. *Invest. Ophthalmol. Vis. Sci.* **18**, 867–70 (1979).
95. Kleineller, A., Fambrough, D. M. & Benos, D. J. *The Eye's Aqueous Humor : From Secretion to Glaucoma*. (Elsevier, 1997). at [https://books.google.co.uk/books?id=y8UI0i-F4YsC&pg=PA25&lpg=PA25&dq=Molecular+approaches+to+the+study+of+the+Na%2B-K%2B-ATPase+and+chloride+channels+in+the+ocular+ciliary+epithelium&source=bl&ots=glg1AutJT8&sig=sC8P0RHmAokj0Q84odeRrbIGkm4&hl=en&sa=X&ved=0ahUKEwis-u\\_D04LaAhWMSsAKHX65BAYQ6AEIYjAE#v=onepage&q=Molecular approaches to the study of the Na%2B-K%2B-ATPase and chloride channels in the ocular ciliary epithelium&f=false](https://books.google.co.uk/books?id=y8UI0i-F4YsC&pg=PA25&lpg=PA25&dq=Molecular+approaches+to+the+study+of+the+Na%2B-K%2B-ATPase+and+chloride+channels+in+the+ocular+ciliary+epithelium&source=bl&ots=glg1AutJT8&sig=sC8P0RHmAokj0Q84odeRrbIGkm4&hl=en&sa=X&ved=0ahUKEwis-u_D04LaAhWMSsAKHX65BAYQ6AEIYjAE#v=onepage&q=Molecular+approaches+to+the+study+of+the+Na%2B-K%2B-ATPase+and+chloride+channels+in+the+ocular+ciliary+epithelium&f=false)
  96. Becker, B. *Vanadate and Aqueous Humor Dynamics-Proctor Lecture. Investigative Ophthalmology & Visual Science* **19**, (C.V. Mosby Co, 1977).
  97. Marcel, Y., Seidler, R. W., Stone, R. A. & Civan, M. M. *Inhibitors of NHE-1 Na<sup>+</sup>/H<sup>+</sup> Exchange Reduce Mouse Intraocular Pressure. Investigative Ophthalmology & Visual Science* **43**, (C.V. Mosby Co, 1977).
  98. Murthy, K. R. *et al.* Proteomics of human aqueous humor. *OMICS* **19**, 283–93 (2015).
  99. Perumal, N. *et al.* Characterization of the human aqueous humour proteome: A comparison of the genders. *PLoS One* **12**, 1–15 (2017).
  100. Tripathi, R. C., Borisuth, N. S. C. & Tripathi, B. J. Growth factors in

- the aqueous humor and their therapeutic implications in glaucoma and anterior segment disorders of the human eye. *Drug Dev. Res.* **22**, 1–23 (1991).
101. Mihaylova, B. et al. Plasma Endothelin-1 and Endothelin-A receptor concentrations in patients with POAG. (2017). doi:10.1080/13102818.2017.1334592
  102. Malina, H. Z. & Martin, X. D. Indoleamine 2,3-dioxygenase activity in the aqueous humor, iris/ciliary body, and retina of the bovine eye. *Graefes Arch. Clin. Exp. Ophthalmol.* **231**, 482–6 (1993).
  103. Ophthalmology, A. A. of. Fundamentals and Principles of Ophthalmology Section 2. 362 (1991).
  104. Tripathi, R. C., Park, J. K., Tripathi, B. J. & Millard, C. B. Tissue plasminogen activator in human aqueous humor and its possible therapeutic significance. *Am. J. Ophthalmol.* **106**, 719–22 (1988).
  105. Kiel, J. W., Hollingsworth, M., Rao, R., Chen, M. & Reitsamer, H. A. Ciliary blood flow and aqueous humor production. *Prog. Retin. Eye Res.* **30**, 1–17 (2011).
  106. Stárka, L., Hampl, R., Bicíková, M. & Obenberger, J. Identification and radioimmunologic estimation of sexual steroid hormones in aqueous humor and vitreous of rabbit eye. *Albrecht Von Graefes Arch. Klin. Exp. Ophthalmol.* **199**, 261–6 (1976).
  107. Navajas, E. V. et al. Concentration of hyaluronic acid in primary open-angle glaucoma aqueous humor. *Exp. Eye Res.* **80**, 853–857 (2005).

108. Wang, Y.-L., Hayashi, M., Yablonski, M. E. & Toris, C. B. Effects of Multiple Dosing of Epinephrine on Aqueous Humor Dynamics in Human Eyes. *J. Ocul. Pharmacol. Ther.* **18**, 53–63 (2002).
109. Smith, S. D. Measurement of the Rate of Aqueous Humor Flow. *YALE J. Biol. Med.* **64**, 89–102 (1991).
110. Brubaker, R. F. Measurement of uveoscleral outflow in humans. *J. Glaucoma* **10**, S45-8 (2001).
111. Fautsch, M. P. & Johnson, D. H. Aqueous humor outflow: what do we know? Where will it lead us? *Invest. Ophthalmol. Vis. Sci.* **47**, 4181–7 (2006).
112. Gabelt, B. T. & Kaufman, P. L. Changes in aqueous humor dynamics with age and glaucoma. *Prog. Retin. Eye Res.* **24**, 612–637 (2005).
113. Ou, Y. Glaucoma and the Importance of the Eye’s Drainage System | BrightFocus Foundation. at <<https://www.brightfocus.org/glaucoma/article/glaucoma-and-importance-eyes-drainage-system>>
114. Overby, D. R. *et al.* The Structure of the Trabecular Meshwork, Its Connections to the Ciliary Muscle, and the Effect of Pilocarpine on Outflow Facility in Mice. *Investig. Ophthalmology Vis. Sci.* **55**, 3727 (2014).
115. Abu-Hassan, D. W., Acott, T. S. & Kelley, M. J. The Trabecular Meshwork: A Basic Review of Form and Function. *J. Ocul. Biol.* **2**, (2014).

116. Vranka, J. A., Kelley, M. J., Acott, T. S. & Keller, K. E. Extracellular matrix in the trabecular meshwork: Intraocular pressure regulation and dysregulation in glaucoma. *Exp. Eye Res.* **133**, 112–125 (2015).
117. Llobet, A., Gasull, X. & Gual, A. Understanding trabecular meshwork physiology: a key to the control of intraocular pressure? *News Physiol. Sci.* **18**, 205–9 (2003).
118. Tektas, O.-Y. & Lütjen-Drecoll, E. Structural changes of the trabecular meshwork in different kinds of glaucoma. *Exp. Eye Res.* **88**, 769–775 (2009).
119. Vranka, J. A., Kelley, M. J., Acott, T. S. & Keller, K. E. Extracellular matrix in the trabecular meshwork: intraocular pressure regulation and dysregulation in glaucoma. *Exp. Eye Res.* **133**, 112–25 (2015).
120. Keller, K. E. & Acott, T. S. The Juxtacanalicular Region of Ocular Trabecular Meshwork: A Tissue with a Unique Extracellular Matrix and Specialized Function. at <https://www.ncbi.nlm.nih.gov/pmc/articles/PMC3867143/pdf/nihms-520258.pdf>
121. Lutjen-Drecoll, E., Futa, R. & Rohen, J. W. Ultrahistochemical studies on tangential sections of the trabecular meshwork in normal and and glaucomatous eyes. *Investig. Ophthalmol. Vis. Sci.* **21**, 563–573 (1981).
122. Acott, T. S. *et al.* Intraocular pressure homeostasis: maintaining balance in a high-pressure environment. *J. Ocul. Pharmacol. Ther.*

**30**, 94–101

123. Lütjen-Drecoll, E., Shimizu, T., Rohrbachand, M. & Rohen, J. W. Quantitative Analysis of 'Plaque Material' Between Ciliary Muscle Tips in Normal- and Glaucomatous Eyes. *Eye Res* **42**, 457–465 (1986).
124. Tamm, E. R. The trabecular meshwork outflow pathways: Structural and functional aspects. *Exp. Eye Res.* **88**, 648–655 (2009).
125. Johnson, M. 'What controls aqueous humour outflow resistance?'. *Exp. Eye Res.* **82**, 545–57 (2006).
126. Keller, K. E. & Acott, T. S. The Juxtacanalicular Region of Ocular Trabecular Meshwork: A Tissue with a Unique Extracellular Matrix and Specialized Function. *J. Ocul. Biol.* **1**, 3 (2013).
127. Ueda, J., Wentz-Hunter, K. & Yue, B. Y. J. T. Distribution of myocilin and extracellular matrix components in the juxtacanalicular tissue of human eyes. *Invest. Ophthalmol. Vis. Sci.* **43**, 1068–76 (2002).
128. Hann, C. R., Springett, M. J., Wang, X. & Johnson, D. H. Ultrastructural Localization of Collagen IV, Fibronectin, and Laminin in the Trabecular Meshwork of Normal and Glaucomatous Eyes GL 61L TM Extracellular Matrix. *Ophthalmic Res* **3333**, (2001).
129. Acott, T. S. *et al.* Intraocular pressure homeostasis: maintaining balance in a high-pressure environment. *J. Ocul. Pharmacol. Ther.*

- 30**, 94–101 (2014).
130. Tamm, E. R. & Fuchshofer, R. What Increases Outflow Resistance in Primary Open-angle Glaucoma? *Surv. Ophthalmol.* **52**, 101–104 (2007).
  131. Winkler, N. S. & Fautsch, M. P. Effects of prostaglandin analogues on aqueous humor outflow pathways. *J. Ocul. Pharmacol. Ther.* **30**, 102–9 (2014).
  132. Gold, M. E. *et al.* Age-related changes in trabecular meshwork imaging. *Biomed Res. Int.* **2013**, (2013).
  133. Babizhayev, M. A. & Brodskaya, M. W. Fibronectin detection in drainage outflow system of human eyes in ageing and progression of open-angle glaucoma. *Mech. Ageing Dev.* **47**, 145–57 (1989).
  134. Freddo, F. Age-related Changes of Sulfated Proteoglycans Human Trabecular Meshwork in the Normal. 691–709 (1992).
  135. Knepper, P. A., Goossens, W., Hvizd, M. & Palmberg, P. F. Glycosaminoglycans of the human trabecular meshwork in primary open-angle glaucoma. *Investig. Ophthalmol. Vis. Sci.* **37**, 1360–1367 (1996).
  136. Boldea, R. C., Roy, S. & Mermoud, A. Ageing of Schlemm's canal in nonglaucomatous subjects. *Int. Ophthalmol.* **24**, 67–77 (2002).
  137. Han, X. *et al.* Age-Related Changes of Intraocular Pressure in Elderly People in Southern China: Lingtou Eye Cohort Study. *PLoS One* **11**, e0151766 (2016).
  138. Nomura, H., Shimokata, H., Ando, F., Miyake, Y. & Kuzuya, F. Age-

- related changes in intraocular pressure in a large Japanese population: a cross-sectional and longitudinal study. *Ophthalmology* **106**, 2016–22 (1999).
139. Baek, S. U., Kee, C. & Suh, W. Longitudinal analysis of age-related changes in intraocular pressure in South Korea. *Eye (Lond)*. **29**, 625–9 (2015).
140. Zhao, D. *et al.* A longitudinal study of age-related changes in intraocular pressure: the Kangbuk Samsung Health Study. *Invest. Ophthalmol. Vis. Sci.* **55**, 6244–50 (2014).
141. Vecino, E., Rodriguez, F. D., Ruzafa, N., Pereiro, X. & Sharma, S. C. Glia-neuron interactions in the mammalian retina. *Prog. Retin. Eye Res.* **51**, 1–40 (2016).
142. Wang, W., Tan, M., Yu, J. & Tan, L. Role of pro-inflammatory cytokines releases from microglia in Alzheimer’s disease. **3**, 1–15 (2015).
143. Rawji, K. S. *et al.* Immunosenescence of microglia and macrophages: Impact on the ageing central nervous system. *Brain* **139**, 653–661 (2016).
144. Harwerth, R. S., Wheat, J. L. & Rangaswamy, N. V. Age-Related Losses of Retinal Ganglion Cells and Axons. *Investig. Ophthalmology Vis. Sci.* **49**, 4437 (2008).
145. Patel, N. B., Lim, M., Gajjar, A., Evans, K. B. & Harwerth, R. S. Age-associated changes in the retinal nerve fiber layer and optic nerve head. *Investig. Ophthalmol. Vis. Sci.* **55**, 5134–5143 (2014).

146. Formichella, C. R., Abella, S. K., Sims, S. M., Cathcart, H. M. & Sappington, R. M. Astrocyte Reactivity: A Biomarker for Retinal Ganglion Cell Health in Retinal Neurodegeneration. *J Clin Cell Immunol* **5**,
147. Hernandez, M. R. The optic nerve head in glaucoma: Role of astrocytes in tissue remodeling. *Prog. Retin. Eye Res.* **19**, 297–321 (2000).
148. Kotecha, A., Izadi, S. & Jeffery, G. Age-related changes in the thickness of the human lamina cribrosa. *Br J Ophthalmol* **90**, 1531–1534 (2006).
149. Hernandez, M. R., Luo, X. X., Andrzejewska, W. & Neufeld, A. H. Age-Related Changes in the Extracellular Matrix of the Human Optic Nerve Head. *Am. J. Ophthalmol.* **107**, 476–484 (1989).
150. Albon, J., Purslow, P. P., Karwatowski, W. S. & Easty, D. L. Age related compliance of the lamina cribrosa in human eyes. *Br. J. Ophthalmol.* **84**, 318–23 (2000).
151. Tezel, G., Luo, C. & Yang, X. Accelerated Aging in Glaucoma: Immunohistochemical Assessment of Advanced Glycation End Products in the Human Retina and Optic Nerve Head. at <https://www.ncbi.nlm.nih.gov/pmc/articles/PMC2492883/pdf/nihms55493.pdf>
152. Amano, S. *et al.* Advanced glycation end products in human optic nerve head. *Br. J. Ophthalmol.* **85**, 52–5 (2001).
153. Vranka, J. A. Extracellular matrix in the trabecular meshwork:

- Intraocular pressure regulation and dysregulation in glaucoma. **52**, 566–584 (2016).
154. Keller, K. E., Bradley, J. M., Kelley, M. J. & Acott, T. S. Effects of modifiers of glycosaminoglycan biosynthesis on outflow facility in perfusion culture. *Investig. Ophthalmol. Vis. Sci.* **49**, 2495–2505 (2008).
155. Keller, K. E., Aga, M., Bradley, J. M., Kelley, M. J. & Acott, T. S. Extracellular matrix turnover and outflow resistance. *Exp. Eye Res.* **88**, 676–82 (2009).
156. Furuyoshi, N., Furuyoshi, M., Futa, R., Gottanka, J. & Lütjen-Drecoll, E. Ultrastructural changes in the trabecular meshwork of juvenile glaucoma. *Ophthalmologica.* **211**, 140–6 (1997).
157. Acott, T. S. & Kelley, M. J. Extracellular matrix in the trabecular meshwork. *Exp. Eye Res.* **86**, 543–561 (2008).
158. O'Brien, E. T., Wang, Y., Ying, H. & Yue, B. Y. J. T. Differential Expression of Genes in Cells Cultured from Juxtacanalicular Trabecular Meshwork and Schlemm's Canal. *J. Ocul. Pharmacol. Ther.* **30**, 291–299 (2014).
159. Acott, T. S. & Kelley, M. J. NIH Public Access. *Science (80-. ).* **86**, 543–561 (2009).
160. Alexander, J. P., Samples, J. R. & Acott, T. S. Growth factor and cytokine modulation of trabecular meshwork matrix metalloproteinase and TIMP expression. *Curr. Eye Res.* **17**, 276–285 (1998).

161. Doucette, L. P., Rasnitsyn, A., Seifi, M. & Walter, M. A. The interactions of genes, age, and environment in glaucoma pathogenesis. *Surv. Ophthalmol.* **60**, 310–326 (2015).
162. Janssen, S. F. *et al.* The vast complexity of primary open angle glaucoma: disease genes, risks, molecular mechanisms and pathobiology. *Prog. Retin. Eye Res.* **37**, 31–67 (2013).
163. Fini, M. E. *et al.* Steroid-induced ocular hypertension/glaucoma: Focus on pharmacogenomics and implications for precision medicine. *Prog. Retin. Eye Res.* **56**, 58–83 (2017).
164. Wang, J. *et al.* Targeting Transforming Growth Factor- $\beta$  Signaling in Primary Open-Angle Glaucoma. *J. Glaucoma* **26**, 390–395 (2017).
165. Taves, M. D., Gomez-Sanchez, C. E. & Soma, K. K. Extra-adrenal glucocorticoids and mineralocorticoids: evidence for local synthesis, regulation, and function. *Am. J. Physiol. Endocrinol. Metab.* **301**, E11-24 (2011).
166. Chung, S., Son, G. H. & Kim, K. Circadian rhythm of adrenal glucocorticoid: Its regulation and clinical implications. *Biochim. Biophys. Acta - Mol. Basis Dis.* **1812**, 581–591 (2011).
167. Verhoeven, F., Prati, C., Maguin-Gaté, K., Wendling, D. & Demougeot, C. Glucocorticoids and endothelial function in inflammatory diseases: focus on rheumatoid arthritis. *Arthritis Res. Ther.* **18**, 258 (2016).
168. Barnes, P. J. Anti-inflammatory actions of glucocorticoids:

- molecular mechanisms. *Clin. Sci. (Lond)*. **94**, 557–72 (1998).
169. Stahn, C. & Buttgereit, F. Genomic and nongenomic effects of glucocorticoids. *Nat. Clin. Pract. Rheumatol*. **4**, 525–533 (2008).
170. De Iudicibus, S., Franca, R., Martelossi, S., Ventura, A. & Decorti, G. Molecular mechanism of glucocorticoid resistance in inflammatory bowel disease. *World J. Gastroenterol*. **17**, 1095–108 (2011).
171. Guyre, P. M. & Munck, A. in *Encyclopedia of Immunology* 996–1001 (Elsevier, 1998). doi:10.1006/rwei.1999.0258
172. LU, N. Z. & CIDLOWSKI, J. A. The Origin and Functions of Multiple Human Glucocorticoid Receptor Isoforms. *Ann. N. Y. Acad. Sci*. **1024**, 102–123 (2004).
173. Sánchez-Vega, B., Krett, N., Rosen, S. T. & Gandhi, V. Glucocorticoid receptor transcriptional isoforms and resistance in multiple myeloma cells. *Mol. Cancer Ther*. **5**, 3062–70 (2006).
174. Oakley, R. H. & Cidlowski, J. A. The biology of the glucocorticoid receptor: new signaling mechanisms in health and disease. *J. Allergy Clin. Immunol*. **132**, 1033–44 (2013).
175. Kino, T. *et al*. Glucocorticoid receptor (GR) beta has intrinsic, GRalpha-independent transcriptional activity. *Biochem. Biophys. Res. Commun*. **381**, 671–5 (2009).
176. Wikstrom, A.-C., Bakke, O., Okret, S., Bronnegard, M. & Gustafsson, J. Intracellular Localization of the Glucocorticoid Receptor: Evidence for Cytoplasmic and Nuclear Localization\*.

- Endocrinology* **120**, 1232–1242 (1987).
177. Strehl, C. & Buttgereit, F. Unraveling the functions of the membrane-bound glucocorticoid receptors: first clues on origin and functional activity. *Ann. N. Y. Acad. Sci.* **1318**, 1–6 (2014).
  178. Presman, D. M. *et al.* Insights on Glucocorticoid Receptor Activity Modulation through the Binding of Rigid Steroids. *PLoS One* **5**, e13279 (2010).
  179. Harrell, J. M. *et al.* Evidence for Glucocorticoid Receptor Transport on Microtubules by Dynein. *J. Biol. Chem.* **279**, 54647–54654 (2004).
  180. Beato, M., Truss, M. & Chávez, S. Control of transcription by steroid hormones. *Ann. N. Y. Acad. Sci.* **784**, 93–123 (1996).
  181. Truss, M. & Beato, M. Steroid Hormone Receptors: Interaction with Deoxyribonucleic Acid and Transcription Factors\*. *Endocr. Rev.* **14**, 459–479 (1993).
  182. Smith, C. L., Oñate, S. A., Tsai, M. J. & O'Malley, B. W. CREB binding protein acts synergistically with steroid receptor coactivator-1 to enhance steroid receptor-dependent transcription. *Proc. Natl. Acad. Sci.* **93**, (1996).
  183. Li, X., Wong, J., Tsai, S. Y., Tsai, M.-J. & O'Malley, B. W. Progesterone and glucocorticoid receptors recruit distinct coactivator complexes and promote distinct patterns of local chromatin modification. *Mol. Cell. Biol.* **23**, 3763–73 (2003).
  184. Hua, G., Ganti, K. P. & Chambon, P. Glucocorticoid-induced

- tethered transrepression requires SUMOylation of GR and formation of a SUMO-SMRT/NCoR1-HDAC3 repressing complex. *Proc. Natl. Acad. Sci. U. S. A.* **113**, E635-43 (2016).
185. R. Oakley, J. C. The Biology of the Glucocorticoid Receptor: New Signaling Mechanism in Health and Disease. *J allergy clin immunol* **132**, 1033–1044 (2013).
186. Almawi, W. Y. & Melemedjian, O. K. Negative regulation of nuclear factor-kappaB activation and function by glucocorticoids. *J. Mol. Endocrinol.* **28**, 69–78 (2002).
187. Sulaiman, R. S., Kadmiel, M. & Cidlowski, J. A. Glucocorticoid receptor signaling in the eye. *Steroids* 0–1 (2017).  
doi:10.1016/j.steroids.2017.11.002
188. Pleyer, U. & Sherif, Z. in *Recent Advances in Glucocorticoid Receptor Action* 65–81 (Springer Berlin Heidelberg, 2002).  
doi:10.1007/978-3-662-04660-9\_5
189. Petroustos, G., Guimaraes, R., Giraud, J. P. & Pouliquen, Y. Corticosteroids and corneal epithelial wound healing. *Br. J. Ophthalmol.* **66**, 705–8 (1982).
190. Ashton, N. & Cook, C. Effect of Cortisone on Healing of Corneal Wounds. *Brit. J. Ophthal* **35**,
191. Cook, C. & MacDonald, R. K. Effect of cortisone on the permeability of the blood-aqueous barrier to fluorescein. *Br. J. Ophthalmol.* **35**, 730–40 (1951).
192. Dinning, W. J. Steroids and the eye-indications and complications.

- Postgraduate Med. J.* **52**, 634–638 (1976).
193. Moghadam-Kia, S. & Werth, V. P. Prevention and treatment of systemic glucocorticoid side effects. *Int. J. Dermatol.* **49**, 239–248 (2010).
194. Renfro, L. & Snow, J. S. Ocular effects of topical and systemic steroids. *Dermatol. Clin.* **10**, 505–12 (1992).
195. Zhang, X., Ognibene, C. M., Clark, A. F. & Yorio, T. Dexamethasone Inhibition of Trabecular Meshwork Cell Phagocytosis and Its Modulation by Glucocorticoid Receptor $\beta$ . *Exp Eye Res* **84**, 275–284 (2007).
196. Dismuke, W. M., Klingeborn, M. & Stamer, W. D. Mechanism of Fibronectin Binding to Human Trabecular Meshwork Exosomes and Its Modulation by Dexamethasone. *PLoS One* **11**, e0165326 (2016).
197. Benedek, T. G. History of the development of corticosteroid therapy. *Clin. Exp. Rheumatol.* **29**, S-5-12
198. Shields, C. L. & Shields, J. A. Basic understanding of current classification and management of retinoblastoma. *Curr. Opin. Ophthalmol.* **17**, 228–234 (2006).
199. Kersey, J. P. & Broadway, D. C. Corticosteroid-induced glaucoma: a review of the literature. *Eye* **20**, 407–416 (2006).
200. Edelman, J. L. Differentiating intraocular glucocorticoids. *Ophthalmologica* **224**, 25–30 (2010).
201. Cantrill, H. L. *et al.* COMPARISON O F IN VITRO POTENCY O F

CORTICOSTEROIDS WITH ABILITY TO RAISE INTRAOCULAR PRESSURE. at

<<http://www.sciencedirect.com/sdfe/pdf/download/eid/1-s2.0-000293947590687X/first-page-pdf>>

202. Lewis, J. M. *et al.* Intraocular pressure response to topical dexamethasone as a predictor for the development of primary open-angle glaucoma. *Am. J. Ophthalmol.* **106**, 607–12 (1988).
203. Tripathi, R. C., Parapuram, S. K., Tripathi, B. J., Zhong, Y. & Chalam, K. V. Corticosteroids and glaucoma risk. *Drugs Aging* **15**, 439–450 (1999).
204. Wilson, K., McCartney, M. D., Miggans, S. T. & Clark, A. F. Dexamethasone induced ultrastructural changes in cultured human trabecular meshwork cells. *Curr. Eye Res.* **12**, 783–793 (1993).
205. Rybkin, I., Gerometta, R., Fridman, G., Candia, O. & Danias, J. Model systems for the study of steroid-induced IOP elevation. *Exp. Eye Res.* **158**, 51–58 (2017).
206. Mao, W., Tovar-Vidales, T., Yorio, T., Wordinger, R. J. & Clark, A. F. Perfusion-Cultured Bovine Anterior Segments as an Ex Vivo Model for Studying Glucocorticoid-Induced Ocular Hypertension and Glaucoma. *Investig. Ophthalmology Vis. Sci.* **52**, 8068 (2011).
207. Clark, A. F., Wilson, K., De Kater, A. W., Allingham, R. R. & McCartney, M. D. Dexamethasone-induced ocular hypertension in perfusion-cultured human eyes. *Investig. Ophthalmol. Vis. Sci.* **36**, 478–489 (1995).

208. Wordinger, R. J. & Clark, A. F. Effects of glucocorticoids on the trabecular meshwork: Towards a better understanding of glaucoma. *Prog. Retin. Eye Res.* **18**, 629–667 (1999).
209. Zhang, X., Ognibene, C. M., Clark, A. F. & Yorio, T. Dexamethasone inhibition of trabecular meshwork cell phagocytosis and its modulation by glucocorticoid receptor beta. *Exp. Eye Res.* **84**, 275–84 (2007).
210. Raghunathan, V. K. *et al.* Dexamethasone Stiffens Trabecular Meshwork, Trabecular Meshwork Cells, and Matrix. *Invest. Ophthalmol. Vis. Sci.* **56**, 4447–59 (2015).
211. Weiss, A. & Attisano, L. The TGFbeta Superfamily Signaling Pathway. *WIREs Dev Biol* **2**, 47–63 (2013).
212. Poniatoski, L. A., Wojdasiewicz, P., Gasik, R. & Szukiewicz, D. Transforming growth factor beta family: Insight into the role of growth factors in regulation of fracture healing biology and potential clinical applications. *Mediators Inflamm.* **2015**, (2015).
213. Mathews, L. S. & Vale, W. W. Expression cloning of an activin receptor, a predicted transmembrane serine kinase. *Cell* **65**, 973–982 (1991).
214. Annes, J. P. Making sense of latent TGFbeta activation. *J. Cell Sci.* **116**, 217–224 (2003).
215. Fortunel, N. O., Hatzfeld, A. & Hatzfeld, J. A. Transforming growth factor- $\beta$ : pleiotropic role in the regulation of hematopoiesis. at <http://www.bloodjournal.org/content/bloodjournal/96/6/2022.f>

ull.pdf>

216. Huang, T. & Hinck, A. P. Production, Isolation, and Structural Analysis of Ligands and Receptors of the TGF- $\beta$  Superfamily. *Methods Mol. Biol.* **1344**, 63–92 (2016).
217. Gleizes, P. *et al.* TGF-beta; Latency: Biological Significance and Mechanisms of Activation. *Stem Cells* **15**, 190–197 (1997).
218. Walton, K. L. *et al.* Two Distinct Regions of Latency-associated Peptide Coordinate Stability of the Latent Transforming Growth Factor- $\beta$ 1 Complex \*. (2010). doi:10.1074/jbc.M110.110288
219. Miyazono, K., Hellman, U., Wernstedt, C. & Heldins, C.-H. Latent High Molecular Weight Complex of Transforming Growth Factor B 1 Purification From Human Platelets And Structural Characterisation. *J. Biol. Chem.* **263**, 6407–6415 (1988).
220. Taipale, J., Saharinen, J. & Keski-Oja, J. Extracellular Matrix-Associated Transforming Growth Factor- $\beta$ : Role in Cancer Cell Growth and Invasion. *Adv. Cancer Res.* **75**, 87–134 (1998).
221. Dabovic, B. *et al.* Dual functions for LTBP in lung development: LTBP-4 independently modulates elastogenesis and TGF-beta activity. *J. Cell. Physiol.* **219**, 14–22 (2009).
222. Munger, J. S. *et al.* Latent transforming growth factor- $\beta$ : Structural features and mechanisms of activation. *Kidney Int.* **51**, 1376–1382 (1997).
223. Robertson, I. B. *et al.* Latent TGF- $\beta$ -binding proteins. *Matrix Biol.* **47**, 44–53 (2015).

224. Murphy-Ullrich, J. E. & Poczatek, M. Activation of latent TGF-beta by thrombospondin-1: mechanisms and physiology. *Cytokine Growth Factor Rev.* **11**, 59–69 (2000).
225. Schultz-Cherry, S. & Murphy-Ullrich, J. E. Thrombospondin causes activation of latent transforming growth factor-beta secreted by endothelial cells by a novel mechanism. *J Cell Biol* **122**, 923–932 (1993).
226. Abdelouahed, M., Ludlow, A., Brunner, G. & Lawler, J. Activation of platelet-transforming growth factor beta-1 in the absence of thrombospondin-1. *J. Biol. Chem.* **275**, 17933–6 (2000).
227. Chen, Y. *et al.* ALK4 functions as a receptor for multiple TGF $\beta$ -related ligands to regulate left–right axis determination and mesoderm induction in *Xenopus*. *Dev. Biol.* **268**, 280–294 (2004).
228. Hinck, A. P. Structural studies of the TGF- $\beta$ s and their receptors - Insights into evolution of the TGF- $\beta$  superfamily. *FEBS Lett.* **586**, 1860–1870 (2012).
229. Nagaraj, N. S., Datta, P. K., Datta, P. K. & Dr. Targeting the transforming growth factor-beta signaling pathway in human cancer. *Expert Opin. Investig. Drugs* **19**, 77–91 (2010).
230. Miyazawa, K. Two major SMAD pathways on the TGF-beta superfamily signalling.
231. Verrecchia, F. & Mauviel, A. Transforming growth factor- $\beta$  signaling through the Smad pathway: Role in extracellular matrix gene expression and regulation. *J. Invest. Dermatol.* **118**, 211–215

(2002).

232. Massagué, J. & Gomis, R. R. The logic of TGF $\beta$  signaling. *FEBS Lett.* **580**, 2811–2820 (2006).
233. Massagué, J. TGF $\beta$  in cancer. *Cell* **134**, 215–230 (2008).
234. Min, S. H., Lee, T.-I., Chung, Y. S. & Kim, H. K. Transforming growth factor-beta levels in human aqueous humor of glaucomatous, diabetic and uveitic eyes. *Korean J. Ophthalmol.* **20**, 162–5 (2006).
235. Pena, J. D., Taylor, A. W., Ricard, C. S., Vidal, I. & Hernandez, M. R. Transforming growth factor beta isoforms in human optic nerve heads. *Br. J. Ophthalmol.* **83**, 209–18 (1999).
236. Tripathi, R. C., Li, J., Chan, W. F. & Tripathi, B. J. Aqueous humor in glaucomatous eyes contains an increased level of TGF-beta 2. *Exp. Eye Res.* **59**, 723–7 (1994).
237. Bollinger, K. E. *et al.* Quantitative Proteomics: TGF $\beta$ 2 Signaling in Trabecular Meshwork Cells. *Investig. Ophthalmology Vis. Sci.* **52**, 8287 (2011).
238. Tripathi, R. C., Li, J., Borisuth, N. S. C. & Tripathi, B. J. Trabecular cells of the eye express messenger RNA for transforming growth factor- $\beta$ 1 and secrete this cytokine. *Investig. Ophthalmol. Vis. Sci.* **34**, 2562–2569 (1993).
239. Tripathi, R. C., Borisuth, N. S., Kolli, S. P. & Tripathi, B. J. Trabecular cells express receptors that bind TGF-beta 1 and TGF-beta 2: a qualitative and quantitative characterization. *Invest. Ophthalmol. Vis. Sci.* **34**, 260–3 (1993).

240. Wallace, D. M., Downs, J. C. & O'Brien, C. J. The role of matricellular proteins in glaucoma. *Matrix Biol.* **37**, 174–182 (2014).
241. Verrecchia, F. & Mauviel, A. Transforming growth factor-beta and fibrosis. *World J. Gastroenterol.* **13**, 3056–62 (2007).
242. Li, J., Tripathi, B. J. & Tripathi, R. C. Modulation of Pre-mRNA Splicing and Protein Production of Fibronectin by TGF- $\beta$ 2 in Porcine Trabecular Cells. *Invest. Ophthalmol. Vis. Sci.* **41**, 3437–3443 (2000).
243. Fuchshofer, R., Welge-Lussen, U. & Lütjen-Drecoll, E. The effect of TGF- $\beta$ 2 on human trabecular meshwork extracellular proteolytic system. *Exp. Eye Res.* **77**, 757–765 (2003).
244. Fleenor, D. L. *et al.* TGF $\beta$ 2-induced changes in human trabecular meshwork: Implications for intraocular pressure. *Investig. Ophthalmol. Vis. Sci.* **47**, 226–234 (2006).
245. Morgan, J. T., Raghunathan, V. K., Chang, Y.-R., Murphy, C. J. & Russell, P. The intrinsic stiffness of human trabecular meshwork cells increases with senescence. *Oncotarget* **6**, 15362–74 (2015).
246. Wang, K., Read, A. T., Sulchek, T. & Ethier, C. R. Trabecular meshwork stiffness in glaucoma. *Exp. Eye Res.* **158**, 3–12 (2017).
247. Tovar-Vidales, T., Clark, A. F. & Wordinger, R. J. Transforming growth factor-beta2 utilizes the canonical Smad-signaling pathway to regulate tissue transglutaminase expression in human trabecular meshwork cells. *Exp. Eye Res.* **93**, 442–451 (2011).

248. Tovar-Vidales, T., Roque, R., Clark, A. F. & Wordinger, R. J. Tissue Transglutaminase Expression and Activity in Normal and Glaucomatous Human Trabecular Meshwork Cells and Tissues. *Investig. Ophthalmology Vis. Sci.* **49**, 622 (2008).
249. Sethi, A., Wordinger, R. J. & Clark, A. F. Gremlin utilizes canonical and non-canonical TGF $\beta$  signaling to induce lysyl oxidase (LOX) genes in human trabecular meshwork cells. *Exp. Eye Res.* **113**, 117–27 (2013).
250. Wiederholt, M., Thieme, H. & Stumpff, F. The regulation of trabecular meshwork and ciliary muscle contractility. *Prog Retin Eye Res* **19**, 271–295 (2000).
251. Carthy, J. M. TGF $\beta$  signaling and the control of myofibroblast differentiation: Implications for chronic inflammatory disorders. *J. Cell. Physiol.* **233**, 98–106 (2018).
252. Pattabiraman, P. P. & Rao, P. V. Mechanistic basis of Rho GTPase-induced extracellular matrix synthesis in trabecular meshwork cells. *Am. J. Physiol. Physiol.* **298**, C749–C763 (2010).
253. Bermudez, J. Y., Montecchi-Palmer, M., Mao, W. & Clark, A. F. Cross-linked actin networks (CLANs) in glaucoma. *Exp. Eye Res.* **159**, 16–22 (2017).
254. Montecchi-Palmer, M. *et al.* TGF $\beta$ 2 Induces the Formation of Cross-Linked Actin Networks (CLANs) in Human Trabecular Meshwork Cells Through the Smad and Non-Smad Dependent Pathways. *Investig. Ophthalmology Vis. Sci.* **58**, 1288 (2017).

255. Clark, A. F. *et al.* Dexamethasone alters F-actin architecture and promotes cross-linked actin network formation in human trabecular meshwork tissue. *Cell Motil. Cytoskeleton* **60**, 83–95 (2005).
256. Duffy, L. & O'Reilly, S. Functional Implications of Cross-Linked Actin Networks in Trabecular Meshwork Cells. *Cell. Physiol. Biochem.* **45**, 783–794 (2018).
257. Clark, A. F. *et al.* Glucocorticoid-Induced Formation of Cross-Linked Actin Networks in Cultured Human Trabecular Meshwork Cells. **35**, (1994).
258. Mattick, J. S. & Makunin, I. V. Non-coding RNA. *Hum. Mol. Genet.* **15 Spec No**, 17–29 (2006).
259. Lodish H, Berk A, Zipursky SL, *et al.* *The Three Roles of RNA in Protein Synthesis. Molecular Cell Biology. 4th edition.* (New York: W. H. Freeman, 2000). at  
<<https://www.ncbi.nlm.nih.gov/books/NBK21603/>>
260. Lee, R. C., Feinbaum, R. L. & Ambrost, V. The C.elegans Heterochronic Gene lin-4 Encodes Small RNAs with Antisense Complementarity to lin-14. *Cell* **75**, 843–854 (1993).
261. Wightman, B., Lho Ha, T. & Ruvkun, G. Posttranscriptional Regulation of the Heterochronic Gene lin-14 by lin-4 Mediates Temporal Pattern Formation in C. elegans. **75**, 855–862 (1993).
262. Wahid, F., Shehzad, A., Khan, T. & Kim, Y. Y. MicroRNAs: Synthesis, mechanism, function, and recent clinical trials. *Biochim. Biophys.*

*Acta - Mol. Cell Res.* **1803**, 1231–1243 (2010).

263. Lai, E. C., Tomancak, P., Williams, R. W. & Rubin, G. M. Computational identification of *Drosophila* microRNA genes. *Genome Biol.* **4**, R42 (2003).
264. Nam, J. *et al.* Human microRNA prediction through a probabilistic co-learning model of sequence and structure. *academic.oup.com* (2005). at <<https://academic.oup.com/nar/article-abstract/33/11/3570/1106539>>
265. Monticelli, S. *et al.* MicroRNA profiling of the murine hematopoietic system. *Genome Biol.* **6**, R71.1-R71.15 (2005).
266. Zhao, Y., Samal, E. & Srivastava, D. Serum response factor regulates a muscle-specific microRNA that targets Hand2 during cardiogenesis. *Nature* **436**, 214–220 (2005).
267. Naguibneva, I. *et al.* The microRNA miR-181 targets the homeobox protein Hox-A11 during mammalian myoblast differentiation. *Nat. Cell Biol.* **8**, 278–284 (2006).
268. Garzon, R. *et al.* MicroRNA fingerprints during human megakaryocytopoiesis. *Proc. Natl. Acad. Sci.* **103**, 5078–5083 (2006).
269. Esau, C. *et al.* miR-122 regulation of lipid metabolism revealed by in vivo antisense targeting. *Cell Metab.* **3**, 87–98 (2006).
270. Yong, S. L. & Dutta, A. The tumor suppressor microRNA let-7 represses the HMGA2 oncogene. *Genes Dev.* **21**, 1025–1030 (2007).

271. Hwang, H. W. & Mendell, J. T. MicroRNAs in cell proliferation, cell death, and tumorigenesis. *Br. J. Cancer* **94**, 776–780 (2006).
272. MacFarlane, L.-A. & R. Murphy, P. MicroRNA: Biogenesis, Function and Role in Cancer. *Curr. Genomics* **11**, 537–561 (2010).
273. Iorio, M. V. *et al.* MicroRNA gene expression deregulation in human breast cancer. *Cancer Res.* **65**, 7065–7070 (2005).
274. Peter, M. E. Let-7 and miR-200 microRNAs: Guardians against pluripotency and cancer progression. *Cell Cycle* **8**, 843–852 (2009).
275. Wang, J. *et al.* CREB up-regulates long non-coding RNA, HULC expression through interaction with microRNA-372 in liver cancer. *Nucleic Acids Res.* **38**, 5366–5383 (2010).
276. Ambs, S. *et al.* Genomic profiling of microRNA and messenger RNA reveals deregulated microRNA expression in prostate cancer. *Cancer Res.* **68**, 6162–6170 (2008).
277. Tang, X., Tang, G. & Özcan, S. Role of microRNAs in diabetes. *Biochim. Biophys. Acta - Gene Regul. Mech.* **1779**, 697–701 (2008).
278. Delay, C., Mandemakers, W. & Hébert, S. S. MicroRNAs in Alzheimer's disease. *Neurobiol. Dis.* **46**, 285–290 (2012).
279. Wang, W.-X. *et al.* The Expression of MicroRNA miR-107 Decreases Early in Alzheimer's Disease and May Accelerate Disease Progression through Regulation of -Site Amyloid Precursor Protein-Cleaving Enzyme 1. *J. Neurosci.* **28**, 1213–1223 (2008).
280. Femminella, G. D., Ferrara, N. & Rengo, G. The emerging role of

- microRNAs in Alzheimer's disease. *Front. Physiol.* **6**, 1–5 (2015).
281. Hebert, S. S. *et al.* Loss of microRNA cluster miR-29a/b-1 in sporadic Alzheimer's disease correlates with increased BACE1/ - secretase expression. *Proc. Natl. Acad. Sci.* **105**, 6415–6420 (2008).
282. Breving, K. & Esquela-Kerscher, A. The complexities of microRNA regulation: Mirandering around the rules. *Int. J. Biochem. Cell Biol.* **42**, 1316–1329 (2010).
283. Catalanotto, C., Cogoni, C. & Zardo, G. MicroRNA in Control of Gene Expression: An Overview of Nuclear Functions. *Int. J. Mol. Sci.* **17**, (2016).
284. Rajewsky, N. L ( ou ) sy miRNA targets ? NEWS AND VIEWS. *Nat. Struct. Mol. Biol.* **13**, 754–755 (2006).
285. Rajewsky, N. MicroRNA target predictions in animals. *Nat. Genet.* **38**, S8–S13 (2006).
286. AMBROS, V. A uniform system for microRNA annotation. *RNA* **9**, 277–279 (2003).
287. Bartel, D. P. MicroRNAs: Genomics, Biogenesis, Mechanism, and Function. *Cell* **116**, 281–297 (2004).
288. Kim, V. N. Small RNAs: classification, biogenesis, and function. *Mol. Cells* **19**, 1–15 (2005).
289. Ramalingam, P. *et al.* Biogenesis of intronic miRNAs located in clusters by independent transcription and alternative splicing. *RNA* **20**, 76–87 (2014).

290. Baldrich, P., Hsing, Y.-I. C. & San Segundo, B. Genome-Wide Analysis of Polycistronic MicroRNAs in Cultivated and Wild Rice. *Genome Biol. Evol.* **8**, 1104–14 (2016).
291. Lagos-quintana, M., Rauhut, R., Meyer, J., Borkhardt, A. & Tuschl, T. New microRNAs from mouse and human New microRNAs from mouse and human. 175–179 (2003).  
doi:10.1261/rna.2146903.Our
292. Lagos-Quintana, M. Identification of Novel Genes Coding for Small Expressed RNAs. *Science (80-. )*. **294**, 853–858 (2001).
293. Lee, Y. MicroRNA maturation: stepwise processing and subcellular localization. (2002).
294. Lee, Y. *et al.* MicroRNA genes are transcribed by RNA polymerase II. *EMBO J.* **23**, 4051–4060 (2004).
295. Jeong, G., Lim, Y.-H. & Kim, Y.-K. Precise mapping of the transcription start sites of human microRNAs using DROSHA knockout cells. *BMC Genomics* **17**, 908 (2016).
296. Monteys, A. M. *et al.* Structure and activity of putative intronic miRNA promoters. *Rna* **16**, 495–505 (2010).
297. He, L. & Hannon, G. J. MicroRNAs: Small RNAs with a big role in gene regulation. *Nat. Rev. Genet.* **5**, 522–531 (2004).
298. Heman-Ackah, S. M., Hallegger, M., Rao, M. S. & Wood, M. J. A. RISC in PD: the impact of microRNAs in Parkinson’s disease cellular and molecular pathogenesis. *Front. Mol. Neurosci.* **6**, (2013).

299. Han, J. The Drosha-DGCR8 complex in primary microRNA processing. *Genes Dev.* **18**, 3016–3027 (2004).
300. Graves, P. & Zeng, Y. Biogenesis of Mammalian MicroRNAs: A Global View. *Genomics, Proteomics Bioinforma.* **10**, 239–245 (2012).
301. Zeng, Y., Yi, R. & Cullen, B. R. Recognition and cleavage of primary microRNA precursors by the nuclear processing enzyme Drosha. *EMBO J.* **24**, 138–148 (2005).
302. Lee, Y. *et al.* The nuclear RNase III Drosha initiates microRNA processing. *Nature* **425**, 415–419 (2003).
303. Faller, M. *et al.* DGCR8 recognizes primary transcripts of microRNAs through highly cooperative binding and formation of higher-order structures. *Rna* **16**, 1570–1583 (2010).
304. Berezikov, E. *et al.* Phylogenetic shadowing and computational identification of human microRNA genes. *Cell* **120**, 21–24 (2005).
305. Faller, M. *et al.* DGCR8 recognizes primary transcripts of microRNAs through highly cooperative binding and formation of higher-order structures. *RNA* **16**, 1570–83 (2010).
306. Han, J. *et al.* Posttranscriptional crossregulation between Drosha and DGCR8. *Cell* **136**, 75–84 (2009).
307. Han, J. *et al.* Posttranscriptional Crossregulation between Drosha and DGCR8. **136**, 75–84 (2010).
308. Chong, M. M. W. *et al.* Canonical and alternate functions of the microRNA biogenesis machinery. *Genes Dev.* **24**, 1951–1960

- (2010).
309. Ha, M. & Kim, V. N. Regulation of microRNA biogenesis. *Nat. Rev. Mol. Cell Biol.* **15**, 509–524 (2014).
310. Auyeung, V. . Beyond Secondary structure: primary-sequence determinants license pri-miRNA hairpins for processing. *Cell* **152**, 844–858 (2013).
311. Fang, W. & Bartel, D. P. The Menu of Features that Define Primary MicroRNAs and Enable De Novo Design of MicroRNA Genes. *Mol. Cell* **60**, 131–45 (2015).
312. Kim, Y. K. & Kim, V. N. Processing of intronic microRNAs. *EMBO J.* **26**, 775–783 (2007).
313. Boivin, V., Deschamps-Francoeur, G. & Scott, M. S. Protein coding genes as hosts for noncoding RNA expression. *Semin. Cell Dev. Biol.* **75**, 3–12 (2018).
314. Sundaram, G. M. *et al.* ‘See-saw’ expression of microrna-198 and fstl1 from a single transcript in wound healing. *Nature* **495**, 103–106 (2013).
315. Wu, Q. *et al.* The RNase III enzyme DROSHA is essential for microRNA production and spermatogenesis. *J. Biol. Chem.* **287**, 25173–90 (2012).
316. Wada, T., Kikuchi, J. & Furukawa, Y. Histone deacetylase 1 enhances microRNA processing via deacetylation of DGCR8. *EMBO Rep.* **13**, 142–149 (2012).
317. Tang, X. *et al.* Acetylation of Drosha on the N-Terminus Inhibits Its

- Degradation by Ubiquitination. *PLoS One* **8**, (2013).
318. Herbert, K. M., Pimienta, G., DeGregorio, S. J., Alexandrov, A. & Steitz, J. A. Phosphorylation of DGCR8 increases its intracellular stability and induces a progrowth miRNA profile. *Cell Rep.* **5**, 1070–81 (2013).
  319. Hata, A. & Blahna, M. T. Smad-mediated Regulation of microRNA biosynthesis. **344**, 1173–1178 (2015).
  320. Davis, B. N., Hilyard, A. C., Lagna, G. & Hata, A. SMAD proteins control DROSHA-mediated microRNA maturation. **454**, 56–61 (2009).
  321. Slezak-Prochazka, I., Durmus, S., Kroesen, B. J. & van den Berg, A. MicroRNAs, macrocontrol: Regulation of miRNA processing. *Rna* **16**, 1087–1095 (2010).
  322. Yi, R., Qin, Y., Macara, I. G. & Cullen, B. R. Exportin-5 mediates the nuclear export of pre-microRNAs and short hairpin RNAs. *Genes Dev.* **17**, 3011–6 (2003).
  323. Bohnsack, M. T., Czaplinski, K. & Gorlich, D. Exportin 5 is a RanGTP-dependent dsRNA-binding protein that mediates nuclear export of pre-miRNAs. *RNA* **10**, 185–91 (2004).
  324. Wang, X. *et al.* Dynamic mechanisms for pre-miRNA binding and export by Exportin-5. *RNA* **17**, 1511–28 (2011).
  325. Koscianska, E., Starega-Roslan, J. & Krzyzosiak, W. J. The role of Dicer protein partners in the processing of microRNA precursors. *PLoS One* **6**, e28548 (2011).

326. Starega-Roslan, J., Galka-Marciniak, P. & Krzyzosiak, W. J. Nucleotide sequence of miRNA precursor contributes to cleavage site selection by Dicer. *Nucleic Acids Res.* **43**, 10939–51 (2015).
327. Benoit, M. P. M. H. *et al.* The RNA-binding region of human TRBP interacts with microRNA precursors through two independent domains. doi:10.1093/nar/gkt086
328. Hammond, S. M. Argonaute2, a Link Between Genetic and Biochemical Analyses of RNAi. *Science (80-. ).* **293**, 1146–1150 (2001).
329. Höck, J. & Meister, G. The Argonaute protein family. *Genome Biol.* **9**, 210 (2008).
330. Janas, M. M. *et al.* Alternative RISC assembly: binding and repression of microRNA-mRNA duplexes by human Ago proteins. *RNA* **18**, 2041–55 (2012).
331. Khvorova, A., Reynolds, A. & Jayasena, S. D. Functional siRNAs and miRNAs Exhibit Strand Bias. *Cell* **115**, 209–216 (2003).
332. Kawamata, T., Seitz, H., Molecular, Y. T.-N. S. and & 2009, undefined. Structural determinants of miRNAs for RISC loading and slicer-independent unwinding. *nature.com* at <<https://www.nature.com/articles/nsmb.1630>>
333. Pratt, A. J. & MacRae, I. J. The RNA-induced silencing complex: a versatile gene-silencing machine. *J. Biol. Chem.* **284**, 17897–901 (2009).
334. Ameres, S. L. & Zamore, P. D. Diversifying microRNA sequence and

- function. *Nat. Rev. Mol. Cell Biol.* **14**, 475–488 (2013).
335. Rügger, S. & Großhans, H. MicroRNA turnover: when, how, and why. *Trends Biochem. Sci.* **37**, 436–446 (2012).
336. Yang, J.-S. & Lai, E. C. Alternative miRNA Biogenesis Pathways and the Interpretation of Core miRNA Pathway Mutants. *Mol. Cell* **43**, 892–903 (2011).
337. Babiarz, J. E., Ruby, J. G., Wang, Y., Bartel, D. P. & Blelloch, R. Mouse ES cells express endogenous shRNAs, siRNAs, and other Microprocessor-independent, Dicer-dependent small RNAs. *Genes Dev.* **22**, 2773–2785 (2008).
338. Chong, M. M. W. *et al.* Canonical and alternate functions of the microRNA biogenesis machinery. *Genes Dev.* **24**, 1951–1960 (2010).
339. Berezikov, E., Chung, W.-J., Willis, J., Cuppen, E. & Lai, E. C. Mammalian Mirtron Genes. *Mol. Cell* **28**, 328–336 (2007).
340. Yang, J.-S. *et al.* Conserved vertebrate mir-451 provides a platform for Dicer-independent, Ago2-mediated microRNA biogenesis. *Proc. Natl. Acad. Sci. U. S. A.* **107**, 15163–8 (2010).
341. Yang, J.-S. & Lai, E. C. Dicer-independent, Ago2-mediated microRNA biogenesis in vertebrates. *Cell Cycle* **9**, 4455–60 (2010).
342. Cifuentes, D. *et al.* A novel miRNA processing pathway independent of Dicer requires Argonaute2 catalytic activity. *Science* **328**, 1694–8 (2010).
343. Cheloufi, S., Dos Santos, C. O., Chong, M. M. W. & Hannon, G. J. A

- dicer-independent miRNA biogenesis pathway that requires Ago catalysis. *Nature* **465**, 584–9 (2010).
344. Peter, M. E. Targeting of mRNAs by multiple miRNAs: the next step. *Oncogene* **29**, 2161–2164 (2010).
345. Doench, J. G. & Sharp, P. A. Specificity of microRNA target selection in translational repression. *Genes Dev.* **18**, 504–11 (2004).
346. Friedman, R. C., Farh, K. K. H., Burge, C. B. & Bartel, D. P. Most mammalian mRNAs are conserved targets of microRNAs. *Genome Res.* **19**, 92–105 (2009).
347. Mullany, L. E., Herrick, J. S., Wolff, R. K. & Slattery, M. L. MicroRNA Seed Region Length Impact on Target Messenger RNA Expression and Survival in Colorectal Cancer. *PLoS One* **11**, e0154177 (2016).
348. Felekis, K., Touvana, E., Stefanou, C. & Deltas, C. microRNAs: a newly described class of encoded molecules that play a role in health and disease. *Hippokratia* **14**, 236–40 (2010).
349. Farazi, T. A., Juranek, S. A. & Tuschl, T. The growing catalog of small RNAs and their association with distinct Argonaute/Piwi family members. *Development* **135**, 1201–1214 (2008).
350. Stark, A., Brennecke, J., Bushati, N., Russell, R. B. & Cohen, S. M. Animal MicroRNAs Confer Robustness to Gene Expression and Have a Significant Impact on 3'UTR Evolution. *Cell* **123**, 1133–1146 (2005).
351. Carthew, R. W. & Sontheimer, E. J. Origins and Mechanisms of

miRNAs and siRNAs. doi:10.1016/j.cell.2009.01.035

352. Aleman, L. M., Doench, J. & Sharp, P. A. Comparison of siRNA-induced off-target RNA and protein effects. *RNA* **13**, 385–395 (2007).
353. Pillai, R. S. MicroRNA function: multiple mechanisms for a tiny RNA? *RNA* **11**, 1753–61 (2005).
354. Pfaff, J. *et al.* Structural features of Argonaute-GW182 protein interactions. *Proc. Natl. Acad. Sci. U. S. A.* **110**, E3770-9 (2013).
355. Wilson, R. C. & Doudna, J. A. Molecular Mechanisms of RNA Interference. *Annu. Rev. Biophys.* **42**, 217–239 (2013).
356. Guo, H., Ingolia, N. T., Weissman, J. S. & Bartel, D. P. Mammalian microRNAs predominantly act to decrease target mRNA levels. *Nature* **466**, 835–40 (2010).
357. Braun, J. E., Huntzinger, E. & Izaurralde, E. in 147–163 (Springer, New York, NY, 2013). doi:10.1007/978-1-4614-5107-5\_9
358. Li, Z. & Rana, T. M. Molecular Mechanisms of RNA-Triggered Gene Silencing Machineries. *Acc. Chem. Res.* **45**, 1122–1131 (2012).
359. Fabian, M. R. *et al.* Mammalian miRNA RISC Recruits CAF1 and PABP to Affect PABP-Dependent Deadenylation. *Mol. Cell* **35**, 868–880 (2009).
360. Chu, C. & Rana, T. M. Translation Repression in Human Cells by MicroRNA-Induced Gene Silencing Requires RCK/p54. *PLoS Biol.* **4**, e210 (2006).

361. Fukao, A. *et al.* MicroRNAs Trigger Dissociation of eIF4A1 and eIF4AII from Target mRNAs in Humans. *Mol. Cell* **56**, 79–89 (2014).
362. Li, Y. & Kowdley, K. V. MicroRNAs in Common Human Diseases. *Genomics. Proteomics Bioinformatics* **10**, 246–253 (2012).
363. Mattick, J. S. & Makunin, I. V. Small regulatory RNAs in mammals. *Hum. Mol. Genet.* **14**, R121–R132 (2005).
364. Schetter, A. J., Heegaard, N. H. H. & Harris, C. C. Inflammation and cancer: interweaving microRNA, free radical, cytokine and p53 pathways. *Carcinogenesis* **31**, 37–49 (2010).
365. O'Reilly, S. MicroRNAs in fibrosis: Opportunities and challenges. *Arthritis Res. Ther.* **18**, 1–10 (2016).
366. van Rooij, E. *et al.* Dysregulation of microRNAs after myocardial infarction reveals a role of miR-29 in cardiac fibrosis. *Proc. Natl. Acad. Sci.* **105**, 13027–13032 (2008).
367. Suzuki, H., Maruyama, R., Yamamoto, E. & Kai, M. DNA methylation and microRNA dysregulation in cancer. *Mol. Oncol.* **6**, 567–578 (2012).
368. Ardekani, A. M. & Naeini, M. M. The Role of MicroRNAs in Human Diseases. *Avicenna J. Med. Biotechnol.* **2**, 161–79 (2010).
369. Naeini, M. M. & Ardekani, A. M. Noncoding RNAs and Cancer. *Avicenna J. Med. Biotechnol.* **1**, 55–70 (2009).
370. Xu, S. microRNA expression in the eyes and their significance in relation to functions. *Prog. Retin. Eye Res.* **28**, 87–116 (2009).

371. Leichter, A. L., Sullivan, M. J., Eccles, M. R. & Chatterjee, A. MicroRNA expression patterns and signalling pathways in the development and progression of childhood solid tumours. *Mol. Cancer* **16**, 15 (2017).
372. Peng, C.-H. *et al.* MicroRNAs and cataracts: correlation among let-7 expression, age and the severity of lens opacity. *Br. J. Ophthalmol.* **96**, 747–751 (2012).
373. Chen, K.-C. *et al.* MicroRNA-328 May Influence Myopia Development by Mediating the *PAX6* Gene. *Investig. Ophthalmology Vis. Sci.* **53**, 2732 (2012).
374. Romano, G. L. *et al.* Retinal and Circulating miRNAs in Age-Related Macular Degeneration: An In vivo Animal and Human Study. *Front. Pharmacol.* **8**, 168 (2017).
375. Wang, L.-L., Hu, H.-F. & Feng, Y.-Q. Suppressive effect of microRNA-143 in retinoblastoma. *Int. J. Ophthalmol.* **9**, 1584–1590 (2016).
376. Wu, C. *et al.* Discrepant Expression of MicroRNAs in Transparent and Cataractous Human Lenses. *Investig. Ophthalmology Vis. Sci.* **53**, 3906 (2012).
377. Tanaka, Y. *et al.* Profiles of extracellular miRNAs in the aqueous humor of glaucoma patients assessed with a microarray system. *Sci. Rep.* **4**, 5089 (2014).
378. Yu, X., Zheng, H., Chan, M. T. & Wu, W. K. K. MicroRNAs: new players in cataract. *Am. J. Transl. Res.* **9**, 3896–3903 (2017).

379. Drewry, M. D. *et al.* Differentially expressed microRNAs in the aqueous humor of patients with exfoliation glaucoma or primary open-angle glaucoma. *Hum. Mol. Genet.* **0**, 1–13 (2018).
380. Guo, R., Shen, W., Su, C., Jiang, S. & Wang, J. Relationship between the Pathogenesis of Glaucoma and miRNA. *Ophthalmic Res.* **57**, 194–199 (2017).
381. Gonzalez, P., Li, G., Qiu, J., Wu, J. & Luna, C. Role of MicroRNAs in the Trabecular Meshwork. *J. Ocul. Pharmacol. Ther.* **30**, 128–137 (2014).
382. Putten, J. Van. Growth characteristics. *Infect. Dis. (Auckl)*. 1676–1689 (2005). doi:10.1016/B978-0-323-04579-7.00168-4
383. Barber, R. D., Harmer, D. W., Coleman, R. A. & Clark, B. J. GAPDH as a housekeeping gene: analysis of GAPDH mRNA expression in a panel of 72 human tissues. *Physiol. Genomics* **21**, 389–395 (2005).
384. Vandesompele, J. *et al.* Accurate normalization of real-time quantitative RT-PCR data by geometric averaging of multiple internal control genes. *Genome Biol.* **3**, RESEARCH0034 (2002).
385. Yamashita, H. *et al.* [Functions of the transforming growth factor-beta superfamily in eyes]. *Nihon. Ganka Gakkai Zasshi* **101**, 927–47 (1997).
386. Pasquaie, L. R., Dorman-pease, M. E., Lutty, G. A., Quigley, H. A. & Jampel, H. D. Immunolocalisation of TGF-beta 1, TGF-beta 2, and TGF-beta 3 in the anterior segment of the human eye. *Ophthalmology* **34**, (1993).

387. Saika, S. TGF $\beta$  pathobiology in the eye. *Lab. Investig.* **86**, 106–115 (2006).
388. Connor, T. B. *et al.* Correlation of fibrosis and transforming growth factor- $\beta$  type 2 levels in the eye. *J. Clin. Invest.* **83**, 1661–6 (1989).
389. Knisely, T. L., Bleicher, P. A., Vibbard, C. A. & Granstein, R. D. Production of latent transforming growth factor-beta and other inhibitory factors by cultured murine iris and ciliary body cells. *Curr. Eye Res.* **10**, 761–71 (1991).
390. Edward, D. P. & Bouhenni, R. Anterior segment alterations and comparative aqueous humor proteomics in the buphthalmic rabbit (an American Ophthalmological Society thesis). *Trans. Am. Ophthalmol. Soc.* **109**, 66–114 (2011).
391. Horn, V. *et al.* 868 Reports Growth factors in aqueous humor of normal and inflamed eyes of rabbits . D . Reports 869 Table I . Effect of various aqueous humors on the specific blast transformation induced by Origin of. 868–870 (2018).
392. Cousins, S. W., McCabe, M. M., Danielpour, D. & Streilin, J. W. Identification of transforming growth factor beta as an immunosuppressive factor in aqueous humour. *Invest. Ophthalmol. Vis. Sci.* **32**, 2201–2211 (1991).
393. Inatani, M. *et al.* Transforming growth factor-beta 2 levels in aqueous humor of glaucomatous eyes. *Graefes Arch. Clin. Exp. Ophthalmol.* **239**, 109–13 (2001).
394. Agarwal, P., Daher, A. M. & Agarwal, R. Aqueous humor TGF- $\beta$ 2

- levels in patients with open-angle glaucoma: A meta-analysis. *Mol. Vis.* **21**, 612–20 (2015).
395. Picht, G., Welge-Luessen, U., Grehn, F. & Lütjen-Drecoll, E. Transforming growth factor beta 2 levels in the aqueous humor in different types of glaucoma and the relation to filtering bleb development. *Graefes Arch. Clin. Exp. Ophthalmol.* **239**, 199–207 (2001).
396. Ochiai, Y. & Ochiai, H. Higher concentration of transforming growth factor-beta in aqueous humor of glaucomatous eyes and diabetic eyes. *Jpn. J. Ophthalmol.* **46**, 249–53 (2002).
397. Fuchshofer, R. & Tamm, E. R. The role of TGF- $\beta$  in the pathogenesis of primary open-angle glaucoma. *Cell Tissue Res.* **347**, 279–290 (2012).
398. Erickson-Lamy, K., Schroeder, A. & Epstein, D. L. Ethacrynic acid induces reversible shape and cytoskeletal changes in cultured cells. *Investig. Ophthalmol. Vis. Sci.* **33**, 2631–2640 (1992).
399. Tian, B., Geiger, B., Epstein, D. L. & Kaufman, P. L. Cytoskeletal involvement in the regulation of aqueous humor outflow. *Investig. Ophthalmol. Vis. Sci.* **41**, 619–623 (2000).
400. Vasantha Rao, P., Deng, P. F., Kumar, J. & Epstein, D. L. Modulation of aqueous humor outflow facility by the Rho kinase-specific inhibitor Y-27632. *Investig. Ophthalmol. Vis. Sci.* **42**, 1029–1037 (2001).
401. Wiederholt, M., Bielka, S., Schweig, F., Lütjen-Drecoll, E. & Lepple-

- Wienhues, A. Regulation of outflow rate and resistance in the perfused anterior segment of the bovine eye. *Exp. Eye Res.* **61**, 223–34 (1995).
402. Gottanka, J., Chan, D., Eichhorn, M., Lütjen-Drecoll, E. & Ethier, C. R. Effects of TGF-beta2 in perfused human eyes. *Invest. Ophthalmol. Vis. Sci.* **45**, 153–8 (2004).
403. Peeters, A. *et al.* Quantifying the effect of intraocular pressure reduction on the occurrence of glaucoma. *Acta Ophthalmol.* **88**, 5–11 (2010).
404. Coleman, A. L. & Miglior, S. Risk Factors for Glaucoma Onset and Progression. *Surv. Ophthalmol.* **53**, 3–10 (2008).
405. Zhao, X., Ramsey, K. E., Stephan, D. A. & Russell, P. Gene and protein expression changes in human trabecular meshwork cells treated with transforming growth factor- $\beta$ . *Investig. Ophthalmol. Vis. Sci.* **45**, 4023–4034 (2004).
406. Fuchshofer, R., Stephan, D. A., Russell, P. & Tamm, E. R. Gene expression profiling of TGF $\beta$ 2- and/or BMP7-treated trabecular meshwork cells: Identification of Smad7 as a critical inhibitor of TGF- $\beta$ 2 signaling. *Exp. Eye Res.* **88**, 1020–1032 (2009).
407. Fuchshofer, R., Stephan, D. A., Russell, P. & Tamm, E. R. Gene expression profiling of TGF $\beta$ 2- and/or BMP7-treated trabecular meshwork cells: Identification of Smad7 as a critical inhibitor of TGF- $\beta$ 2 signaling. *Gene Expr.* **88**, 1020–1032 (2011).
408. Fuchshofer, R., Yu, A. H. L., Welge-Lüssen, U. & Tamm, E. R. Bone

- morphogenetic protein-7 is an antagonist of transforming growth factor-beta2 in human trabecular meshwork cells. *Invest. Ophthalmol. Vis. Sci.* **48**, 715–26 (2007).
409. Tamm, E. R., Russell, P., Epstein, D. L., Johnson, D. H. & Piatigorsky, J. Modulation of myocilin/TIGR expression in human trabecular meshwork. *Invest Ophthalmol Vis Sci* **40**, 2577–2582 (1999).
410. Lu, U. W., May, C. A., Eichhorn, M., Bloemendal, H. & Lu, W. AlphaB-crystallin in the TM is inducible by transforming growth factor beta. 2235–2241 (2018).
411. Welge-Lüssen, U., May, C. a & Lütjen-Drecoll, E. Induction of tissue transglutaminase in the trabecular meshwork by TGF-beta1 and TGF-beta2. *Invest. Ophthalmol. Vis. Sci.* **41**, 2229–2238 (2000).
412. Li, J., Tripathi, B. J. & Tripathi, R. C. Modulation of pre-mRNA splicing and protein production of fibronectin by TGF- $\beta$ 2 in porcine trabecular cells. *Investig. Ophthalmol. Vis. Sci.* **41**, 3437–3443 (2000).
413. Flügel-Koch, C., Ohlmann, A., Fuchshofer, R., Welge-Lüssen, U. & Tamm, E. R. Thrombospondin-1 in the trabecular meshwork: Localization in normal and glaucomatous eyes, and induction by TGF- $\beta$ 1 and dexamethasone in vitro. *Exp. Eye Res.* **79**, 649–663 (2004).
414. Bumgarner, R. DNA microarrays: Types, Applications and their future. *Curr Protoc Mol Biol.* **6137**, 1–17 (2013).

415. Medina-Ortiz, W. E., Belmares, R., Neubauer, S., Wordinger, R. J. & Clark, A. F. Cellular Fibronectin Expression in Human Trabecular Meshwork and Induction by Transforming Growth Factor- $\beta$ 2. *Investig. Ophthalmology Vis. Sci.* **54**, 6779 (2013).
416. Wang, Z., Gerstein, M. & Snyder, M. RNA-Seq: a revolutionary tool for transcriptomics. (2009). doi:10.1038/nrg2484
417. Hernandez, M. R. *et al.* Human trabecular meshwork cells in culture: Morphology and extracellular matrix components. *Investig. Ophthalmol. Vis. Sci.* **28**, 1655–1660 (1987).
418. Krämer, A., Green, J., Pollard, J. & Tugendreich, S. Causal analysis approaches in Ingenuity Pathway Analysis. *Bioinformatics* **30**, 523–530 (2014).
419. Wiggs, J. L. *et al.* Common variants at 9p21 and 8q22 are associated with increased susceptibility to optic nerve degeneration in glaucoma. *PLoS Genet.* **8**, (2012).
420. Wiggs, J. L. & Pasquale, L. R. Genetics of glaucoma. *Hum. Mol. Genet.* **26**, R21–R27 (2017).
421. Liu, Y. & Allingham, R. R. Major review: Molecular genetics of primary open-angle glaucoma. *Exp. Eye Res.* **160**, 62–84 (2017).
422. Danford, I. D. *et al.* Characterizing the ‘POAGome’: A bioinformatics-driven approach to primary open-angle glaucoma. *Prog. Retin. Eye Res.* **58**, 89–114 (2017).
423. Polansky, J. R., Fauss, D. J. & Zimmerman, C. C. Regulation of TIGR/MYOC gene expression in human trabecular meshwork cells.

- Eye* **14**, 503–514 (2000).
424. Grierson, I., Marshall, J. & Robins, E. Human Trabecular Meshwork in Primary Culture: A Morphological and Autoradiographic Study. (1983). at <[https://ac.els-cdn.com/0014483583901720/1-s2.0-0014483583901720-main.pdf?\\_tid=a54735f8-feb4-466d-a35e-a8b7ccb013cb&acdnat=1528982557\\_9b6f544627af439f2e53de3dbf9076e6](https://ac.els-cdn.com/0014483583901720/1-s2.0-0014483583901720-main.pdf?_tid=a54735f8-feb4-466d-a35e-a8b7ccb013cb&acdnat=1528982557_9b6f544627af439f2e53de3dbf9076e6)>
425. Goodpaster, T. *et al.* An immunohistochemical method for identifying fibroblasts in formalin-fixed, paraffin-embedded tissue. *J. Histochem. Cytochem.* **56**, 347–58 (2008).
426. Zhang, X., Ognibene, C. M., Clark, A. F. & Yorio, T. Dexamethasone inhibition of trabecular meshwork cell phagocytosis and its modulation by glucocorticoid receptor  $\beta$ . *Exp. Eye Res.* **84**, 275–284 (2007).
427. Matsumoto, Y. & Johnson, D. H. Dexamethasone decreases phagocytosis by human trabecular meshwork cells in situ. *Invest. Ophthalmol. Vis. Sci.* **38**, 1902–7 (1997).
428. Tripathi, R. C., Li, J., Chan, W. A. & Tripathi, B. J. Aqueous Humor in Glaucomatous Eyes Contains an Increased Level of TGF- $\beta$ 2. *Exp. Eye Res.* **59**, 723–728 (1994).
429. Amano, M., Nakayama, M. & Kaibuchi, K. Rho-kinase/ROCK: A key regulator of the cytoskeleton and cell polarity. *Cytoskeleton* **67**, 545–554 (2010).
430. Wang, J., Liu, X. & Zhong, Y. Rho/Rho-associated kinase pathway

- in glaucoma (Review). *Int. J. Oncol.* **43**, 1357–1367 (2013).
431. Loirand, G. Rho Kinases in Health and Disease: From Basic Science to Translational Research. *Pharmacol. Rev.* **67**, 1074–1095 (2015).
432. Nomikou, E., Livitsanou, M., Stournaras, C. & Kardassis, D. Transcriptional and post-transcriptional regulation of the genes encoding the small GTPases RhoA, RhoB, and RhoC: implications for the pathogenesis of human diseases. *Cell. Mol. Life Sci.* (2018). doi:10.1007/s00018-018-2787-y
433. Rao, P. V., Pattabiraman, P. P. & Kopczynski, C. Role of the Rho GTPase/Rho kinase signaling pathway in pathogenesis and treatment of glaucoma: Bench to bedside research. *Exp. Eye Res.* **158**, 23–32 (2017).
434. Katoh, K., Kano, Y. & Noda, Y. Rho-associated kinase-dependent contraction of stress fibres and the organization of focal adhesions. *J. R. Soc. Interface* **8**, 305–11 (2011).
435. Hartmann, S., Ridley, A. J. & Lutz, S. The Function of Rho-Associated Kinases ROCK1 and ROCK2 in the Pathogenesis of Cardiovascular Disease. *Front. Pharmacol.* **6**, 276 (2015).
436. Kassianidou, E., Hughes, J. H. & Kumar, S. Activation of ROCK and MLCK tunes regional stress fiber formation and mechanics via preferential myosin light chain phosphorylation. *Mol. Biol. Cell* **28**, 3832–3843 (2017).
437. Edwards, D. C. & Gill, G. N. Structural features of LIM kinase that control effects on the actin cytoskeleton. *J. Biol. Chem.* **274**,

- 11352–11361 (1999).
438. Amin, E. *et al.* Rho-kinase: Regulation, (dys)function, and inhibition. *Biol. Chem.* **394**, 1399–1410 (2013).
439. Sharanek, A. *et al.* Rho-kinase/myosin light chain kinase pathway plays a key role in the impairment of bile canaliculi dynamics induced by cholestatic drugs. *Sci. Rep.* **6**, 1–18 (2016).
440. Mills, J. C., Stone, N. L., Erhardt, J. & Pittman, R. N. Apoptotic membrane blebbing is regulated by myosin light chain phosphorylation. *J. Cell Biol.* **140**, 627–636 (1998).
441. Nakajima, E., Nakajima, T., Minagawa, Y., Shearer, T. R. & Azuma, M. Contribution of ROCK in contraction of trabecular meshwork: Proposed mechanism for regulating aqueous outflow in monkey and human eyes. *J. Pharm. Sci.* **94**, 701–708 (2005).
442. Steglitz, K. & Universitat, D. F. Differential Smooth Trabecular Muscle-like Meshwork Contractile and Ciliary Muscle of. *Exp Eye Res* **53**, 33–38 (1991).
443. Inoue, T. & Tanihara, H. Rho-associated kinase inhibitors: A novel glaucoma therapy. *Prog. Retin. Eye Res.* **37**, 1–12 (2013).
444. Zhu, Y., Kakinuma, N., Wang, Y. & Kiyama, R. Kank proteins: A new family of ankyrin-repeat domain-containing proteins. *Biochim. Biophys. Acta - Gen. Subj.* **1780**, 128–133 (2008).
445. Walker, M. G. & Volkmuth, W. Cell adhesion and matrix remodeling genes identified by co-expression analysis. *Gene Funct. Dis.* **3**, 109–112 (2002).

446. Pattabiraman, P. P., Rao, P. V. & Carolina, N. Mechanistic basis of Rho GTPase-induced extracellular matrix synthesis in trabecular meshwork cells. 749–763 (2010). doi:10.1152/ajpcell.00317.2009.
447. Afshari, N. A. *et al.* Genome-wide association study identifies three novel loci in Fuchs endothelial corneal dystrophy. *Nat. Commun.* **8**, (2017).
448. Koizumi, N., Kinoshita, S. & Okumura, N. The Role of Rho Kinase Inhibitors in Corneal Endothelial Dysfunction. *Curr. Pharm. Des.* **23**, 660–666 (2017).
449. Richter, K. & Kietzmann, T. Reactive oxygen species and fibrosis: further evidence of a significant liaison. *Cell Tissue Res.* **365**, 591–605 (2016).
450. Latella, G. Redox Imbalance in Intestinal Fibrosis: Beware of the TGF $\beta$ -1, ROS, and Nrf2 Connection. *Dig. Dis. Sci.* **63**, 312–320 (2018).
451. Jiang, F., Liu, G.-S., Dusting, G. J. & Chan, E. C. NADPH oxidase-dependent redox signaling in TGF- $\beta$ -mediated fibrotic responses. *Redox Biol.* **2**, 267–272 (2014).
452. Brown, K. D. *et al.* Transforming growth factor  $\beta$ 1-induced NADPH oxidase-4 expression and fibrotic response in conjunctival fibroblasts. *Investig. Ophthalmol. Vis. Sci.* **58**, 3011–3017 (2017).
453. Das, S. J., Lovicu, F. J. & Collinson, E. J. Nox4 Plays a Role in TGF- $\beta$ -Dependent Lens Epithelial to Mesenchymal Transition. *Investig. Ophthalmology Vis. Sci.* **57**, 3665 (2016).

454. GU, X.-J. *et al.* Involvement of NADPH oxidases in alkali burn-induced corneal injury. *Int. J. Mol. Med.* **38**, 75–82 (2016).
455. Nisimoto, Y., Diebold, B. A., Constantino-Gomes, D. & Lambeth, J. D. Nox4: A hydrogen peroxide-generating oxygen sensor. *Biochemistry* **53**, 5111–5120 (2014).
456. Jiang, F., Liu, G. S., Dusting, G. J. & Chan, E. C. NADPH oxidase-dependent redox signaling in TGF-Beta-mediated fibrotic responses. *Redox Biol.* **2**, 267–272 (2014).
457. O’Callaghan, J., Cassidy, P. S. & Humphries, P. Open-angle glaucoma: therapeutically targeting the extracellular matrix of the conventional outflow pathway. *Expert Opin. Ther. Targets* **21**, 1037–1050 (2017).
458. Ferreira, S. M., Lerner, S. F., Brunzini, R., Evelson, P. A. & Llesuy, S. F. Oxidative stress markers in aqueous humor of glaucoma patients. *Am. J. Ophthalmol.* **137**, 62–69 (2004).
459. Izzotti, A., Sacca, S. C., Longobardi, M. & Cartiglia, C. Mitochondrial Damage in the Trabecular Meshwork of Patients With Glaucoma. *Arch Ophthalmol* **128**, 724–730 (2010).
460. Hogg, P., Calthorpe, M., Batterbury, M. & Grierson, I. Aqueous humor stimulates the migration of human trabecular meshwork cells in vitro. *Invest Ophthalmol Vis Sci* **41**, 1091–1098 (2000).
461. Sampson, N., Berger, P. & Zenzmaier, C. Therapeutic targeting of redox signaling in myofibroblast differentiation and age-related fibrotic disease. *Oxid. Med. Cell. Longev.* **2012**, (2012).

462. Maguire, J. J. & Davenport, A. P. Endothelin Receptors and Their Antagonists. *Semin. Nephrol.* **35**, 125–136 (2015).
463. Yanagisawa, M. *et al.* A novel potent vasoconstrictor peptide produced by vascular endothelial cells. *Nature* **332**, 411–415 (1988).
464. Zee, C. L. Von, Langert, K. A. & Stubbs, E. B. Transforming Growth Factor- $\beta$ 2 Induces Synthesis and Secretion of Endothelin-1 in Human Trabecular Meshwork Cells. *Investig. Ophthalmology Vis. Sci.* **53**, 5279 (2012).
465. Chakravarthy, U., Douglas, A. J., Bailie, J. R., McKibben, B. & Archer, D. B. Immunoreactive endothelin distribution in ocular tissues. *Investig. Ophthalmol. Vis. Sci.* **35**, 2448–2454 (1994).
466. Lepple-Wienhues, A. *et al.* Endothelin-Like Immunoreactivity in the Aqueous Humour and in Conditioned Medium from Cultured Ciliary Epithelial Cells. *Curr. Eye Res.* **11**, 1041–1046 (1992).
467. Noske, W. Endothelin-like immunoreactivity in aqueous humor of patients with primary open-angle glaucoma and cataract. *Graefes Arch. Clin. Exp. Ophthalmol.* **235**, 551–552 (1997).
468. Chauhan, B. C. *et al.* Model of endothelin-1-induced chronic optic neuropathy in rat. *Invest. Ophthalmol. Vis. Sci.* **45**, 144–52 (2004).
469. Luna, C. *et al.* Regulation of trabecular meshwork cell contraction and intraocular pressure by miR-200c. *PLoS One* **7**, e51688 (2012).
470. Cellini, M., Versura, P., Zamparini, E., Bendo, E. & Campos, E. C. Effects of endothelin-1 and flunarizine on human trabecular

- meshwork cell contraction. *Exp. Biol. Med. (Maywood)*. **231**, 1081–4 (2006).
471. Pattabiraman, P. P. & Rao, P. V. Mechanistic basis of Rho GTPase-induced extracellular matrix synthesis in trabecular meshwork cells. *Am. J. Physiol. Cell Physiol.* **298**, C749-63 (2010).
472. Sugiyama, T., Moriya, S., Oku, H. & Azuma, I. Association of endothelin-1 with normal tension glaucoma: clinical and fundamental studies. *Surv. Ophthalmol.* **39 Suppl 1**, S49-56 (1995).
473. Orgul, S., Cioffi, G. A., Bacon, D. R. & Van Buskirk, E. M. An endothelin-1 induced model of chronic optic nerve ischemia in rhesus monkeys. *J. Glaucoma* **5**, 135–138 (1996).
474. Tezel, G., Kass, M. A., Kolker, A. E., Becker, B. & Wax, M. B. Plasma and aqueous humor endothelin levels in primary open-angle glaucoma. *J. Glaucoma* **6**, 83–9 (1997).
475. Yorio, T., Krishnamoorthy, R. & Prasanna, G. Endothelin: is it a contributor to glaucoma pathophysiology? *J. Glaucoma* **11**, 259–70 (2002).
476. Flammer, J., Haefliger, I. O., Orgül, S. & Resink, T. Vascular dysregulation: a principal risk factor for glaucomatous damage? *J. Glaucoma* **8**, 212–9 (1999).
477. Flammer, J. *et al.* The impact of ocular blood flow in glaucoma. *Prog. Retin. Eye Res.* **21**, 359–393 (2002).
478. Granstam, E., Wang, L. & Bill, A. Effects of endothelins (ET-1, ET-2

- and ET-3) in the rabbit eye; role of prostaglandins. *Eur. J. Pharmacol.* **194**, 217–23 (1991).
479. Okada, K., Sugiyama, K., Haque, M. S., Taniguchi, T. & Kitazawa, Y. The effects of endothelin-1 on intraocular pressure and pupillary diameter in rabbits. *Jpn. J. Ophthalmol.* **39**, 233–41 (1995).
480. Holló, G., Lakatos, P. & Vargha, P. Immediate Increase in Aqueous Humour Endothelin 1 Concentration and Intra-Ocular Pressure after Argon Laser Trabeculoplasty in the Rabbit. *Ophthalmologica* **214**, 292–295 (2000).
481. Rosenthal, R. *et al.* Effects of ML-7 and Y-27632 on carbachol- and endothelin-1-induced contraction of bovine trabecular meshwork. *Exp. Eye Res.* **80**, 837–845 (2005).
482. Rosenthal, R. & Fromm, M. Endothelin antagonism as an active principle for glaucoma therapy. *Br. J. Pharmacol.* **162**, 806–16 (2011).
483. Polak, K. *et al.* Effect of endothelin and BQ123 on ocular blood flow parameters in healthy subjects. *Invest. Ophthalmol. Vis. Sci.* **42**, 2949–56 (2001).
484. Greene, L. A., Liu, D. X., Troy, C. M. & Biswas, S. C. Cell cycle molecules define a pathway required for neuron death in development and disease. *Biochim. Biophys. Acta - Mol. Basis Dis.* **1772**, 392–401 (2007).
485. Hannon, G. J. & Beach, D. p15INK4B is a potential effector of TGF-beta-induced cell cycle arrest. *Nature* **371**, 257–61 (1994).

486. Nanda, V. & Leeper, N. CDKN2B Regulates TGF-Beta Signalling and Smooth Muscle Cell Investment of Hypoxic Neovessels. **21**, 129–139 (2017).
487. Ravitz, M. J. & Wenner, C. E. Cyclin-dependent kinase regulation during G1 phase and cell cycle regulation by TGF-beta. *Adv. Cancer Res.* **71**, 165–207 (1997).
488. Takamoto, M. *et al.* Common variants on chromosome 9p21 are associated with normal tension Glaucoma. *PLoS One* **7**, (2012).
489. Vishal, M. *et al.* Evaluation of genetic association of the INK4 locus with primary open angle glaucoma in east indian population. *Sci. Rep.* **4**, 7–10 (2014).
490. Ng, S. K. *et al.* Genetic association at the 9p21 glaucoma locus contributes to sex bias in normal-tension glaucoma. *Investig. Ophthalmol. Vis. Sci.* **57**, 3416–3421 (2016).
491. Osman, W., Low, S.-K., Takahashi, A., Kubo, M. & Nakamura, Y. A genome-wide association study in the Japanese population confirms 9p21 and 14q23 as susceptibility loci for primary open angle glaucoma. *Hum. Mol. Genet.* **21**, 2836–2842 (2012).
492. Cunnington, M. S., Koref, M. S., Mayosi, B. M., Burn, J. & Keavney, B. Chromosome 9p21 SNPs associated with multiple disease phenotypes correlate with ANRIL expression. *PLoS Genet.* **6**, (2010).
493. Baker, A. *et al.* A Common Variant on Chromosome 9p21 affects the risk of myocardial infarction. 1491–1494 (2007).

494. Mcpherson, R. *et al.* A Common Allele on Chromosome 9 Associated with Coronary Heart Disease. *Heart Dis.* **316**, 1488–1491 (2009).
495. Zeggini, E. *et al.* Multiple type 2 diabetes susceptibility genes following genome-wide association scan in UK samples. *Science (80-. ).* **316**, 1336–1341 (2007).
496. Wrensch, M. *et al.* Variants in the CDKN2B and RTEL1 regions are associated with high grade glioma susceptibility. **41**, 905–908 (2010).
497. Burdon, K. P. *et al.* Genome-wide association study identifies susceptibility loci for open angle glaucoma at TMCO1 and CDKN2B-AS1. *Nat. Genet.* **43**, 574–578 (2011).
498. Pasmant, E., Sabbagh, A., Vidaud, M. & Bièche, I. ANRIL, a long, noncoding RNA, is an unexpected major hotspot in GWAS. *FASEB J.* **25**, 444–448 (2011).
499. Jarinova, O. *et al.* Functional Analysis of the Chromosome 9p21.3 Coronary Artery Disease Risk Locus. *Arterioscler. Thromb. Vasc. Biol.* **29**, 1671–1677 (2009).
500. Wiggs, J. L. Glaucoma Genes and Mechanisms. *Prog. Mol. Biol. Transl. Sci.* **134**, 315–342 (2015).
501. Yamaguchi, T. P. Heads or tails: Wnts and anterior-posterior patterning. *Curr. Biol.* **11**, 713–724 (2001).
502. Fuhrmann, S. Wnt signaling in eye organogenesis. *Organogenesis* **4**, 60–67 (2008).

503. de longh, R. U., Abud, H. E. & Hime, G. R. WNT/Frizzled signaling in eye development and disease. *Front. Biosci.* **11**, 2442–64 (2006).
504. Mao, W. *et al.* Existence of the Canonical Wnt Signaling Pathway in the Human Trabecular Meshwork. *Investig. Ophthalmology Vis. Sci.* **53**, 7043 (2012).
505. Schulte, G. & Bryja, V. The Frizzled family of unconventional G-protein-coupled receptors. *Trends Pharmacol. Sci.* **28**, 518–525 (2007).
506. He, X. LDL receptor-related proteins 5 and 6 in Wnt/ -catenin signaling: Arrows point the way. *Development* **131**, 1663–1677 (2004).
507. Habas, R. & Dawid, I. B. Dishevelled and Wnt signaling: Is the nucleus the final frontier? *J. Biol.* **4**, 2–5 (2005).
508. Hoang, B. H. *et al.* Expression pattern of two Frizzled-related genes, Frzb-1 and Sfrp-1, during mouse embryogenesis suggests a role for modulating action of Wnt family members. *Dev. Dyn.* **212**, 364–372 (1998).
509. Glinka, A. *et al.* Dickkopf-1 is a member of a new family of secreted proteins and functions in head induction. *Nature* **391**, 357–362 (1998).
510. Webber, H. C., Bermudez, J. Y., Sethi, A., Clark, A. F. & Mao, W. Crosstalk between TGF $\beta$  and Wnt signaling pathways in the human trabecular meshwork. *Exp. Eye Res.* **148**, 97–102 (2016).

511. Wang, W. H. *et al.* Increased expression of the WNT antagonist sFRP-1 in glaucoma elevates intraocular pressure. *J. Clin. Invest.* **118**, 1056–1064 (2008).
512. Shyam, R., Shen, X., Yue, B. Y. J. T. & Wentz-Hunter, K. K. Wnt gene expression in human trabecular meshwork cells. *Mol. Vis.* **16**, 122–129 (2010).
513. Morgan, J. T., Raghunathan, V. K., Chang, Y. R., Murphy, C. J. & Russell, P. Wnt inhibition induces persistent increases in intrinsic stiffness of human trabecular meshwork cells. *Exp. Eye Res.* **132**, 174–178 (2015).
514. Qu, Y. *et al.* High levels of secreted frizzled-related protein 1 correlate with poor prognosis and promote tumorigenesis in gastric cancer. *Eur. J. Cancer* **49**, 3718–3728 (2013).
515. Wang, X. *et al.* Mutual regulation of the Hippo/Wnt/LPA/TGF- $\beta$  signaling pathways and their roles in glaucoma (Review). *Int. J. Mol. Med.* **41**, 1201–1212 (2017).
516. Wang, J. Lian *et al.* TGF- $\beta$  signaling regulates DACT1 expression in intestinal epithelial cells. *Biomed. Pharmacother.* **97**, 864–869 (2018).
517. Jardim, D. P., Poço, P. C. E. & Campos, A. H. Dact1, a Wnt-Pathway Inhibitor, Mediates Human Mesangial Cell TGF- $\beta$ 1-Induced Apoptosis. *J. Cell. Physiol.* **232**, 2104–2111 (2017).
518. Blee, A. M. & Huang, H. PMEPA1 guards against TGF- $\beta$ -mediated prostate cancer bone metastasis. *Asian J. Urol.* **3**, 1–3 (2016).

519. Izzi, L. & Attisano, L. Regulation of the TGF $\beta$  signalling pathway by ubiquitin-mediated degradation. *Oncogene* **23**, 2071–2078 (2004).
520. Fournier, P. G. J. *et al.* The TGF- $\beta$  Signaling Regulator PMEPA1 Suppresses Prostate Cancer Metastases to Bone. *Cancer Cell* **27**, 809–821 (2015).
521. Lukas, T. J. *et al.* Susceptibility to glaucoma: Differential comparison of the astrocyte transcriptome from glaucomatous African American and Caucasian American donors. *Genome Biol.* **9**, (2008).
522. Fournier, P. G. J. *et al.* Cancer Metastases to Bone. **27**, 809–821 (2016).
523. Liu, Z. *et al.* Low density lipoprotein receptor class A domain containing 4 (LDLRAD4) promotes tumorigenesis of hepatic cancer cells. *Exp. Cell Res.* **360**, 189–198 (2017).
524. Nakano, N. *et al.* C18 orf1, a novel negative regulator of transforming growth factor- $\beta$  signaling. *J. Biol. Chem.* **289**, 12680–12692 (2014).
525. Tsuchida, K. Activins, myostatin and related TGF-beta family members as novel therapeutic targets for endocrine, metabolic and immune disorders. *Curr. Drug Targets. Immune. Endocr. Metabol. Disord.* **4**, 157–66 (2004).
526. Wordinger, R. J. *et al.* Expression of bone morphogenetic proteins (BMP), BMP receptors, and BMP associated proteins in human trabecular meshwork and optic nerve head cells and tissues. *Mol.*

- Vis.* **8**, 241–250 (2002).
527. Wordinger, R. J. *et al.* Effects of TGF- $\beta$ 2, BMP-4, and gremlin in the trabecular meshwork: Implications for glaucoma. *Investig. Ophthalmol. Vis. Sci.* **48**, 1191–1200 (2007).
528. Long, W. FSTL3 and its role in mediating fibrosis and hypertrophy in diet-induced obesity. (2016). at [https://open.bu.edu/handle/2144/16818%5Cnfile:///Users/ryanwalker/papers\\_library/Library.papers3/Files/DB/DB83CB9A-8776-4412-AE83-12411F57B3F3.pdf%5Cnpapers3://publication/uuid/5E49BB80-8408-4ECA-B7FB-C6CCD1046C05](https://open.bu.edu/handle/2144/16818%5Cnfile:///Users/ryanwalker/papers_library/Library.papers3/Files/DB/DB83CB9A-8776-4412-AE83-12411F57B3F3.pdf%5Cnpapers3://publication/uuid/5E49BB80-8408-4ECA-B7FB-C6CCD1046C05)
529. Zhavoronkov, A. *et al.* Pro-fibrotic pathway activation in trabecular meshwork and lamina cribrosa is the main driving force of glaucoma. *Cell Cycle* **15**, 1643–52 (2016).
530. Lan, Y., Kingsley, P. D., Cho, E. S. & Jiang, R. *Osr2*, a new mouse gene related to *Drosophila* odd-skipped, exhibits dynamic expression patterns during craniofacial, limb, and kidney development. *Mech. Dev.* **107**, 175–179 (2001).
531. Mullen, J. R. & DiNardo, S. Establishing parasegments in *Drosophila* embryos: Roles of the odd-skipped and naked genes. *Developmental Biology* **169**, 295–308 (1995).
532. Coulter, D. E. & Wieschaus, E. Gene activities and segmental patterning in *Drosophila*: analysis of odd-skipped and pair-rule double mutants. *Genes Dev.* **2**, 1812–1823 (1988).

533. Kawai, S. & Amano, A. Negative regulation of Odd-skipped related 2 by TGF-beta achieves the induction of cellular migration and the arrest of cell cycle. *Biochem. Biophys. Res. Commun.* **421**, 696–700 (2012).
534. Alowayed, N., Salker, M. S., Zeng, N., Singh, Y. & Lang, F. LEFTY2 Controls Migration of Human Endometrial Cancer Cells via Focal Adhesion Kinase Activity (FAK) and miRNA-200a. *Cell. Physiol. Biochem.* **39**, 815–826 (2016).
535. Casey, B. & Kosaki, K. in *Heart Development* 479–489 (Elsevier, 1999). doi:10.1016/B978-012329860-7/50029-5
536. Tabibzadeh, S. Homeostasis Of Extracellular Matrix By TGF-Beta And LEFTY Siamak Tabibzadeh. 1231–1246 (2002).
537. Fuchshofer, R. & Tamm, E. R. The role of TGF- $\beta$  in the pathogenesis of primary open-angle glaucoma. *Cell Tissue Res.* **347**, 279–90 (2012).
538. Bos, J. L. Ras-like GTPases. *Biochim. Biophys. Acta - Rev. Cancer* **1333**, (1997).
539. Hirata, K., Ohashi, Y., Yamochi, W. & Akita, H. Transforming Growth Factor- 1 and Protein Kinase C Synergistically Activate the c-fos Serum Response Element in Myocardial Cells. **562**, 551–562 (1998).
540. Stolle, K. *et al.* Cloning, genomic organization, and tissue-specific expression of the RASL11B gene. *Biochim. Biophys. Acta - Gene Struct. Expr.* **1769**, 514–524 (2007).

541. Liu, Y. *et al.* Gene Expression Profile in Human Trabecular Meshwork From Patients With Primary Open-Angle Glaucoma. *Investig. Ophthalmology Vis. Sci.* **54**, 6382 (2013).
542. Pankov, R. & Yamada, K. M. Fibronectin at a glance. *J. Cell Sci.* **115**, 3861–3863 (2002).
543. Deng, A. Y., Chauvet, C. & Ménard, A. Alterations in Fibronectin Type III Domain Containing 1 Protein Gene Are Associated with Hypertension. *PLoS One* **11**, e0151399 (2016).
544. Anderegg, U. *et al.* MEL4B3, a novel mRNA is induced in skin tumors and regulated by TGF-beta and pro-inflammatory cytokines. *Exp. Dermatol.* **14**, 709–718 (2005).
545. Das, D. K. *et al.* miR-1207-3p regulates the androgen receptor in prostate cancer via FNDC1/fibronectin. **348**, 190–200 (2017).
546. Folmer, D. E., Elferink, R. P. J. O. & Paulusma, C. C. P4 ATPases - Lipid flippases and their role in disease. *Biochim. Biophys. Acta - Mol. Cell Biol. Lipids* **1791**, 628–635 (2009).
547. Naito, T. *et al.* Phospholipid flippase ATP10A translocates phosphatidylcholine and is involved in plasma membrane dynamics. *J. Biol. Chem.* **290**, 15004–15017 (2015).
548. Fan, B. J., Wang, D. Y., Tham, C. C. Y., Lam, D. S. C. & Pang, C. P. Gene expression profiles of human trabecular meshwork cells induced by triamcinolone and dexamethasone. *Investig. Ophthalmol. Vis. Sci.* **49**, 1886–1897 (2008).
549. Allingham, R. R. *et al.* Early Adult-Onset POAG Linked to 15q11-13

- Using Ordered Subset Analysis. *Investig. Ophthalmology Vis. Sci.* **46**, 2002 (2005).
550. Fu, Y. *et al.* Regulation of NADPH Oxidase Activity Is Associated with miRNA-25-Mediated NOX4 Expression in Experimental Diabetic Nephropathy. *Am. J. Nephrol.* **32**, 581–589 (2010).
551. Vajaranant, T. S. *et al.* Visual Acuity and Intraocular Pressure after Descemet's Stripping Endothelial Keratoplasty in Eyes with and without Preexisting Glaucoma. *Ophthalmology* **116**, 1644–1650 (2009).
552. Clark, A. F. & Wordinger, R. J. The role of steroids in outflow resistance. *Exp Eye Res* **88**, 752–759 (2009).
553. Polansky, J. R. *et al.* Cellular pharmacology and molecular biology of the trabecular meshwork inducible glucocorticoid response gene product. *Ophthalmologica.* **211**, 126–39 (1997).
554. Stone, E. M. *et al.* Identification of a gene that causes primary open angle glaucoma. *Science (80- ).* **275**, 668–670 (1997).
555. Armaly, M. F. & Becker, B. Intraocular pressure response to topical corticosteroids. *Fed. Proc.* **24**, 1274–8 (1965).
556. Becker, B. Intraocular Pressure Response To Topical Corticosteroids. *Invest. Ophthalmol.* **4**, 198–205 (1965).
557. Razeghinejad, M. R. & Katz, L. J. Steroid-induced iatrogenic glaucoma. *Ophthalmic Res.* **47**, 66–80 (2012).
558. Bartlett, J. D., Woolley, T. W. & Adams, C. M. Identification of high intraocular pressure responders to topical ophthalmic

- corticosteroids. *J. Ocul. Pharmacol.* **9**, 35–45 (1993).
559. Paterson, G. Studies of the response to topical dexamethasone of glaucoma relatives. *Trans. Ophthalmol. Soc. U. K.* **85**, 295–305 (1965).
560. Becker, B. & Chevrette, L. Topical corticosteroid testing in glaucoma sibilings. *Arch. Ophthalmol. (Chicago, Ill. 1960)* **76**, 484–7 (1966).
561. Johnson, D. H., Bradley, J. M. B. & Acott, T. S. The effect of dexamethasone on glycosaminoglycans of human trabecular meshwork in perfusion organ culture. *Investig. Ophthalmol. Vis. Sci.* **31**, 2568–2571 (1990).
562. Steely, H. T. *et al.* The effects of dexamethasone on fibronectin expression in cultured human trabecular meshwork cells. *Invest. Ophthalmol. Vis. Sci.* **33**, 2242–50 (1992).
563. Yun, A. J., Murphy, C. G., Polansky, J. R., Newsome, D. A. & Alvarado, J. A. Proteins secreted by human trabecular cells: Glucocorticoid and other effects. *Investig. Ophthalmol. Vis. Sci.* **30**, 2012–2022 (1989).
564. Snyder, R. W., Stamer, W. D., Kramer, T. R. & Seftor, R. E. Corticosteroid treatment and trabecular meshwork proteases in cell and organ culture supernatants. *Exp. Eye Res.* **57**, 461–8 (1993).
565. Partridge, C. A., Weinstein, B. I., Southren, A. L. & Gerritsen, M. E. Dexamethasone induces specific proteins in human trabecular

- meshwork cells. *Invest. Ophthalmol. Vis. Sci.* **30**, 1843–7 (1989).
566. Wordinger, R. J. & Clark, A. F. Effects of glucocorticoids on the trabecular meshwork: towards a better understanding of glaucoma. *Prog. Retin. Eye Res.* **18**, 629–67 (1999).
567. Ishibashi, T. *et al.* cDNA microarray analysis of gene expression changes induced by dexamethasone in cultured human trabecular meshwork cells. *Invest Ophthalmol. Vis. Sci.* **43**, 3691–3697 (2002).
568. Lo, W. R. *et al.* Tissue differential microarray analysis of dexamethasone induction reveals potential mechanisms of steroid glaucoma. *Investig. Ophthalmol. Vis. Sci.* **44**, 473–485 (2003).
569. Leung, Y. F. *et al.* The dual role of dexamethasone on anti-inflammation and outflow resistance demonstrated in cultured human trabecular meshwork cells. *Mol. Vis.* **9**, 425–39 (2003).
570. Rozsa, F. W. *et al.* Gene expression profile of human trabecular meshwork cells in response to long-term dexamethasone exposure. *Mol. Vis.* **12**, 125–141 (2006).
571. Nehmé, A., Lobenhofer, E. K., Stamer, W. D. & Edelman, J. L. Glucocorticoids with different chemical structures but similar glucocorticoid receptor potency regulate subsets of common and unique genes in human trabecular meshwork cells. *BMC Med. Genomics* **2**, 58 (2009).
572. Jain, A., Wordinger, R. J., Yorio, T. & Clark, A. F. Role of the Alternatively Spliced Glucocorticoid Receptor Isoform GR $\beta$  in

- Steroid Responsiveness and Glaucoma. *J. Ocul. Pharmacol. Ther.* **30**, 121–127 (2014).
573. Bamberger, C. M., Bamberger, A. M., de Castro, M. & Chrousos, G. P. Glucocorticoid receptor beta, a potential endogenous inhibitor of glucocorticoid action in humans. *J. Clin. Invest.* **95**, 2435–2441 (1995).
574. Lewis-Tuffin, L. J. & Cidlowski, J. A. The Physiology of Human Glucocorticoid Receptor beta (hGRbeta) and Glucocorticoid Resistance. *Ann. N. Y. Acad. Sci.* **1069**, 1–9 (2006).
575. Zhang, X., Clark, A. F. & Yorio, T. Regulation of glucocorticoid responsiveness in glaucomatous trabecular meshwork cells by glucocorticoid receptor-?? *Investig. Ophthalmol. Vis. Sci.* **46**, 4607–4616 (2005).
576. Spandidos, A., Wang, X., Wang, H. & Seed, B. PrimerBank: A resource of human and mouse PCR primer pairs for gene expression detection and quantification. *Nucleic Acids Res.* **38**, 792–799 (2009).
577. Coutinho, A. E. & Chapman, K. E. The anti-inflammatory and immunosuppressive effects of glucocorticoids, recent developments and mechanistic insights. *Mol. Cell. Endocrinol.* **335**, 2–13 (2011).
578. Evans, R. The steroid and thyroid hormone receptor superfamily. *Science (80-. )*. **240**, 889–895 (1988).
579. James, E. R. The Etiology of Steroid Cataract. *J. Ocul. Pharmacol.*

- Ther.* **23**, 403–420 (2007).
580. Armaly, M. F. Effect of Corticosteroids on Intraocular Pressure and Fluid Dynamics. *Arch. Ophthalmol.* **70**, 482 (1963).
581. Clark, A. F. & Wordinger, R. J. The role of steroids in outflow resistance. *Exp. Eye Res.* **88**, 752–759 (2009).
582. Clark, A. F. *et al.* Dexamethasone alters F-actin architecture and promotes cross-linked actin network formation in human trabecular meshwork tissue. *Cell Motil. Cytoskeleton* **60**, 83–95 (2005).
583. Hamid, Q. A. *et al.* Increased glucocorticoid receptor beta in airway cells of glucocorticoid-insensitive asthma. *Am J Respir Crit Care Med* **159**, 1600–1604 (1999).
584. Derijk, R. H. *et al.* A human glucocorticoid receptor gene variant that increases the stability of the glucocorticoid receptor beta-isoform mRNA is associated with rheumatoid arthritis. *J. Rheumatol.* **28**, 2383–8 (2001).
585. Longui, C. *et al.* Low Glucocorticoid Receptor  $\alpha/\beta$  Ratio in T-cell Lymphoblastic Leukemia. *Horm. Metab. Res.* **32**, 401–406 (2000).
586. Hägg, P. M., Hurskainen, T., Palatsi, R., Ilves, M. & Oikarinen, a. Increased expression of glucocorticoid receptor beta in lymphocytes of patients with severe atopic dermatitis unresponsive to topical corticosteroid. *Br. J. Dermatol.* **162**, 318–24 (2010).
587. Honda, M. *et al.* Expression of glucocorticoid receptor beta in

- lymphocytes of patients with glucocorticoid-resistant ulcerative colitis. *Gastroenterology* **118**, 859–66 (2000).
588. Oakley, R. H., Sar, M. & Cidlowski, J. A. The Human Glucocorticoid Receptor beta Isoform. *J. Biol. Chem.* **271**, 9550–9559 (1996).
589. Zhang, H. *et al.* [Relationship between glucocorticoid receptors in the peripheral blood lymphocytes and trabecular meshwork and glucocorticoid induced glaucoma]. *Zhonghua. Yan Ke Za Zhi.* **42**, 431–4 (2006).
590. Jain, A. *et al.* Effects of thalidomide on glucocorticoid response in trabecular meshwork and steroid-induced glaucoma. *Invest. Ophthalmol. Vis. Sci.* **54**, 3137–42 (2013).
591. Revollo, J. R. & Cidlowski, J. A. Mechanisms Generating Diversity in Glucocorticoid Receptor Signaling. *Ann. N. Y. Acad. Sci.* **1179**, 167–178 (2009).
592. Poveda, J. *et al.* MXRA5 is a TGF- $\beta$ 1-regulated human protein with anti-inflammatory and anti-fibrotic properties. *J. Cell. Mol. Med.* **21**, 154–164 (2017).
593. Stojadinovic, O. *et al.* Novel genomic effects of glucocorticoids in epidermal keratinocytes: Inhibition of apoptosis, interferon- $\gamma$  pathway, and wound healing along with promotion of terminal differentiation. *J. Biol. Chem.* **282**, 4021–4034 (2007).
594. Avraham, H., Park, S. Y., Schinkmann, K. & Avraham, S. RAFTK/Pyk2-mediated cellular signalling. *Cell. Signal.* **12**, 123–133 (2000).

595. Xiong, W. C., Macklem, M. & Parsons, J. T. Expression and characterization of splice variants of PYK2, a focal adhesion kinase-related protein. *J. Cell Sci.* **111** ( Pt 1, 1981–91 (1998).
596. Lev, S. *et al.* Identification of a Novel Family of Targets of PYK2 Related to *Drosophila* Retinal Degeneration B (rdgB) Protein. *Mol. Cell. Biol.* **19**, 2278–2288 (1999).
597. Koch, A. E., Castro-Rueda, H. P., Kenneth, G. K. & Koch, A. E. Differential expression of the FAK family kinases in rheumatoid arthritis and osteoarthritis synovial tissues. *Arthritis Res. Ther.* **9**, 1–10 (2007).
598. Dikic, I., Tokiwa, G., Lev, S., Courtneidge, S. A. & Schlessinger, J. A Role for PYK2 and Src in linking G-protein-coupled Receptors with MAP kinase activation. (1996).
599. Takahashi, E., Inoue, T., Fujimoto, T., Kojima, S. & Tanihara, H. Epithelial mesenchymal transition-like phenomenon in trabecular meshwork cells. *Exp. Eye Res.* **118**, 72–79 (2014).
600. Salgia, R. *et al.* The related adhesion focal tyrosine kinase forms a complex with paxillin in hematopoietic cells. *J. Biol. Chem.* **271**, 31222–31226 (1996).
601. Ohba, T., Ishino, M., Aoto, H. & Sasaki, T. Interaction of two proline-rich sequences of cell adhesion kinase beta with SH3 domains of p130(Cas)-related proteins and a GTPase-activating protein, *Graf. Biochem. J.* **330**, 1249–1254 (1998).
602. Lipsky, B. P. Leupaxin Is a Novel LIM Domain Protein That Forms a

- Complex with PYK2. *J. Biol. Chem.* **273**, 11709–11713 (1998).
603. Okigaki, M. *et al.* Pyk2 regulates multiple signaling events crucial for macrophage morphology and migration. *Proc. Natl. Acad. Sci.* **100**, 10740–10745 (2003).
604. Kwon, H. S. & Tomarev, S. I. Myocilin, a glaucoma-associated protein, promotes cell migration through activation of integrin-focal adhesion kinase-serine/threonine kinase signaling pathway. *J. Cell. Physiol.* **226**, 3392–3402 (2011).
605. Gagen, D., Filla, M. S., Clark, R., Liton, P. & Peters, D. M. Activated  $\alpha\beta 3$  integrin regulates  $\alpha\beta 5$  integrin-mediated phagocytosis in trabecular meshwork cells. *Investig. Ophthalmol. Vis. Sci.* **54**, 5000–5011 (2013).
606. Duffy, L. & O'reilly, S. Cellular Physiology and Biochemistry Cellular Physiology and Biochemistry Duffy et al.: Effect of CLANs in TM Cells Functional Implications of Cross-Linked Actin Networks in Trabecular Meshwork Cells. *Cell Physiol Biochem* **45**, 783–794 (2018).
607. Finnemann, S. C. Focal adhesion kinase signaling promotes phagocytosis of integrin-bound photoreceptors. *EMBO J.* **22**, 4143–54 (2003).
608. Saigusa, K. *et al.* RGC32, a novel p53-inducible gene, is located on centrosomes during mitosis and results in G2/M arrest. *Oncogene* **26**, 1110–1121 (2007).
609. Niculescu, F., Badea, T. & Rus, H. Sublytic C5b-9 induces

- proliferation of human aortic smooth muscle cells Role of mitogen activated protein kinase and phosphatidylinositol. **142**, 47–56 (1999).
610. Badea, T. *et al.* RGC-32 increases p34CDC2 kinase activity and entry of aortic smooth muscle cells into S-phase. *J. Biol. Chem.* **277**, 502–508 (2002).
611. Vlaicu, S. I. *et al.* Role of response gene to complement 32 in diseases. *Arch. Immunol. Ther. Exp. (Warsz)*. **56**, 115–122 (2008).
612. Chen, Q. M. *et al.* Corticosteroids inhibit cell death induced by doxorubicin in cardiomyocytes: induction of antiapoptosis, antioxidant, and detoxification genes. *Mol. Pharmacol.* **67**, 1861–1873 (2005).
613. Almon, R. R., Lai, W., DuBois, D. C. & Jusko, W. J. Cortiosteroid-regulated genes in rat kidney: mining time series array data. **66**, 630–635 (2005).
614. James, E. R., Fresco, V. M. & Robertson, L. L. Glucocorticoid-Induced Changes in the Global Gene Expression of Lens Epithelial Cells. *J. Ocul. Pharmacol. Ther.* **21**, 11–27 (2005).
615. Vlaicu, S. I. *et al.* RGC-32 is expressed in the human atherosclerotic arterial wall: Role in C5b-9-induced cell proliferation and migration. *Exp. Mol. Pathol.* **101**, 221–230 (2016).
616. Sun, Q. *et al.* Overexpression of response gene to complement 32 (RGC32) promotes cell invasion and induces epithelial-

mesenchymal transition in lung cancer cells via the NF- $\kappa$ B signaling pathway. *Tumor Biol.* **34**, 2995–3002 (2013).

617. Xu, R. *et al.* Knockdown of response gene to complement 32 (RGC32) induces apoptosis and inhibits cell growth, migration, and invasion in human lung cancer cells. *Mol. Cell. Biochem.* **394**, 109–118 (2014).
618. Gnainsky, Y. *et al.* Gene expression during chemically induced liver fibrosis: Effect of halofuginone on TGF- $\beta$  signaling. *Cell Tissue Res.* **328**, 153–166 (2007).
619. Esson, D. W., Popp, M. P., Liu, L., Schultz, G. S. & Sherwood, M. B. Microarray analysis of the failure of filtering blebs in a rat model of glaucoma filtering surgery. *Investig. Ophthalmol. Vis. Sci.* **45**, 4450–4462 (2004).
620. Huang, W.-Y. *et al.* RGC-32 Mediates Transforming Growth Factor- $\beta$ -induced Epithelial-Mesenchymal Transition in Human Renal Proximal Tubular Cells. *J. Biol. Chem.* **284**, 9426–9432 (2009).
621. Matsuda, A. *et al.* DNA Methylation Analysis of Human Trabecular Meshwork Cells During Dexamethasone Stimulation DNA Methylation Analysis of Trabecular Meshwork Cells. *Investig. Ophthalmol. Vis. Sci.* **56**, 3801–3809 (2015).
622. Peppi, M., Kujawa, S. G. & Sewell, W. F. A Corticosteroid-Responsive Transcription Factor, Promyelocytic Leukemia Zinc Finger Protein, Mediates Protection of the Cochlea from Acoustic Trauma. *Natl. Institutes Heal.* **5**, 3045–3056 (2010).

623. Fahnenstich, J. *et al.* Promyelocytic leukaemia zinc finger protein (PLZF) is a glucocorticoid- and progesterone-induced transcription factor in human endometrial stromal cells and myometrial smooth muscle cells. *Mol. Hum. Reprod.* **9**, 611–23 (2003).
624. Wasim, M. *et al.* PLZF/ZBTB16, a glucocorticoid response gene in acute lymphoblastic leukemia, interferes with glucocorticoid-induced apoptosis. *J. Steroid Biochem. Mol. Biol.* **120**, 218–27 (2010).
625. Yeyati, P. L. *et al.* Leukemia translocation protein PLZF inhibits cell growth and expression of cyclin A. *Oncogene* **18**, 925–934 (1999).
626. Shiraishi, A., Joko, T., Higashiyama, S. & Ohashi, Y. Role of Promyelocytic Leukemia Zinc Finger Protein in Proliferation of Cultured Human Corneal Endothelial Cells. *Mol. Vis.* **13**, 649–658 (2007).
627. Yu, W. Y. *et al.* Progenitors for the corneal endothelium and trabecular meshwork: a potential source for personalized stem cell therapy in corneal endothelial diseases and glaucoma. *J. Biomed. Biotechnol.* **2011**, 412743 (2011).
628. Smith, D. F., Faber, L. E. & Toft, D. O. Purification of unactivated progesterone receptor and identification of novel receptor-associated proteins. *J. Biol. Chem.* **265**, 3996–4003 (1990).
629. Denny, W. B., Valentine, D. L., Reynolds, P. D., Smith, D. F. & Scammell, J. G. Squirrel monkey immunophilin FKBP51 is a potent inhibitor of glucocorticoid receptor binding [In Process Citation]. *Endocrinology* **141**, 4107–4113 (2000).

630. Riggs, D. L. *et al.* The Hsp90-binding peptidylprolyl isomerase FKBP52 potentiates glucocorticoid signaling in vivo. *EMBO J.* **22**, 1158–1167 (2003).
631. Scammell, J. G., Denny, W. B., Valentine, D. L. & Smiths, D. F. Overexpression of the FK506-binding immunophilin FKBP51 is the common cause of glucocorticoid resistance in three New World primates. *Gen. Comp. Endocrinol.* **124**, 152–165 (2001).
632. Fries, G., Gassen, N. & Rein, T. The FKBP51 Glucocorticoid Receptor Co-Chaperone: Regulation, Function, and Implications in Health and Disease. *Int. J. Mol. Sci.* **18**, 2614 (2017).
633. FKBP Pharma Ltd. FKBP51 | Immunodepressants FK-506 and Rapamycin | Asthma drug development. at <<http://fkbp-pharma.co.uk/fkbp/fkbp51.html>>
634. Pratt, W. B. & Toft, D. O. Steroid receptor interactions with heat shock protein and immunophilin chaperones. *Endocr. Rev.* **18**, 306–360 (1997).
635. Davies, T. H., Ning, Y.-M. & Sánchez, E. R. A New First Step in Activation of Steroid Receptors. *J. Biol. Chem.* **277**, 4597–4600 (2002).
636. Trebble, P. J. *et al.* A ligand-specific kinetic switch regulates glucocorticoid receptor trafficking and function. *J. Cell Sci.* **126**, 3159–69 (2013).
637. Zhang, X., Clark, A. F. & Yorio, T. FK506-binding protein 51 regulates nuclear transport of the glucocorticoid receptor beta

- and glucocorticoid responsiveness. *Invest. Ophthalmol. Vis. Sci.* **49**, 1037–47 (2008).
638. Faralli, J. A., Dimeo, K. D., Trane, R. M. & Peters, D. Absence of a secondary glucocorticoid response in C57BL / 6J mice treated with topical dexamethasone. 1–18 (2018).
639. Lee, R. S. *et al.* Chronic corticosterone exposure increases expression and decreases deoxyribonucleic acid methylation of Fkbp5 in mice. *Endocrinology* **151**, 4332–43 (2010).
640. Matsuda, A. *et al.* DNA Methylation Analysis of Human Trabecular Meshwork Cells During Dexamethasone StimulationDNA Methylation Analysis of Trabecular Meshwork Cells. *Investig. Ophthalmol. Vis. Sci.* **56**, 3801–3809 (2015).
641. Fingert, J. H., Alward, W. L., Wang, K., Yorio, T. & Clark, A. F. Assessment of SNPs associated with the human glucocorticoid receptor in primary open-angle glaucoma and steroid responders. *Mol. Vis.* **16**, 596–601 (2010).
642. Oakley, R. H., Jewell, C. M., Yudt, M. R., Bofetiado, D. M. & Cidlowski, J. A. The dominant negative activity of the human glucocorticoid receptor beta isoform. Specificity and mechanisms of action. *J. Biol. Chem.* **274**, 27857–66 (1999).
643. Pelleymounter, L. L. *et al.* A novel application of pattern recognition for accurate SNP and indel discovery from high-throughput data: targeted resequencing of the glucocorticoid receptor co-chaperone FKBP5 in a Caucasian population. **104**, 457–469 (2012).

644. Volk, N. *et al.* Amygdalar MicroRNA-15a Is Essential for Coping with Chronic Stress. *Cell Rep.* **17**, 1882–1891 (2016).
645. Zheng, D. *et al.* MicroRNA-511 binds to FKBP5 mRNA, which encodes a chaperone protein, and regulates neuronal differentiation. *J. Biol. Chem.* **291**, 17897–17906 (2016).
646. Pierce, N., Tang, X., Lomenick, B., Damoiseaux, R. & Hao, R. Chemical genetics of TOR identifies an SCF family E3 ubiquitin ligase inhibitor. *Nat. Biotechnol.* **28**, 738–742 (2011).
647. Birke, K., Lütjen-Drecoll, E., Kerjaschki, D. & Birke, M. T. Expression of podoplanin and other lymphatic markers in the human anterior eye segment. *Investig. Ophthalmol. Vis. Sci.* **51**, 344–354 (2010).
648. Schacht, V. *et al.* Up-Regulation of the Lymphatic Marker Podoplanin, a Mucin-Type Transmembrane Glycoprotein, in Human Squamous Cell Carcinomas and Germ Cell Tumors. (2005).  
at  
<<https://www.ncbi.nlm.nih.gov/pmc/articles/PMC1602360/pdf/JPATH166000913.pdf>>
649. Comes, N. & Borrás, T. Individual molecular response to elevated intraocular pressure in perfused postmortem human eyes. *Physiol Genomics* **38**, 205–225 (2009).
650. Watanabe, Y., Hamanaka, T., Takemura, T. & Murakami, A. Involvement of Platelet Coagulation and Inflammation in the Endothelium of Schlemm’s Canal. *Investig. Ophthalmology Vis. Sci.* **51**, 277 (2010).

651. Petrova, T. V. & Koh, G. Y. Organ-specific lymphatic vasculature: From development to pathophysiology. *J. Exp. Med.* **215**, 35–49 (2018).
652. Aspelund, A. *et al.* The Schlemm's canal is a VEGF-C/VEGFR-3-responsive lymphatic-like vessel. *J. Clin. Invest.* **124**, 3975–86 (2014).
653. Aspelund, A. *et al.* The Schlemm's canal develops from venous endothelium into a VEGF-C / VEGFR-3 responsive lymphatic vessel. *J. Clin. Invest.* **124**, 1–25 (2014).
654. Krulthof, E. K. ., Baker, M. S. & Bunn, C. L. Biological and Clinical Aspects of Plasminogen Activator Inhibitor Type 2. **84**, 3253–3260 (1994).
655. Medcalf, R. L. & Stasinopoulos, S. J. The undecided serpin: The ins and outs of plasminogen activator inhibitor type 2. *FEBS J.* **272**, 4858–4867 (2005).
656. Darnell, G. A. *et al.* SerpinB2 is an inducible host factor involved in enhancing HIV-1 transcription and replication. *J. Biol. Chem.* **281**, 31348–31358 (2006).
657. Gan, H., Newman, G. W. & Remold, H. G. Plasminogen activator inhibitor type 2 prevents programmed cell death of human macrophages infected with *Mycobacterium avium*, serovar 4. *J. Immunol.* **155**, 1304–1315 (1995).
658. Harris, N. L. E. *et al.* SerpinB2 regulates stromal remodelling and local invasion in pancreatic cancer. *Oncogene* **36**, 4288–4298

(2017).

659. Kohler, H. P. & Grant, P. J. Plasminogen-Activator Inhibitor Type 1 and Coronary Artery Disease. *N. Engl. J. Med.* **342**, 1792–1801 (2000).
660. Hsieh, H.-H., Chen, Y.-C., Jhan, J.-R. & Lin, J.-J. The serine protease inhibitor serpinB2 binds and stabilizes p21 in senescent cells. *J. Cell Sci.* **130**, 3272–3281 (2017).
661. Reith, A., Booth, N. A., Moore, N. R., Cruickshank, D. J. & Bennett, B. Plasminogen activator inhibitors (PAI-1 and PAI-2) in normal pregnancies, pre-eclampsia and hydatidiform mole. *Br. J. Obstet. Gynaecol.* **100**, 370–4 (1993).
662. Woessner, J. F. Matrix metalloproteinases and their inhibitors in connective tissue remodeling. *FASEB J.* **5**, 2145–54 (1991).
663. Matrisian, L. M. Metalloproteinases and their inhibitors in matrix remodeling. *Trends Genet.* **6**, 121–5 (1990).
664. Markiewicz, L. *et al.* Altered expression levels of MMP1, MMP9, MMP12, TIMP1, and IL-1  $\beta$  as a risk factor for the elevated IOP and optic nerve head damage in the primary open-angle glaucoma patients. *Biomed Res. Int.* **2015**, (2015).
665. Porter, K. M., Epstein, D. L. & Liton, P. B. Up-regulated expression of extracellular matrix remodeling genes in phagocytically challenged trabecular meshwork cells. *PLoS One* **7**, 7–9 (2012).
666. Spiga, M. G. & Borrás, T. Development of a gene therapy virus with a glucocorticoid-inducible MMP1 for the treatment of steroid

- glaucoma. *Investig. Ophthalmol. Vis. Sci.* **51**, 3029–3040 (2010).
667. Kim, W. H., Jee, D. H. & Choi, J. A. Elevated Matrix Metalloproteinase in Aqueous Humor in Patients with Open-Angle Glaucoma. **57**, 601–606 (2016).
668. Schneyer, A. L., Wang, Q. I. F. A., Weiss, J. & Boepple, P. F. Follistatin Physiology and Potential Mechanisms of Action in the Human. 28–29 (1997).
669. Zhang, L., Liu, K., Han, B., Xu, Z. & Gao, X. The emerging role of follistatin under stresses and its implications in diseases. *Gene* **639**, 111–116 (2018).
670. Welt, C., Sidis, Y., Keutmann, H. & Schneyer, A. Activins, inhibins, and follistatins: from endocrinology to signaling. A paradigm for the new millennium. *Exp. Biol. Med. (Maywood)*. **227**, 724–752 (2002).
671. Avsian-Kretchmer, O. & Hsueh, A. J. W. Comparative Genomic Analysis of the Eight-Membered Ring Cystine Knot-Containing Bone Morphogenetic Protein Antagonists. *Mol. Endocrinol.* **18**, 1–12 (2004).
672. de Kretser, D. M., O’Hehir, R. E., Hardy, C. L. & Hedger, M. P. The roles of activin A and its binding protein, follistatin, in inflammation and tissue repair. *Mol. Cell. Endocrinol.* **359**, 101–106 (2012).
673. Fitzgerald, A. M., Benz, C., Clark, A. F. & Wordinger, R. J. The effects of transforming growth factor-beta2 on the expression of

- follistatin and activin a in normal and glaucomatous human trabecular meshwork cells and tissues. *Investig. Ophthalmol. Vis. Sci.* **53**, 7358–7369 (2012).
674. Lim, R. *et al.* Activin and NADPH-oxidase in preeclampsia: Insights from in vitro and murine studies. *Am. J. Obstet. Gynecol.* **212**, 86.e1-86e12 (2015).
675. Lin, C. *et al.* Transcriptional activation of follistatin by Nrf2 protects pulmonary epithelial cells against silica nanoparticle-induced oxidative stress. *Sci. Rep.* **6**, 1–11 (2016).
676. Chen, C. Y. A. & Shyu, A. Bin. AU-rich elements: characterization and importance in mRNA degradation. *Trends Biochem. Sci.* **20**, 465–470 (1995).
677. Dzikiewicz-Krawczyk, A. *et al.* Polymorphisms in microRNA target sites modulate risk of lymphoblastic and myeloid leukemias and affect microRNA binding. *J. Hematol. Oncol.* **7**, 43 (2014).
678. Gong, W. *et al.* Type 2 diabetes mellitus-related genetic polymorphisms in microRNAs and microRNA target sites. (2014). doi:10.1111/1753-0407.12143
679. Askou, A. L., Alsing, S., Holmgaard, A., Bek, T. & Corydon, T. J. Dissecting microRNA dysregulation in age-related macular degeneration: new targets for eye gene therapy. *Acta Ophthalmol.* **96**, 9–23 (2018).
680. Landers, J., Goldberg, I. & Graham, S. L. Analysis of risk factors that may be associated with progression from ocular

- hypertension to primary open angle glaucoma. *Clin. Experiment. Ophthalmol.* **30**, 242–7 (2002).
681. Kasetti, R. B., Maddineni, P., Millar, J. C., Clark, A. F. & Zode, G. S. Increased synthesis and deposition of extracellular matrix proteins leads to endoplasmic reticulum stress in the trabecular meshwork. *Sci. Rep.* **7**, 1–14 (2017).
682. Dunmire, J. J., Lagorous, E., Bouhenni, R. A., Jones, M. & Edward, D. P. MicroRNA in aqueous humor from patients with cataract. *Exp. Eye Res.* **108**, 68–71 (2013).
683. Tanaka, Y. *et al.* Profiles of extracellular miRNAs in the aqueous humor of glaucoma patients assessed with a microarray system. *Sci. Rep.* **4**, 1–7 (2014).
684. Jayaram, H. *et al.* Comparison of MicroRNA Expression in Aqueous Humor of Normal and Primary Open-Angle Glaucoma Patients Using PCR Arrays: A Pilot Study. *Investig. Ophthalmology Vis. Sci.* **58**, 2884 (2017).
685. O’Callaghan, J., Cassidy, P. S. & Humphries, P. Open-angle glaucoma: therapeutically targeting the extracellular matrix of the conventional outflow pathway. *Expert Opin. Ther. Targets* **21**, 1037–1050 (2017).
686. Cushing, L. *et al.* miR-29 is a major regulator of genes associated with pulmonary fibrosis. *Am. J. Respir. Cell Mol. Biol.* **45**, 287–294 (2011).
687. Luna, C., Li, G., Qiu, J., Epstein, D. L. & Gonzalez, P. Role of miR-

- 29b on the regulation of the extracellular matrix in human trabecular meshwork cells under chronic oxidative stress. *Mol. Vis.* **15**, 2488–97 (2009).
688. Luna, C., Li, G., Qiu, J., Epstein, D. L. & Gonzalez, P. Cross-talk between miR-29 and transforming growth factor-betas in trabecular meshwork cells. *Invest. Ophthalmol. Vis. Sci.* **52**, 3567–72 (2011).
689. Villarreal, G., Oh, D.-J., Kang, M. H. & Rhee, D. J. Coordinated Regulation of Extracellular Matrix Synthesis by the MicroRNA-29 Family in the Trabecular Meshwork. *Investig. Ophthalmology Vis. Sci.* **52**, 3391 (2011).
690. Shen, W. *et al.* MicroRNA-483-3p inhibits extracellular matrix production by targeting smad4 in human trabecular meshwork cells. *Investig. Ophthalmol. Vis. Sci.* **56**, 8419–8427 (2015).
691. Challa, P. & Arnold, J. J. Rho-kinase inhibitors offer a new approach in the treatment of glaucoma. *Expert Opin. Investig. Drugs* **23**, 81–95 (2014).
692. Xu, B. *et al.* Hsa-miR-146a-5p modulates androgen-independent prostate cancer cells apoptosis by targeting ROCK1. *Prostate* **75**, 1896–1903 (2015).
693. Brabletz, S. & Brabletz, T. The ZEB/miR-200 feedback loop—a motor of cellular plasticity in development and cancer? *EMBO Rep.* **11**, 670–677 (2010).
694. Li, X. *et al.* Regulation of intraocular pressure by microRNA cluster

- miR-143/145. *Sci. Rep.* **7**, 915 (2017).
695. Sabbah, M. *et al.* Molecular signature and therapeutic perspective of the epithelial-to-mesenchymal transitions in epithelial cancers. *Drug Resist. Updat.* **11**, 123–151 (2008).
696. Xie, T. *et al.* Comprehensive microRNA analysis in bleomycin-induced pulmonary fibrosis identifies multiple sites of molecular regulation. *Physiol. Genomics* **43**, 479–487 (2011).
697. Luna, C., Li, G., Qiu, J., Epstein, D. L. & Gonzalez, P. MicroRNA-24 regulates the processing of latent TGF $\beta$ 1 during cyclic mechanical stress in human trabecular meshwork cells through direct targeting of FURIN. *J. Cell. Physiol.* **226**, 1407–1414 (2011).
698. Branton, M. H. & Kopp, J. B. TGF-beta and fibrosis. *Microbes Infect.* **1**, 1349–65 (1999).
699. Kang, H. & Hara. Role of MicroRNAs in TGF- $\beta$  Signaling Pathway-Mediated Pulmonary Fibrosis. *Int. J. Mol. Sci.* **18**, 2527 (2017).
700. Davis-Dusenbery, B. N. & Hata, A. Mechanisms of control of microRNA biogenesis. *J. Biochem.* **148**, 381–92 (2010).
701. Butz, H., Roly Rá Cz, K., Szló Hunyady, L. & Pató Cs, A. Crosstalk between TGF-b signaling and the microRNA machinery. (2012). doi:10.1016/j.tips.2012.04.003
702. Davis, B. N. & Hata, A. Regulation of MicroRNA Biogenesis: A miRiad of mechanisms. *Cell Commun. Signal.* **7**, 1–22 (2009).
703. Davis, B. N., Hilyard, A. C., Nguyen, P. H., Lagna, G. & Hata, A. SMAD proteins bind a conserved RNA sequence to promote

- microRNA maturation by DROSHA. **31**, 1713–1723 (2013).
704. Suzuki, H. I. *et al.* Modulation of microRNA processing by p53. *Nature* **460**, 529–533 (2009).
705. Guo, Y. *et al.* Characterization of the mammalian miRNA turnover landscape. *Nucleic Acids Res.* **43**, 2326–41 (2015).
706. Ji Diana Lee, Y., Kim, V., Muth, D. C. & Witwer, K. W. Validated MicroRNA Target Databases: An Evaluation. *Drug Dev. Res.* **76**, 389–396 (2015).
707. Dweep, H. & Gretz, N. miRWalk2.0: a comprehensive atlas of microRNA-target interactions. *Nat. Methods* **12**, 697–697 (2015).
708. Chou, C.-H. *et al.* miRTarBase update 2018: a resource for experimentally validated microRNA-target interactions. *Nucleic Acids Res.* **46**, D296–D302 (2018).
709. Zhao, N. *et al.* MicroRNA miR145 regulates TGFBR2 expression and matrix synthesis in vascular smooth muscle cells. *Circ. Res.* **116**, 23–34 (2015).
710. Wang, L., He, J., Xu, H., Xu, L. & Li, N. MiR-143 targets CTGF and exerts tumor-suppressing functions in epithelial ovarian cancer. *Am. J. Transl. Res.* **8**, 2716–26 (2016).
711. Shimizu, C. *et al.* Differential Expression of miR-145 in Children with Kawasaki Disease. *PLoS One* **8**, e58159 (2013).
712. Junglas, B. *et al.* Connective tissue growth factor causes glaucoma by modifying the actin cytoskeleton of the trabecular meshwork. *Am. J. Pathol.* **180**, 2386–2403 (2012).

713. Hu, H. *et al.* MiR-145 and miR-203 represses TGF- $\beta$ -induced epithelial-mesenchymal transition and invasion by inhibiting SMAD3 in non-small cell lung cancer cells. *Lung Cancer* **97**, 87–94 (2016).
714. Hoffman, E. a, Conley, S. M., Stamer, W. D. & McKay, B. S. Barriers to productive transfection of trabecular meshwork cells. *Mol. Vis.* **11**, 869–875 (2005).
715. Braunger, B. M., Fuchshofer, R. & Tamm, E. R. The aqueous humor outflow pathways in glaucoma: A unifying concept of disease mechanisms and causative treatment. *Eur. J. Pharm. Biopharm.* **95**, 173–181 (2015).
716. Varkonyi-Gasic, E., Wu, R., Wood, M., Walton, E. F. & Hellens, R. P. Protocol: a highly sensitive RT-PCR method for detection and quantification of microRNAs. *Plant Methods* **3**, 12 (2007).
717. Li, C. *et al.* Comparative study of microRNA profiling in keloid fibroblast and annotation of differential expressed microRNAs. *Acta Biochim. Biophys. Sin. (Shanghai)*. **45**, 692–699 (2013).
718. Chang, M., Lin, H., Luo, M., Wang, J. & Han, G. Integrated miRNA and mRNA expression profiling of tension force-induced bone formation in periodontal ligament cells. *Vitr. Cell. Dev. Biol. - Anim.* **51**, 797–807 (2015).
719. Licheng Wu, R., Ali, S., Sarkar, F. H. & Beydoun, R. Identification of Differentially Expressed Mirnas in Appendiceal Mucinous Cystadenocarcinoma from Mucinous Cystadenoma. *J. Cancer Sci. Ther.* **7**, 328–335 (2015).

720. Liu, F., Gong, R., Lv, X. & Li, H. The expression profiling and ontology analysis of non-coding RNAs in dexamethasone induced steatosis in hepatoma cell. *Gene* **650**, 19–26 (2018).
721. Li, C. *et al.* Comparative study of microRNA profiling in keloid fibroblast and annotation of differential expressed microRNAs. *Acta Biochim. Biophys. Sin. (Shanghai)*. **45**, 692–699 (2013).
722. Kent, O. A., McCall, M. N., Cornish, T. C. & Halushka, M. K. Lessons from miR-143/145: The importance of cell-type localization of miRNAs. *Nucleic Acids Res.* **42**, 7528–7538 (2014).
723. Gomes, S. E. *et al.* Convergence of miR-143 overexpression, oxidative stress and cell death in HCT116 human colon cancer cells. *PLoS One* **13**, e0191607 (2018).
724. Das, A. V. & Pillai, R. M. Implications of miR cluster 143/145 as universal anti-oncomiRs and their dysregulation during tumorigenesis. *Cancer Cell Int.* **15**, 92 (2015).
725. Cordes, K. R. *et al.* miR-145 and miR-143 regulate smooth muscle cell fate and plasticity. *Nature* **460**, 705–10 (2009).
726. Zhao, W., Zhao, S.-P. & Zhao, Y.-H. MicroRNA-143/-145 in Cardiovascular Diseases. *Biomed Res. Int.* **2015**, 1–9 (2015).
727. Iio, A., Nakagawa, Y., Hirata, I., Naoe, T. & Akao, Y. Identification of non-coding RNAs embracing microRNA-143/145 cluster. *Mol. Cancer* **9**, 136 (2010).
728. Cheng, Y. *et al.* MicroRNA-145, a Novel Smooth Muscle Cell Phenotypic Marker and Modulator, Controls Vascular Neointimal

- Lesion Formation. *Circ. Res.* **105**, 158–166 (2009).
729. Rangrez, A. Y., Massy, Z. A., Meuth, V. M. Le & Metzinger, L. MiR-143 and miR-145 molecular keys to switch the phenotype of vascular smooth muscle cells. *Circ. Cardiovasc. Genet.* **4**, 197–205 (2011).
730. Davis-Dusenbery, B. N., Wu, C., Hata, A. & Sessa, W. C. Micromanaging Vascular Smooth Muscle Cell Differentiation and Phenotypic Modulation. *Arterioscler. Thromb. Vasc. Biol.* **31**, 2370–2377 (2011).
731. Lagna, G. *et al.* Control of Phenotypic Plasticity of Smooth Muscle Cells by Bone Morphogenetic Protein Signaling through the Myocardin-related Transcription Factors. *J. Biol. Chem.* **282**, 37244–37255 (2007).
732. Tsapara, A. *et al.* The RhoA Activator GEF-H1/Lfc Is a Transforming Growth Factor- Target Gene and Effector That Regulates - Smooth Muscle Actin Expression and Cell Migration. *Mol. Biol. Cell* **21**, 860–870 (2010).
733. Read, A. T., Chan, D. W.-H. & Ethier, C. R. Actin structure in the outflow tract of normal and glaucomatous eyes. *Exp. Eye Res.* **84**, 214–26 (2007).
734. Wade, N. C. *et al.* Cross-linked actin networks (CLANs) in bovine trabecular meshwork cells. *Exp. Eye Res.* **89**, 648–659 (2009).
735. Clark, A. F., Miggans, S. T., Wilson, K., Browder, S. & McCartney, M. D. Cytoskeletal changes in cultured human glaucoma

- trabecular meshwork cells. *J. Glaucoma* **4**, 183–8 (1995).
736. Hoare, M.-J. *et al.* Cross-Linked Actin Networks (CLANs) in the Trabecular Meshwork of the Normal and Glaucomatous Human Eye In Situ. *Investig. Ophthalmology Vis. Sci.* **50**, 1255 (2009).
737. Lee, H. K. *et al.* MicroRNA-145 Is Downregulated in Glial Tumors and Regulates Glioma Cell Migration by Targeting Connective Tissue Growth Factor. *PLoS One* **8**, e54652 (2013).
738. Mu, S., Kang, B., Zeng, W., Sun, Y. & Yang, F. MicroRNA-143-3p inhibits hyperplastic scar formation by targeting connective tissue growth factor CTGF/CCN2 via the Akt/mTOR pathway. *Mol. Cell. Biochem.* **416**, 99–108 (2016).
739. Kuosmanen, S. M., Kansanen, E., Sihvola, V. & Levonen, A.-L. MicroRNA Profiling Reveals Distinct Profiles for Tissue-Derived and Cultured Endothelial Cells. *Sci. Rep.* **7**, 10943 (2017).
740. Zhu, H.-Y., Yeo, S.-W., Ng, J., Htoon, H. M. & Beuerman, R. W. Moesin as a Key Cytoskeleton Regulator in Corneal Fibrosis. *Ocul. Surf.* **11**, 119–132 (2013).
741. Kalouche, G. *et al.* Prostaglandin EP2 receptor signaling protects human trabecular meshwork cells from apoptosis induced by ER stress through down-regulation of p53. *Biochim. Biophys. Acta - Mol. Cell Res.* **1863**, 2322–2332 (2016).
742. Guo, Y. *et al.* Association of TP53 Polymorphisms with Primary Open-Angle Glaucoma: A Meta-Analysis. *Investig. Ophthalmology Vis. Sci.* **53**, 3756 (2012).

743. Costa, C., Giménez-Capitán, A., Karachaliou, N. & Rosell, R. Comprehensive molecular screening: from the RT-PCR to the RNA-seq. *Transl. lung cancer Res.* **2**, 87–91 (2013).
744. Hanrahan, K. *et al.* The role of epithelial-mesenchymal transition drivers ZEB1 and ZEB2 in mediating docetaxel-resistant prostate cancer. *Mol. Oncol.* **11**, 251–265 (2017).
745. Xin, M. *et al.* MicroRNAs miR-143 and miR-145 modulate cytoskeletal dynamics and responsiveness of smooth muscle cells to injury. *Genes Dev.* **23**, 2166–2178 (2009).
746. Long, X. & Miano, J. M. Transforming growth factor-beta1 (TGF-beta1) utilizes distinct pathways for the transcriptional activation of microRNA 143/145 in human coronary artery smooth muscle cells. *J. Biol. Chem.* **286**, 30119–29 (2011).
747. Quintavalle, M., Elia, L., Condorelli, G. & Courtneidge, S. A. MicroRNA control of podosome formation in vascular smooth muscle cells in vivo and in vitro. *J. Cell Biol.* **189**, 13–22 (2010).
748. Donegan, R. K. & Lieberman, R. L. Discovery of Molecular Therapeutics for Glaucoma: Challenges, Successes, and Promising Directions. *J. Med. Chem.* **59**, 788–809 (2016).
749. Bagnis, A., Papadia, M., Scotto, R. & Traverso, C. E. Current and emerging medical therapies in the treatment of glaucoma. *Expert Opin. Emerg. Drugs* **16**, 293–307 (2011).
750. Wiederholt, M., Schäfer, R., Wagner, U. & Lepple-Wienhues, A. Contractile response of the isolated trabecular meshwork and

- ciliary muscle to cholinergic and adrenergic agents. *Ger. J. Ophthalmol.* **5**, 146–53 (1996).
751. Realini, T. A History of Glaucoma Pharmacology. *Optom. Vis. Sci.* **88**, 36–38 (2011).
752. Toris, C. B., Yablonski, M. E., Wang, Y. L. & Hayashi, M. Prostaglandin A2 increases uveoscleral outflow and trabecular outflow facility in the cat. *Exp. Eye Res.* **61**, 649–57 (1995).
753. Weinreb, R. N., Toris, C. B., Gabelt, B. T., Lindsey, J. D. & Kaufman, P. L. Effects of prostaglandins on the aqueous humor outflow pathways. *Surv. Ophthalmol.* **47 Suppl 1**, S53-64 (2002).
754. Reitsamer, H. A., Posey, M. & Kiel, J. W. Effects of a topical  $\alpha_2$  adrenergic agonist on ciliary blood flow and aqueous production in rabbits. *Exp. Eye Res.* **82**, 405–415 (2006).
755. Zimmerman, T. J., Harbin, R., Pett, M. & Kaufman, H. E. Timolol and facility of outflow. *Invest. Ophthalmol. Vis. Sci.* **16**, 623–4 (1977).
756. Coakes, R. L. & Brubaker, R. F. The mechanism of timolol in lowering intraocular pressure. In the normal eye. *Arch. Ophthalmol. (Chicago, Ill. 1960)* **96**, 2045–8 (1978).
757. Hoyng, P. F. & van Beek, L. M. Pharmacological therapy for glaucoma: a review. *Drugs* **59**, 411–34 (2000).
758. Melamed, S., Ben Simon, G. J. & Levkovitch-Verbin, H. Selective Laser Trabeculoplasty as Primary Treatment for Open-angle Glaucoma. *Arch. Ophthalmol.* **121**, 957 (2003).

759. Johnson, D. H. & Johnson, M. How does nonpenetrating glaucoma surgery work? Aqueous outflow resistance and glaucoma surgery. *J. Glaucoma* **10**, 55–67 (2001).
760. Gedde, S. J. *et al.* Treatment Outcomes in the Tube Versus Trabeculectomy (TVT) Study After Five Years of Follow-up. *Am. J. Ophthalmol.* **153**, 789–803.e2 (2012).
761. Spiegel, D. & Kobuch, K. Trabecular meshwork bypass tube shunt: initial case series. *Br. J. Ophthalmol.* **86**, 1228–31 (2002).
762. Weinreb, R., Cotlier, E. & Yue, B. Y. J. T. The extracellular matrix and its modulation in the trabecular meshwork. *Surv. Ophthalmol.* **40**, 379–390 (1996).
763. Morrison, J. C., Dorman-Pease, M. E., Dunkelberger, G. R. & Quigley, H. A. Optic nerve head extracellular matrix in primary optic atrophy and experimental glaucoma. *Arch. Ophthalmol. (Chicago, Ill. 1960)* **108**, 1020–4 (1990).
764. Kvanta, A., Seregard, S., Sejersen, S., Kull, B. & Fredholm, B. Localization of Adenosine Receptor Messenger RNAs in the Rat Eye. *Exp. Eye Res.* **65**, 595–602 (1997).
765. Fleischhauer, J. C. *et al.* Common actions of adenosine receptor agonists in modulating human trabecular meshwork cell transport. *J. Membr. Biol.* **193**, 121–136 (2003).
766. Karl, M. O. *et al.* Differential P1-purinergic modulation of human Schlemm's canal inner-wall cells. *Am. J. Physiol. Physiol.* **288**, C784–C794 (2005).

767. Husain, S., Shearer, T. W. & Crosson, C. E. Mechanisms Linking Adenosine A1 Receptors and Extracellular Signal-Regulated Kinase 1/2 Activation in Human Trabecular Meshwork Cells. *J. Pharmacol. Exp. Ther.* **320**, 258–265 (2006).
768. Agarwal, R. & Agarwal, P. Newer targets for modulation of intraocular pressure: focus on adenosine receptor signaling pathways. *Expert Opin. Ther. Targets* **18**, 527–539 (2014).
769. Crosson, C. E., Sloan, C. F. & Yates, P. W. Modulation of Conventional Outflow Facility by the Adenosine A<sub>1</sub> Agonist N<sup>6</sup>-Cyclohexyladenosine. *Investig. Ophthalmology Vis. Sci.* **46**, 3795 (2005).
770. Shearer, T. W. & Crosson, C. E. Adenosine A<sub>1</sub> receptor modulation of MMP-2 secretion by trabecular meshwork cells. *Invest. Ophthalmol. Vis. Sci.* **43**, 3016–20 (2002).
771. Borrás, T., Buie, L. K. & Spiga, M. G. Inducible scAAV2.GRE.MMP1 lowers IOP long-term in a large animal model for steroid-induced glaucoma gene therapy. *Gene Ther.* **23**, 438–449 (2016).
772. Hoy, S. M. Netarsudil Ophthalmic Solution 0.02%: First Global Approval. *Drugs* **78**, 389–396 (2018).
773. Leung, T., Chen, X. Q., Manser, E. & Lim, L. The p160 RhoA-binding kinase ROK alpha is a member of a kinase family and is involved in the reorganization of the cytoskeleton. *Mol. Cell. Biol.* **16**, 5313–27 (1996).
774. Mueller, B. K., Mack, H. & Teusch, N. Rho kinase, a promising drug

- target for neurological disorders. *Nat. Rev. Drug Discov.* **4**, 387–398 (2005).
775. Satoh, K., Fukumoto, Y. & Shimokawa, H. Rho-kinase: important new therapeutic target in cardiovascular diseases. *Am. J. Physiol. Circ. Physiol.* **301**, H287–H296 (2011).
776. Riento, K. & Ridley, A. J. Rocks: Multifunctional kinases in cell behaviour. *Nat. Rev. Mol. Cell Biol.* **4**, 446–456 (2003).
777. Fukata, Y., Amano, M. & Kaibuchi, K. Rho-Rho-kinase pathway in smooth muscle contraction and cytoskeletal reorganization of non-muscle cells. *Trends Pharmacol. Sci.* **22**, 32–9 (2001).
778. Whitlock, N. A. *et al.* Decreased Intraocular Pressure in Mice Following Either Pharmacological or Genetic Inhibition of ROCK. *J. Ocul. Pharmacol. Ther.* **25**, 187–194 (2009).
779. Noda, K. *et al.* Rho-Kinase Inhibition Ameliorates Metabolic Disorders through Activation of AMPK Pathway in Mice. *PLoS One* **9**, e110446 (2014).
780. Aznar, S., Fernández-Valerón, P., Espina, C. & Lacal, J. C. Rho GTPases: potential candidates for anticancer therapy. *Cancer Lett.* **206**, 181–191 (2004).
781. Hidaka, H., Inagaki, M., Kawamoto, S. & Sasaki, Y. Isoquinolinesulfonamides, novel and potent inhibitors of cyclic nucleotide dependent protein kinase and protein kinase C. *Biochemistry* **23**, 5036–41 (1984).
782. Davies, S. P., Reddy, H., Caivano, M. & Cohen, P. Specificity and

- mechanism of action of some commonly used protein kinase inhibitors. *Biochem. J.* **351**, 95–105 (2000).
783. Tamura, M. *et al.* Development of specific Rho-kinase inhibitors and their clinical application. *Biochim. Biophys. Acta - Proteins Proteomics* **1754**, 245–252 (2005).
784. Jacobs, M. *et al.* The Structure of Dimeric ROCK I Reveals the Mechanism for Ligand Selectivity. *J. Biol. Chem.* **281**, 260–268 (2006).
785. Sumi, K. *et al.* IOP-lowering effect of isoquinoline-5-sulfonamide compounds in ocular normotensive monkeys. *Bioorg. Med. Chem. Lett.* **24**, 831–834 (2014).
786. Yamamoto, K. *et al.* The Novel Rho Kinase (ROCK) Inhibitor K-115: A New Candidate Drug for Neuroprotective Treatment in Glaucoma. *Investig. Ophthalmology Vis. Sci.* **55**, 7126 (2014).
787. Chang, R. & Wang, S. An emerging treatment option for glaucoma: Rho kinase inhibitors. *Clin. Ophthalmol.* **8**, 883 (2014).
788. Rao, P. V, Deng, P. F., Kumar, J. & Epstein, D. L. Modulation of aqueous humor outflow facility by the Rho kinase-specific inhibitor Y-27632. *Invest. Ophthalmol. Vis. Sci.* **42**, 1029–37 (2001).
789. Harrison, B. A. *et al.* Discovery and Development of LX7101, a Dual LIM-Kinase and ROCK Inhibitor for the Treatment of Glaucoma. *ACS Med. Chem. Lett.* **6**, 84–88 (2015).
790. Lu, Z., Overby, D. R., Scott, P. A., Freddo, T. F. & Gong, H. The

- mechanism of increasing outflow facility by rho-kinase inhibition with Y-27632 in bovine eyes. *Exp. Eye Res.* **86**, 271–281 (2008).
791. Sugiyama, T. *et al.* Effects of Fasudil, a Rho-Associated Protein Kinase Inhibitor, on Optic Nerve Head Blood Flow in Rabbits. *Investig. Ophthalmology Vis. Sci.* **52**, 64 (2011).
792. Tokushige, H., Waki, M., Takayama, Y. & Tanihara, H. Effects of Y-39983, a Selective Rho-Associated Protein Kinase Inhibitor, on Blood Flow in Optic Nerve Head in Rabbits and Axonal Regeneration of Retinal Ganglion Cells in Rats. *Curr. Eye Res.* **36**, 964–970 (2011).
793. Honjo, M. *et al.* Potential Role of Rho-Associated Protein Kinase Inhibitor Y-27632 in Glaucoma Filtration Surgery. *Investig. Ophthalmology Vis. Sci.* **48**, 5549 (2007).
794. Wang, S. K. & Chang, R. T. An emerging treatment option for glaucoma: Rho kinase inhibitors. *Clin. Ophthalmol.* **8**, 883–90 (2014).
795. Harrison, B. A. *et al.* Discovery and Development of LX7101, a Dual LIM-Kinase and ROCK Inhibitor for the Treatment of Glaucoma. *ACS Med. Chem. Lett.* **6**, 84–8 (2015).
796. Manetti, F. Recent findings confirm LIM domain kinases as emerging target candidates for cancer therapy. *Curr. Cancer Drug Targets* **12**, 543–60 (2012).
797. Menzies, A. M., Long, G. V & Murali, R. Dabrafenib and its potential for the treatment of metastatic melanoma. *Drug Des.*

*Devel. Ther.* **6**, 391–405 (2012).

798. Wang, Y. *et al.* ROCK Isoform Regulation of Myosin Phosphatase and Contractility in Vascular Smooth Muscle Cells. *Circ. Res.* **104**, 531–540 (2009).
799. Harrison, B. A. *et al.* Novel Class of LIM-Kinase 2 Inhibitors for the Treatment of Ocular Hypertension and Associated Glaucoma. *J. Med. Chem.* **52**, 6515–6518 (2009).
800. Cherecheanu, A. P., Garhofer, G., Schmidl, D., Werkmeister, R. & Schmetterer, L. Ocular perfusion pressure and ocular blood flow in glaucoma. *Curr. Opin. Pharmacol.* **13**, 36–42 (2013).
801. San Martin, A. *et al.* Dual Regulation of Cofilin Activity by LIM Kinase and Slingshot-1L Phosphatase Controls Platelet-Derived Growth Factor-Induced Migration of Human Aortic Smooth Muscle Cells. *Circ. Res.* **102**, 432–438 (2008).
802. Siddle, K. Signalling by insulin and IGF receptors: supporting acts and new players. *J. Mol. Endocrinol.* **47**, R1-10 (2011).
803. Smith, L. E. H. *et al.* Regulation of vascular endothelial growth factor-dependent retinal neovascularization by insulin-like growth factor-1 receptor. *Nat. Med.* **5**, 1390–1395 (1999).
804. Haurigot, V. *et al.* Increased intraocular insulin-like growth factor-1 triggers blood-retinal barrier breakdown. *J. Biol. Chem.* **284**, 22961–9 (2009).
805. Mathew, R. & Barton, K. Anti-Vascular Endothelial Growth Factor Therapy in Glaucoma Filtration Surgery. *Am. J. Ophthalmol.* **152**,

- 10–15.e2 (2011).
806. Ruberte, J. *et al.* Increased ocular levels of IGF-1 in transgenic mice lead to diabetes-like eye disease. *J. Clin. Invest.* **113**, 1149–57 (2004).
807. Beckwith, H. & Yee, D. Minireview: Were the IGF Signaling Inhibitors All Bad? *Mol. Endocrinol.* **29**, 1549–57 (2015).
808. Kuespert, S., Junglas, B., Braunger, B. M., Tamm, E. R. & Fuchshofer, R. The regulation of connective tissue growth factor expression influences the viability of human trabecular meshwork cells. doi:10.1111/jcmm.12492
809. Nakajima, E., Nakajima, T., Minagawa, Y., Shearer, T. R. & Azuma, M. Contribution of ROCK in Contraction of Trabecular Meshwork: Proposed Mechanism for Regulating Aqueous Outflow in Monkey and Human Eyes. *J. Pharm. Sci.* **94**, 701–708 (2005).
810. Teixeira, G. *et al.* Therapeutic potential of NADPH oxidase 1/4 inhibitors. *Br. J. Pharmacol.* **174**, 1647–1669 (2017).
811. Altenhöfer, S., Radermacher, K. A., Kleikers, P. W. M., Wingler, K. & Schmidt, H. H. H. W. Evolution of NADPH Oxidase Inhibitors: Selectivity and Mechanisms for Target Engagement. *Antioxid. Redox Signal.* **23**, 406–27 (2015).
812. Laleu, B. *et al.* First in Class, Potent, and Orally Bioavailable NADPH Oxidase Isoform 4 (Nox4) Inhibitors for the Treatment of Idiopathic Pulmonary Fibrosis. *J. Med. Chem.* **53**, 7715–7730 (2010).

813. Cifuentes-Pagano, M. E., Meijles, D. N. & Pagano, P. J. Nox Inhibitors & Therapies: Rational Design of Peptidic and Small Molecule Inhibitors. *Curr. Pharm. Des.* **21**, 6023–35 (2015).
814. Deliyanti, D. & Wilkinson-Berka, J. L. Inhibition of NOX1/4 with GKT137831: a potential novel treatment to attenuate neuroglial cell inflammation in the retina. *J. Neuroinflammation* **12**, 136 (2015).
815. Murphy-Marshman, H. *et al.* Antioxidants and NOX1/NOX4 inhibition blocks TGF $\beta$ 1-induced CCN2 and  $\alpha$ -SMA expression in dermal and gingival fibroblasts. *PLoS One* **12**, e0186740 (2017).
816. Weinreb, R. N. *et al.* Primary open-angle glaucoma. *Nat. Rev. Dis. Prim.* **2**, 16067 (2016).
817. Zhang, X., Clark, A. F. & Yorio, T. Interactions of endothelin-1 with dexamethasone in primary cultured human trabecular meshwork cells. *Invest. Ophthalmol. Vis. Sci.* **44**, 1–8 (2003).
818. Nathanson, J. A. Direct application of a guanylate cyclase activator lowers intraocular pressure. *Eur. J. Pharmacol.* **147**, 155–6 (1988).
819. Wiederholt, M., Sturm, A. & Lepple-Wienhues, A. Relaxation of trabecular meshwork and ciliary muscle by release of nitric oxide. *Invest. Ophthalmol. Vis. Sci.* **35**, 2515–20 (1994).
820. Attinà, T., Camidge, R., Newby, D. E. & Webb, D. J. Endothelin antagonism in pulmonary hypertension, heart failure, and beyond. *Heart* **91**, 825–31 (2005).
821. Neidhart, W. *et al.* Discovery of Ro 48-5695: A potent mixed

- endothelin receptor antagonist optimized from bosentan. *Bioorg. Med. Chem. Lett.* **7**, 2223–2228 (1997).
822. Verhaar, M. C. *et al.* Endothelin-A receptor antagonist-mediated vasodilatation is attenuated by inhibition of nitric oxide synthesis and by endothelin-B receptor blockade. *Circulation* **97**, 752–6 (1998).
823. Strachan, F. E. *et al.* Systemic blockade of the endothelin-B receptor increases peripheral vascular resistance in healthy men. *Hypertens. (Dallas, Tex. 1979)* **33**, 581–5 (1999).
824. Logallo, N. *et al.* Tenecteplase versus alteplase for management of acute ischaemic stroke (NOR-TEST): a phase 3, randomised, open-label, blinded endpoint trial. *Lancet Neurol.* **16**, 781–788 (2017).
825. Izuhara, Y. *et al.* Inhibition of Plasminogen Activator Inhibitor-1: Its Mechanism and Effectiveness on Coagulation and Fibrosis. *Arterioscler. Thromb. Vasc. Biol.* **28**, 672–677 (2008).
826. Huang, Y. *et al.* A mutant, noninhibitory plasminogen activator inhibitor type 1 decreases matrix accumulation in experimental glomerulonephritis. *J. Clin. Invest.* **112**, 379–388 (2003).
827. Mendell, J. R. *et al.* A phase 1/2a follistatin gene therapy trial for becker muscular dystrophy. *Mol. Ther.* **23**, 192–201 (2015).
828. Mendell, J. R. *et al.* Follistatin Gene Therapy for Sporadic Inclusion Body Myositis Improves Functional Outcomes. *Mol. Ther.* **25**, 870–879 (2017).
829. Demetriades, A.-M. Gene therapy for glaucoma. *Curr. Opin.*

- Ophthalmol.* **22**, 73–77 (2011).
830. De Groef, L., Van Hove, I., Dekeyster, E., Stalmans, I. & Moons, L. MMPs in the Trabecular Meshwork: Promising Targets for Future Glaucoma Therapies? *Investig. Ophthalmology Vis. Sci.* **54**, 7756 (2013).
831. O’Callaghan, J. *et al.* Therapeutic potential of AAV-mediated MMP-3 secretion from corneal endothelium in treating glaucoma. *Hum. Mol. Genet.* **26**, 1230–1246 (2017).
832. Vidal, L., Blagden, S., Attard, G. & de Bono, J. Making sense of antisense. *Eur. J. Cancer* **41**, 2812–2818 (2005).
833. Baumann, V. & Winkler, J. Medicinal Chemistry miRNA-based therapies: strategies and delivery platforms for oligonucleotide and non-oligonucleotide agents. *Futur. Med. Chem* **6**, 1967–1984 (2014).
834. Christopher, A. F. *et al.* MicroRNA therapeutics: Discovering novel targets and developing specific therapy. *Perspect. Clin. Res.* **7**, 68–74 (2016).
835. Beg, M. S. *et al.* Phase I study of MRX34, a liposomal miR-34a mimic, administered twice weekly in patients with advanced solid tumors. *Invest. New Drugs* **35**, 180–188 (2017).
836. Rupaimoole, R. & Slack, F. J. MicroRNA therapeutics: towards a new era for the management of cancer and other diseases. *Nat. Rev. Drug Discov.* **16**, 203–222 (2017).
837. Krützfeldt, J. *et al.* Silencing of microRNAs in vivo with

- 'antagomirs'. *Nature* **438**, 685–689 (2005).
838. Janssen, H. L. A. *et al.* Treatment of HCV Infection by Targeting MicroRNA. *N. Engl. J. Med.* **368**, 1685–1694 (2013).
839. Elmén, J. *et al.* LNA-mediated microRNA silencing in non-human primates. *Nature* **452**, 896–899 (2008).
840. Gebert, L. F. R. *et al.* Miravirsin (SPC3649) can inhibit the biogenesis of miR-122. *Nucleic Acids Res.* **42**, 609–621 (2014).
841. Broderick, J. A. & Zamore, P. D. MicroRNA therapeutics. *Gene Ther.* **18**, 1104–1110 (2011).
842. Carè, A. *et al.* MicroRNA-133 controls cardiac hypertrophy. *Nat. Med.* **13**, 613–618 (2007).
843. Roderburg, C. *et al.* Micro-RNA profiling reveals a role for miR-29 in human and murine liver fibrosis. *Hepatology* **53**, 209–218 (2011).
844. Wadhwa, S., Paliwal, R., Paliwal, S. & Vyas, S. Nanocarriers in Ocular Drug Delivery: An Update Review. *Curr. Pharm. Des.* **15**, 2724–2750 (2009).
845. de Salamanca, A. E. *et al.* Chitosan Nanoparticles as a Potential Drug Delivery System for the Ocular Surface: Toxicity, Uptake Mechanism and In Vivo Tolerance. *Investig. Ophthalmology Vis. Sci.* **47**, 1416 (2006).
846. Borrás, T., Gabelt, B. T., Klintworth, G. K., Peterson, J. C. & Kaufman, P. L. Non-invasive observation of repeated adenoviral GFP gene delivery to the anterior segment of the monkey eye

- vivo. *J. Gene Med.* **3**, 437–449 (2001).
847. Borrás, T. Gene therapy strategies in glaucoma and application for steroid-induced hypertension. *Saudi J. Ophthalmol.* **25**, 353–362 (2011).
848. True Gabelt, A. *et al.* Caldesmon transgene expression disrupts focal adhesions in HTM cells and increases outflow facility in organ-cultured human and monkey anterior segments. (2006). doi:10.1016/j.exer.2005.12.002
849. Gerometta, R., Spiga, M.-G., Borrás, T. & Candia, O. A. Treatment of Sheep Steroid-Induced Ocular Hypertension with a Glucocorticoid-Inducible MMP1 Gene Therapy Virus. *Investig. Ophthalmology Vis. Sci.* **51**, 3042 (2010).
850. Hellström, M., Pollett, M. A. & Harvey, A. R. Post-Injury Delivery of rAAV2-CNTF Combined with Short-Term Pharmacotherapy Is Neuroprotective and Promotes Extensive Axonal Regeneration after Optic Nerve Trauma. *J. Neurotrauma* **28**, 2475–2483 (2011).
851. Schlimgen, R. *et al.* Risks Associated With Lentiviral Vector Exposures and Prevention Strategies. *J. Occup. Environ. Med.* **58**, 1159–1166 (2016).
852. Miyazaki, M. *et al.* Pigment Epithelium-Derived Factor Gene Therapy Targeting Retinal Ganglion Cell Injuries: Neuroprotection against Loss of Function in Two Animal Models. *Hum. Gene Ther.* **22**, 559–565 (2011).
853. Comes, N. & Borrás, T. Functional delivery of synthetic naked

- siRNA to the human trabecular meshwork in perfused organ cultures. *Mol. Vis.* **13**, 1363–74 (2007).
854. Chen, Y., Gao, D.-Y. & Huang, L. In vivo delivery of miRNAs for cancer therapy: challenges and strategies. *Adv. Drug Deliv. Rev.* **81**, 128–41 (2015).
855. Huang, L. & Liu, Y. In Vivo Delivery of RNAi with Lipid-Based Nanoparticles. *Annu. Rev. Biomed. Eng.* **13**, 507–530 (2011).
856. Tripathi, R. C., Li, J., Chan, W. F. & Tripathi, B. J. Aqueous humor in glaucomatous eyes contains an increased level of TGF-beta 2. *Experimental eye research* **59**, 723–727 (1994).
857. Gerzenstein, S. M. *et al.* Glucocorticoid Receptor Polymorphisms and Intraocular Pressure Response to Intravitreal Triamcinolone Acetonide. *Ophthalmic Genet.* **29**, 166–170 (2008).
858. Johnson, D. H. & Tschumper, R. C. Human Trabecular Meshwork Organ Culture, A New Method. **28**, 1802–1806 (1995).
859. Kearns, V. R. & Williams, R. L. Drug delivery systems for the eye. *Expert Rev. Med. Devices* **6**, 277–290 (2009).
860. Edgar Edward Wilson. Anatomy & Physiology I Chapter ppt video online download. at  
<<http://slideplayer.com/slide/9195506/>>
861. Tulane University. Glucocorticoid Pharmacology.  
doi:10.2174/1874325001206010449

